Summer 8-15-2019

Brain Blood Flow and Metabolism: Variable Relationships in Altered Metabolic States

Tyler M. Blazey
Washington University in St. Louis

WASHINGTON UNIVERSITY IN ST. LOUIS

Division of Biology and Biomedical Sciences
Neurosciences

Dissertation Examination Committee:
Marcus E. Raichle, Chair
Amy L. Bauernfeind
Tamara Hershey
Shannon L. Macauley-Rambach
Abraham Z. Snyder

Brain Blood Flow and Metabolism: Variable Relationships in Altered Metabolic States

by
Tyler Matthew Blazey

A dissertation presented to
The Graduate School
of Washington University in
partial fulfillment of the
requirements for the degree
of Doctor of Philosophy

August 2019
St. Louis, Missouri

Table of Contents

List of Figures

List of Tables

Acknowledgments

People who know me are well aware that I tend to try to work things out by myself. Over the last few years, however, I often found myself in the same situation: trying to solve a tricky problem by myself but failing to do so and feeling rather stuck. At this point, I would continue to struggle for far too long before eventually giving up and asking for help. Unsurprisingly, the problem quickly became much more manageable once I asked for help. I would therefore like to thank the many people that have helped me complete this dissertation. I know I couldn't have done it without them. My only regret is that I didn't reach out for help sooner. It is clear to me now there were always people willing to help me, and that all I had to do was ask.

First, I would like to thank my primary advisors Marc Raichle and Avi Snyder for their endless support of me as I completed this dissertation. More than once while trying to complete this thesis I wondered if I was going to be able to finish it. I don't doubt that at one point or another, many other advisors would have given up on me. But Marc and Avi always believed that I could finish my work, and I will always be grateful for their belief in me. Marc has been incredibly understanding these last few years, and always supported me when I was struggling inside or outside of lab. Although he is well-known for his many scientific achievements, I think he deserves equal acclaim for the way he treats everyone around him. Avi too has gone well beyond what is required of a mentor. He never hesitated in doing what was needed to help me, whether it was daily meetings to make sure I kept on track or watching an old movie with me so that I had some fun. New students in the lab often find meeting with Avi a cause for anxiety. There is no need. Although he can be a bit abrasive during scientific discussions, he is a uniquely kind and selfless person.

Intellectually, I could not have asked for better mentors. Marc has such a thorough, unique understanding of brain metabolism. He is also easily the most imaginative and thoughtful person I have ever met. Sometimes I, as a rather concrete thinker, found it hard to keep up with the wide-ranging connections that he seemed to make so easily. These discussions always made my work better though and going forward I think I will be fine if I can work with a fraction of his creativity. Avi was an indispensable asset whenever I had trouble with a technical aspect of my work. Despite his intelligence, he shares my preference for simple solutions and helped me come up with solutions without relying too much on complicated or flashy techniques. He has also been exceedingly helpful with my writing. He was the first person to read everything I wrote for my thesis and never failed to increase the clarify of my writing.

Of course, many other people helped me along the way as well. I would be remiss if I did not thank Brian Gordon, who tolerated with good grace the many times I came into his office to talk about science or some other nerdy topic. He also gave me the opportunity to work on several interesting side projects. I learned a great deal about PET analysis from Lars Couture, John Lee, and Yi Su. John, in particular, deserves acknowledgment, as much of the data I used in this thesis would not exist without his diligence. Similarly, I owe a debt to Ana María Arbeláez and her amazing team, who acquired all of the data used in chapters 4 and 5. I was also very fortunate to work with Manu Goyal and Andrei Vlassenko, who were great collaborators.

I would also like to thank Tammie Benzinger, Denise Head, and Russ Hornbeck for hiring me as a research technician before I started graduate school. Despite the fact that I was an employee, they allowed me a great deal of freedom to work on unassigned tasks. During this time, I was able to learn many of technical skills that I relied upon to complete my thesis. I greatly appreciate the chance they took on me.

I also need to acknowledge my other committee members: Amy Bauernfeind, Tammy Hershey, and Shannon Macauley-Rambach. They were all very supportive, provided me with invaluable feedback, and encouraged me to think more broadly about my work. I should also note that they never complained about a rather irregular committee meeting schedule. I would especially like to think Tammy for serving as my committee chair. She was always encouraging, even during periods when I felt my work was not progressing as much as it should. She also has been a great source of practical advice about my thesis and life after graduate school.

Finally, I would like to my father for a lifetime of unconditional support. I would have never made it this far without him. I particularly feel the need to acknowledge how he encouraged me to learn growing up. As a child, the one thing I always knew he would buy for me were books. I like to think that this thesis is proof that he made a good investment.

Tyler Blazey

Washington University in St. Louis

August 2019

ABSTRACT OF THE DISSERTATION

Brain Blood Flow and Metabolism: Variable Relationships in Altered Metabolic States

by

Tyler Matthew Blazey

Doctor of Philosophy in Biology and Biomedical Sciences

Neurosciences

Washington University in St. Louis, 2019

Professor Marcus E. Raichle, Chair

Brain metabolism is usually thought of in terms of energy production. Decades of research has shown that the brain derives the majority of its energy from the oxidative phosphorylation of glucose transported from the blood into the brain. Because of this, cerebral blood flow (CBF), the cerebral metabolic rate of glucose consumption (CMRglc), and the cerebral metabolic rate of oxygen consumption ($CMRO_2$) generally are tightly coupled. Indeed, the coupling between CBF, CMRglc, and $CMRO_2$ is robust enough such that many investigators believe them to be equivalent measures of brain activity.

Nevertheless, research over the last few decades has shown that cerebral metabolic coupling is not stoichiometrically exact. Perhaps the best example of metabolic uncoupling occurs during focal increases in brain activity. Sensory stimulation, for instance, increases CBF and CMRglc to a much greater extent than $CMRO_2$. This response results in: 1) an increase in nonoxidative glucose consumption, and 2) an increase in oxygenated blood in the brain's vasculature, the phenomenon which underlies blood oxygen dependent (BOLD) functional magnetic resonance imaging (fMRI).

Importantly, metabolic uncoupling is not restricted to periods of increased neural activity. The primary goal of this thesis is to investigate other examples of uncoupling between CBF, CMRglc, and $CMRO_2$. I performed four separate studies that all examine metabolic uncoupling from a different perspective. In the first study, I performed a meta-analysis of published papers to show that at rest, nearly 10% of the brain's glucose consumption uses nonoxidative pathways that do not end in lactate efflux. If CMRglc and $CMRO_2$ were completely coupled, then one would not expect to find any nonoxidative glucose consumption (NOglc). The second study expands upon the first by showing that there are regional differences in the amount of glucose consumed using nonoxidative pathways. In some brain regions, such as the precuneus and medial prefrontal cortex, NOglc accounts for nearly 20% of resting CMRglc. Conversely, there does not appear to by any NOglc in the cerebellum.

The aim of the remaining two studies was to determine if changes in blood glucose concentration produce similar changes in CBF, CMRglc, and $CMRO_2$. Although multiple studies have reported that hypoglycemia focally increases CBF in humans, it is not clear how it impacts regional CMRglc. Therefore, I examined both regional CBF and regional CMRglc during moderate hypoglycemia. Although hypoglycemia decreased CMRglc in every region of the brain, it only increased CBF significantly in the globus pallidus. This suggests that CBF does not increase during hypoglycemia to prevent a fall in CMRglc. Next, I examined regional changes in brain metabolism during hyperglycemia. Previous studies have established that acute hyperglycemia alters the topography of cerebral glucose metabolism. However, the impact of hyperglycemia on regional CBF and $CMRO_2$ has not yet been determined. Therefore, I examined CBF, CMRglc, and $CMRO_2$ in several brain regions during hyperglycemia. Hyperglycemia did not change CBF or $CMRO_2$ in any brain region. However, hyperglycemia did increase CMRglc

in white matter and in the brain stem by over 30%. CMRglc was not altered by hyperglycemia in any other region. Therefore, hyperglycemia appears to selectively increase NOglc in the brain stem and white matter.

Taken together, the four studies that make up this thesis show that metabolic uncoupling, in particular NOglc, is an important part of brain metabolism. These results also highlight the need for future studies that can elucidate the mechanisms behind uncoupling in both health and disease.

Chapter 1: A historical review on regional cerebral blood flow and metabolism

1.1 Chapter organization

The focus of this thesis is uncoupling between three major aspects of metabolism in the adult human brain: cerebral blood flow (CBF), the cerebral metabolic rate of glucose (CMRglc), and the cerebral metabolic rate of oxygen consumption ($CMRO_2$). The underlying theme of all the original work presented here is that uncoupling between these three measures of metabolism has important physiological consequences that need to be understood. As such, the primary goal of this introductory chapter is to review what is known about uncoupling between CBF, CMRglc, and $CMRO_2$. With this goal in mind, I have divided this introductory chapter into six sections. The first section discusses early studies of brain metabolism, with a particular emphasis on how techniques for measuring regional brain metabolism support the hypothesis that cerebral metabolism is coupled to neural activity. In the following section, I review the fairly large literature which shows that the coupling between cerebral metabolism and neural activity is not quite as tight as early studies suggested. Then, in section three, I explore the various mechanisms that have been proposed to explain metabolic uncoupling during neural responses to imposed tasks. After section three, the remaining text focuses on resting brain metabolism. In section four, I review the evidence that a significant proportion of the brain's resting CMRglc is not consumed via oxidative pathways. Next, I argue, in section five, that metabolic uncoupling occurs in many different brain diseases and altered physiological states. Finally, I preview chapters 2-5 in section six.

1.2 Early studies of brain metabolism

The idea that brain activity is coupled to cerebral blood flow and metabolism is often attributed to the work of Roy and Sherrington in 1890[1]. Since then, establishing how metabolism supports brain activity has been the focus of an extensive body of literature. One of the important early discoveries, made by several investigators in the early 20th century, was that oxidative consumption of blood-borne glucose is the brain's primary fuel source under normal conditions. These studies used cerebral arterio-venous differences of CO_2 and O_2 to show that the respiratory quotient (the ratio of CO_2 produced to O_2 consumed) was nearly 1.0, which would only occur if nearly all of cerebral oxygen consumption was used for the oxidation of glucose[2-4]. The implication of these studies is that brain activity is maintained using ATP generated solely through the oxidative phosphorylation of glucose. Subsequent studies provided support for this hypothesis by showing that reductions in the availability of glucose have profound effects on brain function. Insulin-induced hypoglycemia, for example, decreases cerebral glucose and oxygen consumption and can result in coma[5-7]. The brain is also extremely sensitive to oxygen availability, with electrical activity in the brain effectively ceasing after several seconds without oxygen[8].

Early evidenced seemed to indicate that brain activity was supported by metabolism. However, if the Roy-Sherrington hypothesis was to be proven correct, a correlation would have to be shown between brain activity, cerebral blood flow, and metabolism. Perhaps the first researcher to address this question was Angelo Masso, who as early as 1879 reported that mental activity increases fluctuations in cerebral blood volume[9,10]. However, the first group to specifically measure blood flow and metabolism in humans during a cognitive task was Louis Sokoloff and colleagues in 1955[11]. Using the Kety-Schmidt method[12], an early technique that

used cerebral arteriovenous differences to obtain metabolic rates, Sokoloff et al. measured global CBF and $CMRO_2$ in young men while they performed a mental arithmetic task. While substantial shifts in EEG patterns were reported, a finding consistent with an alteration in neural activity, neither CBF nor $CMRO_2$ increased during the mental arithmetic task. To explain their seemingly contradictory results, Sokoloff et al. proposed that, although global CBF and $CMRO_2$ may not change during periods of task-driven increased brain activity, changes may occur in specific brain regions. However, establishing that regional CBF is elevated by neural activity would require the development of techniques that could quantify brain metabolism at the regional level in healthy individuals.

Fortunately, methods for assessing regional brain metabolism were developed quickly. In 1955, the same year as the Sokoloff et al. report, Seymour Kety and colleagues introduced a method that allowed for the regional quantification of CBF in animal models[13]. This technique used a relatively simple model of inert gas exchange to relate the cerebral uptake of a radioactive tracer, trifluorolodomethane (CF_3I^{131}), to local CBF. Louis Sokoloff and others quickly applied this technique to the question of brain activation in the cat[14]. They found that visual stimulation increased CBF in several brain regions, including the visual cortex, lateral geniculate nucleus, and superior colliculus. Unfortunately, the CF_3I^{131} technique could not be applied to living humans, as the quantification of tracer uptake required tissue samples from each brain region. An early attempt at solving this problem was developed by Ingvar and Lassen[15]. Instead of tissue samples, their technique measured the concentration of [^{85}Kr] using scintillation detectors placed directly on the scalp. Although this technique was severely limited in spatial resolution, as tracer concentration could only be measured near the detector, it did allow for the measurement of CBF in humans[16,17]. Using this technique, Ingvar and Risberg found that a backwards digit-span task

increased average gray matter CBF, with a particular focus in brain regions superior to the lateral sulcus[18]. This finding, along with the animal work discussed above, provided support for the Roy-Sherrington hypothesis that increases in neural activity are accompanied by increases in cerebral blood flow. Other techniques, however, were necessary to determine if cerebral glucose and oxygen consumption were also increased by task engagement.

The [^{14}C]-2-deoxyglucose ([^{14}C]-DG) tracer method was the first robust strategy for measuring the CMRglc within specific brain regions. Published by Sokoloff et al. in 1977, the technique relied on the fact that like glucose, deoxyglucose is transported into brain cells and phosphorylated by hexokinase[19]. However, unlike glucose, deoxyglucose is effectively trapped within cells after it is converted to 2-deoxyglucose-6-phosphate by hexokinase. It cannot move further down the glycolytic pathway because the lack of a hydroxyl group on the second carbon atom of deoxyglucose-6-phosphate prevents it from being converted to fructose-6-phosophate by phosphoglucose isomerase[20]. Furthermore, the relatively low activity of glucose-6-phosphtate in the brain[21] limits the amount of deoxyglucose-6-phosphate being converted back to deoxyglucose. As a result of the trapping of 2-deoxyglucose-6-phosphate within brain cells, the amount of [^{14}C]-DG taken up by a tissue is directly proportional to CMRglc. Moreover, no corrections need to be made for loss of tracer due to the efflux of metabolites.

Several studies relating CMRglc to functional activity were quickly published using the [^{14}C]-DG tracer. Sharp et al. reported that CMRglc was increased in the olfactory bulb of rats after exposure to amyl acetate[22]. In a pair of influential studies, Kennedy et al. found that: 1) Electrical stimulation of the sciatic nerve in the rat increased CMRglc in the ipsilateral lateral dorsal horn of the spinal cord, 2) Inducing a seizure in the motor cortex of the monkey with potassium benzyl penicillin increased CMRglc in the motor cortex, putamen, globus pallidus,

caudate, and thalamus, 3) Unilateral visual deprivation in the rat reduces CMRglc in the superior colliculus, lateral geniculate, and visual cortex, and 4) Unilateral visual deprivation in the monkey decreases CMRglc in alternating 0.3 – 0.4 mm stripes in visual cortex, revealing the presence of ocular dominance columns[23,24]. Finally, the increase in CMRglc within the rat superior cervical ganglion following electrical stimulation of its afferent fibers is proportional to the frequency of stimulation[25]. From these and other reports in the literature (for a review see[26]), it became clear that, at least in animal models, cerebral glucose consumption is coupled to brain activity.

Like the CF_3I^{131} technique for measuring CBF, the original [^{14}C]-DG method was unsuited for human studies because tissue samples were required to quantify tracer uptake. However, the development of positron-emission topography (PET) in the 1970s by Michel Ter-Pogossian and colleagues[27] provided a way to track radioisotopes in the brains of within living, healthy humans. PET imaging took advantage of the fact that radioisotopes, such as ^{15}O, ^{11}C, ^{18}F, that emit positrons as they undergo radioactive decay. After traveling a few millimeters, an emitted positron undergoes an annihilation event with an electron, producing two photons. Because the two photons have equal energy (511 keV) and travel in approximately opposite directions, the location in space of the original positron can be determined if the two photons are detected simultaneously by a pair of scintillation counters (i.e., a coincidence event). If one employs a series of scintillation detectors, a 3D image representing the tissue concentration of the radioactive tracer can be reconstructed using mathematical algorithms. For more information on the development of PET, see the review by Raichle and the references therein[28].

The first study using PET imaging to measure glucose metabolism in the brain was published in 1978 by Raichle et al. [29], who used [^{11}C]-glucose to measure CMRglc in rhesus

monkeys. However, the measurement of CMRglc with [^{11}C]-glucose can be complex as [^{11}C]-glucose is metabolized by cells throughout the body, resulting in radiometabolites that must be accounted for. The following year Reivich et al. used [^{18}F]-2-deoxy-2-fluoro-D-glucose ([^{18}F]-FDG) to measure regional CMRglc in humans[30]. Like [^{14}C]-DG, [^{18}F]-FDG is also effectively trapped within cells after it is phosphorylated by hexokinase[31], greatly simplifying the quantification of CMRglc. Within a few years of the report by Reivich et al., several studies used [^{18}F]-FDG to assess the relationship between functional activity and regional CMRglc in humans (for a review of early findings see Phelps et al.[32]). In 1981, Phelps, Kuhl, and Mazziotta showed that visual simulation increased CMRglc in the primary and associative visual cortex[33]. The magnitude of the increase in CMRglc was found to be proportional to the complexity of the visual stimulus; stimulation with a constant white light increased CMRglc by approximately 10%, whereas a complex visual scene resulted in increases of 40 to 60%. Unstructured illumination is similarly a weak driver of neural responses in primate visual cortex[34].

A little over a month later, Greenberg et al. used [^{18}F]-FDG to study the effect of visual, tactile, and auditory stimulation on local CMRglc[35]. They found that CMRglc was significantly increased from resting controls in the visual cortex during the visual task and in the primary auditory cortex during auditory task. Tactile simulation also increased CMRglc in the postcentral gyrus, although the increase was not statistically significant. Taken together, the results of these early [^{18}F]-FDG PET studies made it clear that like CBF, CMRglc increases in specific brain regions during periods of heightened brain activity.

1.3 Metabolic uncoupling during neural activity

By the early 1980s, strong evidence had been presented that both CBF and CMRglc increase in specific brain regions as a result of functional activity. The remaining piece of the puzzle was to determine how activity affects the cerebral metabolic rate of oxygen consumption ($CMRO_2$). Early methods for measuring regional $CMRO_2$ in humans were presented as early as 1970[36]. Similar to the [^{85}Kr] technique for quantifying regional CBF, Ter-Pogossian et al. measured regional $CMRO_2$ using five external scintillation detectors following the injection of [^{15}O]-O_2. Using this technique, Ter-Pogossian et al. were able to quantify $CMRO_2$ in very large brain regions (i.e., frontal, parietal, and occipital lobe). The resolution was greatly improved, however, with the adaptation of the [^{15}O]-O_2 PET imaging by Frackowiak et al. in 1980[37]. A few years later, Fox and Raichle used [^{15}O]-O_2 PET to determine if $CMRO_2$ was focally increased by vibratory stimulation of a single hand[38]. Although they found that vibratory stimuli slightly increased $CMRO_2$ in the sensorimotor cortex (~ 5%), the increase was not statistically significant. Conversely, they found that CBF, measured with [^{15}O]-H_2O PET, increased by 29% percent in the sensorimotor cortex. As a result, the oxygen extraction fraction (OEF), or the fraction of arterial oxygen that is extracted by the brain, actually decreased during the stimulation trials. Although unexpected, these results provided some of the first evidence that cerebral blood flow and metabolism are not entirely coupled to neural activity in the healthy human brain.

Two years later in 1988 Fox and Raichle published a follow-up study that was even more influential than their previous work[39]. In this study Fox and Raichle showed that although visual stimulation increases CBF and CMRglc by nearly 50%, it only increases $CMRO_2$ by a small nonsignificant amount (~5%). This result has two primary implications. First it shows that metabolic uncoupling between CBF and $CMRO_2$ during task-evoked activity is not limited to the

sensorimotor cortex. Second, and more importantly, because CMRglc increases to a greater extent than $CMRO_2$, it shows that a significant portion of the glucose that is consumed during task performance is metabolized via non-oxidative pathways. In their 1998 paper, Fox and Raichle suggested that the excess CMRglc is converted to lactate via glycolysis[39]. Since then, many investigators have referred to non-oxidative increases in CMRglc during task performance as an increase in "aerobic glycolysis". The term was originally used to refer to Otto Warburg's discovery that cancers cells produce excess lactate via glycolysis despite sufficient oxygen to completely metabolize glucose via oxidative phosphorylation[40]. It is important to note, however, that in this context, the term aerobic glycolysis does not necessarily mean that the ultimate fate of all of non-oxidative glucose consumption (NOglc) is lactate. There are many metabolic pathways in the brain that do not require complete oxidation of glucose to CO_2 and H_2O, some of which bypass lactate production entirely (**Error! Reference source not found.**)

Fox and Raichle's 1988 paper was immediately controversial[41]. The prevailing view at the time accepted the Roy-Sherrington hypothesis, which postulated that increases in neural activity necessitated greater energy production than what would be possible if a portion of glucose were to be metabolized anaerobically. This hypothesis was supported by the large body of literature reviewed in the first several paragraphs of this chapter. The work of Fox and Raichle showed that CBF, CMRglc, and $CMRO_2$ were not completely coupled during functional activation and that the increase in energy production during visual stimulation performance was a small fraction of the brain's resting energy needs. Specifically, they estimated that, due to the high rate of NOglc, the maximum increase in the rate of ATP production during visual stimulation was 8% of baseline[39]. Raichle and Fox's work was supported by earlier evidence for uncoupling during neural. In 1975, Cooper and colleagues reported that visual stimulation, motor

activity, and reading produce focal elevations in oxygen concentration[42], suggesting that increases in CBF during activation are not matched by increases in $CMRO_2$.

Despite the initial skepticism, subsequent research has largely confirmed the findings of Fox and Raichle that task-evoked activity results in greater increases in CBF and CMRglc than $CMRO_2$. Both Ginsberg et al. and Kuwabara et al. reported that CBF and CMRglc are generally well-coupled during somatosensory activation[43,44]. Blomqvist et al. combined [^{18}-F]-FDG PET with [1-^{11}C]-glucose PET to show that NOglc is increased in the motor cortex during voluntary motor activity[45]. Several studies using magnetic resonance spectroscopy (MRS) reported focal increases in brain lactate concentration in humans during visual[46-56], motor[57-59], and other cognitive[60] tasks. Although some investigators have reported no significant changes in regional $CMRO_2$ during task performance[44,61-63], the majority of studies have found modest (~10-20%) increases in $CMRO_2$ during task performance[51,64-71]. Consistent with moderate task-induced increases in $CMRO_2$, Buxton performed a meta-analysis of studies which measured ΔCBF (%) and $\Delta CMRO_2$ (%) during activation, and found that in most studies ΔCBF was 2-4 times greater than $\Delta CMRO_2$[72].

Perhaps the best evidence corroborating the Fox and Raichle result came with the discovery of the bold oxygen level dependent (BOLD) effect and functional magnetic resonance imaging (fMRI)[73,74]. BOLD contrast relies on the fact that deoxyhemoglobin, which is paramagnetic, attenuates the MRI signal because it creates small local distortions in the main MRI magnetic field[75]. During periods of increased neural activity, CBF increases more than $CMRO_2$ causing a relative increase in the concentration of oxyhemoglobin over deoxyhemoglobin and producing a measurable increase in the MRI signal. Therefore, the

thousands of papers that employ BOLD imaging each year to measure brain function[76] depend on uncoupling between CBF and $CMRO_2$.

1.4 Proposed mechanisms underlying uncoupling

Metabolic uncoupling during functional activity, particularly that resulting in an increase in NOglc, is perplexing from an energetic perspective. Complete oxidative phosphorylation of glucose yields approximately 30 molecules of ATP, whereas glycolysis creates only 2. Why would the brain utilize an energetically less efficient pathway during periods of increased activity? First, it is important to recall that only a small increase in oxidative phosphorylation is necessary because the increase in ATP during task performance is small fraction of the baseline production rate[39]. This was confirmed by Lin et al., who used magnetic resonance spectroscopy (MRS) to show that visual stimulation increased ATP production by only about 15%[51] (see Zhu et al. for a higher estimate[77]). Furthermore, Lin et al. found that the moderate increase in ATP production could be accounted for by a modest increase in $CMRO_2$ from baseline values (~15%). This is consistent with early animal model studies that reported that task-induced increases in energy production could be almost entirely accounted for by oxidative consumption of glucose[78,79]. Similarly, a meta-analysis of human studies estimated that nearly 90% of the task-induced increase in ATP production is met by oxidative phosphorylation[80]. Thus it appears that although it takes up more glucose that is necessary for oxidative phosphorylation, the brain still relies on oxidative phosphorylation to meet its energy needs during periods of increases activity.

Why then does the brain consume an excessive amount of glucose? One explanation, suggested by Raichle and Mintun, is that glycolysis is used to quickly generate the ATP that is not created by oxidative phosphorylation[81]. This hypothesis is supported by the fact that

glycolysis can operate at a much faster rate than oxidative phosphorylation, at least in active skeletal muscle[82,83]. Another hypothesis that predicts that neural activity should increase glycolytic ATP production is the astrocyte-neuron lactate shuttle hypothesis (ANLS)[84]. Pellerin and Magistretti developed the ANLS to explain their finding that glutamate stimulated glycolysis and subsequently lactate release from cultured astrocytes[85]. The first step in the ANLS model is the astrocytic uptake of glutamate from the synaptic clef during neural activity. The uptake of glutamate by astrocytes is facilitated thorough the GLT-1 and GLAST transporters, which couple glutamate influx with the uptake of 3 molecules of Na+[86]. Therefore, astrocytes must remove both excess intracellular glutamate and Na+ in order to retain the ability to remove glutamate from the synapse. To remove excess glutamate, astrocytes convert it glutamine using glutamine synthetase, a reaction that costs 1 ATP. Glutamine is then transferred back to neurons where it can be synthesized back into glutamate. At the same time, excess Na+ is removed from astrocytes using the Na+/K+ ATPase. The Na+/K+ ATPase requires one molecule of ATP to remove 3 Na+ ions. According to the ANLS, the two molecules of ATP that are needed to remove glutamate and Na+ are met by the two ATP generated by glycolysis. Finally, the lactate that is produced as the end point of glycolysis is shuttled to neurons where it undergoes oxidative phosphorylation.

A large body of experimental evidence supports the ANLS mechanism (for a comprehensive review, see Magistretti and Allaman[87]). Several studies have shown that the structure and enzymatic organization of astrocytes and neurons is set up to promote a transfer of lactate between the two cell types. The endfeet of astrocytes surround capillaries[88] and express glucose transporters[89], making them well positioned to take up glucose from the blood. Astrocytes also are in direct contact with synaptic terminals[90], which have been shown to be the

site of the majority of glucose uptake during electrical stimulation[91,92]. Lactate dehydrogenase (LDH), the enzyme that converts lactate to pyruvate, exists in five distinct isozymes[93]. Astrocytes contain a high concentration of LDH5[94,95], the form of LDH typically found in glycolytic tissues such as muscle[96]. Conversely, neurons primarily express LDH1[94], which is usually found in oxidative tissues such as the heart[96]. Similarly, neurons, but not astrocytes, contain high quantities of pyruvate dehydrogenase[95], the enzyme necessary to convert pyruvate to acetyl-CoA, the first molecule in the TCA cycle. Finally, astrocytes have a significantly higher NAD+/NADH ratio as compared to neurons, which is consistent with greater lactate production in astrocytes[97].

There is also a good deal of functional evidence supporting the ANLS. Studies employing whisker stimulation in rodents have shown that increases in barrel cortex CMRglc: 1) occur primarily in astrocytes[98], and 2) are strongly attenuated in mice with GLT-1 and GLAST knockout mutations[99]. Studies in culture have also shown that neurons prefer to oxidize external cellular lactate over glucose[100,101]. Consistent with this fact, elevated blood lactate decreases CMRglc in humans[102,103]. Finally, studies using MRS in rats have reported a nearly 1:1 relationship between cerebral glucose oxidation and glutamate cycling[104,105]. This is exactly what one would expect if astrocytes use glycolysis to generate 2 ATP to power glutamate turnover and then shuttle lactate over to neurons for complete oxidation[80].

Despite this evidence, the ANLS remains controversial, having been criticized on both experimental[106,107] and theoretical grounds[108] (for an extremely detailed critical discussion see the review by Dienel[109]). For example, Lundgaard et al. used two-photon microscopy with a fluorescence 2-deoxyglucose analogue to show that glucose consumption is higher in neurons than astrocytes at rest and during neural stimulation[106]. More generally, one of the most

pervasive critiques of the ANLS is that most of the evidence in its favor comes mostly from *in vitro* studies; in particular no study has shown that glucose-derived lactate is transported from astrocytes to neurons *in vivo*. However, recent results have begun to address this criticism. Zimmer et al. reported that simulation of glutamate uptake increases CMRglc in rats[110]. Furthermore, Mächler et al. showed that in transgenic mice: 1) Astrocytes have higher lactate concentration than neurons at baseline, 2) Intravenous lactate injections increase lactate more in neurons than astrocytes, and 3) Intravenous pyruvate injections result in greater lactate efflux from astrocytes than neurons[111]. Taken together, these findings suggest that glycolysis in astrocytes creates a lactate gradient between astrocytes and neurons, which supports lactate flow down this gradient. It is likely, though, that the ANLS will remain a source of controversy until shuttling of glucose-derived lactate from astrocytes is observed directly *in vivo.*

It is important to note, however, that in its original formation the ANLS does not explain the rise in NOglc during increased neural activity. Instead, the ANLS predicts a rise in non-oxidative glucose use in astrocytes, followed by an increase in oxidative phosphorylation in neurons[85]. In this model, there is in no total increase in non-oxidative glucose use, which contradicts the NOglc reported by Fox and Raichle[39]. To explain this discrepancy, several alternative explanations have been proposed. Pellerin et al. hypothesized that increased neural activity produces different metabolic alterations at different time scales[84]. According to their model, immediately following depolarization, neurons undergo oxidative metabolism to provide the Na+/K+ ATPase with the ATP necessary to remove excess Na+. This is consistent with the work of Kasischke et al., who reported that in the first 10 seconds after electrical stimulation, NADH levels are decreased in neurons[112]. Next the inhibition of neuronal glucose uptake by glutamate release[113], causes an increase in lactate consumption in neurons. Experiments in both

rats[114] and humans[115] which show decreased cerebral lactate concentration immediately following activation support this hypothesis. The continued release of glutamate from neurons activates the Na+/K+ in astrocytes[84], which results in enhanced astrocytic glucose uptake and lactate production as described earlier[85]. The excess lactate is then is transported to neurons, where it can be used to oxidatively generate the ATP necessary for continue neural activity. Multiple studies in humans[46-57,59,60,116] and animals[114,117-123] have shown that neural activity stimulates lactate production. Furthermore, Kasischke et al. showed that NADH activity starts to increase in astrocytes approximately 10 seconds after activation[112].

During periods of sustained activity, however, the model proposed by Pellerin et al. predicts that astrocytes use glycogen to supplement the glucose supplied from the blood. According to this model, it is glycogen replenishment that is responsible for the increase in NOglc during neural activity. A similar hypothesis was also proposed by Shulman and colleagues[124], who pointed out that glycogen synthesis reduces the ATP generated from glycolysis from 2 ATP per mole of glucose to 1 ATP per mole. Therefore, to generate the same amount of ATP from glycolysis, twice the amount of glucose would need to be consumed, resulting in twice the amount of lactate production. Although shunting glucose down the glycogen pathway is energetically less efficient and results in substantial NOglc, Shulman et al. hypothesize that it is used during neural activity because glycogen can be quickly broken down during periods of greater energy requirements.

Brain tissue contains approximately 5-10 $\mu Mol \cdot g^{-1}$ [119,120,122,125] of glycogen, although the exact value is fairly sensitive to measurement technique[119,125]. At euglycemia, the concentration of glycogen in the brain is considerably higher than that of glucose, which typically exists in concentrations around 1.0 $\mu Mol \cdot g^{-1}$[126-129]. Interestingly, glycogen in the brain is largely confined

to astrocytes[130]. Consistent with the models proposed by Pellerin et al. and Shulman et al., neural activity has been shown to deplete glycogen stores in animal models[118-120,122,131]. Furthermore, prolonged periods of wakefulness have been shown to reduce cerebral glycogen content in rodents[132] (but see[133]), and to increase glycogen turnover in astrocytic processes near synapses[134], further implicating glycogen use during neural activity. However, glycogen turnover has been shown to be quite slow in the resting brain in both humans[135] and rats[136]. Moreover, a study in humans reported that glycogen concentration in the occipital lobe was not changed by visual stimulation[135]. Although it is has been argued that the experimental methods and kinetic modeling used by this study were not sufficient to detect glycogen breakdown[137], there are, to our knowledge, no other studies examining glycogen change during task-evoked activity in humans. Studies in rats have also reported that there is little evidence of non-oxidative glucose use 15 minutes after activation[118], even though glycogen levels are still below baseline[118,119]. Therefore, more studies are needed to clarify how much glycogen turnover contributes to non-oxidative glucose metabolism driven by neural activity. In particular, methods are need to properly assess glycogen flux *in vivo*, as changes in glycogen concentration might not accurately reflect changes in the flux of glucose through the glycogen pool[122].

An alternative hypothesis is that astrocytes produce more lactate during increased neural activity than can be oxidized by neurons. This would result in a temporary increase in NOglc. Then, after activity has returned to basal levels, the excess lactate could either be removed from the brain or oxidized. Studies employing MRS in humans have reported that lactate levels peak after a few minutes of stimulation and then decline thereafter, either towards a new slightly elevated baseline[46,47,60], or to pre-stimulation levels[48,52]. Studies in both humans[116] and rats[138] have shown that increased brain activity stimulates lactate efflux from the brain. Other evidence

suggests that lactate oxidation is increased after functional activity. Specifically, PET studies in humans have reported that $CMRO_2$ increases during prolonged stimulation[71,139], whereas CMRglc decreases[140]. Similarly, Madsen et al. reported in rats that as brain lactate concentration returns to baseline following sensory stimulation, the brain uses more oxygen than can be accounted for by glucose consumption[118].

Not all the evidence is consistent with the idea that NOglc is elevated during task because of a temporary increase in lactate consumption. Several human MRS studies have reported that lactate concentration remains elevated during prolonged stimulation[49,50,53,54,58]. Furthermore, additional human studies have shown that NOglc persists well after task-performance[116,141]. Finally, rodent studies have argued that lactate production has a limited role in explaining NOglc. The same Madsen et al. report mentioned previously estimated that less than 54% of the NOglc that occurred during stimulation could be accounted for by lactate production[118]. Based on metabolite measurements from extracellular fluid following the infusion of [3,4-^{14}C]-glucose, Ball et al. estimated that lactate oxidation can only account for a very small fraction of activity dependent increases in NOglc[138]. Therefore, although the existing evidence suggests that excessive lactate production plays a role NOglc during neural activity, it is unlikely to be the only factor.

An alternative, albeit non-exclusive, hypothesis is that NOglc during task-evoked activity is directed towards glutamate synthesis. Specially, Hertz and Fillenz proposed that increased neural activity stimulates the production of glutamate, which is then consumed via oxidative phosphorylation once activity levels have returned to baseline[142]. In support of this hypothesis, a [6-^{14}C]-glucose labeling studying in rats reported a significant increase in the labeling of glutamate during sensory stimulation[120]. In addition, most[50,53,54,56,58,143,144], but not all[48,55], studies

have reported that sensory stimulation increases glutamate concentration in humans by a small amount (typically less than 5% averaged over a large ROI in the appropriate sensory area). Interestingly, some investigators have also found that brain aspartate concentration decreases as glutamate concentration increases[50,54,56]. This suggests that some of the increase in glutamate production may be due to the malate-aspartate shuttle[49,145]. The malate-aspartate shuttle is a critical metabolic pathway, as it generates NAD+ needed for glycolysis and transfers reducing equivalents, in the form of NADH, from the cytosol to mitochondria, where they are required for oxidative phosphorylation[109,146]. However, not all studies have reported decreases in aspartate concentration with sensory simulation[53,55,143]. Therefore, more research is needed to determine what role the malate-aspartate shuttle plays in glutamate production during neural activity. More generally, the extent to which glutamate synthesis is responsible for NOglc during task performance remains unclear. Although the evidence discussed above indicates that glutamate concentration is elevated during sensory stimulation, the increases are typically only a small percent of baseline values. Quantitative studies are clearly needed to establish how much NOglc is dedicated to glutamate production during neural activity.

One final hypothesis deserves to be discussed. Multiple authors have proposed that NOglc provides the brain with the biosynthetic precursors needed for neural development and plasticity[147,148]. Early support for this hypothesis was obtained by Madsen et al. in 1995, who found that the whole-brain average NOglc remained elevated for more than 40 minutes after participants performed the Wisconsin Card Sorting Test[116]. Interestingly, Madsen et al. later reported in rats, that cerebral NOglc was effectively eliminated only minutes after tactile simulation[118]. These discrepant results suggest that increases in NOglc following task performance may be species dependent. More recently, Shannon and colleagues expanded upon

the work of Madsen et al. using PET imaging[141]. They reported that approximately 2 to 3 hours after performing a motor learning task, NOglc was increased in Brodmann area 44, an area which is active during motor responses[149]. Taken together, these two studies suggest that NOglc plays a role in learning-induced synaptic plasticity.

Studies employing radiolabeled glucose infusions in rats have also provided evidence that glucose is used for biosynthesis during neural activity. Cruz et al. reported that, after acoustic stimulation, 10-25% of the recovered radiolabel was found in products of the pentose phosphate shunt[121,150], a pathway used for nucleic acid synthesis[151]. Similarly, Dienel et al. found that tactile stimulation increased the amount of radiolabel recovered in a large number of glucose metabolites, including the amino acids glutamate, GABA, and alanine[120]. Finally, advocates of the biosynthesis hypothesis often point out that, during human development, a period characterized by brain growth and synaptic development[152], approximately 30% of the brain's glucose is consumed via non-oxidative pathways[153] (but see[154]). Similarly, developmental studies in primates have shown that glucose consumption peaks at around the same time as rates of myelination and synaptogenesis[148].

There is, therefore, credible evidence that part of the brain's NOglc passes through biosynthetic pathways. However, despite the fact that biosynthesis plays an important role in synaptic plasticity[155], there is currently no evidence that glycolytic by-products are directly incorporated into new structural elements (e.g.., synapses) during learning. Critics of the biosynthesis hypothesis also argue that use of glucose for biosynthesis would result in uncontrolled brain growth[154]. Although this criticism ignores turnover of synaptic elements[156,157] and proteins[158,159], as well as alternative mechanisms for the efflux of glucose metabolites[138,160], it does highlight the fact that we do not yet know how carbon consumed via biosynthetic

pathways leaves the brain. Methods that can track the movement of glucose in and out of the brain's biosynthetic machinery are needed to clarify the relationship between plasticity and NOglc.

Currently, no single hypothesis entirely explains why NOglc is elevated during periods of increased neural activity. It is more likely that a combination of mechanisms, including those discussed in the previous paragraphs, is needed to account for all glucose consumption in excess of oxygen utilization. An accurate model of task-evoked NOglc will likely be complex, as it will need to account for, among other things, multiple metabolic pathways and interactions among cell types. Moreover, the effect of NOglc may not be confined to the area of activation, as glucose metabolites can spread to neighboring tissues via gap junctions in astrocytes[121]. Finally, a useful working model will need to consider non-oxidative uses of glucose that go beyond merely energy metabolism. Recent work has begun to establish the role of lactate as signaling molecule[161], with a critical role in formation of long-term memories[87]. For example, Suzuki et al. showed that blocking the transfer of lactate from astrocytes to neurons impairs long-term memory formation in rats[162]. Importantly, it does not appear that blocking lactate transport impairs energy metabolism, as direct injection of glucose does not rescue memory formation. Instead, lactate appears to induce the expression of genes such as Arc[162,163] that are related to synaptic plasticity[155]. These studies suggest that NOglc may promote biosynthesis in more ways than just providing metabolic precursors for biosynthesis. Furthermore, studies linking lactate signaling and learning reinforce the need for a model of metabolism during neural activity that incorporates more than just the energetic perspective.

1.5 Non-oxidative glucose consumption at rest

Since the work of Fox and Raichle in 1988, the majority of research on metabolic uncoupling in the brain has focused on understanding uncoupling during periods of increased neural activity. However, it is important to realize that it was recognized as early as 1942 that during periods of rest the brain consumes more glucose than would be expected given its rate of oxygen consumption[4]. Early studies reported that the whole-brain average oxygen-to-glucose index (OGI), which is the molar ratio of oxygen to glucose consumption, was around 5.5 (for review see[164]). If glucose is entirely consumed via oxidative pathways, the OGI should be 6, as 6 moles of oxygen are required to oxidize 1 mole of glucose. An OGI of 5.5 indicates that nearly 10% of the brain's glucose consumption at rest does not undergo oxidative phosphorylation. Following its discovery, the importance of non-oxidative glucose metabolism was largely underappreciated. Most investigators argued that lactate (or pyruvate) efflux accounted for nearly all of the NOglc in the brain[4,165,166]. This argument was also presented by Siesjö in his influential textbook *Brain Energy Metabolism*[167]. According to Siesjö, "… an OGI of less than 100% [6.0] could be explained in terms of production of lactate … there is no need to explain an OGI value of less than 100% [6.0] in terms of synthesis of amino acids or other compounds." To this day, many investigators still hold to this view. For example, in recent review, Dienel wrote that "Submaximal OGI in resting brain is ascribed mainly to lactate production and efflux from brain…"[109].

Despite the widely held view that non-oxidative glucose metabolism at rest merely reflects lactate efflux, and is therefore of little physiological importance, there is evidence suggesting otherwise. Based differential arterio-venous measurements of glucose, lactate, and oxygen in humans, Scheinberg et al. reported in 1965 that cerebral NOglc could not be explained by lactate efflux to venous blood[168]. They also presciently concluded that "… the portion of

utilized glucose not accounted for by oxidation may be involved in the synthesis of other substances, in particular amino acids of cerebral proteins." More recently, Vaishnavi et al., using PET measurements of CMRglc and $CMRO_2$, showed that there are regional differences in NOglc[147]. The lowest rates of NOglc were found in the cerebellum and medial temporal lobe, whereas the highest were found in the prefrontal and parietal cortices. Interestingly, the regions with elevated NOglc overlapped strongly with two resting state networks (RSNs), that is, regions of the brain whose spontaneous activity is highly correlated at rest[169]. The first RSN was the cognitive control network, a network that encompasses parts of the lateral prefrontal and parietal cortices and is thought to be involved in attention and working memory[170]. The second RSN was the default mode network (DMN), a collection of regions including the prefrontal cortex, precuneus, and lateral parietal cortex[171]. The defining feature of the DMN is that, although it is metabolically active at rest, it becomes less so during goal-directed task performance[171-173]. The DMN has traditionally been associated with self-referential processes such as mind-wandering[174,175]; however there is evidence that the DMN has more expansive role (for a review see[176]). The fact that resting NOglc is spatially correlated with regions associated with RSNs suggests that these regions may have unique metabolic needs compared to other brain regions.

More recently, Goyal et al. reported that the expression of genes related to synaptic plasticity and development is enriched in brain regions with high levels of NOglc[153] (but see[177]). This suggests that a portion of the brain's non-oxidative glucose metabolism in spent on plasticity and other biosynthetic processes (for a similar argument during task-evoked activity see ***Proposed mechanisms underlying uncoupling*** **above**). In support of this idea, Glasser et al. showed that there is a negative spatial correlation between regional NOglc and a putative measure of cortical myelination[178]. Furthermore, Segarra-Mondejar et al. reported that glucose

consumption, specifically glycolysis, is necessary for neurite growth *in vitro* and *in vivo* in mice[179]. Although intriguing, these and the studies discussed in the preceding two paragraphs do not definitively establish the function of NOglc in the resting brain. As in metabolic uncoupling during task-evoked activity, it is likely that multiple mechanisms are at play. To further establish the role of NOglc at rest, there is a need for techniques that can quantify the flux of glucose into multiple metabolic pathways, including those responsible for biosynthesis. To address these issues,[13]C MRS[180,181] and hyperpolarized [13]C MRI[182] *in vivo* and metabolic flux analysis *in vitro*[183] provide intriguing opportunities.

1.6 Brain metabolism in altered metabolic states and disease

So far, this chapter has focused almost exclusively on brain metabolism in healthy individuals. However, understanding the effect of acute metabolic states and neurological diseases on brain metabolism has been an active area of study since methods for measuring brain metabolism in humans were first developed. The same year that he published his influential article establishing the nitrous oxide technique for measuring CBF in humans[12], Kety published five papers studying the relationship between whole-brain CBF and $CMRO_2$ and schizophrenia[184], intracranial pressure[185], diabetic coma[6], hypertension[186], and hypercapnia[187]. One of the interesting findings that emerged from these studies is that CBF and $CMRO_2$ often are uncoupled during metabolic challenges. For example, Kety reported that hypercapnia dramatically increases CBF, without a proportional increase in $CMRO_2$[187]. Conversely, Kety found that, although patients experiencing diabetic coma had a greatly reduced $CMRO_2$, their CBF values were largely in the normal range[6].

Since these initial studies by Kety and colleagues, multiple investigators have reported uncoupling between CBF, $CMRO_2$, and CMRglc during acute metabolic challenges. Hypoglycemia was intensively studied in the 1940 and 1950s since insulin shock was, at the time, considered a viable treatment for schizophrenia[188]. Consistent with Kety's study in patients suffering from diabetic coma, profound hypoglycemia decreased whole-brain CMRglc greatly, whereas CBF and $CMRO_2$ changed modestly[7,184,189,190]. Another notable example is hypoxia. Studies in both humans[166,187,191] and rats[192] have shown that hypoxia dramatically increases global CBF without altering $CMRO_2$. Furthermore, CMRglc increases modestly during hypoxia[166]. The increase in CMRglc without a proportional increase in $CMRO_2$, results in increased NOglc during hypoxia[166,193], which appears to be due to lactate production[166,194]. This is consistent with the finding that acute hypocapnia results an in a temporary increase in NOglc[195].

The variety of the examples discussed in the previous two paragraphs should make it clear that alterations in systematic metabolism often disrupts metabolic coupling in the brain. In some cases it is fairly simple to come up with a reasonable hypothesis to explain the divergent changes metabolism. During hypoxia, for example, it is possible that CBF and lactate production increase to prevent energy failure[167]. In other cases, coming up with a satisfactory explanation is more difficult. Despite a great deal work, there is still no complete account of what fuel sources the brain uses to maintain $CMRO_2$ during hypoglycemia (for a review see[196]).

In addition to its role in acute disorders, metabolic uncoupling has also been implicated in chronic neurological disease. For example, temporal lobe epilepsy has been shown to decrease CMRglc in the temporal lobe to a greater extent than it does CBF[197-199]. Interestingly, metabolic uncoupling also occurs during traumatic brain injury, which increases whole-brain NOglc[200].

Given these results, one would expect that metabolic uncoupling would be an active area of study for those interested in understanding neurological diseases, but this is not always true. A promising example of where research on metabolic uncoupling could contribute to the study of neurological disease is in Alzheimer's disease (AD) research. AD research is a field which has grown quickly in the last few decades[201], due, in part, to the increased economic and social burden that AD is expected to have on aging populations[202].

Pathologically, AD is defined by the development of amyloid-beta plaques, followed by tangles of hyperphosphorylated tau[203]. However, another hallmark of AD is focal decreases in glucose consumption. AD patients typically show deficits in glucose consumption in the frontal, parietal, and temporal lobes, as well as in the precuneus and posterior cingulate[204]. It is generally accepted in the field that decreased glucose use in AD is a sign of synaptic dysfunction[203,204]; a conclusion that is based on studies that have shown that most of the glucose consumed during neural activity is taken up by synapses[91,92]. There is, however, a lack of empirical evidence that decreased glucose consumption in AD patients is entirely due to energy failure at synapses. Although glucose metabolism measured using FDG PET is one of the most common biomarkers reported in AD studies[205], cerebral oxygen metabolism is rarely assessed. Early studies showed that in patients with severe dementia, global $CMRO_2$ declines by about 20%[206], with the largest declines occurring in the parietal lobe[207]. However, as these studies did not simultaneous measure glucose consumption, it is not clear if CMRglc declines in proportional to oxygen consumption. Indeed, regional decreases in CMRglc in excess of 30-40% have been reported in individuals with AD[208,209]. Therefore, the claim that AD patients have lower cerebral glucose consumption entirely because of synaptic dysfunction relies on the assumption that there is a tight coupling between synaptic activity and glucose consumption in individuals with AD.

However, as we have seen, metabolic coupling becomes much less pronounced in many neurological diseases. Indeed, there is evidence for uncoupling in AD patients (for a review see[210]). CMRglc has been shown to decrease to a greater extent than $CMRO_2$ in individuals with both early-onset[211] and late onset AD[212-214]. This indicates that NOglc decreases during AD, in addition to the decline of NOglc that has been noted during healthy aging[215]. Intriguingly, Hoyer et al. also showed that in later stages of AD, $CMRO_2$ drops sharply, which eliminates much of the difference between changes in CMRglc and $CMRO_2$[212]. This suggests that the relationship between AD and brain metabolism may evolve as the disease progresses. Consistent with this hypothesis, it was recently reported that there is a negative correlation between tau deposition and NOglc in cognitively normal individuals[216]. However, this correlation was only found in individuals that were at risk for developing AD due to high levels of amyloid plaques. It is therefore possible that amyloid plaques mediate the relationship between NOglc and AD. In agreement with this proposal, Vlassenko et al. reported that the regions of the brain with high levels of amyloid plaques in individuals with AD are the same regions that have high levels of NOglc in healthy young adults[217]. A few years later, Bero et al. replicated this finding by showing a positive regional correlation between lactate production and amyloid plaque loads in a transgenic mouse model of AD[123]. Together, these results suggest that high rates of NOglc may put a brain region at risk for developing amyloid plaques later in life. Determining if deficits in NOglc lead to the development of AD pathology, or if they are merely an epiphenomenon, will require more direct research.

1.7 Overview of dissertation

The previous sections in this introductory chapter have argued that metabolic uncoupling, in particular that resulting in NOglc, has important consequences that extend beyond energy

metabolism. This is in contrast to the conventional view, which posits that metabolic uncoupling is a minor phenomenon of relatively little physiological importance. Therefore, the goal of the remaining chapters in this thesis is to further explore discrepancies between CBF, CMRglc, and $CMRO_2$.

In Chapter 2, I will examine whole-brain NOglc at rest in healthy individuals. As previously mentioned, an early review by Kety concluded that the whole-brain OGI was approximately 5.5[164], which shows that around 9% of CMRglc is metabolized without oxygen consumption. Conversely, a recent small meta-analysis (n=8) reported that the whole-brain OGI may be as low as 5.1[218]. To resolve the quantitative discrepancy, I performed a large meta-analysis of studies reporting whole-brain OGI (n=40). Also because it is widely believed that excess glucose in the brain is accounted for by lactate production[167], we analyzed studies (n=39) that reported the whole-brain oxygen-to-carbohydrate index (OCI), a measure that includes lactate as well as glucose consumption. If the OGI is less than 6.0 due to lactate production, then the average whole-brain OCI from our meta-analysis should not be statistically different from 6.0. Alternatively, an OCI significantly less than 6.0 suggests that some of the brain's NOglc proceeds down metabolic pathways that do not end in lactate production (e.g., biosynthetic pathways). A slightly modified version of Chapter 2 has been published elsewhere[219].

The topic of Chapter 3 is regional differences in NOglc in the brain at rest. A previous study from our laboratory reported that the fraction of glucose consumed via non-oxidative pathways varies across the human brain[147]. The precuneus, frontal lobe, and parietal lobe have high rates of NOglc, whereas the cerebellum and medial temporal lobe have lower rates. This report was recently challenged by Hyder et al., who argued that these regional differences are methodical artifacts[220]. In the original report, Vaishnavi et al. calculated cerebral glucose and

oxygen consumption using local-to-global tracer uptake ratios[147], instead of quantifying absolute CMRglc and $CMRO_2$ directly in each region. Although the lack of absolute units can result in misleading inferences[221], uptake ratios are a commonly used technique because they remove global variance and do not require invasive arterial sampling. In their paper, Hyder et al. attempted to show that there are no regional differences in NOglc if a proper kinetic model is used to compute absolute CMRglc and $CMRO_2$[220]. However, a careful reading of the Hyder et al. paper suggested that the authors actually reported regional differences in their data that were simply masked by a combination of misleading data visualization and improper statistical techniques. I therefore reanalyzed the Hyder et al. data using simple, direct methods to confirm this impression. The results of this analysis were also reported in a previous article[222].

Although the focus of Chapters 2 and 3 are on brain metabolism in healthy individuals under normal physiological conditions, the goal of Chapter 4 is to examine regional cerebral blood flow and glucose metabolism in participants experiencing moderate hypoglycemia. Many studies have examined how regional CBF changes in response to hypoglycemia (for a review see[223]). These studies have found that, in humans, hypoglycemia focally increases CBF in the thalamus, globus pallidus, and medial prefrontal cortex[224-226]. In contrast, most of the studies measuring CMRglc during hypoglycemia have reported only global values. Although global CMRglc is substantially lower in subjects experiencing profound hypoglycemia[184,189], it does not begin to decline until moderate hypoglycemia (~50 mg/dL) occurs[227,228]. The sole study examining regional CMRglc during moderate hypoglycemia humans reported changes in every region examined[229,230]. Thus, hypoglycemia seems to affect CBF, which changes focally, differently than CMRglc, which changes uniformly across the brain. To test this hypothesis, I

used [^{15}O]-H_2O and 1-[^{11}C]-D-glucose PET to measure regional CBF and CMRglc in 18 patients during stepped hypoglycemia.

Lastly, Chapter 5 will investigate regional changes in blood flow, glucose consumption, and oxygen metabolism in hyperglycemic individuals. It is well-known that during euglycemia, more glucose is present in the blood than is taken up by cells in the brain [231]. Therefore, one would predict that increases in blood glucose concentration would not change CMRglc. However, there is evidence that this may not be true. Although statistically significant in only one report[232], multiple studies have reported that hyperglycemia increases global CMRglc slightly[232-235]. More interestingly, two separate studies have reported that white matter is particularly affected by hyperglycemia, with CMRglc increasing by over 40% in both studies[232,234]. Conversely, the same two studies found that the increases in CMRglc within gray matter where either much smaller (~20%)[232], or not significant[234].There currently is no explanation as to why hyperglycemia increases CMRglc specifically in white matter. As metabolic uncoupling occurs in so many neurological conditions (see ***Brain metabolism and disease*** above), it is possible that hyperglycemia selectively increases NOglc. I used [^{18}F]-FDG and [^{15}O]-O_2 PET imaging to determine if changes in glucose consumption during hyperglycemia are matched by changes in oxygen consumption. Finally, I used [^{15}O]-H_2O PET and arterial spin labeling MRI to test how regional blood flow if affected during hyperglycemia.

1.8 Figures

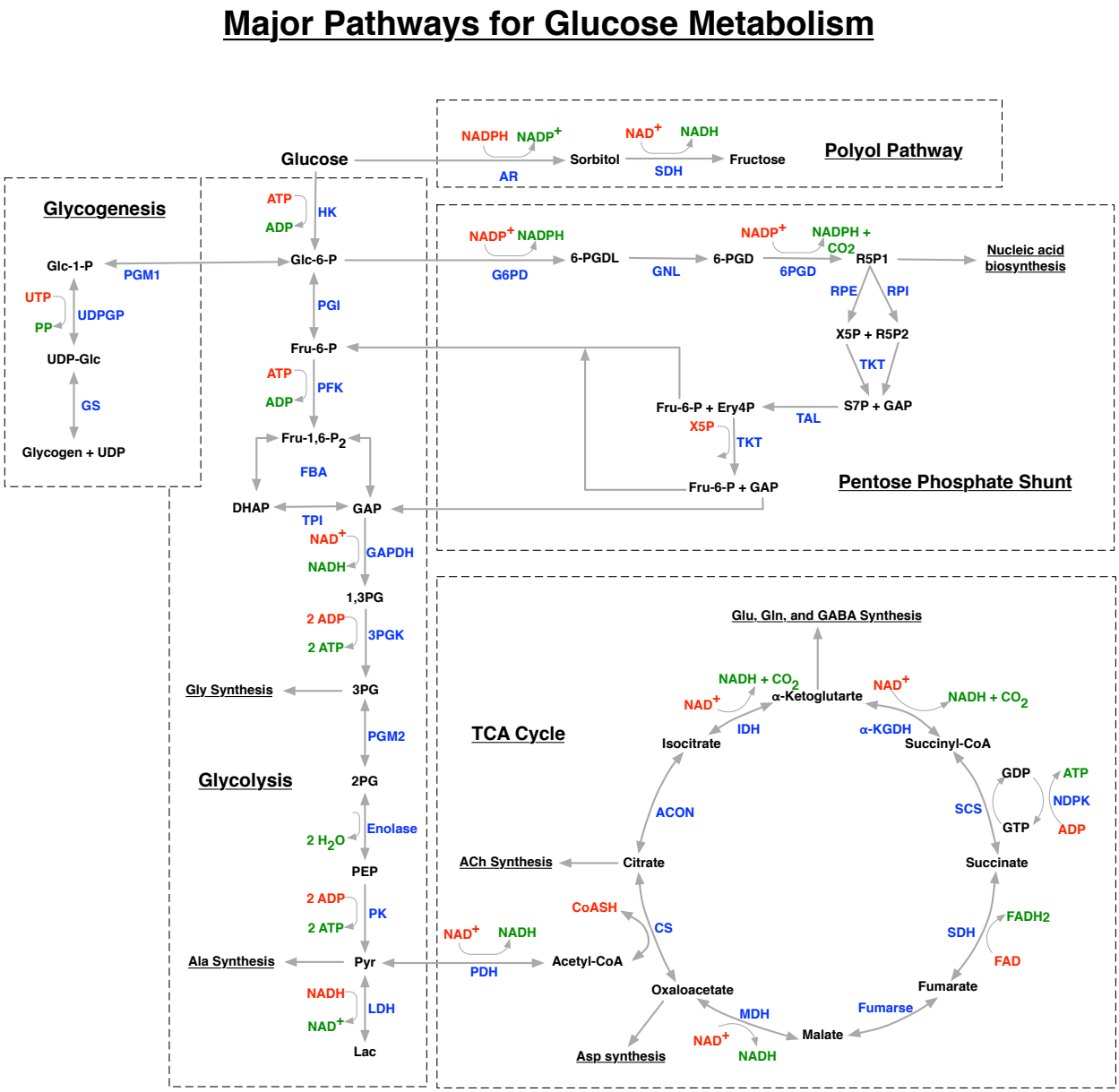

Figure 1.1: Major metabolic pathways for cerebral glucose metabolism

Gray boxes denote each separate pathway that glucose can enter once inside the brain. The majority of glucose enters the glycolytic pathway and then is reduced to CO_2 and water in the TCA cycle. However, the TCA cycle also produces many important amino acids such as glutamate. Furthermore, glucose can also be stored as glycogen, be converted into fructose by

the polyol pathway, or used to generate intermediates for nucleic acid biosynthesis via the pentose phosphate shunt. Abbreviations are as follows: 1,3-Bisphosphoglycerate (1,3PG), 2-Phosphoglycerate (2PG). 3-Phosphoglycerate (3PG), Phosphoglycerate kinase (3PGK), 6-Phosphogluconate (6-PGD), 6-Phosphogluconolactone (6-PGDL), Acetylcholine (ACh), Aconitase (ACON), Adenosine diphosphate (ADP), α-Ketoglutarate dehydrogenase (α-KGDH), Alanine (Ala), Aldose reductase (AR), Aspartate (Asp), Adenosine-triphosphate (ATP), Coenzyme A (CoASH), Citrate synthase (CS), Dihydroxyacetone phosphate (DHAP), Erythrose 4-phosphate (Ery4P), Flavin adenine dinucleotide (FAD), Dihydroflavine adenine dinucleotide ($FADH_2$), Fructose-bisphosphate aldolase (FBA), Fructose 1,6-bisphosphate (Fru-1-6-P_2), Fructose 6-phosphate (Fru-6-P), Glucose-6-phosphate dehydrogenase (G6PD), Glyceraldehyde 3-phosphate dehydrogenase (GAPDH), Glyceraldehyde 3-phosphate (GAP), Guanosine diphosphaste (GDP), Glucose-1-phosophate (Glc-1-P), Glucose-6-phosphate (Glc-6-P), Glutamine (Gln), Glutamate (Glu), Glycine (Gly), Gluconolactonase (GNL), Glycogen synthase (GS), Guanosine triphosphaste (GTP), Hexokinsae (HK), Isocitrate dehydrogenase (IDH), Lactate dehydrogenase (LDH), Malate dehydrogenase (MDH), Nicotinamide adenine dinucleotide (NAD^+, NADH), Nicotinamide adenine dinucleotide phosphate ($NADP^+$, NADPH), Nucleoside-diphosphate kinase (NDPK), Pyruvate dehydrogenase (PDH), Phosphoenolpyruvate (PEP), Phosphofructosekinase (PFK), Phosphoglucose isomerase (PGI), Phosphoglucomutase (PGM1), Phosphoglycerate mutase (PGM2), Pyruvate kinase (PK), Pyrophosphate (PP), Pyruvate (Pyr), Ribulose-5-phosophate (R5P1), Ribose-5-phosphate (R5P2), Ribulose-5-phosphate 3-Epimerase (RPE), Ribulose-5-phosphate Isomerase (RPI), Sedoheptulose 7-phosphate(S7P), Succinyl coenzyme A synthetase (SCS), Succinate dehydrogenase (SDH), Transaldolase (TAL), Transketolase (TKT), Triose-phosphate isomerase (TPI), Uridine

diphosphate (UDP), UTP-glucose-1-phosphate uridylytransferase (UDPGP), Uridine triphosphate (UTP), Xylulose-5-phosphate (X5P). Adapted from Dienel[109] and Garrett and Grisham[236].

1.9 References

1 Roy CS, Sherrington CS. On the Regulation of the Blood-supply of the Brain. *J Physiol (Lond)* 1890; **11**: 85–158.17.

2 Lennox WG, Leonhardt E. The respiratory quotient of the brain and of extremities in man. *Arch Neurol Psychiat* 1931; **26**: 719–724.

3 Wortis J, Bowman KM, Goldfarb W. Human Brain Metabolism: Normal Values and Values in Certain Clinical States. *Am J Psychiatry* 1940; **97**: 552–565.

4 Gibbs EL, Lennox WG, Nims LF, Gibbs FA. Arterial and cerebral venous blood arterial-venous differences in man. *J Biol Chem* 1942; **144**: 325–332.

5 Himwich HE, Bowman KM, Daly C, Fazekas JF, Wortis J, Goldfarb W. Cerebral blood flow and brain metabolism during insulin hypoglycemia. *Am J Physiol* 1941; **132**: 640–647.

6 Kety SS, Polis BD. The blood flow and oxygen consumption of the human brain in diabetic acidosis and coma. *J Clin Investig* 1948; **27**: 500–510.

7 Porta PD, Maiolo AT, Negri VU, Rossella E. Cerebral Blood Flow and Metabolism in Therapeutic Insulin Coma. *Metab Clin Exp* 1964; **13**: 131–140.

8 Moss J, Rockoff M. EEG monitoring during cardiac arrest and resuscitation. *JAMA* 1980; **244**: 2750–2751.

9 Zago S, Ferrucci R, Marceglia S, Priori A. The Mosso method for recording brain pulsation: the forerunner of functional neuroimaging. *Neuroimage* 2009; **48**: 652–656.

10 Mosso A. *Angelo Mosso's Circulation of Blood in the Human Brain*. Oxford University Press: New York, NY, 2014.

11 Sokoloff L, Mangold R, Wechsler RL, Kenney C, Kety SS. The effect of mental arithmetic on cerebral circulation and metabolism. *J Clin Investig* 1955; **34**: 1101–1108.

12 Kety SS, Schmidt CF. The Nitrous Oxide Method for the Quantitative Determination of Cerebral Blood Flow in Man: Theory, Procedure and Normal Values. *J Clin Investig* 1948; **27**: 476–483.

13 Landau WM, Feygang WH, Roland LP, Sokoloff L, Kety SS. The local circulation of the living brain; values in the unanesthetized and anesthetized cat. *Trans Am Neurol Assoc* 1955; 125–129.

14 Sokoloff L. Local Cerebral Circulation at Rest and During Altered Cerebral Activity Induced by Anesthesia or Visual Stimulation. In: Kety SS, Elkes J (eds). *Regional Neurochemistry*. Pergamon Press, 1961, pp 107–117.

15 Lassen NA, Ingvar DH. The blood flow of the cerebral cortex determined by radioactive krypton. *Experientia* 1961; **17**: 42–43.

16 Ingvar DH, Lassen NA. Quantitative Determination of Regional Cerebral Blood-Flow in Man. *The Lancet* 1961; **278**: 806–807.

17 Lassen NA, Hoedt-Rasmussen K, Sorensen SC, Skinhoj E, Cronquist S, Bodforss B *et al.* Regional Cerebral Blood Flow in Man Determined by Krypton. *Neurology* 1963; **13**: 719–727.

18 Ingvar DH, Risberg J. Increase of regional cerebral blood flow during mental effort in normals and in patients with focal brain disorders. *Exp Brain Res* 1967; **3**: 195–211.

19 Sokoloff L, Reivich M, Kennedy C, Rosiers Des MH, Patlak CS, Pettigrew KD *et al.* The [14C]Deoxyglucose Method for the Measurement of Local Cerebral Glucose Utilization: Theory, Procedure, and Normal Values in the Conscious and Anesthetized Albino Rat. *J Neurochem* 1977; **28**: 897–916.

20 Wick AN, Drury DR, Nakada HI, Wolfe JB. Localization of the primary metabolic block produced by 2-deoxyglucose. *J Biol Chem* 1957; **224**: 963–969.

21 Prasannan KG, Subrahmanyam K. Effect of insulin on the synthesis of glycogen in cerebral cortical slices of alloxan diabetic rats. *Endocrinology* 1968; **82**: 1–6.

22 Sharp FR, Kauer JS, Shepherd GM. Local sites of activity-related glucose metabolism in rat olfactory bulb during olfactory stimulation. *Brain Res* 1975; **98**: 596–600.

23 Kennedy C, Rosiers Des MH, Jehle JW, Reivich M, Sharpe F, Sokoloff L. Mapping of functional neural pathways by autoradiographic survey of local metabolic rate with (14C)deoxyglucose. *Science* 1975; **187**: 850–853.

24 Kennedy C, Rosiers Des MH, Sakurada O, Shinohara M, Reivich M, Jehle JW *et al.* Metabolic mapping of the primary visual system of the monkey by means of the autoradiographic [14C]deoxyglucose technique. *Proc Natl Acad Sci USA* 1976; **73**: 4230–4234.

25 Yarowsky P, Kadekaro M, Sokoloff L. Frequency-dependent activation of glucose utilization in the superior cervical ganglion by electrical stimulation of cervical sympathetic trunk. *Proc Natl Acad Sci USA* 1983; **80**: 4179–4183.

26 Sokoloff L. Localization of functional activity in the central nervous system by measurement of glucose utilization with radioactive deoxyglucose. *J Cereb Blood Flow Metab* 1981; **1**: 7–36.

27 Ter-Pogossian MM, Phelps ME, Hoffman EJ, Mullani NA. A positron-emission transaxial tomograph for nuclear imaging (PETT). *Radiology* 1975; **114**: 89–98.

28 Raichle ME. Positron emission tomography. *Annu Rev Neurosci* 1983; **6**: 249–267.

29 Raichle ME, welch MJ, Grubb RL, Higgins CS, Ter-Pogossian MM, Larson KB. Measurement of regional substrate utilization rates by emission tomography. *Science* 1978; **199**: 986–987.

30 Reivich M, Kuhl D, Wolf A, Greenberg J, Phelps M, Ido T *et al.* The [18F]fluorodeoxyglucose method for the measurement of local cerebral glucose utilization in man. *Metabolism* 1979; **44**: 127–137.

31 Gallagher BM, Fowler JS, Gutterson NI, MacGregor RR, Wan CN, Wolf AP. Metabolic trapping as a principle of radiopharmaceutical design: some factors resposible for the biodistribution of [18F] 2-deoxy-2-fluoro-D-glucose. *J Nucl Med* 1978; **19**: 1154–1161.

32 Phelps ME, Mazziotta JC, Huang SC. Study of cerebral function with positron computed tomography. *J Cereb Blood Flow Metab* 1982; **2**: 113–162.

33 Phelps ME, Kuhl DE, Mazziota JC. Metabolic mapping of the brain's response to visual stimulation: studies in humans. *Science* 1981; **211**: 1445–1448.

34 Richmond BJ, Optican LM, Spitzer H. Temporal encoding of two-dimensional patterns by single units in primate primary visual cortex. I. Stimulus-response relations. *Journal of Neurophysiology* 1990; **64**: 351–369.

35 Greenberg JH, Reivich M, Alavi A, Hand P, Rosenquist A, Rintelmann W *et al.* Metabolic mapping of functional activity in human subjects with the [18F]fluorodeoxyglucose technique. *Science* 1981; **212**: 678–680.

36 Ter-Pogossian MM, Eichling JO, Davis DO, welch MJ. The measure in vivo of regional cerebral oxygen utilization by means of oxyhemoglobin labeled with radioactive oxygen-15. *J Clin Investig* 1970; **49**: 381–391.

37 Frackowiak RS, Jones T, Lenzi GL, Heather JD. Regional cerebral oxygen utilization and blood flow in normal man using oxygen-15 and positron emission tomography. *Acta Neurol Scand* 1980; **62**: 336–344.

38 Fox PT, Raichle ME. Focal physiological uncoupling of cerebral blood flow and oxidative metabolism during somatosensory stimulation in human subjects. *Proc Natl Acad Sci USA* 1986; **83**: 1140–1144.

39 Fox PT, Raichle ME, Mintun MA, Dence C. Nonoxidative glucose consumption during focal physiologic neural activity. *Science* 1988; **241**: 462–464.

40 Warburg O. On the origin of cancer cells. *Science* 1956; **123**: 309–314.

41 Fox PT. The coupling controversy. *Neuroimage* 2012; **62**: 594–601.

42 Cooper R, Papakostopoulos D, Crow HJ. Rapid Changes of Cortical Oxyen Associated with Motor and Cognitive Function in Man. In: Harper M, Jennett B, MIller D, Rowan J

(eds). *Blood Flow and Metabolism in the Brain*. 7th International Symposium on Cerebral Blood Flow and Metabolism: Edinburgh, 1975.

43 Ginsberg MD, Chang JY, Kelley RE, Yoshii F, Barker WW, Ingenito G *et al.* Increases in both cerebral glucose utilization and blood flow during execution of a somatosensory task. *Annals of Neurology* 1988; **23**: 152–160.

44 Kuwabara H, Ohta S, Brust P, Meyer E, Gjedde A. Density of perfused capillaries in living human brain during functional activation. *Prog Brain Res* 1992; **91**: 209–215.

45 Blomqvist G, Seitz RJ, Sjögren I, Halldin C, Stone-Elander S, Widén L *et al.* Regional cerebral oxidative and total glucose consumption during rest and activation studied with positron emission tomography. *Acta Physiol Scand* 1994; **151**: 29–43.

46 Prichard J, Rothman D, Novotny E, Petroff O, Kuwabara T, Avison M *et al.* Lactate rise detected by 1H NMR in human visual cortex during physiologic stimulation. *Proc Natl Acad Sci USA* 1991; **88**: 5829–5831.

47 Sappey-Marinier D, Calabrese G, Fein G, Hugg JW, Biggins C, Weiner MW. Effect of photic stimulation on human visual cortex lactate and phosphates using 1H and 31P magnetic resonance spectroscopy. *J Cereb Blood Flow Metab* 1992; **12**: 584–592.

48 Frahm J, Krüger G, Merboldt KD, Kleinschmidt A. Dynamic uncoupling and recoupling of perfusion and oxidative metabolism during focal brain activation in man. *Magn Reson Med* 1996; **35**: 143–148.

49 Mangia S, Tkac I, Logothetis NK, Gruetter R, Van De Moortele P-F, Ugurbil K. Dynamics of lactate concentration and blood oxygen level-dependent effect in the human visual cortex during repeated identical stimuli. *Journal of Neuroscience Research* 2007; **85**: 3340–3346.

50 Mangia S, Tkac I, Gruetter R, Van De Moortele P-F, Maraviglia B, Ugurbil K. Sustained neuronal activation raises oxidative metabolism to a new steady-state level: evidence from 1H NMR spectroscopy in the human visual cortex. *J Cereb Blood Flow Metab* 2007; **27**: 1055–1063.

51 Lin AL, Fox PT, Hardies J, Duong TQ, Gao JH. Nonlinear coupling between cerebral blood flow, oxygen consumption, and ATP production in human visual cortex. *Proc Natl Acad Sci USA* 2010; **107**: 8446–8451.

52 Lin Y, Stephenson MC, Xin L, Napolitano A, Morris PG. Investigating the metabolic changes due to visual stimulation using functional proton magnetic resonance spectroscopy at 7 T. *J Cereb Blood Flow Metab* 2012; **32**: 1484–1495.

53 Schaller B, Mekle R, Xin L, Kunz N, Gruetter R. Net increase of lactate and glutamate concentration in activated human visual cortex detected with magnetic resonance spectroscopy at 7 tesla. *Journal of Neuroscience Research* 2013; **91**: 1076–1083.

54 Bednařík P, Tkac I, Giove F, DiNuzzo M, Deelchand DK, Emir UE *et al.* Neurochemical and BOLD responses during neuronal activation measured in the human visual cortex at 7 Tesla. *J Cereb Blood Flow Metab* 2015; **35**: 601–610.

55 Mekle R, Kühn S, Pfeiffer H, Aydin S, Schubert F, Ittermann B. Detection of metabolite changes in response to a varying visual stimulation paradigm using short-TE 1 H MRS at 7 T. *NMR Biomed* 2017; **30**. doi:10.1002/nbm.3672.

56 Bednařík P, Tkac I, Giove F, Eberly LE, Deelchand DK, Barreto FR *et al.* Neurochemical responses to chromatic and achromatic stimuli in the human visual cortex. *J Cereb Blood Flow Metab* 2018; **38**: 347–359.

57 Kuwabara T, Watanabe H, Tsuji S, Yuasa T. Lactate rise in the basal ganglia accompanying finger movements: a localized 1H-MRS study. *Brain Res* 1995; **670**: 326–328.

58 Schaller B, Xin L, O'Brien K, Magill AW, Gruetter R. Are glutamate and lactate increases ubiquitous to physiological activation? A (1)H functional MR spectroscopy study during motor activation in human brain at 7Tesla. *Neuroimage* 2014; **93 Pt 1**: 138–145.

59 Koush Y, de Graaf RA, Jiang L, Rothman DL, Hyder F. Functional MRS with J-edited lactate in human motor cortex at 4 T. *Neuroimage* 2019; **184**: 101–108.

60 Urrila AS, Hakkarainen A, Heikkinen S, Vuori K, Stenberg D, Häkkinen A-M *et al.* Metabolic imaging of human cognition: an fMRI/1H-MRS study of brain lactate response to silent word generation. *J Cereb Blood Flow Metab* 2003; **23**: 942–948.

61 Seitz RJ, Roland PE. Vibratory stimulation increases and decreases the regional cerebral blood flow and oxidative metabolism: a positron emission tomography (PET) study. *Acta Neurol Scand* 1992; **86**: 60–67.

62 Fujita H, Kuwabara H, Reutens DC, Gjedde A. Oxygen consumption of cerebral cortex fails to increase during continued vibrotactile stimulation. *J Cereb Blood Flow Metab* 1999; **19**: 266–271.

63 Vafaee MS, Vang K, Bergersen LH, Gjedde A. Oxygen consumption and blood flow coupling in human motor cortex during intense finger tapping: implication for a role of lactate. *J Cereb Blood Flow Metab* 2012; **32**: 1859–1868.

64 Roland PE, Eriksson L, Stone-Elander S, Widén L. Does mental activity change the oxidative metabolism of the brain? *J Neurosci* 1987; **7**: 2373–2389.

65 Davis TL, Kwong KK, Weisskoff RM, Rosen BR. Calibrated functional MRI: mapping the dynamics of oxidative metabolism. *Proc Natl Acad Sci USA* 1998; **95**: 1834–1839.

66 Vafaee MS, Marrett S, Meyer E, Evans AC, Gjedde A. Increased oxygen consumption in human visual cortex: response to visual stimulation. *Acta Neurol Scand* 1998; **98**: 85–89.

67 Vafaee MS, Meyer E, Marrett S, Paus T, Evans AC, Gjedde A. Frequency-dependent changes in cerebral metabolic rate of oxygen during activation of human visual cortex. *J Cereb Blood Flow Metab* 1999; **19**: 272–277.

68 Hoge RD, Atkinson J, Gill B, Crelier GR, Marrett S, Pike GB. Linear coupling between cerebral blood flow and oxygen consumption in activated human cortex. *Proc Natl Acad Sci USA* 1999; **96**: 9403–9408.

69 Gjedde A, Marrett S. Glycolysis in neurons, not astrocytes, delays oxidative metabolism of human visual cortex during sustained checkerboard stimulation in vivo. *J Cereb Blood Flow Metab* 2001; **21**: 1384–1392.

70 Vafaee MS, Gjedde A. Spatially dissociated flow-metabolism coupling in brain activation. *Neuroimage* 2004; **21**: 507–515.

71 Lin A-L, Fox PT, Yang Y, Lu H, Tan L-H, Gao J-H. Time-dependent correlation of cerebral blood flow with oxygen metabolism in activated human visual cortex as measured by fMRI. *Neuroimage* 2009; **44**: 16–22.

72 Buxton RB. Interpreting oxygenation-based neuroimaging signals: the importance and the challenge of understanding brain oxygen metabolism. *Front Neuroenergetics* 2010; **2**: 8.

73 Kwong KK, Belliveau JW, Chesler DA, Goldberg IE, Weisskoff RM, Poncelet BP *et al.* Dynamic magnetic resonance imaging of human brain activity during primary sensory stimulation. *Proc Natl Acad Sci USA* 1992; **89**: 5675–5679.

74 Ogawa S, Tank DW, Menon R, Ellermann JM, Kim SG, Merkle H *et al.* Intrinsic signal changes accompanying sensory stimulation: functional brain mapping with magnetic resonance imaging. *Proc Natl Acad Sci USA* 1992; **89**: 5951–5955.

75 Buxton RB. The physics of functional magnetic resonance imaging (fMRI). *Rep Prog Phys* 2013; **76**: 096601.

76 Rosen BR, Savoy RL. fMRI at 20: has it changed the world? *Neuroimage* 2012; **62**: 1316–1324.

77 Zhu X-H, Lee B-Y, Chen W. Functional energetic responses and individual variance of the human brain revealed by quantitative imaging of adenosine triphosphate production rates. *J Cereb Blood Flow Metab* 2018; **38**: 959–972.

78 Hyder F, Chase JR, Behar KL, Mason GF, Siddeek M, Rothman DL *et al.* Increased tricarboxylic acid cycle flux in rat brain during forepaw stimulation detected with 1H[13C]NMR. *Proc Natl Acad Sci USA* 1996; **93**: 7612–7617.

79 Hyder F, Rothman DL, Mason GF, Rangarajan A, Behar KL, Shulman RG. Oxidative glucose metabolism in rat brain during single forepaw stimulation: a spatially localized 1H[13C] nuclear magnetic resonance study. *J Cereb Blood Flow Metab* 1997; **17**: 1040–1047.

80 Rothman DL, Behar KL, Hyder F, Shulman RG. In vivo NMR studies of the glutamate neurotransmitter flux and neuroenergetics: implications for brain function. *Annu Rev Physiol* 2003; **65**: 401–427.

81 Brain work and brain imaging. *Annu Rev Neurosci* 2006; **29**: 449–476.

82 Parolin ML, Chesley A, Matsos MP, Spriet LL, Jones NL, Heigenhauser GJ. Regulation of skeletal muscle glycogen phosphorylase and PDH during maximal intermittent exercise. *Am J Physiol* 1999; **277**: E890–900.

83 Baker JS, McCormick MC, Robergs RA. Interaction among Skeletal Muscle Metabolic Energy Systems during Intense Exercise. *J Nutr Metab* 2010; **2010**: 905612–13.

84 Pellerin L, Bouzier-Sore A-K, Aubert A, Serres S, Merle M, Costalat R *et al.* Activity-dependent regulation of energy metabolism by astrocytes: an update. *Glia* 2007; **55**: 1251–1262.

85 Pellerin L, Magistretti PJ. Glutamate uptake into astrocytes stimulates aerobic glycolysis: a mechanism coupling neuronal activity to glucose utilization. *Proc Natl Acad Sci USA* 1994; **91**: 10625–10629.

86 Anderson CM, Swanson RA. Astrocyte glutamate transport: review of properties, regulation, and physiological functions. *Glia* 2000; **32**: 1–14.

87 Magistretti PJ, Allaman I. Lactate in the brain: from metabolic end-product to signalling molecule. *Nat Rev Neurosci* 2018; **27**: 476–249.

88 Kacem K, Lacombe P, Seylaz J, Bonvento G. Structural organization of the perivascular astrocyte endfeet and their relationship with the endothelial glucose transporter: a confocal microscopy study. *Glia* 1998; **23**: 1–10.

89 McCall AL, Van Bueren AM, Nipper V, Moholt-Siebert M, Downes H, Lessov N. Forebrain ischemia increases GLUT1 protein in brain microvessels and parenchyma. *J Cereb Blood Flow Metab* 1996; **16**: 69–76.

90 Ventura R, Harris KM. Three-dimensional relationships between hippocampal synapses and astrocytes. *J Neurosci* 1999; **19**: 6897–6906.

91 Kadekaro M, Crane AM, Sokoloff L. Differential effects of electrical stimulation of sciatic nerve on metabolic activity in spinal cord and dorsal root ganglion in the rat. *Proc Natl Acad Sci USA* 1985; **82**: 6010–6013.

92 Nudo RJ, Masterton RB. Stimulation-induced [14C]2-deoxyglucose labeling of synaptic activity in the central auditory system. *J Comp Neurol* 1986; **245**: 553–565.

93 Markert CL, Møller F. Multiple Forms of Enzymes: Tissue, Ontogenetic, and Species Specific Patterns. *Proc Natl Acad Sci USA* 1959; **45**: 753–763.

94 Bittar PG, Charnay Y, Pellerin L, Bouras C, Magistretti PJ. Selective distribution of lactate dehydrogenase isoenzymes in neurons and astrocytes of human brain. *J Cereb Blood Flow Metab* 1996; **16**: 1079–1089.

95 Laughton JD, Bittar P, Charnay Y, Pellerin L, Kovari E, Magistretti PJ *et al.* Metabolic compartmentalization in the human cortex and hippocampus: evidence for a cell- and region-specific localization of lactate dehydrogenase 5 and pyruvate dehydrogenase. *BMC Neurosci* 2007; **8**: 35.

96 Cahn RD, Zwilling E, Kaplan NO, Levine L. Nature and Development of Lactic Dehydrogenases: The two major types of this enzyme form molecular hybrids which change in makeup during development. *Science* 1962; **136**: 962–969.

97 Mongeon R, Venkatachalam V, Yellen G. Cytosolic NADH-NAD(+) Redox Visualized in Brain Slices by Two-Photon Fluorescence Lifetime Biosensor Imaging. *Antioxid Redox Signal* 2016; **25**: 553–563.

98 Chuquet J, Quilichini P, Nimchinsky EA, Buzsáki G. Predominant enhancement of glucose uptake in astrocytes versus neurons during activation of the somatosensory cortex. *J Neurosci* 2010; **30**: 15298–15303.

99 Voutsinos-Porche B, Bonvento G, Tanaka K, Steiner P, Welker E, Chatton J-Y *et al.* Glial glutamate transporters mediate a functional metabolic crosstalk between neurons and astrocytes in the mouse developing cortex. *Neuron* 2003; **37**: 275–286.

100 Itoh Y, Esaki T, Shimoji K, Cook M, Law MJ, Kaufman E *et al.* Dichloroacetate effects on glucose and lactate oxidation by neurons and astroglia in vitro and on glucose utilization by brain in vivo. *Proc Natl Acad Sci USA* 2003; **100**: 4879–4884.

101 Bouzier-Sore A-K, Voisin P, Canioni P, Magistretti PJ, Pellerin L. Lactate is a preferential oxidative energy substrate over glucose for neurons in culture. *J Cereb Blood Flow Metab* 2003; **23**: 1298–1306.

102 Smith D, Pernet A, Hallett WA, Bingham E, Marsden PK, Amiel SA. Lactate: a preferred fuel for human brain metabolism in vivo. *J Cereb Blood Flow Metab* 2003; **23**: 658–664.

103 van Hall G, Strømstad M, Rasmussen P, Jans O, Zaar M, Gam C *et al.* Blood lactate is an important energy source for the human brain. *J Cereb Blood Flow Metab* 2009; **29**: 1121–1129.

104 Sibson NR, Dhankhar A, Mason GF, Rothman DL, Behar KL, Shulman RG. Stoichiometric coupling of brain glucose metabolism and glutamatergic neuronal activity. *Proc Natl Acad Sci USA* 1998; **95**: 316–321.

105 Hyder F, Patel AB, Gjedde A, Rothman DL, Behar KL, Shulman RG. Neuronal-glial glucose oxidation and glutamatergic-GABAergic function. *J Cereb Blood Flow Metab* 2006; **26**: 865–877.

106 Lundgaard I, Li B, Xie L, Kang H, Sanggaard S, Haswell JDR *et al.* Direct neuronal glucose uptake heralds activity-dependent increases in cerebral metabolism. *Nature Communications* 2015; **6**: 6807.

107 Díaz-García CM, Mongeon R, Lahmann C, Koveal D, Zucker H, Yellen G. Neuronal Stimulation Triggers Neuronal Glycolysis and Not Lactate Uptake. *Cell Metab* 2017; **26**: 361–374.e4.

108 Dienel GA. Lack of appropriate stoichiometry: Strong evidence against an energetically important astrocyte-neuron lactate shuttle in brain. *Journal of Neuroscience Research* 2017; **95**: 2103–2125.

109 Dienel GA. Brain Glucose Metabolism: Integration of Energetics with Function. *Physiol Rev* 2019; **99**: 949–1045.

110 Zimmer ER, Parent MJ, Souza DG, Leuzy A, Lecrux C, Kim H-I *et al.* [18F]FDG PET signal is driven by astroglial glutamate transport. 2017; **20**: 393–395.

111 Mächler P, Wyss MT, Elsayed M, Stobart J, Gutierrez R, Faber-Castell von A *et al.* In Vivo Evidence for a Lactate Gradient from Astrocytes to Neurons. *Cell Metab* 2016; **23**: 94–102.

112 Kasischke KA, Vishwasrao HD, Fisher PJ, Zipfel WR, Webb WW. Neural activity triggers neuronal oxidative metabolism followed by astrocytic glycolysis. *Science* 2004; **305**: 99–103.

113 Porras OH, Loaiza A, Barros LF. Glutamate mediates acute glucose transport inhibition in hippocampal neurons. *J Neurosci* 2004; **24**: 9669–9673.

114 Hu Y, Wilson GS. A temporary local energy pool coupled to neuronal activity: fluctuations of extracellular lactate levels in rat brain monitored with rapid-response enzyme-based sensor. *J Neurochem* 1997; **69**: 1484–1490.

115 Mangia S, Garreffa G, Bianciardi M, Giove F, Di Salle F, Maraviglia B. The aerobic brain: lactate decrease at the onset of neural activity. *Neuroscience* 2003; **118**: 7–10.

116 Madsen PL, Hasselbalch SG, Hagemann LP, Olsen KS, Bülow J, Holm S *et al.* Persistent resetting of the cerebral oxygen/glucose uptake ratio by brain activation: evidence obtained with the Kety-Schmidt technique. *J Cereb Blood Flow Metab* 1995; **15**: 485–491.

117 Fellows LK, Boutelle MG, Fillenz M. Physiological stimulation increases nonoxidative glucose metabolism in the brain of the freely moving rat. *J Neurochem* 1993; **60**: 1258–1263.

118 Madsen PL, Cruz NF, Sokoloff L, Dienel GA. Cerebral oxygen/glucose ratio is low during sensory stimulation and rises above normal during recovery: excess glucose

consumption during stimulation is not accounted for by lactate efflux from or accumulation in brain tissue. *J Cereb Blood Flow Metab* 1999; **19**: 393–400.

119 Cruz NF, Dienel GA. High glycogen levels in brains of rats with minimal environmental stimuli: implications for metabolic contributions of working astrocytes. *J Cereb Blood Flow Metab* 2002; **22**: 1476–1489.

120 Dienel GA, Wang RY, Cruz NF. Generalized sensory stimulation of conscious rats increases labeling of oxidative pathways of glucose metabolism when the brain glucose-oxygen uptake ratio rises. *J Cereb Blood Flow Metab* 2002; **22**: 1490–1502.

121 Cruz NF, Ball KK, Dienel GA. Functional imaging of focal brain activation in conscious rats: Impact of [14C]glucose metabolite spreading and release. *Journal of Neuroscience Research* 2007; **85**: 3254–3266.

122 Dienel GA, Ball KK, Cruz NF. A glycogen phosphorylase inhibitor selectively enhances local rates of glucose utilization in brain during sensory stimulation of conscious rats: implications for glycogen turnover. *J Neurochem* 2007; **102**: 466–478.

123 Bero AW, Yan P, Roh JH, Cirrito JR, Stewart FR, Raichle ME *et al.* Neuronal activity regulates the regional vulnerability to amyloid-β deposition. *Nat Neurosci* 2011; **14**: 750–756.

124 Shulman RG, Hyder F, Rothman DL. Cerebral energetics and the glycogen shunt: neurochemical basis of functional imaging. *Proc Natl Acad Sci USA* 2001; **98**: 6417–6422.

125 Öz G, DiNuzzo M, Kumar A, Moheet A, Seaquist ER. Revisiting Glycogen Content in the Human Brain. *Neurochem Res* 2015; **40**: 2473–2481.

126 Blomqvist G, Stone-Elander S, Halldin C, Roland PE, Widén L, Lindqvist M *et al.* Positron emission tomographic measurements of cerebral glucose utilization using [1-11C]D-glucose. *J Cereb Blood Flow Metab* 1990; **10**: 467–483.

127 Gruetter R, Novotny EJ, Boulware SD, Rothman DL, Mason GF, Shulman GI *et al.* Direct measurement of brain glucose concentrations in humans by 13C NMR spectroscopy. *Proc Natl Acad Sci USA* 1992; **89**: 1109–1112.

128 Gruetter R, Novotny EJ, Boulware SD, Rothman DL, Shulman RG. 1H NMR studies of glucose transport in the human brain. *J Cereb Blood Flow Metab* 1996; **16**: 427–438.

129 Gruetter R, Ugurbil K, Seaquist ER. Steady-state cerebral glucose concentrations and transport in the human brain. *J Neurochem* 1998; **70**: 397–408.

130 Cataldo AM, Broadwell RD. Cytochemical identification of cerebral glycogen and glucose-6-phosphatase activity under normal and experimental conditions: I. Neurons and glia. *Journal of Electron Microscopy Technique* 1986; **3**: 413–437.

131 Swanson RA, Morton MM, Sagar SM, Sharp FR. Sensory stimulation induces local cerebral glycogenolysis: demonstration by autoradiography. *Neuroscience* 1992; **51**: 451–461.

132 Kong J, Shepel PN, Holden CP, Mackiewicz M, Pack AI, Geiger JD. Brain glycogen decreases with increased periods of wakefulness: implications for homeostatic drive to sleep. *J Neurosci* 2002; **22**: 5581–5587.

133 Franken P, Gip P, Hagiwara G, Ruby NF, Heller HC. Glycogen content in the cerebral cortex increases with sleep loss in C57BL/6J mice. *Neuroscience Letters* 2006; **402**: 176–179.

134 Bellesi M, de Vivo L, Koebe S, Tononi G, Cirelli C. Sleep and Wake Affect Glycogen Content and Turnover at Perisynaptic Astrocytic Processes. *Front Cell Neurosci* 2018; **12**: 308.

135 Öz G, Seaquist ER, Kumar A, Criego AB, Benedict LE, Rao JP *et al.* Human brain glycogen content and metabolism: implications on its role in brain energy metabolism. *Am J Physiol Endocrinol Metab* 2007; **292**: E946–51.

136 Choi IY, Tkác I, Ugurbil K, Gruetter R. Noninvasive measurements of [1-(13)C]glycogen concentrations and metabolism in rat brain in vivo. *J Neurochem* 1999; **73**: 1300–1308.

137 DiNuzzo M. Kinetic analysis of glycogen turnover: relevance to human brain 13C-NMR spectroscopy. *J Cereb Blood Flow Metab* 2013; **33**: 1540–1548.

138 Ball KK, Cruz NF, Mrak RE, Dienel GA. Trafficking of glucose, lactate, and amyloid-beta from the inferior colliculus through perivascular routes. *J Cereb Blood Flow Metab* 2010; **30**: 162–176.

139 Mintun MA, Vlassenko AG, Shulman GL, Snyder AZ. Time-related increase of oxygen utilization in continuously activated human visual cortex. *Neuroimage* 2002; **16**: 531–537.

140 Vlassenko AG, Rundle MM, Mintun MA. Human brain glucose metabolism may evolve during activation: findings from a modified FDG PET paradigm. *Neuroimage* 2006; **33**: 1036–1041.

141 Shannon BJ, Vaishnavi SN, Vlassenko AG, Shimony JS, Rutlin J, Raichle ME. Brain aerobic glycolysis and motor adaptation learning. *Proc Natl Acad Sci USA* 2016; **113**: E3782–91.

142 Hertz L, Fillenz M. Does the ‘mystery of the extra glucose’ during CNS activation reflect glutamate synthesis? *Neurochem Int* 1999; **34**: 71–75.

143 Apšvalka D, Gadie A, Clemence M, Mullins PG. Event-related dynamics of glutamate and BOLD effects measured using functional magnetic resonance spectroscopy (fMRS) at 3T in a repetition suppression paradigm. *Neuroimage* 2015; **118**: 292–300.

144 Ip IB, Berrington A, Hess AT, Parker AJ, Emir UE, Bridge H. Combined fMRI-MRS acquires simultaneous glutamate and BOLD-fMRI signals in the human brain. *Neuroimage* 2017; **155**: 113–119.

145 Mangia S, Giove F, Tkac I, Logothetis NK, Henry P-G, Olman CA *et al.* Metabolic and hemodynamic events after changes in neuronal activity: current hypotheses, theoretical predictions and in vivo NMR experimental findings. *J Cereb Blood Flow Metab* 2009; **29**: 441–463.

146 McKenna MC, Waagepetersen HS, Schousboe A, Sonnewald U. Neuronal and astrocytic shuttle mechanisms for cytosolic-mitochondrial transfer of reducing equivalents: current evidence and pharmacological tools. *Biochem Pharmacol* 2006; **71**: 399–407.

147 Vaishnavi SN, Vlassenko AG, Rundle MM, Snyder AZ, Mintun MA, Raichle ME. Regional aerobic glycolysis in the human brain. *Proc Natl Acad Sci USA* 2010; **107**: 17757–17762.

148 Bauernfeind AL, Barks SK, Duka T, Grossman LI, Hof PR, Sherwood CC. Aerobic glycolysis in the primate brain: reconsidering the implications for growth and maintenance. *Brain Struct Funct* 2014; **219**: 1149–1167.

149 Fadiga L, Craighero L, D'Ausilio A. Broca's area in language, action, and music. *Ann N Y Acad Sci* 2009; **1169**: 448–458.

150 Dienel GA. Fueling and imaging brain activation. *ASN Neuro* 2012; **4**. doi:10.1042/AN20120021.

151 Nelson DL, Cox MM. *Lehninger Principles of Biochemistry*. 6 ed. W.H. Freeman and Company: New York, 2013.

152 Goyal MS, Venkatesh S, Milbrandt J, Gordon JI, Raichle ME. Feeding the brain and nurturing the mind: Linking nutrition and the gut microbiota to brain development. *Proc Natl Acad Sci USA* 2015; **112**: 14105–14112.

153 Goyal MS, Hawrylycz M, Miller JA, Snyder AZ, Raichle ME. Aerobic glycolysis in the human brain is associated with development and neotenous gene expression. *Cell Metab* 2014; **19**: 49–57.

154 Benveniste H, Dienel G, Jacob Z, Lee H, Makaryus R, Gjedde A *et al.* Trajectories of Brain Lactate and Re-visited Oxygen-Glucose Index Calculations Do Not Support Elevated Non-oxidative Metabolism of Glucose Across Childhood. *Front Neurosci* 2018; **12**: 631.

155 Caroni P, Donato F, Muller D. Structural plasticity upon learning: regulation and functions. *Nat Rev Neurosci* 2012; **13**: 478–490.

156 Lendvai B, Stern EA, Chen B, Svoboda K. Experience-dependent plasticity of dendritic spines in the developing rat barrel cortex in vivo. *Nature* 2000; **404**: 876–881.

157 Trachtenberg JT, Chen BE, Knott GW, Feng G, Sanes JR, Welker E *et al.* Long-term in vivo imaging of experience-dependent synaptic plasticity in adult cortex. *Nature* 2002; **420**: 788–794.

158 Ehlers MD. Activity level controls postsynaptic composition and signaling via the ubiquitin-proteasome system. *Nat Neurosci* 2003; **6**: 231–242.

159 Cohen LD, Zuchman R, Sorokina O, Müller A, Dieterich DC, Armstrong JD *et al.* Metabolic turnover of synaptic proteins: kinetics, interdependencies and implications for synaptic maintenance. *PLoS ONE* 2013; **8**: e63191.

160 Lundgaard I, Lu ML, Yang E, Peng W, Mestre H, Hitomi E *et al.* Glymphatic clearance controls state-dependent changes in brain lactate concentration. *J Cereb Blood Flow Metab* 2017; **37**: 2112–2124.

161 Bergersen LH, Gjedde A. Is lactate a volume transmitter of metabolic states of the brain? *Front Neuroenergetics* 2012; **4**: 5.

162 Suzuki A, Stern SA, Bozdagi O, Huntley GW, Walker RH, Magistretti PJ *et al.* Astrocyte-Neuron Lactate Transport Is Required for Long-Term Memory Formation. *Cell* 2011; **144**: 810–823.

163 Yang J, Ruchti E, Petit J-M, Jourdain P, Grenningloh G, Allaman I *et al.* Lactate promotes plasticity gene expression by potentiating NMDA signaling in neurons. *Proc Natl Acad Sci USA* 2014; **111**: 12228–12233.

164 Kety SS. The General Metabolism Of The Brain *In Vivo*. In: Richter D (ed). *Metabolism Of The Nervous System*. London, 1957, pp 221–327.

165 Himwich WA, Himwich HE. Pyruvic acid exchange of the brain. *Journal of Neurophysiology* 1946; **9**: 133–136.

166 Cohen PJ, Alexander SC, Smith TC, Reivich M, Wollman H. Effects of hypoxia and normocarbia on cerebral blood flow and metabolism in conscious man. *J Appl Physiol* 1967; **23**: 183–189.

167 Siesjö BK. *Brain energy metabolism*. John Wiley & Sons, 1978.

168 Scheinberg P, Bourne B, Reinmuth OM. Human Cerebral Lactate And Pyruvate Extraction. *Arch Neurol* 1965; **12**: 246–250.

169 Fox MD, Raichle ME. Spontaneous fluctuations in brain activity observed with functional magnetic resonance imaging. *Nat Rev Neurosci* 2007; **8**: 700–711.

170 Seeley WW, Menon V, Schatzberg AF, Keller J, Glover GH, Kenna H *et al.* Dissociable Intrinsic Connectivity Networks for Salience Processing and Executive Control. *Journal of Neuroscience* 2007; **27**: 2349–2356.

171 Raichle ME, MacLeod AM, Snyder AZ, Powers WJ, Gusnard DA, Shulman GL. A default mode of brain function. 2001; **98**: 676–682.

172 Shulman GL, Fiez JA, Corbetta M, Buckner RL, Miezin FM, Raichle ME *et al.* Common Blood Flow Changes across Visual Tasks: II. Decreases in Cerebral Cortex. *J Cogn Neurosci* 1997; **9**: 648–663.

173 Fox MD, Snyder AZ, Vincent JL, Corbetta M, Van Essen DC, Raichle ME. The human brain is intrinsically organized into dynamic, anticorrelated functional networks. *Proc Natl Acad Sci USA* 2005; **102**: 9673–9678.

174 Gusnard DA, Akbudak E, Shulman GL, Raichle ME. Medial prefrontal cortex and self-referential mental activity: relation to a default mode of brain function. *Proc Natl Acad Sci USA* 2001; **98**: 4259–4264.

175 Andrews-Hanna JR, Reidler JS, Huang C, Buckner RL. Evidence for the default network's role in spontaneous cognition. *Journal of Neurophysiology* 2010; **104**: 322–335.

176 Raichle ME. The brain's default mode network. *Annu Rev Neurosci* 2015; **38**: 433–447.

177 Roy M, Sorokina O, Skene N, Simonnet C, Mazzo F, Zwart R *et al.* Proteomic analysis of postsynaptic proteins in regions of the human neocortex. *Nat Neurosci* 2018; **21**: 130–138.

178 Glasser MF, Goyal MS, Preuss TM, Raichle ME, Van Essen DC. Trends and properties of human cerebral cortex: correlations with cortical myelin content. *Neuroimage* 2014; **93 Pt 2**: 165–175.

179 Segarra Mondejar M, Casellas Díaz S, Ramiro Pareta M, Müller Sánchez C, Martorell Riera A, Hermelo I *et al.* Synaptic activity-induced glycolysis facilitates membrane lipid provision and neurite outgrowth. *EMBO J* 2018; **37**. doi:10.15252/embj.201797368.

180 Cheshkov S, Dimitrov IE, Jakkamsetti V, Good L, Kelly D, Rajasekaran K *et al.* Oxidation of [U-13 C]glucose in the human brain at 7T under steady state conditions. *Magn Reson Med* 2017; **78**: 2065–2071.

181 Lai M, Lanz B, Poitry-Yamate C, Romero JF, Berset CM, Cudalbu C *et al.* In vivo 13C MRS in the mouse brain at 14.1 Tesla and metabolic flux quantification under infusion of [1,6-13C2]glucose. *J Cereb Blood Flow Metab* 2018; **38**: 1701–1714.

182 Grist JT, McLean MA, Riemer F, Schulte RF, Deen SS, Zaccagna F *et al.* Quantifying normal human brain metabolism using hyperpolarized [1-13C]pyruvate and magnetic resonance imaging. *Neuroimage* 2019; **189**: 171–179.

183 Amaral AI, Teixeira AP, Håkonsen BI, Sonnewald U, Alves PM. A comprehensive metabolic profile of cultured astrocytes using isotopic transient metabolic flux analysis and C-labeled glucose. *Front Neuroenergetics* 2011; **3**: 5.

184 Kety SS, Woodford RB. Cerebral blood flow and metabolism in schizophrenia; the effects of barbiturate semi-narcosis, insulin coma and electroshock. *Am J Psychiatry* 1948; **104**: 765–770.

185 Kety SS, Skenkin HA, Schmidt CF. The effects of increased intracranial pressure on cerebral circulatory functions in man. *J Clin Investig* 1948; **27**: 493–499.

186 Kety SS, Hafkenschiel JH. The blood flow, vascular resistance, and oxygen consumption of the brain in essential hypertension. *J Clin Investig* 1948; **27**: 511–514.

187 Kety SS, Schmidt CF. The Effects of Altered Arterial Tensions of Carbon Dioxide and Oxygen on Cerebral Blood Flow and Cerebral Oxygen Consumption of Normal Young Men. *J Clin Investig* 1948; **27**: 484–492.

188 Sakel M. A New Treatment of Schizophrenia. *Am J Psychiatry* 1937; **93**: 829–841.

189 Eisenberg S, Seltzer HS. The cerebral metabolic effects of acutely induced hypoglycemia in human subjects. *Metabolism* 1962; **11**: 1162–1168.

190 Gottstein U, Held K. The effect of insulin on brain metabolism in metabolically healthy and diabetic patients. *Klin Wochenschr* 1967; **45**: 18–23.

191 Mintun MA, Lundstrom BN, Snyder AZ, Vlassenko AG, Shulman GL, Raichle ME. Blood flow and oxygen delivery to human brain during functional activity: theoretical modeling and experimental data. *Proc Natl Acad Sci USA* 2001; **98**: 6859–6864.

192 Jóhannsson H, Siesjö BK. Cerebral blood flow and oxygen consumption in the rat in hypoxic hypoxia. *Acta Physiol Scand* 1975; **93**: 269–276.

193 Borgström L, Norberg K, Siesjö BK. Glucose consumption in rat cerbral cortex in normoxia, hypoxia and hypercapnia. *Acta Physiol Scand* 1976; **96**: 569–574.

194 Siesjö BK, Nilsson L. The influence of arterial hypoxemia upon labile phosphates and upon extracellular and intracellular lactate and pyruvate concentrations in the rat brain. *Scand J Clin Lab Invest* 1971; **27**: 83–96.

195 Raichle ME, Posner JB, Plum F. Cerebral blood flow during and after hyperventilation. *Arch Neurol* 1970; **23**: 394–403.

196 Siesjö BK. Hypoglycemia, brain metabolism, and brain damage. *Diabetes Metab Rev* 1988; **4**: 113–144.

197 Gaillard WD, Fazilat S, White S, Malow B, Sato S, Reeves P *et al.* Interictal metabolism and blood flow are uncoupled in temporal lobe cortex of patients with complex partial epilepsy. *Neurology* 1995; **45**: 1841–1847.

198 Fink GR, Pawlik G, Stefan H, Pietrzyk U, Wienhard K, Heiss WD. Temporal lobe epilepsy: evidence for interictal uncoupling of blood flow and glucose metabolism in temporomesial structures. *Journal of the Neurological Sciences* 1996; **137**: 28–34.

199 Breier JI, Mullani NA, Thomas AB, Wheless JW, Plenger PM, Gould KL *et al.* Effects of duration of epilepsy on the uncoupling of metabolism and blood flow in complex partial seizures. *Neurology* 1997; **48**: 1047–1053.

200 Bergsneider M, Hovda DA, Shalmon E, Kelly DF, Vespa PM, Martin NA *et al.* Cerebral hyperglycolysis following severe traumatic brain injury in humans: a positron emission tomography study. *J Neurosurg* 1997; **86**: 241–251.

201 Serrano-Pozo A, Aldridge GM, Zhang Q. Four Decades of Research in Alzheimer's Disease (1975-2014): A Bibliometric and Scientometric Analysis. *J Alzheimers Dis* 2017; **59**: 763–783.

202 Alzheimer's Association. 2015 Alzheimer's disease facts and figures. *Alzheimers Dement* 2015; **11**: 332–384.

203 Jack CR, Knopman DS, Jagust WJ, Shaw LM, Aisen PS, Weiner MW *et al.* Hypothetical model of dynamic biomarkers of the Alzheimer's pathological cascade. *The Lancet Neurology* 2010; **9**: 119–128.

204 Mosconi L. Brain glucose metabolism in the early and specific diagnosis of Alzheimer's disease. FDG-PET studies in MCI and AD. *Eur J Nucl Med Mol Imaging* 2005; **32**: 486–510.

205 Jack CR, Vemuri P, Wiste HJ, Weigand SD, Lesnick TG, Lowe V *et al.* Shapes of the trajectories of 5 major biomarkers of Alzheimer disease. *Arch Neurol* 2012; **69**: 856–867.

206 Lassen NA, Feinberg I, Lane MH. Bilateral studies of cerebral oxygen uptake in young and aged normal subjects and in patients with organic dementia. *J Clin Investig* 1960; **39**: 491–500.

207 Frackowiak RS, Pozzilli C, Legg NJ, Boulay Du GH, Marshall J, Lenzi GL *et al.* Regional cerebral oxygen supply and utilization in dementia. A clinical and physiological study with oxygen-15 and positron tomography. *Brain* 1981; **104**: 753–778.

208 Benson DF, Kuhl DE, Hawkins RA, Phelps ME, Cummings JL, Tsai SY. The fluorodeoxyglucose 18F scan in Alzheimer's disease and multi-infarct dementia. *Arch Neurol* 1983; **40**: 711–714.

209 Jagust WJ, Seab JP, Huesman RH, Valk PE, Mathis CA, Reed BR *et al.* Diminished glucose transport in Alzheimer's disease: dynamic PET studies. *J Cereb Blood Flow Metab* 1991; **11**: 323–330.

210 Vlassenko AG, Raichle ME. Brain aerobic glycolysis functions and Alzheimer's disease. *Clinical and Translational Imaging* 2015; **3**: 27–37.

211 Hoyer S, Oesterreich K, Wagner O. Glucose metabolism as the site of the primary abnormality in early-onset dementia of Alzheimer type? *J Neurol* 1988; **235**: 143–148.

212 Hoyer S, Nitsch R, Oesterreich K. Predominant abnormality in cerebral glucose utilization in late-onset dementia of the Alzheimer type: a cross-sectional comparison against advanced late-onset and incipient early-onset cases. *J Neural Transm Park Dis Dement Sect* 1991; **3**: 1–14.

213 Fukuyama H, Ogawa M, Yamauchi H, Yamaguchi S, Kimura J, Yonekura Y *et al.* Altered cerebral energy metabolism in Alzheimer's disease: a PET study. *J Nucl Med* 1994; **35**: 1–6.

214 Ogawa M, Fukuyama H, Ouchi Y, Yamauchi H, Kimura J. Altered energy metabolism in Alzheimer's disease. *Journal of the Neurological Sciences* 1996; **139**: 78–82.

215 Goyal MS, Vlassenko AG, Blazey TM, Su Y, Couture LE, Durbin TJ *et al.* Loss of Brain Aerobic Glycolysis in Normal Human Aging. *Cell Metab* 2017; **26**: 353–360.e3.

216 Vlassenko AG, Gordon BA, Goyal MS, Su Y, Blazey TM, Durbin TJ *et al.* Aerobic glycolysis and tau deposition in preclinical Alzheimer's disease. *Neurobiol Aging* 2018; **67**: 95–98.

217 Vlassenko AG, Vaishnavi SN, Couture L, Sacco D, Shannon BJ, Mach RH *et al.* Spatial correlation between brain aerobic glycolysis and amyloid-β (Aβ) deposition. *Proc Natl Acad Sci USA* 2010; **107**: 17763–17767.

218 Rasmussen P, Wyss MT, Lundby C. Cerebral glucose and lactate consumption during cerebral activation by physical activity in humans. *FASEB J* 2011; **25**: 2865–2873.

219 Blazey TM, Snyder AZ, Goyal MS, Vlassenko AG, Raichle ME. A systematic meta-analysis of oxygen-to-glucose and oxygen-to-carbohydrate ratios in the resting human brain. *PLoS ONE* 2018; **13**: e0204242.

220 Hyder F, Herman P, Bailey CJ, Møller A, Globinsky R, Fulbright RK *et al.* Uniform distributions of glucose oxidation and oxygen extraction in gray matter of normal human brain: No evidence of regional differences of aerobic glycolysis. *J Cereb Blood Flow Metab* 2016; **36**: 903–916.

221 Borghammer P, Aanerud J, Gjedde A. Data-driven intensity normalization of PET group comparison studies is superior to global mean normalization. *Neuroimage* 2009; **46**: 981–988.

222 Blazey TM, Snyder AZ, Su Y, Goyal MS, Lee JJ, Vlassenko AG *et al.* Quantitative positron emission tomography reveals regional differences in aerobic glycolysis within the human brain. *J Cereb Blood Flow Metab* 2018; **144**: 271678X18767005.

223 Rooijackers HMM, Wiegers EC, Tack CJ, van der Graaf M, de Galan BE. Brain glucose metabolism during hypoglycemia in type 1 diabetes: insights from functional and metabolic neuroimaging studies. *Cell Mol Life Sci* 2016; **73**: 705–722.

224 Teves D, Videen TO, Cryer PE, Powers WJ. Activation of human medial prefrontal cortex during autonomic responses to hypoglycemia. *Proc Natl Acad Sci USA* 2004; **101**: 6217–6221.

225 Arbelaez AM, Su Y, Thomas JB, Hauch AC, Hershey T, Ances BM. Comparison of regional cerebral blood flow responses to hypoglycemia using pulsed arterial spin labeling and positron emission tomography. *PLoS ONE* 2013; **8**: e60085.

226 Wiegers EC, Becker KM, Rooijackers HM, Samson-Himmelstjerna von FC, Tack CJ, Heerschap A *et al.* Cerebral blood flow response to hypoglycemia is altered in patients with type 1 diabetes and impaired awareness of hypoglycemia. *J Cereb Blood Flow Metab* 2017; **37**: 1994–2001.

227 Boyle PJ, Nagy RJ, O'Connor AM, Kempers SF, Yeo RA, Qualls C. Adaptation in brain glucose uptake following recurrent hypoglycemia. *Proc Natl Acad Sci USA* 1994; **91**: 9352–9356.

228 Lee JJ, Khoury N, Shackleford AM, Nelson S, Herrera H, Antenor-Dorsey JA *et al.* Dissociation Between Hormonal Counterregulatory Responses and Cerebral Glucose Metabolism During Hypoglycemia. *Diabetes* 2017; **66**: 2964–2972.

229 Gutniak M, Blomqvist G, Widén L, Stone-Elander S, Hamberger B, Grill V. D-[U-11C]glucose uptake and metabolism in the brain of insulin-dependent diabetic subjects. *Am J Physiol* 1990; **258**: E805–12.

230 Blomqvist G, Gjedde A, Gutniak M, Grill V, Widén L, Stone-Elander S *et al.* Facilitated transport of glucose from blood to brain in man and the effect of moderate hypoglycaemia on cerebral glucose utilization. *Eur J Nucl Med* 1991; **18**: 834–837.

231 Lund-Andersen H. Transport of glucose from blood to brain. *Physiol Rev* 1979; **59**: 305–352.

232 Blomqvist G, Grill V, Ingvar M, Widén L, Stone-Elander S. The effect of hyperglycaemia on regional cerebral glucose oxidation in humans studied with [1-11C]-D-glucose. *Acta Physiol Scand* 1998; **163**: 403–415.

233 Gottstein U, Held K, Sebening H, Walpurger G. Der Glucoseverbrauch des menschlichen Gehirns unter dem Einfluß intravenöser Infusionen von Glucose, Glucagon und Glucose-Insulin. *Klin Wochenschr* 1965; **43**: 965–975.

234 Hasselbalch SG, Knudsen GM, Capaldo B, Postiglione A, Paulson OB. Blood-brain barrier transport and brain metabolism of glucose during acute hyperglycemia in humans. *J Clin Endocrinol Metab* 2001; **86**: 1986–1990.

235 Ishibashi K, Wagatsuma K, Ishiwata K, Ishii K. Alteration of the regional cerebral glucose metabolism in healthy subjects by glucose loading. *Hum Brain Mapp* 2016; **37**: 2823–2832.

236 Garrett RH, Grisham CM. *Principles of Biochemistry with a Human Focus*. Thomson Learning: Boston, MA, 2002.

Chapter 2: A systematic meta-analysis of oxygen-to-glucose and oxygen-to-carbohydrate ratios in the resting human brain[i]

2.1 Abstract

Glucose is the predominant fuel supporting brain function. If the brain's entire glucose supply is consumed by oxidative phosphorylation, the molar ratio of oxygen to glucose consumption (OGI) is equal to 6. An OGI of less than 6 is evidence of non-oxidative glucose metabolism. Several studies have reported that the OGI in the resting human brain is less than 6.0, but the exact value remains uncertain. Additionally, it is not clear if lactate efflux accounts for the difference between OGI and its theoretical value of 6.0. To address these issues, we conducted a meta-analysis of OGI and oxygen-to-carbohydrate (glucose + 0.5*lactate; OCI) ratios in healthy young and middle-aged adults. We identified 47 studies that measured at least one of these ratios using arterio-venous differences of glucose, lactate, and oxygen. Using a Bayesian random effects model, the population median OGI was 5.46 95% credible interval (5.25-5.66), indicating that approximately 9% of the brain's glucose metabolism is non-oxidative. The population median OCI was 5.60 (5.36-5.84), suggesting that lactate efflux does not account for all non-oxidative glucose consumption (NOglc). Significant heterogeneity across studies was observed, which implies that further work is needed to characterize how demographic and methodological factors influence measured cerebral metabolic ratios.

2.2 Introduction

[i] This chapter is slightly modified version of a previously published article: Blazey TM, Snyder AZ, Goyal MS, Vlassenko AG, Raichle ME. A systematic meta-analysis of oxygen-to-glucose and oxygen-to-carbohydrate ratios in the resting human brain. *PLoS ONE* 2018; **13**: e0204242.

Glucose and oxygen consumption are tightly coupled in the brain at rest, with the majority of glucose undergoing complete oxidative phosphorylation[1]. Furthermore, the ratio of carbon dioxide production to oxygen consumption is very close to one[2], indicating that nearly all of oxygen consumption is used for carbohydrates. The standard measure of coupling between oxygen and glucose utilization is the oxygen-to-glucose index (OGI), which is the molar ratio of oxygen to glucose consumption. An OGI of 6 indicates that all glucose is consumed via oxidative pathways.

The measurement of cerebral arterio-venous differences of oxygen and glucose is regarded as the gold-standard technique for obtaining OGI. With this method, arterial samples are collected from a peripheral artery (e.g. radial or brachial artery) and venous samples from the internal jugular vein at the jugular bulb. The primary assumption of this technique is that the venous blood in the jugular bulb comes solely from the brain. If blood from other sources is present, than the arterio-venous difference is no longer only the result of cerebral metabolism. This bias is likely to be small, however, as it has been estimated that 97.4% of the blood in the jugular bulb comes from cerebral sources[3].

Although the arterio-venous technique has been used to study whole-brain OGI for over sixty years[4], there remains some uncertainty as to the exact value. Individual studies using arterio-venous differences in humans at rest have reported values ranging from 4.6[5] to 7.5[6]. In 1957, Kety reviewed sixteen studies of both healthy and diseased populations and reported a mean value of 5.54[4]. A more recent meta-analysis of eight studies of metabolism during exercise found a whole-brain OGI of 5.1[7]. These two reviews suggest that anywhere from 8 to 15% of the brain's glucose uptake is consumed via non-oxidative metabolism. Thus, the value of cerebral OGI in resting, healthy humans is known only approximately.

The fate of glucose consumed by non-oxidative pathways is also a matter of some debate. It has been suggested that lactate efflux to venous blood may completely account for non-oxidative glucose metabolism[8]. Two more recent reviews have reported conflicting results[7,9]. Both studies performed a meta-analysis of the oxygen-to-carbohydrate index (OCI), also referred to as the cerebral metabolic ratio (CMR). The OCI is computed as the molar ratio of the arterio-venous difference of oxygen to glucose plus ½ lactate. (The factor of ½ arises because each mole of glucose theoretically yields two moles of lactate). If lactate efflux to venous blood completely accounts for an OGI less than 6, then the OCI should equal 6 or greater. Alternatively, an OCI less than 6 indicates that lactate efflux to venous blood does not alone account for all of non-oxidative glucose metabolism. Consistent with the original finding of Siesjö[8], Quistroff et al. reported that the population mean OCI from eight studies is approximately 6. However, Rasmussen et al., in a partially overlapping sample of eight studies, reported that the resting OCI was 5.3. Thus, it remains unclear whether lactate fully accounts for non-oxidative glucose metabolism in the resting human brain.

To provide a more accurate estimate of both OGI and OCI in the healthy human brain at rest, we conducted a systematic meta-analysis[10] of studies reporting arterio-venous differences for glucose, oxygen, and lactate. We identified 40 studies with OGI data and 37 partially overlapping studies with OCI data. We then performed a random effects Bayesian meta-analysis[11] to determine the population average OGI and OCI ratios and their credible intervals (CIs).

2.3 Methods

Study Design

Our meta-analysis was conducted using the Preferred Reports Items for Systematic Reviews and Meta-Analyses (PRISMA) guidelines[10]. Figure 2.1 shows a flow diagram of the study procedures. Table 2.1 contains the PRISMA checklist. We did not complete or register an *a priori* study protocol.

Eligibility Criteria

We included studies that reported mean OGI and/or OCI along with either SD or standard error of the mean (SE), or the data necessary to estimate the mean and SE. Only studies that used arterio-venous differences to measure whole-brain OGI and/or OCI were included. OGI and OGI data were typically taken from text or tables, but were extracted from figures if necessary. Table 2.2 lists the data source for each study. If a study did not report either ratio but contained the necessary arterio-venous data, we contacted the corresponding author via the listed email address and requested the required data. Although positron emission tomography (PET) can be used to measure whole-brain OGI[12,13], we chose to exclude these studies because of uncertainty in the value of the lumped constant for [^{18}F]-FDG[14]. We did not include studies from older adult cohorts or from diseased populations (e.g., cardiac, neurological, or mental disorders).

Study Identification

We searched the PUBMED database with several combinations of the terms “Arterial”, “Arterio”, “Brain”, “Carbohydrate”, “Cerebral”, “Glucose”, “Index”, “OCI”, “OGI”, “Oxygen”, “Ratio”, and “Venous” (Table 2.3). In total, we performed 24 separate search queries. All searches were constrained to articles published between 1900 and August 10th, 2017. To limit the amount of animal model studies returned by our searches, we added the Medical Subject Heading (MeSH) keyword “Human” to every search. In addition, the first author (TB) conducted a search of his personal archives for any papers that included measures of cerebral oxygen,

glucose, and lactate metabolism. The papers in the final dataset that were only found in the first authors archives are listed in Table 2.2.

Statistics

A random effects Bayesian meta-analysis[11] was performed to calculate the population average OGI and OCI. A random effects model accounts for differing variance in each study's estimates of OGI and OCI, while simultaneously allowing for heterogeneity between studies. Separate models were run for OGI and OCI. If a study reported multiple values for OGI or OCI, a fixed effects meta-analysis was performed to calculate an overall estimate for that study[15]. Our model assumed that each study's estimate, y_i, is a random sample from a normal distribution:

$$y_i \sim N(\mu + \mu_i, \sigma_i) \qquad (2.1)$$

whereμ is the population mean, $\mu_i$is random offset for study *i*, and σ_i is the study standard deviation. No covariates or other explanatory factors were included in the model. We assume that σ_i is equal to each study's standard error of the mean. The random offsets for each study were also assumed to follow a normal distribution:

$$\mu_i \sim N(0, \tau) \qquad (2.2)$$

where τ is the random effects standard deviation, which reflects the heterogeneity across studies.

The model parameters, μ, μ_i, and τ were estimated using Hamilton Markov Chain Monte Carlo (MCMC) implemented in Stan[16]. The population mean, μ, was given a broad normal prior with a mean of 6 and standard deviation of 2. The random effects standard deviation, τ , was given a uniform prior with a lower limit of 0. Eight randomly initialized chains of 20,000 samples were run for each model. The first 10,000 samples of each chain were discarded as

warm-up. Sample autocorrelation was minimized by only considering every 5th sample. As a result, all inferences are based upon 16,000 posterior samples. Convergence was assessed using the Gelman and Rubin potential reduction statistic, $\hat{R}$[17,18]. $\hat{R}$ is the ratio of within chain variance to the pooled between chain variance. At convergence, $\hat{R}$ should be equal to one. For both models, $\hat{R}$ was with within 10^{-3} of 1 for every parameter. All results are summarized with medians and 95% equal-tailed credible intervals.

The primary parameters of interest where the population means, μ, for OGI and OCI. We also computed the percent of glucose metabolism that is entirely non-oxidative. This was done by assuming a 6:1 stoichiometric ratio: $100 \cdot (1 - OGI/6.0)$. Replacing OGI in this expression with OCI gives the percent of carbohydrate metabolism that is non-oxidative.

Assessment of Bias and Heterogeneity

Risk of bias within studies was assessed by considering four factors: study population, interval between catheterization and measurement, the presence of experimental manipulations, and fasting state. Bias assessment was not a factor in the random effects meta-analysis, and no sub-group analyses are reported. The possibility for bias across studies was assessed using funnel plots[19]. A funnel plot is used to determine if there is any relationship between the reported OGI/OCI value and its standard error. If a meta-analysis is free from publication bias and heterogeneity, the plot should resemble a funnel with the studies with the smallest standard errors clustered around the population average. An asymmetric funnel plot can be an indication of reporting bias or study heterogeneity[20]. To test for funnel plot asymmetry, we used the method recommended by Egger et al.[19,21], which involves a regression model with effect size as the dependent variable and standard error as the independent variable. Our regression model, implemented in the R metafor package[15], also estimated a random effect for each study.

The possibility of study heterogeneity was further quantified using posterior predictive intervals[22] for a random new study. Posterior predictive intervals, which incorporate the uncertainty in parameter estimates, provide a credible interval in which we would expect a new study to fall. All posterior predictive intervals were computed using 16,000 random samples. Finally, we computed the I^2 statistic[23,24]:

$$I^2 = 100 \cdot \frac{\hat{\tau}^2}{\hat{\tau}^2 + \hat{\sigma}^2} \qquad (2.3)$$

where $\hat{\tau}^2$ is the estimated between study variance from the random effects model, and $\hat{\sigma}^2$ is the within study variance:

$$\hat{\sigma}^2 = \frac{\sum_{i=1}^{k} w_i(k-1)}{\left(\sum_{i=1}^{k} w_i\right)^2 - \sum_{i=1}^{k} w_i^2} \qquad (2.4)$$

where k is the number of studies and w_i is the precision of the mean for study *i:* $w_i = 1/\sigma_i^2$. We calculated I^2 for each MCMC sample of $\hat{\tau}^2$ and then computed the median I^2 along with its 95% equal-tailed credible intervals. Higher values of I^2 indicated a greater relative proportion of between study variance and thus greater study heterogeneity.

2.4 Results

Included Studies

Our searches of PUBMED (see Methods) and our own archives identified 927 potential records (Figure 2.1). After reviewing the titles, and if necessary, abstracts of all 927 records, 810 were discarded from further consideration. Records were discarded at this step if they were clearly irrelevant for our purposes (e.g. animal studies). The remaining 117 papers were then subjected to a critical full text review. This review resulted in the rejection of 65 papers (Table

2.4). The majority of papers were rejected because they did not acquire the data necessary to calculate OGI/OCI (n=38) or because they reported values only in experimental states (n=17). For OGI, we found 52 papers that met our requirements for inclusion, 34 of which reported OGI. In addition, we sent 19 requests for data to authors of studies that had the data necessary to report OGI but did not do so. We received data from 6 of these authors, resulting in a total of 40 studies. For OCI, 43 papers met our inclusion requirements. Of these, 32 papers reported the required data, and data requests were sent for the remaining 11. After receiving data from 5 authors, our final OCI dataset contained 37 studies. A summary of the characteristics for the included studies is in Table 2.2. A total of 30 studies measured both OGI and OCI.

Population Average OGI and OCI

Forest plots for OGI and OCI are shown in Figure 2.2 and Figure 2.3, respectively. Note that the random effects models effectively decrease the weight of studies with high standard errors. The population average OGI was 5.46 with a 95% CI of 5.25 to 5.66. As the CI does not overlap 6.0, we can infer that there is significant NOglc at rest. The population average OCI was 5.60 with a 95% CI of 5.36 to 5.84. The fact that the credible intervals do not contain 6 indicates that a significant portion of the brain's glucose consumption is non-oxidative and cannot be accounted for by lactate efflux to the blood.

Bias and Heterogeneity

Within-study bias was assessed in four separate categories: study population, waiting period between catheterization and measurement, experimental manipulations, and fasting state (Table 2.5). The most frequent bias in study population was the use of all male subjects. Nineteen studies included only male subjects. No study included only female subjects. The majority of studies consisted of younger subjects (Table 2.5). Across all studies that reported an average age,

the mean age was 27.2 with a standard deviation (SD) of 4.6. Only five studies specifically mentioned including subjects over the age of 40[25-29]. A few other studies included only hospital patients (e.g. Scheinberg et al., 1949, Takeshita et al., 1972) or competitive athletes (e.g., Voliantis et al., 2008 and Bain et al., 2016). More than half (24/47) of studies included no mention of a waiting period between catheterization and blood sampling. Blood sampling was performed in a variety of positions, the two most common being supine (13) and semi-supine (20). The majority of measurements were performed in the absence of any overt experimental manipulation, however a few studies did include the injection of labeled compounds (e.g., Boyle et al., 1994 and Glenn et al., 2015) or saline (Hasselbalch et al., 1996 and Volianitis et al., 2011). Finally, the requirement for fasting subjects was mixed, with 19 requiring at least some fasting period, 20 including no mention of performing measurements in a fasting state, and the remaining 8 studies assessed subjects in a post-absorptive state.

To assess bias across studies, funnel plots were constructed for both OGI (Figure 2.4A) and OCI (Figure 2.4B). No asymmetry was apparent in either plot. This impression was quantified with a regression test for asymmetry[19]. No significant evidence for asymmetry was found for either OGI (p=0.2013) or OCI (p=0.1948). The lack of asymmetry suggests the absence of reporting bias in our sample. There was, however, substantial horizontal scatter around the population averages, indicating heterogeneity across studies. To further assess this heterogeneity, we computed posterior predictive intervals for a new random study for each ratio. Both ratios showed considerable variability, with the 95% posterior predictive interval for OGI spanning 4.35 to 6.60 and from 4.32 to 6.91 for OCI. Furthermore, the I^2 values were consistent with substantial between study heterogeneity. An estimated 85.03% [95 CI 75.88-91.35] of the

total variance in the OGI meta-analysis was due to study heterogeneity. A similar value of 84.96% [95 CI 75.09-91.60] was found in the OCI analysis.

2.5 Discussion

Our meta-analyses of OGI and OCI reveals that both measures are significantly less than 6. The fact that OGI is less than 6 indicates that a proportion of glucose consumption is non-oxidative, while OCI being less than 6 shows that not all of non-oxidative metabolism can be accounted for by lactate efflux to venous blood. Expressed in terms of percentages non-oxidative metabolism accounts for 9.0% 95 CI [5.67-12.5] of glucose consumption and 6.7% 95 CI [2.67-10.67] of carbohydrate metabolism. Our estimates of the population average OGI (5.46 95% CI [5.25-5.66], and OCI (5.60 with a 95% CI [5.36-5.84]) are based on a much larger set of studies than previous reviews, and are therefore more likely to accurately reflect the true population means. It is of some interest to note the close agreement between our population average OGI and the value of 5.54 originally reported by Kety[4].

Although we did not find any evidence for publication bias, we did find considerable heterogeneity across studies. We computed I^2 for each ratio, which indicated that ~85% of the total variance is attributable to study heterogeneity. Substantial methodical differences (Table 2.5) may account for the variability in measured OGI and OCI values. Many studies included only males and there is evidence of differences in metabolism between males and females[30,31]. Thus, it is likely that our population averages are more representative of male metabolic ratios. Similarly, our population averages are weighted towards the predominantly young adult samples included in our meta-analysis. Many studies also did not specify if they included a waiting period between catheterization and measurement. This may have influenced the reported values, as

metabolic ratios have been shown to decrease during arousal[32]. Finally, not all investigators insured that measurements were performed while subjects were in a basal metabolic state. A few studies infused labeled carbohydrates, and many studies did require that subjects be in a fasting state. Either factor could have affected the published results. For example, OGI is known to increase during hypoglycemia[29]. More direct studies are clearly needed to quantify the sources of heterogeneity in studies measuring OGI and OCI.

There is no clear consensus concerning the role of non-oxidative glucose metabolism in the brain[33]. It has been variously proposed that NOglc (i) allows for the rapid creation of ATP for the Na^+/K^+ ATPase in astrocytes[34], (ii) regulates cellular redox potentials[35], (iii) is a by-product of glycogen breakdown during increased neuronal activation[36], (iv) is necessary for the degradation of glutamate by astrocytes[37], (v) reduces oxidative stress, particularly during periods of cellular growth[38], or (vi) is used to fuel biosynthetic processes[39,40]. Part of the difficulty here is the uncertainty regarding the ultimate fate of glucose that enters non-oxidative pathways. It was traditionally thought that lactate production, and subsequent efflux to venous blood, could completely account for any non-oxidative glucose use[8]. The results of our meta-analysis are not consistent with this idea. The fact that the population average OCI was greater than the average OGI does show that some glucose is converted to lactate and leaves the brain via the venous system. The OCI was less than 6, however, which means this route does not account for all non-oxidative glucose use.

One potential explanation for the OCI being less than 6 is that resting arterio-venous differences simply underestimate the amount of lactate that leaves the brain. Brain lactate concentration has been shown to decrease during sleep[41], suggesting that measurements taken during conscious rest do not fully account for all of lactate efflux. Alternatively, lactate may

leave the brain via routes that bypass the sampling sites used for arterio-venous differences. This idea is supported by a study by Ball et al., who found that injection of radiolabeled glucose and lactate into the inferior colliculus labeled the meninges[42]. Subsequent tracer experiments identified a potential perivascular clearance pathway from the inferior colliculus to the cervical lymph nodes[42]. More recently, components of the glymphatic system have been shown in mice to regulate lactate efflux, as well as the concentration of lactate in cervical lymph nodes[41]. Neither of these experiments, however, quantified the proportion of lactate efflux that occurs via these pathways. Furthermore, if perivascular/glymphatic clearance does play a role in lactate removal, it is not clear what impact it would have on arterio-venous difference measurements. In sheep, rats, and rabbits approximately half of CSF is cleared through lymphatic pathways[43]. The other half enters the venous sinuses through the arachnoid villi, and therefore would presumably be accounted for by venous samples taken at the level of the jugular bulb. Although exact proportions are not available, it has been proposed that the arachnoid pathway plays a much a larger role in humans[43]. If true, this would suggest that perivascular/glymphatic clearance cannot fully account for the OCI being less than 6. Direct experimental approaches are clearly needed to address this question.

An alternative possibility is that the carbon from non-oxidative glucose metabolism leaves the brain as metabolites other than CO_2 or lactate. Although pyruvate is well-known to have a net efflux from the brain, it is unlikely to account for much of the unexplained fraction, as net pyruvate efflux is nearly an order of magnitude less than that of lactate[44]. Numerous other carbon-containing compounds, however, have also been shown to leave the brain. For example, there is a small net efflux of glutamine from the brain[45,46]. In addition, peptides and proteins are known to exit the brain via the CSF[47]. The most well-studied of these are amyloid-beta[48,49] and

tau[50], which are both markers of Alzheimer's disease[51]. Other molecules, such as leptin[52] and cholesterol[53], have also been shown to leave the brain in small amounts. In contrast, Rasmussen et al. reported that using nuclear magnetic resonance spectroscopy , there were no detectable cerebral arterio-venous differences for any carbon sources other than glucose and lactate[54]. However, it is unclear exactly which carbon-based compounds were examined by Rasmussen et al. Therefore, future experiments with labeled compounds are needed to elucidate how, and in what proportions, glucose derived carbon leaves the brain.

Although we are not aware of any studies directly linking NOglc with the synthesis, and subsequence efflux, of specific glucose metabolites, there is evidence linking non-oxidative metabolism with biosynthesis more generally. Madsen et al., found that OGI was depressed after the performance of the Wisconsin Card Sorting task, while lactate efflux returned to baseline values[55]. Similarly, our group recently reported that, hours after the performance of a covert motor learning task, non-oxidative glucose use was elevated in Brodmann Area 44[56]. Moreover, the change in non-oxidative glucose use was positively correlated with performance during the learning task. Both of these studies are consistent with the hypothesis that glucose is used in a non-oxidative manner to support learning-induced synaptic plasticity. Extending these findings to other learning paradigms (e.g. episodic memory) would provide additional evidence along these lines.

A prior meta-analysis from our group found that non-oxidative glucose use is markedly elevated during early childhood[40], a period of brain growth[57]. This finding was recently supported by Segarra-Mondejar et al., who found that glucose consumption is necessary for neurite outgrowth *in vitro* and *in vivo* [58]. Interestingly, the findings of Segarra-Mondejar et al. also suggest that at least a part of the glucose necessary for neurite outgrowth is directly

incorporated into newly synthesized lipids[58]. Finally, regional differences in non-oxidative metabolism[39,59] have been shown to correlate positively with expression of genes related to synaptic plasticity and development[40]. Taken together, these findings strongly suggest that NOglc contributes to biosynthetic processes in the brain. Quantifying the contribution of non-oxidative glucose metabolism to biosynthesis will be an important topic for future studies. Combining a PET marker of protein synthesis[60], such as L-[1-^{11}C]-leucine PET[61,62] with measures of non-oxidative glucose use during a learning task could provide further evidence that learning is accompanied by increases in biosynthesis and non-oxidative glucose metabolism. ^{13}C magnetic resonance spectroscopy could also be used to measure the movement of glucose and other carbohydrates through different metabolic pathways[63,64].

In summary, on the basis of a meta-analysis of 47 studies, we estimated that non-oxidative processes account for 9% of glucose metabolism in the brain, a significant portion of which cannot be accounted for by lactate efflux to the blood. We also found substantial heterogeneity across studies, likely attributable to differences in methodology. Future studies are needed to determine both the function of non-oxidative metabolism and the ultimate fate of glucose consumed in the brain.

2.6 Figures

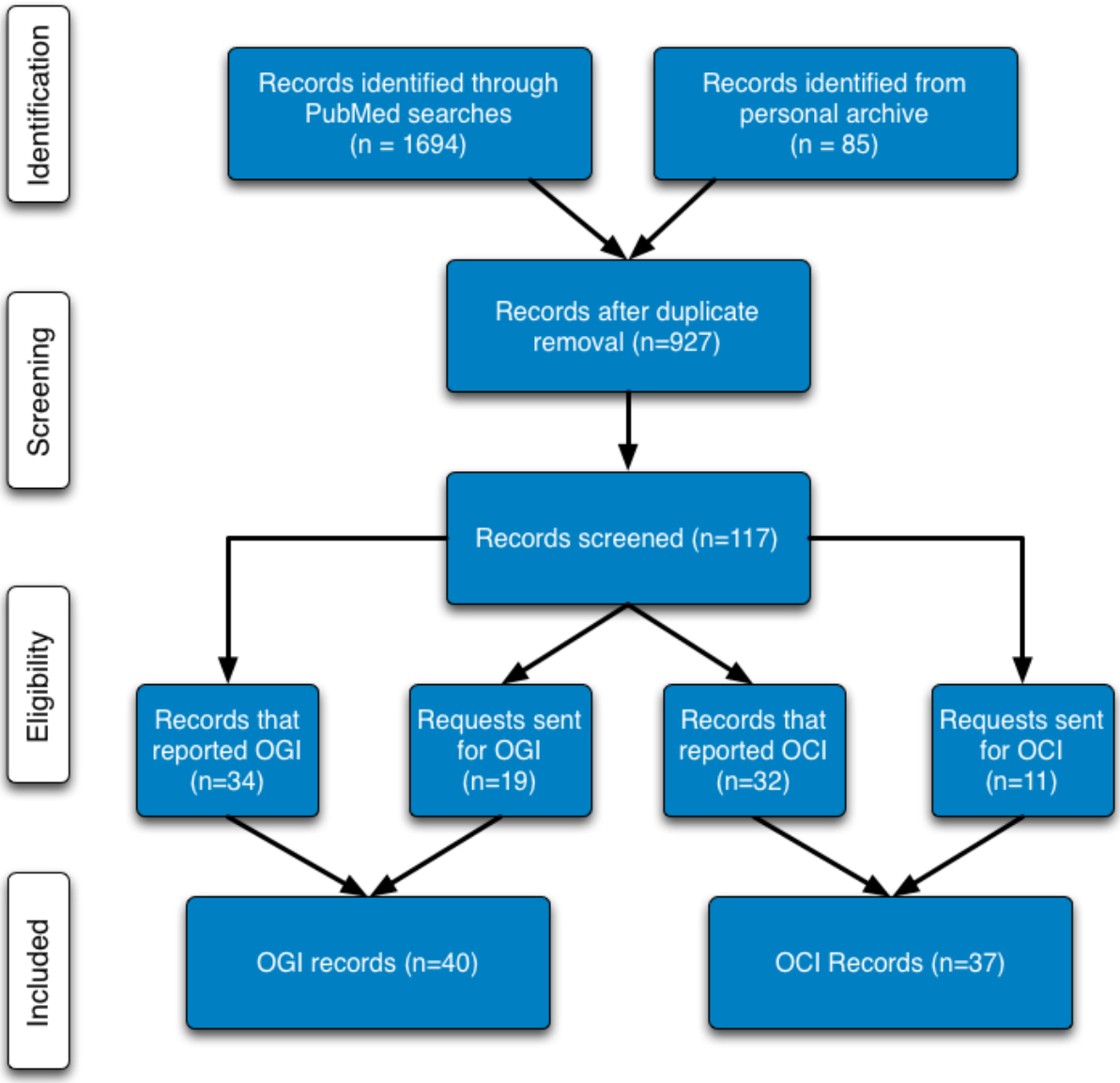

Figure 2.1: Modified PRISMA flow diagram

Included studies were selected using the indicated selection criteria.

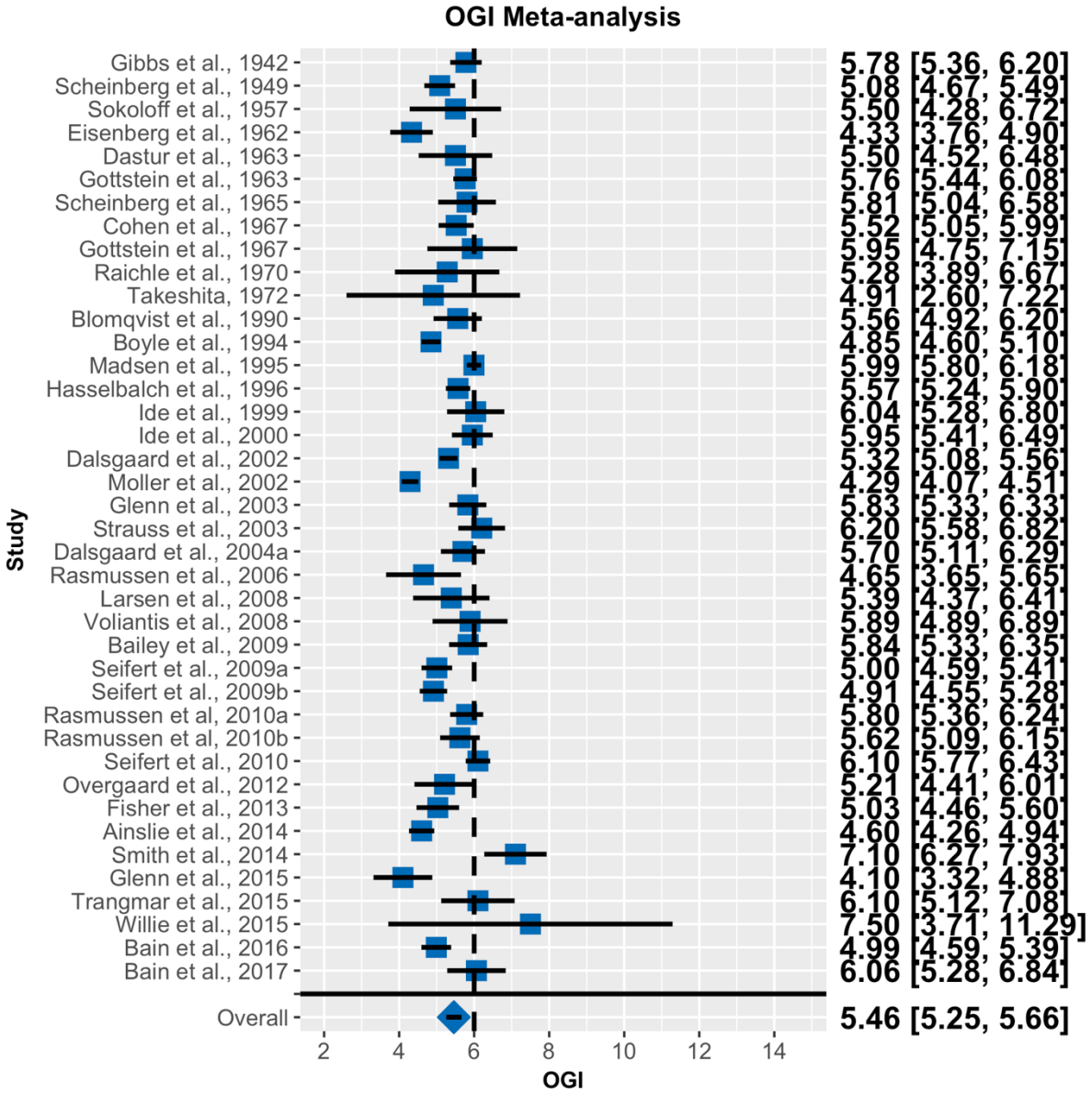

Figure 2.2: Forest plot for OGI meta-analysis

Blue squares represent the reported mean OGI for each study. Black lines represent 95% confidence intervals. Numeric values for these quantities are also listed. The blue diamond is the population average from the Bayesian random effects meta-analysis. Error bars/values for the population mean are 95% CIs (n=40).

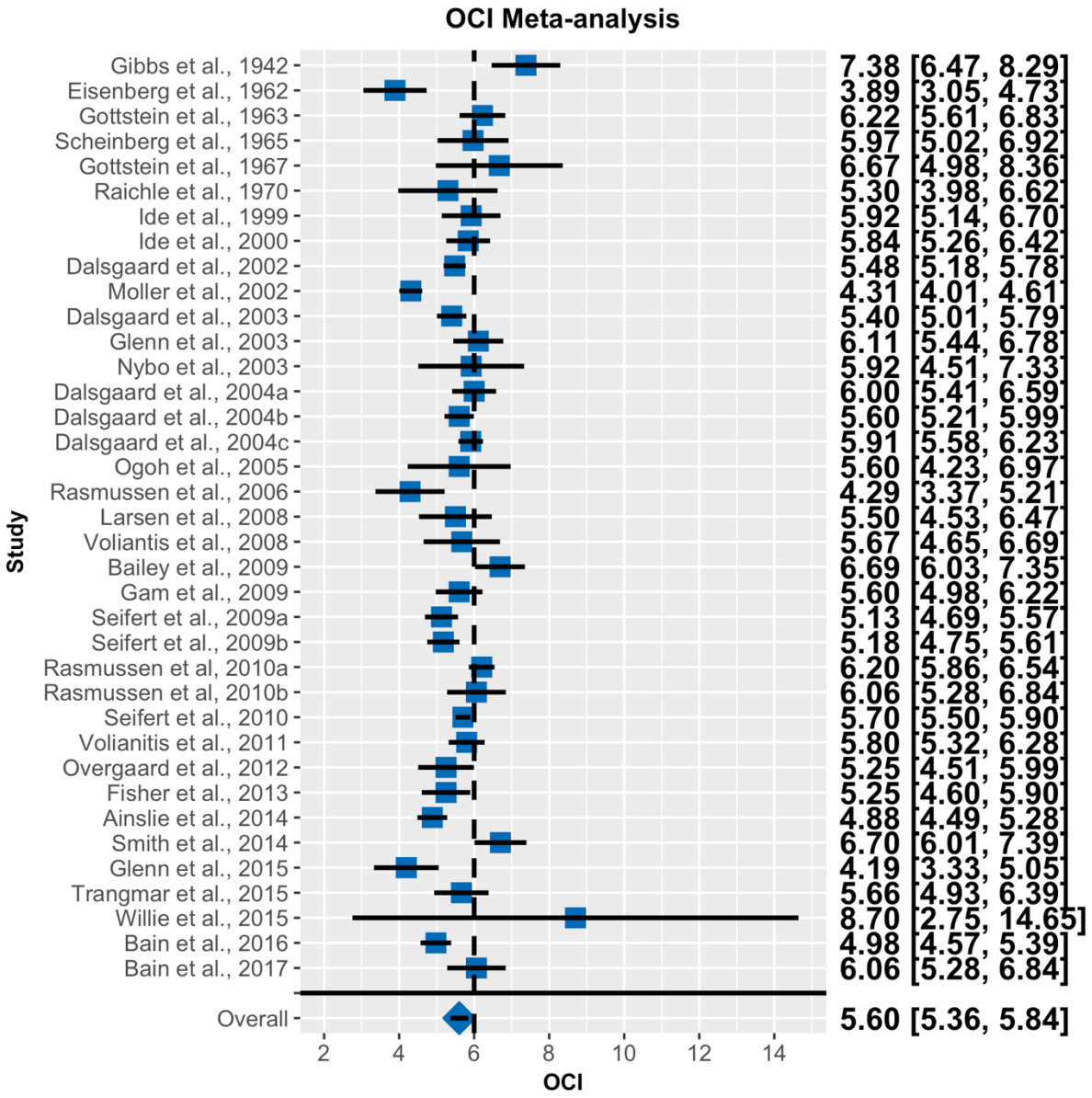

Figure 2.3: Forest plot for OCI meta-analysis

Same convention as in Fig 2 (n=37).

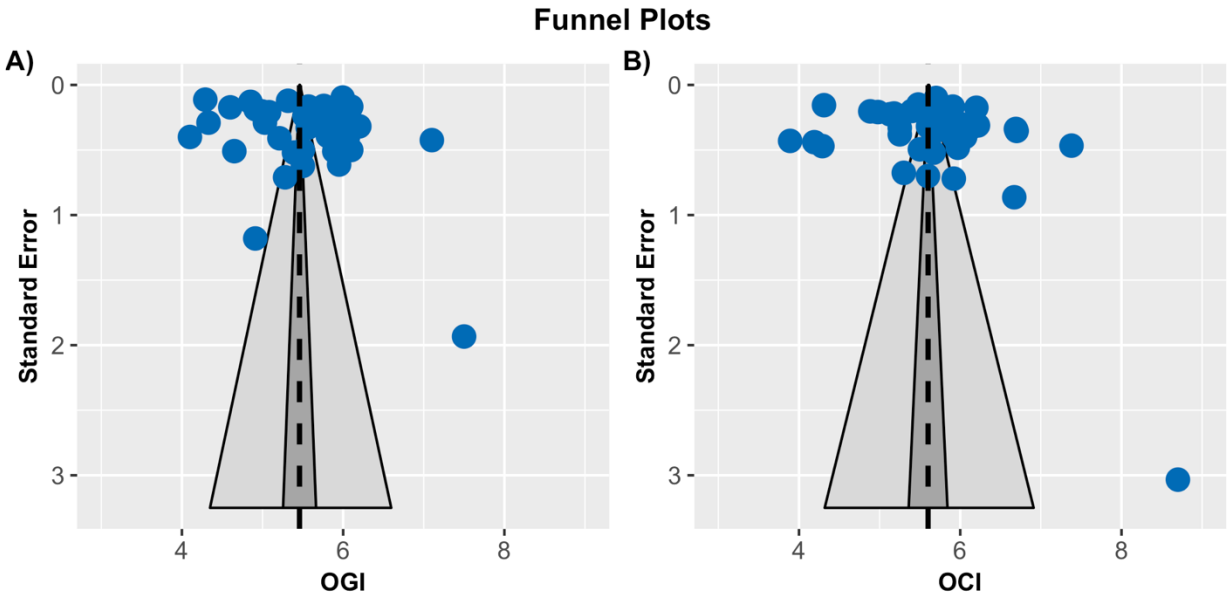

Figure 2.4: Publican bias and between study heterogeneity

Funnel plots for **A)** OGI and **B)** OCI. In each plot, the reported study mean is plotted against its standard error. The population average is the dashed black line, its 95% percent CI is in dark gray, and its 95% prediction interval is in light gray. The lack of any asymmetry is evidence against substantial publication bias. The wide scatter around the population average, however, suggests that there is substantial heterogeneity between studies.

2.7 Tables

Table 2.1: PRISMA checklist

Section/topic	#	Checklist item	Reported on page #
TITLE			
Title	1	Identify the report as a systematic review, meta-analysis, or both.	1
ABSTRACT			
Structured summary	2	Provide a structured summary including, as applicable: background; objectives; data sources; study eligibility criteria, participants, and interventions; study appraisal and synthesis methods; results; limitations; conclusions and implications of key findings; systematic review registration number.	51
INTRODUCTION			
Rationale	3	Describe the rationale for the review in the context of what is already known.	51
Objectives	4	Provide an explicit statement of questions being addressed with reference to participants, interventions, comparisons, outcomes, and study design (PICOS).	51
METHODS			
Protocol and registration	5	Indicate if a review protocol exists, if and where it can be accessed (e.g., Web address), and, if available, provide registration information including registration number.	53
Eligibility criteria	6	Specify study characteristics (e.g., PICOS, length of follow-up) and report characteristics (e.g., years considered, language, publication status) used as criteria for eligibility, giving rationale.	53
Information sources	7	Describe all information sources (e.g., databases with dates of coverage, contact with study authors to identify additional studies) in the search and date last searched.	53
Search	8	Present full electronic search strategy for at least one database, including any limits used, such that it could be repeated.	53, 69
Study selection	9	State the process for selecting studies (i.e., screening, eligibility, included in systematic review, and, if applicable, included in the meta-analysis).	53
Data collection process	10	Describe method of data extraction from reports (e.g., piloted forms, independently, in duplicate) and any processes for obtaining and confirming data from investigators.	53
Data items	11	List and define all variables for which data were sought (e.g., PICOS, funding sources) and any assumptions and simplifications made.	53
Risk of bias in individual studies	12	Describe methods used for assessing risk of bias of individual studies (including specification of whether this was done at the study or outcome level), and how this information is to be used in any data synthesis.	53

Summary measures	13	State the principal summary measures (e.g., risk ratio, difference in means).	53
Synthesis of results	14	Describe the methods of handling data and combining results of studies, if done, including measures of consistency (e.g., I^2) for each meta-analysis.	53
Risk of bias across studies	15	Specify any assessment of risk of bias that may affect the cumulative evidence (e.g., publication bias, selective reporting within studies).	53
Additional analyses	16	Describe methods of additional analyses (e.g., sensitivity or subgroup analyses, meta-regression), if done, indicating which were pre-specified.	NA
RESULTS			
Study selection	17	Give numbers of studies screened, assessed for eligibility, and included in the review, with reasons for exclusions at each stage, ideally with a flow diagram.	57, 65
Study characteristics	18	For each study, present characteristics for which data were extracted (e.g., study size, PICOS, follow-up period) and provide the citations.	71
Risk of bias within studies	19	Present data on risk of bias of each study and, if available, any outcome level assessment (see item 12).	57, 84
Results of individual studies	20	For all outcomes considered (benefits or harms), present, for each study: (a) simple summary data for each intervention group (b) effect estimates and confidence intervals, ideally with a forest plot.	57, 66, 67
Synthesis of results	21	Present results of each meta-analysis done, including confidence intervals and measures of consistency.	57, 66, 67
Risk of bias across studies	22	Present results of any assessment of risk of bias across studies (see Item 15).	57, 68
Additional analysis	23	Give results of additional analyses, if done (e.g., sensitivity or subgroup analyses, meta-regression [see Item 16]).	NA
DISCUSSION			
Summary of evidence	24	Summarize the main findings including the strength of evidence for each main outcome; consider their relevance to key groups (e.g., healthcare providers, users, and policy makers).	60
Limitations	25	Discuss limitations at study and outcome level (e.g., risk of bias), and at review-level (e.g., incomplete retrieval of identified research, reporting bias).	60
Conclusions	26	Provide a general interpretation of the results in the context of other evidence, and implications for future research.	60
FUNDING			
Funding	27	Describe sources of funding for the systematic review and other support (e.g., supply of data); role of funders for the systematic review.	NA

Table 2.2: Summary characteristics of included studies

Studies that were found only through searching the first authors records are indicated by a *. (NA = Not Applicable).

Reference	PMID	Journal	Population	Year	OGI N	OGI Source	OCI N	OCI Source	Age	Age Error	Age Error Type	Sub-Study
Gibbs et al., 1942[1]*	NA	Journal of Biological Chemistry	Healthy young men	1942	33	Table	33	Table	22.9	2.36	SD	NA
Scheinberg et al., 1949[65]*	16695788	The Journal of Clinical Investigation	Normal men (17 medical students, 3 hospital patients without disease)	1949	14	Table	NA	NA	25.1	4.04	SD	Erect
Scheinberg et al., 1949[65]*	16695788	The Journal of Clinical Investigation	Normal men (17 medical students, 3 hospital patients without disease)	1949	18	Table	NA	NA	25.1	4.04	SD	Supine
Sokoloff et al., 1957[25]*	13425236	Annals of the New York	Normal patients	1957	8	Table	NA	NA	24.5	9.1	SD	NA

		Academy of Sciences										
Eisenberg et al.,1962[26]*	NA	Metabolism	Healthy subjects	1962	21	Table	10	Table	40.3	6.2	SD	Control
Dastur et al., 1963[66]*	NA	Human Aging: A Biological and Behavioral Study	Normal young subjects	1963	15	Table	NA	NA	20.8	0.4	SE	NA
Gottstein et al., 1963[67]*	14103599	Klin Wochenschr	NA	1963	32	Table	18	Table	21-69	NA	NA	NA
Scheinberg et al., 1965[28]*	14247382	Journal of Neurological Sciences	Normal volunteers and hospitalized patients without evidence for disease	1965	21	Table	20	Table	32.3	6.9	SD	NA
Cohen et al., 1967[68]*	6031186	The Journal of Applied Physiology	Healthy adult male volunteers	1967	9	Table	NA	NA	21-25	NA	NA	NA
Gottstein et al., 1967[29]*	NA	Klinische Wochenschrift	Normal patients	1967	12	Table	12	Table	30-60	NA	NA	NA

Raichle et al., 1970[69]*	5471647	Archives of Neurology	Healthy men	1970	3	Table	3	Table	NA	NA	NA	NA
Takeshita, 1972[70]*	5006989	Anesthesiology	Healthy patients prior to elective surgery (no cardiopulmonary or neurologic disorders)	1972	6	Table	NA	NA	43	3	SE	NA
Blomqvist et al., 1990[71]*	2112135	Journal of Cerebral Blood Flow and Metabolism	Healthy normal volunteers	1990	7	Table	NA	NA	NA	NA	NA	NA
Boyle et al., 1994[72]*	8113391	The Journal of Clinical Investigation	Normal volunteers	1994	12	Table	NA	NA	25	2	SE	NA
Madsen et al., 1995[55]	7714007	Journal of Cerebral Blood Flow and Metabolism	Healthy, young, non-medicated volunteers	1995	8	Table	NA	NA	25	NA	NA	Study 2
Madsen et al., 1995[55]	7714007	Journal of Cerebral Blood Flow and Metabolism	Healthy, young, non-medicated volunteers	1995	9	Table	NA	NA	25	NA	NA	Study 1

Hasselbalch et al., 1996[73]*	8967461	American Journal of Physiology	Healthy volunteers of normal weight	1996	8	Table	NA	NA	24	4	SD	NA
Ide et al., 1999[74]	10562597	Journal of Applied Physiology	Healthy volunteers	1999	12	Table	12	Table	23	1	SE	NA
Ide et al., 2000[75]	10618160	The Journal of Physiology	Healthy volunteers	2000	6	Table	6	Table	25	2	SD	NA
Dalsgaard et al., 2002[76]	11956354	The Journal of Physiology	Healthy subjects	2002	10	Table	10	Table	25	4	SE	Study 1
Dalsgaard et al., 2002[76]	11956354	The Journal of Physiology	Healthy subjects	2002	10	Table	10	Table	25	1	SE	Study 2
Møller et al., 2002[77]*	12368665	Journal of Cerebral Blood Flow and Metabolism	Healthy human volunteers	2002	8	Author	8	Author	25	NA	NA	NA
Dalsgaard et al., 2003[78]	12621535	Experimental Physiology	Healthy subjects	2003	NA	NA	10	Text	24	NA	NA	NA
Glenn et al., 2003[79]*	14526234	Journal of Cerebral Blood Flow and Metabolism	Normal volunteers	2003	31	Table	31	Author	33.3	8.3	SD	Control

Nybo et al., 2003[80]	12754171	Journal of Applied Physiology	Healthy endurance-trained men	2003	NA	NA	8	Figure	27	2	SE	NA
Strauss et al., 2003[81]	14625823	Liver Transplantation	Healthy subjects	2003	8	Table	NA	NA	NA	NA	NA	NA
Dalsgaard et al., 2004a[82]	14608005	The Journal of Physiology	Healthy subjects	2004	9	Text	9	Text	25	1	SE	NA
Dalsgaard et al., 2004b[83]	15155282	Regulatory, Integrative and Comparative Physiology	Healthy non-athlete males	2004	NA	NA	8	Text	22	1	SE	NA
Dalsgaard et al., 2004c[84]	15208287	The Journal of Applied Physiology	Healthy young men	2004	NA	NA	7	Text	22	1	SE	Cycling
Dalsgaard et al., 2004c[84]	15208287	The Journal of Applied Physiology	Healthy young men	2004	NA	NA	8	Text	26	1	SE	Arm cranking
Ogoh et al., 2005[85]	15498819	Heart and Circulatory Physiology	Healthy adults	2005	NA	NA	7	Table	23	2	SD	NA
Rasmussen et al., 2006[44]	16794025	Journal of Applied Physiology	Healthy men	2006	8	Author	8	Author	22-29	NA	NA	NA

Larsen et al., 2008[86]	18403423	The Journal of Physiology	Healthy males	2008	8	Figure	8	Text	27	6	SD	NA
Voliantis et al., 2008[87]	17932151	The Journal of Physiology	Healthy males	2008	6	Table	6	Table	32	4	SE	NA
Bailey et al., 2009[88]	19726713	Regulatory, Integrative and Comparative Physiology	Healthy men	2009	11	Author	10	Author	27	4	SD	Normoxia
Gam et al., 2009[89]	19659603	Clinical Physiology and Functional Imaging	Sedentary trained males	2009	NA	NA	8	Text	33	6	SD	NA
Seifert et al., 2009a[90]	19605762	Regulatory, Integrative and Comparative Physiology	Sedentary healthy males	2009	7	Figure	7	Figure	32	6	SD	Control After
Seifert et al., 2009a[90]	19605762	Regulatory, Integrative and Comparative Physiology	Sedentary healthy males	2009	7	Figure	7	Figure	32	6	SD	Training Before
Seifert et al., 2009a[90]	19605762	Regulatory, Integrative and	Sedentary healthy males	2009	10	Figure	7	Figure	30	5	SD	Control Before

		Comparative Physiology										
Seifert et al., 2009b[91]	19015195	The Journal of Physiology	Healthy subjects	2009	10	Text	10	Text	24	3	SD	Adrenaline
Seifert et al., 2009b[91]	19015195	The Journal of Physiology	Healthy subjects	2009	8	Text	8	Text	27	7	SD	Noradrenaline
Rasmussen et al, 2010a[92]	20403976	The Journal of Physiology	Young adult males	2010	16	Table	16	Table	20-34	NA	NA	NA
Rasmussen et al, 2010b[93]	20522733	Journal of Applied Physiology	Young males	2010	7	Figure	7	Figure	18-34	NA	NA	NA
Seifert et al., 2010[94]	20660020	Experimental Physiology	Young healthy males	2010	9	Table	9	Table	23	4	SD	NA
Volianitis et al., 2011[95]	21098003	The Journal of Physiology	Healthy males	2011	NA	NA	6	Text	23	2	SD	NA
Overgaard et al., 2012[96]	22441982	The FASEB Journal	Healthy individuals	2012	9	Table	9	Table	26	6	SD	NA
Fisher et al., 2013[97]	23230234	The Journal of Physiology	Young adults	2013	11	Figure	11	Figure	22	1	SE	NA
Ainslie et al., 2014[5]	24117382	Clinical Science	Healthy adults	2014	10	Table	10	Table	28	4.5	SD	Hypoxia trial

Ainslie et al., 2014[5]	24117382	Clinical Science	Healthy adults	2014	10	Table	10	Table	28	4.5	SD	Hyperoxia trial
Smith et al., 2014[98]	25362150	The Journal of Physiology	Young adult males	2014	8	Table	8	Table	30	6	SD	NA
Glenn et al., 2015[99]*	25594628	Journal of Neurotrauma	Healthy volunteers	2015	6	Author	6	Author	28.2	8.2	SD	Control
Trangmar et al., 2015[100]	26371170	Heart and Circulatory Physiology	Endurance trained males	2015	10	Text	10	Figure	29	5	SD	NA
Willie et al., 2015[6]	25690474	Journal of Cerebral Blood Flow and Metabolism	Healthy-young subjects	2015	9	Table	9	Table	30.4	7	SD	NA
Bain et al., 2016[101]*	27256521	The Journal of Physiology	Breath-hold divers	2016	14	Author	14	Table	29.5	7.3	SD	NA
Bain et al., 2017[102]*	28071964	Journal of Cerebral Blood Flow and Metabolism	Breath-hold divers	2017	11	Author	11	Table	31	8	SD	NA

Table 2.3: PubMed search terms

Number	Terms
1	Oxygen AND Arterio AND Venous AND Brain
2	Oxygen AND Arterio AND Venous AND Cerebral
3	Lactate AND Arterio AND Venous AND Brain
4	Lactate AND Arterio AND Venous AND Cerebral
5	Glucose AND Arterio AND Venous AND Brain
6	Glucose AND Arterio AND Venous AND Cerebral
7	Oxygen AND Arterial AND Venous AND Brain
8	Oxygen AND Arterial AND Venous AND Cerebral
9	Lactate AND Arterial AND Venous AND Brain
10	Lactate AND Arterial AND Venous AND Cerebral
11	Glucose AND Arterial AND Venous AND Brain
12	Glucose AND Arterial AND Venous AND Cerebral
13	OGI AND Brain
14	OGI AND Cerebral
15	OCI AND Brain
16	OCI AND Cerebral
17	Oxygen AND Glucose AND Index AND Brain
18	Oxygen AND Glucose AND Index AND Cerebral
19	Oxygen AND Carbohydrate AND Index AND Brain
20	Oxygen AND Carbohydrate AND Index AND Cerebral
21	Oxygen AND Glucose AND Ratio AND Brain

22	Oxygen AND Glucose AND Ratio AND Cerebral
23	Oxygen AND Carbohydrate AND Ratio AND Brain
24	Oxygen AND Carbohydrate AND Ratio AND Cerebral

Table 2.4: Papers excluded after a full-text review

Reference	PMID	Journal	Reason for Exclusion
Wortis et al. 1940[103]	NA	The American journal of psychiatry	Data not sufficient
Gibbs et al. 1945[104]	NA	The American journal of psychiatry	No control data
Kety et al. 1948a[105]	16695569	The Journal of clinical investigation	Data not sufficient
Kety et al. 1948b[106]	16695568	The Journal of clinical investigation	Data not sufficient
Kety et al. 1951[107]	14833874	Pharmacological reviews	Data not sufficient
Fazekas et al. 1952[108]	14902811	The American journal of the medical sciences	Data not sufficient
Novack et al. 1953[109]	13042927	Circulation	No control data
Scheinberg et al. 1953[110]	13057407	A.M.A. archives of neurology and psychiatry	Data not sufficient
Sokoloff et al. 1953[111]	13044828	The Journal of clinical investigation	Data not sufficient
Schieve et al. 1953[112]	13065315	The American journal of medicine	Data not sufficient
Shenkin et al. 1953[113]	13052708	The Journal of clinical investigation	Data not sufficient
Sokoloff et al. 1955[114]	14392225	The Journal of clinical investigation	Data not sufficient
Mangold et al. 1955[115]	14392224	The Journal of clinical investigation	Data not sufficient
Kety et al. 1956[116]	13306754	Journal of chronic diseases	Data not sufficient
Kennedy et al. 1957[117]	13449166	The Journal of clinical investigation	Data not sufficient
Rowe et al. 1959[118]	14439685	The Journal of clinical investigation	Data not sufficient
Kety et al. 1960[119]	NA	Methods in Medical Research	Data not sufficient
Porta et al. 1964[120]	14127087	Metabolism: clinical and experimental	No control data
Alexander et al. 1968[121]	5635772	Journal of applied physiology	No control data
Lewis et al. 1974[122]	4154353	Journal of neurochemistry	Data not sufficient
Raichle et al. 1975[123]	1155625	The American journal of physiology	Data not sufficient
Gottstein et al. 1976[124]	1271691	Klinische Wochenschrift	No control data
Van Aken et al. 1976[125]	1015217	Acta anaesthesiologica Belgica	Data not sufficient

Juhlin-Dannfelt et al. 1977[126]	929098	Scandinavian journal of clinical and laboratory investigation	Data not sufficient
Hertz et al. 1981[127]	7009645	The Journal of clinical investigation	No control data
Eriksson et al. 1983[128]	6619869	Journal of neurochemistry	Data not sufficient
Dastur et al. 1985[129]	3972914	Journal of cerebral blood flow and metabolism	Data not sufficient
Fox et al. 1988[12]	3260686	Science	PET study
Hatazawa et al. 1988[130]	3259242	Journal of cerebral blood flow and metabolism	PET study
Warrell et al. 1988[131]	2900921	Lancet	No control data
Blomqvist et al. 1998[132]	9789584	Acta physiologica Scandinavica	Data not sufficient
Grill et al. 1990[133]	2110424	The American journal of physiology	Error of OGI/OCI not reported
Leenders et al. 1990[134]	2302536	Brain	Data not sufficient
Gutniak et al. 1990[135]	2185663	The American journal of physiology	Data not sufficient
Burgess et al. 1991[136]	2020274	Medicine and science in sports and exercise	Data not sufficient
Blomqvist et al. 1991[137]	1743207	European journal of nuclear medicine	Data not sufficient
Pollard et al. 1997[138]	9377885	Critical care medicine	Data not sufficient
Mielck et al. 1998[139]	9813515	British journal of anaesthesia	OGI/OCI not reported
Schaffranietz et al. 1998[140]	9584928	Neurological research	No control data
Wahren et al. 1999[141]	10440122	Diabetologia	OGI/OCI not reported
Madsen et al. 1999[142]	10197509	Journal of cerebral blood flow and metabolism	Data not sufficient
Takahashi et al. 1999[143]	10369366	American journal of neuroradiology	Data not sufficient
Møller et al. 2002[144]	12027852	Acta anaesthesiologica Scandinavica	Repeated data[77]
Nybo et al. 2002[145]	12070186	Journal of applied physiology	Repeated data[80]
Lancaster et al. 2004[146]	15544165	Cell stress & chaperones	Data not sufficient
Dalsgaard et al. 2004[147]	15123562	Experimental physiology	Repeated data[82]

Cremer et al. 2004[148]	15114206	Anesthesiology	Data not sufficient
Blomstrand et al. 2005[149]	16218925	Acta physiologica Scandinavica	Data not sufficient
Chieregato et al. 2007[150]	17893572	Journal of neurosurgical anesthesiology	No control data
Seifert et al. 2008[151]	19053964	Acta physiologica	Data not sufficient
Quistorff et al. 2008[9]	18653766	FASEB journal	Data not sufficient
Holbein et al. 2009[152]	19196488	Critical care	No control data
van Hall et al. 2009[153]	19337275	Journal of cerebral blood flow and metabolism	Data not sufficient
Espenell et al. 2010[154]	20661680	Canadian journal of anesthesia	No control data
Powers et al. 2010[155]	20959851	Journal of cerebral blood flow and metabolism	PET study
Rasmussen et al. 2010[156]	20102344	Acta physiologica	No control data
Smith et al. 2012[157]	23019310	Journal of applied physiology	Data not sufficient
Mikkelsen et al. 2014[158]	25415176	The Journal of clinical endocrinology and metabolism	No control data
Glenn et al. 2015[159]	25279664	Journal of neurotrauma	No control data
Fabricius-Bjerre et al. 2014[160]	24903076	Clinical physiology and functional imaging	No control data
Lewis et al. 2014[161]	25217373	The Journal of physiology	Data not sufficient
Trangmar et al. 2014[162]	24835170	The Journal of physiology	Repeated data[100]
Tholance et al. 2015[163]	25668478	Neurological research	No control data
Slusher et al. 2015[164]	25771935	Journal of neuroendocrinology	Data not sufficient
Grüne et al. 2017[165]	28207907	PloS one	No control data

Table 2.5: Assessment of bias within studies.

Abbreviations: NA = Not Applicable; NS = Not stated

Reference	Study Population	Waiting Period	Position	Experimental Manipulation(s)	Fasting
Gibbs et al., 1942[1]	All males.	~30 min.	Supine	None	NS
Scheinberg et al., 1949[65]	3 illness free hospital patients.	40 to 50 min.	Supine and Erect	None	Yes
Sokoloff et al., 1957[25]	1 participant was a patient with an anxiety disorder.	NS	NS	Some participants had been given LSD a week earlier.	NS
Eisenberg et al., 1962[26]	None	NS	NS	None	Yes
Dastur et al., 1963[66]	None	NS	NS	None	NS
Gottstein et al., 1963[67]	Patients aged up to 61 years	NS	NS	None	NS
Scheinberg et al., 1965[28]	Some subjects were hospital patients without disease	20 min.	Supine	None	Yes (12 hours)
Cohen et al., 1967[68]	All male	NS	Supine	None	Yes

Gottstein et al., 1967[29]	Patients with normal metabolism	NS	NS	None	NS
Raichle et al., 1970[69]	None	NS	Reclining	None	NS
Takeshita, 1972[70]	Patients scheduled for elective surgery	NS	NS	Given atropine	NS
Blomqvist et al., 1990[71]	None	NS	NS	None	NS
Boyle et al., 1994[72]	None	2 hours	NS	Sleep reduction; Subjects were infused with 6,6-D2-glucose;	No
Madsen et al., 1995[55]	None	~1 hour	Supine	None	Yes (14 hours)
Hasselbalch et al., 1996[73]	None	1 hour	Supine	Saline infusion	No
Ide et al., 1999[74]	None	NS	Semi-supine	None	No
Ide et al., 2000[75]	None	NS	Semi-supine	None	NS
Dalsgaard et al., 2002[76]	None	NS	Semi-supine	None	NS
Møller et al., 2002[77]	None	1 hour	Supine	Subjects were infused with isotonic glucose	Yes (Overnight)
Dalsgaard et al., 2003[78]	None	NS	Semi-supine	None	No
Glenn et al., 2003[79]	None	NS	NS	None	NS
Nybo et al., 2003[80]	All trained males	30 min.	NS	None	No

Strauss et al., 2003[81]	None	NS	Supine	Subjects were infused with 5% glucose.	Yes (Overnight)
Dalsgaard et al., 2004a[82]	None	NS	Semi-supine	None	Yes (8 hours)
Dalsgaard et al., 2004b[83]	All male	1 hour	Semi-supine	None	Yes (Overnight)
Dalsgaard et al., 2004c[84]	All male	NS	Semi-supine	None	Yes (Overnight)
Ogoh et al., 2005[85]	All male	NS	Semi-supine	None	Yes (Overnight)
Rasmussen et al., 2006[44]	All male	1.5 hours	Semi-supine	None	Yes (Overnight)
Larsen et al., 2008[86]	All male	1 hour	Semi-supine	None	Yes (Overnight)
Voliantis et al., 2008[87]	All trained male rowers	NS	Semi-supine	None	Yes (8 hours)
Bailey et al., 2009[88]	All male	30 min.	Supine	Subjects breathed 21% O_2	Yes (12 hours)
Gam et al., 2009[89]	All male	1 hour	Semi-supine	None	NS
Seifert et al., 2009a[90]	All overweight males	1 hour	Semi-supine	None	No
Seifert et al., 2009b[91]	None	1 hour	Supine	Some subjects received a saline control infusion	No
Rasmussen et al, 2010a[92]	All male	NS	Semi-supine	None	NS
Rasmussen et al, 2010b[93]	All male	NS	Semi-supine	Saline injected control; Some had received an EPO trial 3 months earlier	NS
Seifert et al., 2010[94]	All male	30 min.	Semi-supine	None	NS

Volianitis et al., 2011[95]	All males and competitive rowers	NS	Semi-supine	Saline infusion control; Some subjects performed bicarbonate trial ~1-2 weeks earlier	Yes (Overnight)
Overgaard et al., 2012[96]	None	2 hours	Supine	Some subjects performed a hypoxia exercise trial at least two weeks prior; Infused with [1-^{13}C] lactate and labeled bicarbonate	No
Fisher et al., 2013[97]	None	1 hour	Semi-supine	None	Yes (2h)
Ainslie et al., 2014[5]	None	30 min.	Supine	Some measurements were performed after hypoxia trials.	Yes (2h)
Smith et al., 2014[98]	All male	25 min.	Supine	None	Yes (4h)
Glenn et al., 2015[99]	None	NS	Semi-supine	Infusion of [3-^{13}C] lactate and D2 glucose	NS
Trangmar et al., 2015[100]	All trained males	~1 hour	Semi-supine	None	NS
Willie et al., 2015[6]	All male	~30 min.	NS	Subjects underwent an arterial blood gas clamp	NS
Bain et al., 2016[101]	All subjects were elite breath hold divers	30 min	NS	None	NS
Bain et al., 2017[102]	All subjects were elite	NS	NS	None	NS

	breath hold divers				

2.8 References

1 Gibbs EL, Lennox WG, Nims LF, Gibbs FA. Arterial and cerebral venous blood arterial-venous differences in man. *J Biol Chem* 1942; **144**: 325–332.

2 Lennox WG, Leonhardt E. The respiratory quotient of the brain and of extremities in man. *Arch Neurol Psychiat* 1931; **26**: 719–724.

3 Shenkin HA, Harmel MH, Kety SS. Dynamic anatomy of the cerebral circulation. *Arch Neurol Psychiat* 1948; **60**: 240–252.

4 Kety SS. The General Metabolism Of The Brain *In Vivo*. In: Richter D (ed). *Metabolism Of The Nervous System*. London, 1957, pp 221–327.

5 Ainslie PN, Shaw AD, Smith KJ, Willie CK, Ikeda K, Graham J *et al.* Stability of cerebral metabolism and substrate availability in humans during hypoxia and hyperoxia. *Clin Sci* 2014; **126**: 661–670.

6 Willie CK, MacLeod DB, Smith KJ, Lewis NC, Foster GE, Ikeda K *et al.* The contribution of arterial blood gases in cerebral blood flow regulation and fuel utilization in man at high altitude. *J Cereb Blood Flow Metab* 2015; **35**: 873–881.

7 Rasmussen P, Wyss MT, Lundby C. Cerebral glucose and lactate consumption during cerebral activation by physical activity in humans. *FASEB J* 2011; **25**: 2865–2873.

8 Siesjö BK. *Brain energy metabolism*. John Wiley & Sons, 1978.

9 Quistorff B, Secher NH, van Lieshout JJ. Lactate fuels the human brain during exercise. *FASEB J* 2008; **22**: 3443–3449.

10 Moher D, Liberati A, Tetzlaff J, Altman DG, PRISMA Group. Preferred reporting items for systematic reviews and meta-analyses: the PRISMA statement. PLoS Med. 2009; **6**: e1000097.

11 Raudenbush SW. Analyzing effect sizes: Random-effects models. In: Cooper H, Hedges LV, Valentine JC (eds). *The Handbook of Research Synthesis and Meta-Analysis*. New York, 2009, pp 296–314.

12 Fox PT, Raichle ME, Mintun MA, Dence C. Nonoxidative glucose consumption during focal physiologic neural activity. *Science* 1988; **241**: 462–464.

13 Sasaki H, Kanno I, Murakami M, Shishido F, Uemura K. Tomographic mapping of kinetic rate constants in the fluorodeoxyglucose model using dynamic positron emission tomography. *J Cereb Blood Flow Metab* 1986; **6**: 447–454.

14 Wu H-M, Bergsneider M, Glenn TC, Yeh E, Hovda DA, Phelps ME *et al.* Measurement of the global lumped constant for 2-deoxy-2-[18F]fluoro-D-glucose in normal human brain using [15O]water and 2-deoxy-2-[18F]fluoro-D-glucose positron emission tomography imaging. A method with validation based on multiple methodologies. *Mol Imaging Biol* 2003; **5**: 32–41.

15 Viechtbauer W. Conducting meta-analyses in R with the metafor package. *J Stat Softw* 2010. doi:10.2307/2246093.

16 Carpenter B, Gelman A, Hoffman MD, Lee D, Goodrich B, Betancourt M *et al.* Stan: A Probabilistic Programming Language. *J Stat Soft* 2017; **76**: 1–32.

17 Gelman A, Rubin DB. Inference from iterative simulation using multiple sequences. *Statistical science* 1992; **7**: 457–511.

18 Brooks SP, Gelman A. General methods for monitoring convergence of iterative simulations. *Journal of Computational and Graphical Statistics* 1998; **7**: 434–455.

19 Egger M, Davey Smith G, Schneider M, Minder C. Bias in meta-analysis detected by a simple, graphical test. *BMJ* 1997; **31**: 629–634.

20 Sterne JAC, Sutton AJ, Ioannidis JPA, Terrin N, Jones DR, Lau J *et al.* Recommendations for examining and interpreting funnel plot asymmetry in meta-analyses of randomised controlled trials. *BMJ* 2011; **343**: d4002–d4002.

21 Moreno SG, Sutton AJ, Ades AE, Stanley TD, Abrams KR, Peters JL *et al.* Assessment of regression-based methods to adjust for publication bias through a comprehensive simulation study. *BMC Med Res Methodol* 2009; **9**: 2.

22 Gelman A, Carlin JB, Stern HS, Dunson DB, Vehtari A, Rubin DB. *Bayesian Data Analysis*. 3rd ed. Chapman and Hall, 2013.

23 Higgins JPT, Thompson SG. Quantifying heterogeneity in a meta-analysis. *Stat Med* 2002; **21**: 1539–1558.

24 Higgins JPT, Thompson SG, Deeks JJ, Altman DG. Measuring inconsistency in meta-analyses. *BMJ* 2003; **327**: 557–560.

25 Sokoloff L, Perlin S, Kornetsky C, Kety SS. The effects of D-lysergic acid diethylamide on cerebral circulation and overall metabolism. *Ann N Y Acad Sci* 1957; **66**: 468–477.

26 Eisenberg S, Seltzer HS. The cerebral metabolic effects of acutely induced hypoglycemia in human subjects. *Metabolism* 1962; **11**: 1162–1168.

27 Gottstein U, Held K, Sebening H, Walpurger G. Der Glucoseverbrauch des menschlichen Gehirns unter dem Einfluß intravenöser Infusionen von Glucose, Glucagon und Glucose-Insulin. *Klin Wochenschr* 1965; **43**: 965–975.

28 Scheinberg P, Bourne B, Reinmuth OM. Human Cerebral Lactate And Pyruvate Extraction. *Arch Neurol* 1965; **12**: 246–250.

29 Gottstein U, Held K. The effect of insulin on brain metabolism in metabolically healthy and diabetic patients. *Klin Wochenschr* 1967; **45**: 18–23.

30 Aanerud J, Borghammer P, Rodell A, Jónsdottir KY, Gjedde A. Sex differences of human cortical blood flow and energy metabolism. *J Cereb Blood Flow Metab* 2017; **37**: 2433–2440.

31 Goyal MS, Blazey TM, Su Y, Couture LE, Durbin TJ, Bateman RJ *et al.* Persistent metabolic youth in the aging female brain. *Proc Natl Acad Sci USA* 2019; **116**: 3251–3255.

32 Dalsgaard MK. Fuelling cerebral activity in exercising man. *J Cereb Blood Flow Metab* 2006; **26**: 731–750.

33 Vlassenko AG, Raichle ME. Brain aerobic glycolysis functions and Alzheimer's disease. *Clinical and Translational Imaging* 2015; **3**: 27–37.

34 Pellerin L, Magistretti PJ. Excitatory amino acids stimulate aerobic glycolysis in astrocytes via an activation of the Na+/K+ ATPase. *Dev Neurosci* 1996; **18**: 336–342.

35 Cerdán S, Rodrigues TB, Sierra A, Benito M, Fonseca LL, Fonseca CP *et al.* The redox switch/redox coupling hypothesis. *Neurochem Int* 2006; **48**: 523–530.

36 Shulman RG, Hyder F, Rothman DL. Cerebral energetics and the glycogen shunt: neurochemical basis of functional imaging. *Proc Natl Acad Sci USA* 2001; **98**: 6417–6422.

37 Sonnewald U. Glutamate synthesis has to be matched by its degradation - where do all the carbons go? *J Neurochem* 2014; **131**: 399–406.

38 Brand KA, Hermfisse U. Aerobic glycolysis by proliferating cells: a protective strategy against reactive oxygen species. *The FASEB Journal* 1997; **11**: 388–395.

39 Vaishnavi SN, Vlassenko AG, Rundle MM, Snyder AZ, Mintun MA, Raichle ME. Regional aerobic glycolysis in the human brain. *Proc Natl Acad Sci USA* 2010; **107**: 17757–17762.

40 Goyal MS, Hawrylycz M, Miller JA, Snyder AZ, Raichle ME. Aerobic glycolysis in the human brain is associated with development and neotenous gene expression. *Cell Metab* 2014; **19**: 49–57.

41 Lundgaard I, Lu ML, Yang E, Peng W, Mestre H, Hitomi E *et al.* Glymphatic clearance controls state-dependent changes in brain lactate concentration. *J Cereb Blood Flow Metab* 2017; **37**: 2112–2124.

42 Ball KK, Cruz NF, Mrak RE, Dienel GA. Trafficking of glucose, lactate, and amyloid-beta from the inferior colliculus through perivascular routes. *J Cereb Blood Flow Metab* 2010; **30**: 162–176.

43 Weller RO, Djuanda E, Yow H-Y, Carare RO. Lymphatic drainage of the brain and the pathophysiology of neurological disease. *Acta Neuropathol* 2009; **117**: 1–14.

44 Rasmussen P, Plomgaard P, Krogh-Madsen R, Kim Y-S, van Lieshout JJ, Secher NH *et al.* MCA Vmean and the arterial lactate-to-pyruvate ratio correlate during rhythmic handgrip. *J Appl Physiol* 2006; **101**: 1406–1411.

45 Lying-Tunell U, Lindblad BS, Malmlund HO, Persson B. Cerebral blood flow and metabolic rate of oxygen, glucose, lactate, pyruvate, ketone bodies and amino acids. *Acta Neurol Scand* 1980; **62**: 265–275.

46 Grill V, Bjorkman O, Gutniak M, Lindqvist M. Brain uptake and release of amino acids in nondiabetic and insulin-dependent diabetic subjects: important role of glutamine release for nitrogen balance. *Metab Clin Exp* 1992; **41**: 28–32.

47 Reiber H. Dynamics of brain-derived proteins in cerebrospinal fluid. *Clin Chim Acta* 2001; **310**: 173–186.

48 Xie L, Kang H, Xu Q, Chen MJ, Liao Y, Thiyagarajan M *et al.* Sleep drives metabolite clearance from the adult brain. *Science* 2013; **342**: 373–377.

49 Patterson BW, Elbert DL, Mawuenyega KG, Kasten T, Ovod V, Ma S *et al.* Age and amyloid effects on human central nervous system amyloid-beta kinetics. *Annals of Neurology* 2015; **78**: 439–453.

50 Fagan AM, Roe CM, Xiong C, Mintun MA, Morris JC, Holtzman DM. Cerebrospinal fluid tau/beta-amyloid(42) ratio as a prediction of cognitive decline in nondemented older adults. *Arch Neurol* 2007; **64**: 343–349.

51 Bateman RJ, Xiong C, Benzinger TLS, Fagan AM, Goate A, Fox NC *et al.* Clinical and biomarker changes in dominantly inherited Alzheimer's disease. *N Engl J Med* 2012; **367**: 795–804.

52 Wiesner G, Vaz M, Collier G, Seals D, Kaye D, Jennings G *et al.* Leptin is released from the human brain: influence of adiposity and gender. *J Clin Endocrinol Metab* 1999; **84**: 2270–2274.

53 Lütjohann D, Breuer O, Ahlborg G, Nennesmo I, Sidén A, Diczfalusy U *et al.* Cholesterol homeostasis in human brain: evidence for an age-dependent flux of 24S-hydroxycholesterol from the brain into the circulation. *Proc Natl Acad Sci USA* 1996; **93**: 9799–9804.

54 Rasmussen P, Nyberg N, Jaroszewski JW, Krogh-Madsen R, Secher NH, Quistorff B. Brain nonoxidative carbohydrate consumption is not explained by export of an unknown

carbon source: evaluation of the arterial and jugular venous metabolome. *J Cereb Blood Flow Metab* 2010; **30**: 1240–1246.

55 Madsen PL, Hasselbalch SG, Hagemann LP, Olsen KS, Bülow J, Holm S *et al.* Persistent resetting of the cerebral oxygen/glucose uptake ratio by brain activation: evidence obtained with the Kety-Schmidt technique. *J Cereb Blood Flow Metab* 1995; **15**: 485–491.

56 Shannon BJ, Vaishnavi SN, Vlassenko AG, Shimony JS, Rutlin J, Raichle ME. Brain aerobic glycolysis and motor adaptation learning. *Proc Natl Acad Sci USA* 2016; **113**: E3782–91.

57 Dobbing J, Sands J. Quantitative growth and development of human brain. *Arch Dis Child* 1973; **48**: 757–767.

58 Segarra Mondejar M, Casellas Díaz S, Ramiro Pareta M, Müller Sánchez C, Martorell Riera A, Hermelo I *et al.* Synaptic activity-induced glycolysis facilitates membrane lipid provision and neurite outgrowth. *EMBO J* 2018; **37**. doi:10.15252/embj.201797368.

59 Blazey TM, Snyder AZ, Su Y, Goyal MS, Lee JJ, Vlassenko AG *et al.* Quantitative positron emission tomography reveals regional differences in aerobic glycolysis within the human brain. *J Cereb Blood Flow Metab* 2018; **144**: 271678X18767005.

60 Vaalburg W, Coenen HH, Crouzel C, Elsinga PH, Långström B, Lemaire C *et al.* Amino acids for the measurement of protein synthesis in vivo by PET. *Int J Rad Appl Instrum B* 1992; **19**: 227–237.

61 Schmidt KC, Cook MP, Qin M, Kang J, Burlin TV, Smith CB. Measurement of regional rates of cerebral protein synthesis with L-[1-11C]leucine and PET with correction for recycling of tissue amino acids: I. Kinetic modeling approach. *J Cereb Blood Flow Metab* 2005; **25**: 617–628.

62 Smith CB, Schmidt KC, Qin M, Burlin TV, Cook MP, Kang J *et al.* Measurement of regional rates of cerebral protein synthesis with L-[1-11C]leucine and PET with correction for recycling of tissue amino acids: II. Validation in rhesus monkeys. *J Cereb Blood Flow Metab* 2005; **25**: 629–640.

63 Boumezbeur F, Petersen KF, Cline GW, Mason GF, Behar KL, Shulman GI *et al.* The contribution of blood lactate to brain energy metabolism in humans measured by dynamic 13C nuclear magnetic resonance spectroscopy. *J Neurosci* 2010; **30**: 13983–13991.

64 Cheshkov S, Dimitrov IE, Jakkamsetti V, Good L, Kelly D, Rajasekaran K *et al.* Oxidation of [U-13 C]glucose in the human brain at 7T under steady state conditions. *Magn Reson Med* 2017; **78**: 2065–2071.

65 Scheinberg P, Stead EA. The Cerebral Blood Flow In Male Subjects As Measured By The Nitrous Oxide Technique. *J Clin Investig* 1949; **28**: 1163–1171.

66 Dastur DK, Lane MH, Hansen DB, Kety SS, Butler RN, Perlin S *et al.* Effects of aging on cerebral circulation and metabolism in man. In: JE B, Butler RN, Greenhouse SW, Sokoloff L, Yarrow MR (eds). *Human Aging: A Biological and Behavioral Study*. Human Aging - A biologicla and Behavioural Study: Bethesda, US., 1963, pp 59–76.

67 Gottstein U, Bernsmeier A, Sedlmeyer I. The Carbohydrate Metabolism Of The Human Brain. *Klin Wochenschr* 1963; **41**: 943–948.

68 Cohen PJ, Alexander SC, Smith TC, Reivich M, Wollman H. Effects of hypoxia and normocarbia on cerebral blood flow and metabolism in conscious man. *J Appl Physiol* 1967; **23**: 183–189.

69 Raichle ME, Posner JB, Plum F. Cerebral blood flow during and after hyperventilation. *Arch Neurol* 1970; **23**: 394–403.

70 Takeshita H, Okuda Y, Sari A. The effects of ketamine on cerebral circulation and metabolism in man. *Anesthesiology* 1972; **36**: 69–75.

71 Blomqvist G, Stone-Elander S, Halldin C, Roland PE, Widén L, Lindqvist M *et al.* Positron emission tomographic measurements of cerebral glucose utilization using [1-11C]D-glucose. *J Cereb Blood Flow Metab* 1990; **10**: 467–483.

72 Boyle PJ, Scott JC, Krentz AJ, Nagy RJ, Comstock E, Hoffman C. Diminished brain glucose metabolism is a significant determinant for falling rates of systemic glucose utilization during sleep in normal humans. *J Clin Invest* 1994; **93**: 529–535.

73 Hasselbalch SG, Madsen PL, Hageman LP, Olsen KS, Justesen N, Holm S *et al.* Changes in cerebral blood flow and carbohydrate metabolism during acute hyperketonemia. *Am J Physiol* 1996; **270**: E746–51.

74 Ide K, Horn A, Secher NH. Cerebral metabolic response to submaximal exercise. *J Appl Physiol* 1999; **87**: 1604–1608.

75 Ide K, Schmalbruch IK, Quistorff B, Horn A, Secher NH. Lactate, glucose and O2 uptake in human brain during recovery from maximal exercise. *J Physiol (Lond)* 2000; **522 Pt 1**: 159–164.

76 Dalsgaard MK, Ide K, Cai Y, Quistorff B, Secher NH. The intent to exercise influences the cerebral O(2)/carbohydrate uptake ratio in humans. *J Physiol (Lond)* 2002; **540**: 681–689.

77 Møller K, Strauss GI, Qvist J, Fonsmark L, Knudsen GM, Larsen FS *et al.* Cerebral blood flow and oxidative metabolism during human endotoxemia. *J Cereb Blood Flow Metab* 2002; **22**: 1262–1270.

78 Dalsgaard MK, Nybo L, Cai Y, Secher NH. Cerebral metabolism is influenced by muscle ischaemia during exercise in humans. *Exp Physiol* 2003; **88**: 297–302.

79 Glenn TC, Kelly DF, Boscardin WJ, McArthur DL, Vespa P, Oertel M *et al.* Energy dysfunction as a predictor of outcome after moderate or severe head injury: indices of oxygen, glucose, and lactate metabolism. *J Cereb Blood Flow Metab* 2003; **23**: 1239–1250.

80 Nybo L, Nielsen B, Blomstrand E, Møller K, Secher N. Neurohumoral responses during prolonged exercise in humans. *J Appl Physiol* 2003; **95**: 1125–1131.

81 Strauss GI, Møller K, Larsen FS, Kondrup J, Knudsen GM. Cerebral glucose and oxygen metabolism in patients with fulminant hepatic failure. *Liver Transpl* 2003; **9**: 1244–1252.

82 Dalsgaard MK, Quistorff B, Danielsen ER, Selmer C, Vogelsang T, Secher NH. A reduced cerebral metabolic ratio in exercise reflects metabolism and not accumulation of lactate within the human brain. *J Physiol (Lond)* 2004; **554**: 571–578.

83 Dalsgaard MK, Ogoh S, Dawson EA, Yoshiga CC, Quistorff B, Secher NH. Cerebral carbohydrate cost of physical exertion in humans. *Am J Physiol Regul Integr Comp Physiol* 2004; **287**: R534–40.

84 Dalsgaard MK, Volianitis S, Yoshiga CC, Dawson EA, Secher NH. Cerebral metabolism during upper and lower body exercise. *J Appl Physiol* 2004; **97**: 1733–1739.

85 Ogoh S, Dalsgaard MK, Yoshiga CC, Dawson EA, Keller DM, Raven PB *et al.* Dynamic cerebral autoregulation during exhaustive exercise in humans. *Am J Physiol Heart Circ Physiol* 2005; **288**: H1461–7.

86 Larsen TS, Rasmussen P, Overgaard M, Secher NH, Nielsen HB. Non-selective beta-adrenergic blockade prevents reduction of the cerebral metabolic ratio during exhaustive exercise in humans. *J Physiol (Lond)* 2008; **586**: 2807–2815.

87 Volianitis S, Fabricius-Bjerre A, Overgaard A, Strømstad M, Bjarrum M, Carlson C *et al.* The cerebral metabolic ratio is not affected by oxygen availability during maximal exercise in humans. *J Physiol (Lond)* 2008; **586**: 107–112.

88 Bailey DM, Taudorf S, Berg RMG, Lundby C, McEneny J, Young IS *et al.* Increased cerebral output of free radicals during hypoxia: implications for acute mountain sickness? *Am J Physiol Regul Integr Comp Physiol* 2009; **297**: R1283–92.

89 Gam CMB, Rasmussen P, Secher NH, Seifert T, Larsen FS, Nielsen HB. Maintained cerebral metabolic ratio during exercise in patients with beta-adrenergic blockade. *Clin Physiol Funct Imaging* 2009; **29**: 420–426.

90 Seifert T, Rasmussen P, Brassard P, Homann PH, Wissenberg M, Nordby P *et al.* Cerebral oxygenation and metabolism during exercise following three months of endurance training in healthy overweight males. *Am J Physiol Regul Integr Comp Physiol* 2009; **297**: R867–76.

91 Seifert TS, Brassard P, Jørgensen TB, Hamada AJ, Rasmussen P, Quistorff B *et al.* Cerebral non-oxidative carbohydrate consumption in humans driven by adrenaline. *J Physiol (Lond)* 2009; **587**: 285–293.

92 Rasmussen P, Nielsen J, Overgaard M, Krogh-Madsen R, Gjedde A, Secher NH *et al.* Reduced muscle activation during exercise related to brain oxygenation and metabolism in humans. *J Physiol (Lond)* 2010; **588**: 1985–1995.

93 Rasmussen P, Foged EM, Krogh-Madsen R, Nielsen J, Nielsen TR, Olsen NV *et al.* Effects of erythropoietin administration on cerebral metabolism and exercise capacity in men. *J Appl Physiol* 2010; **109**: 476–483.

94 Seifert T, Fisher JP, Young CN, Hartwich D, Ogoh S, Raven PB *et al.* Glycopyrrolate abolishes the exercise-induced increase in cerebral perfusion in humans. *Exp Physiol* 2010; **95**: 1016–1025.

95 Volianitis S, Rasmussen P, Seifert T, Nielsen HB, Secher NH. Plasma pH does not influence the cerebral metabolic ratio during maximal whole body exercise. *J Physiol (Lond)* 2011; **589**: 423–429.

96 Overgaard M, Rasmussen P, Bohm AM, Seifert T, Brassard P, Zaar M *et al.* Hypoxia and exercise provoke both lactate release and lactate oxidation by the human brain. *FASEB J* 2012; **26**: 3012–3020.

97 Fisher JP, Hartwich D, Seifert T, Olesen ND, McNulty CL, Nielsen HB *et al.* Cerebral perfusion, oxygenation and metabolism during exercise in young and elderly individuals. *J Physiol (Lond)* 2013; **591**: 1859–1870.

98 Smith KJ, MacLeod D, Willie CK, Lewis NCS, Hoiland RL, Ikeda K *et al.* Influence of high altitude on cerebral blood flow and fuel utilization during exercise and recovery. *J Physiol (Lond)* 2014; **592**: 5507–5527.

99 Glenn TC, Martin NA, Horning MA, McArthur DL, Hovda DA, Vespa P *et al.* Lactate: brain fuel in human traumatic brain injury: a comparison with normal healthy control subjects. *J Neurotrauma* 2015; **32**: 820–832.

100 Trangmar SJ, Chiesa ST, Llodio I, Garcia B, Kalsi KK, Secher NH *et al.* Dehydration accelerates reductions in cerebral blood flow during prolonged exercise in the heat without compromising brain metabolism. *Am J Physiol Heart Circ Physiol* 2015; **309**: H1598–607.

101 Bain AR, Ainslie PN, Hoiland RL, Barak OF, Cavar M, Drvis I *et al.* Cerebral oxidative metabolism is decreased with extreme apnoea in humans; impact of hypercapnia. *J Physiol (Lond)* 2016; **594**: 5317–5328.

102 Bain AR, Ainslie PN, Barak OF, Hoiland RL, Drvis I, Mijacika T *et al.* Hypercapnia is essential to reduce the cerebral oxidative metabolism during extreme apnea in humans. *J Cereb Blood Flow Metab* 2017; **37**: 3231–3242.

103 Wortis J, Bowman KM, Goldfarb W. Human Brain Metabolism: Normal Values and Values in Certain Clinical States. *Am J Psychiatry* 1940; **97**: 552–565.

104 Gibbs EL, Lennox WG. Bilateral internal jugular blood: Comparison of AV differences, oxygen-dextrose ratios and respiratory quotients. *Am J Psychiatry* 1945; : 181–190.

105 Kety SS, Schmidt CF. The Effects of Altered Arterial Tensions of Carbon Dioxide and Oxygen on Cerebral Blood Flow and Cerebral Oxygen Consumption of Normal Young Men. *J Clin Investig* 1948; **27**: 484–492.

106 Kety SS, Schmidt CF. The Nitrous Oxide Method for the Quantitative Determination of Cerebral Blood Flow in Man: Theory, Procedure and Normal Values. *J Clin Investig* 1948; **27**: 476–483.

107 Kety SS. The theory and applications of the exchange of inert gas at the lungs and tissues. *Pharmacol Rev* 1951; **3**: 1–41.

108 Fazekas JF, Alman RW, Bessman AN. Cerebral physiology of the aged. *Am J Med Sci* 1952; **223**: 245–257.

109 Novack P, Goluboff B, Bortin L, Soffe A, Shenkin HA, Batson P *et al.* Studies of the Cerebral Circulation and Metabolism in Congestive Heart Failure. *Circulation* 1953; **7**: 724–731.

110 Scheinberg P, Blackburn I, Rich M, Saslaw M. Effects of aging on cerebral circulation and metabolism. *AMA Arch Neurol Psychiatry* 1953; **70**: 77–85.

111 Sokoloff L, Wechsler RL, Mangold R, Balls K, Kety SS. Cerebral Blood Flow and Oxygen Consumption in Hyperthyroidsim Berfore and After Treatment. *J Clin Investig* 1953; **32**: 202–208.

112 Schieve JF, Wilson WP. The influence of age, anesthesia and cerebral arteriosclerosis on cerebral vascular activity to CO2. *Am J Med* 1953; **15**: 171–174.

113 Shenkin HA, Novak P, Goluboff B, Soffe AM, Bortin L, Golden D *et al.* The Effects of Aging, Aarteriosclerosis, and Hypertension Upon the Cerebral Circulation. *J Clin Investig* 1953; **32**: 459–465.

114 Sokoloff L, Mangold R, Wechsler RL, Kenney C, Kety SS. The effect of mental arithmetic on cerebral circulation and metabolism. *J Clin Investig* 1955; **34**: 1101–1108.

115 Mangold R, Sokoloff L, Conner E, Kleinerman J, Therman PO, Kety SS. The effects of sleep and lack of sleep on the cerebral circulation and metabolism of normal young men. *J Clin Invest* 1955; **34**: 1092–1100.

116 Kety SS. Human cerebral blood flow and oxygen consumption as related to aging. *J Chronic Dis* 1956; **3**: 478–486.

117 Kennedy C, Sokoloff L. An adaptation of the nitrous oxide method to the study of the cerebral circulation in children; normal values for cerebral blood flow and cerebral metabolic rate in childhood. *J Clin Invest* 1957; **36**: 1130–1137.

118 Rowe GG, Maxwell GM, Castillo CA, Freeman DJ, Crumpton CW. A study in man of cerebral blood flow and cerebral glucose, lactate and pyruvate metabolism before and after eating. *J Clin Investig* 1959; **38**: 2154–2158.

119 Kety SS. Measurement of local blood flow by the exchange of an inert, diffusible substance. *Meth Med Res* 1960; **8**: 228–238.

120 Porta PD, Maiolo AT, Negri VU, Rossella E. Cerebral Blood Flow and Metabolism in Therapeutic Insulin Coma. *Metab Clin Exp* 1964; **13**: 131–140.

121 Alexander SC, Smith TC, Strobel G, Stephen GW, Wollman H. Cerebral carbohydrate metabolism of man during respiratory and metabolic alkalosis. *J Appl Physiol* 1968; **24**: 66–72.

122 Lewis LD, Ljunggren B, Norberg K, Siesjö BK. Changes in carbohydrate substrates, amino acids and ammonia in the brain during insulin-induced hypoglycemia. *J Neurochem* 1974; **23**: 659–671.

123 Raichle ME, Larson KB, Phelps ME, Grubb RL, welch MJ, Ter-Pogossian MM. In vivo measurement of brain glucose transport and metabolism employing glucose-11C. *Am J Physiol* 1975; **228**: 1936–1948.

124 Gottstein U, Zahn U, Held K, Gabriel FH, Textor T, Berghoff W. Effect of hyperventilation on cerebral blood flow and metabolism in man; continuous monitoring of arterio-cerebral venous glucose differences. *Klin Wochenschr* 1976; **54**: 373–381.

125 Van Aken J, Rolly G. Influence of etomidate, a new short acting anesthetic agent, on cerebral blood flow in man. *Acta Anaesthesiol Belg* 1976; **27 suppl**: 175–180.

126 Juhlin-Dannfelt A. Ethanol effects of substrate utilization by the human brain. *Scand J Clin Lab Invest* 1977; **37**: 443–449.

127 Hertz MM, Paulson OB, Barry DI, Christiansen JS, Svendsen PA. Insulin increases glucose transfer across the blood-brain barrier in man. *J Clin Investig* 1981; **67**: 597–604.

128 Eriksson LS, Law DH, Hagenfeldt L, Wahren J. Nitrogen metabolism of the human brain. *J Neurochem* 1983; **41**: 1324–1328.

129 Dastur DK. Cerebral blood flow and metabolism in normal human aging, pathological aging, and senile dementia. *J Cereb Blood Flow Metab* 1985; **5**: 1–9.

130 Hatazawa J, Ito M, Matsuzawa T, Ido T, Watanuki S. Measurement of the ratio of cerebral oxygen consumption to glucose utilization by positron emission tomography: its consistency with the values determined by the Kety-Schmidt method in normal volunteers. *J Cereb Blood Flow Metab* 1988; **8**: 426–432.

131 Warrell DA, White NJ, Veall N, Looareesuwan S, Chanthavanich P, Phillips RE *et al.* Cerebral anaerobic glycolysis and reduced cerebral oxygen transport in human cerebral malaria. *Lancet* 1988; **2**: 534–538.

132 Blomqvist G, Grill V, Ingvar M, Widén L, Stone-Elander S. The effect of hyperglycaemia on regional cerebral glucose oxidation in humans studied with [1-11C]-D-glucose. *Acta Physiol Scand* 1998; **163**: 403–415.

133 Grill V, Gutniak M, Bjorkman O, Lindqvist M, Stone-Elander S, Seitz RJ *et al.* Cerebral blood flow and substrate utilization in insulin-treated diabetic subjects. *Am J Physiol* 1990; **258**: E813–20.

134 Leenders KL, Perani D, Lammertsma AA, Heather JD, Buckingham P, Healy MJ *et al.* Cerebral blood flow, blood volume and oxygen utilization. Normal values and effect of age. *Brain* 1990; **113 (Pt 1)**: 27–47.

135 Gutniak M, Blomqvist G, Widén L, Stone-Elander S, Hamberger B, Grill V. D-[U-11C]glucose uptake and metabolism in the brain of insulin-dependent diabetic subjects. *Am J Physiol* 1990; **258**: E805–12.

136 Burgess ML, Robertson RJ, Davis JM, Norris JM. RPE, blood glucose, and carbohydrate oxidation during exercise: effects of glucose feedings. *Med Sci Sports Exerc* 1991; **23**: 353–359.

137 Blomqvist G, Gjedde A, Gutniak M, Grill V, Widén L, Stone-Elander S *et al.* Facilitated transport of glucose from blood to brain in man and the effect of moderate hypoglycaemia on cerebral glucose utilization. *Eur J Nucl Med* 1991; **18**: 834–837.

138 Pollard V, Prough DS, Deyo DJ, Conroy B, Uchida T, Daye A *et al.* Cerebral blood flow during experimental endotoxemia in volunteers. *Crit Care Med* 1997; **25**: 1700–1706.

139 Mielck F, Stephan H, Buhre W, Weyland A, Sonntag H. Effects of 1 MAC desflurane on cerebral metabolism, blood flow and carbon dioxide reactivity in humans. *Br J Anaesth* 1998; **81**: 155–160.

140 Schaffranietz L, Heinke W. The effect of different ventilation regimes on jugular venous oxygen saturation in elective neurosurgical patients. *Neurological Research* 1998; **20 Suppl 1**: S66–70.

141 Wahren J, Ekberg K, Fernqvist-Forbes E, Nair S. Brain substrate utilisation during acute hypoglycaemia. *Diabetologia* 1999; **42**: 812–818.

142 Madsen PL, Cruz NF, Sokoloff L, Dienel GA. Cerebral oxygen/glucose ratio is low during sensory stimulation and rises above normal during recovery: excess glucose consumption during stimulation is not accounted for by lactate efflux from or accumulation in brain tissue. *J Cereb Blood Flow Metab* 1999; **19**: 393–400.

143 Takahashi T, Shirane R, Sato S, Yoshimoto T. Developmental changes of cerebral blood flow and oxygen metabolism in children. *AJNR Am J Neuroradiol* 1999; **20**: 917–922.

144 Moller K, Strauss GI, Thomsen G, Larsen FS, Holm S, Sperling BK *et al.* Cerebral blood flow, oxidative metabolism and cerebrovascular carbon dioxide reactivity in patients with acute bacterial meningitis. *Acta Anaesthesiol Scand* 2002; **46**: 567–578.

145 Nybo L, Møller K, Volianitis S, Nielsen B, Secher NH. Effects of hyperthermia on cerebral blood flow and metabolism during prolonged exercise in humans. *J Appl Physiol* 2002; **93**: 58–64.

146 Lancaster GI, Moller K, Nielsen B, Secher NH, Febbraio MA, Nybo L. Exercise induces the release of heat shock protein 72 from the human brain in vivo. *Cell Stress Chaperones* 2004; **9**: 276–280.

147 Dalsgaard MK, Ott P, Dela F, Juul A, Pedersen BK, Warberg J *et al.* The CSF and arterial to internal jugular venous hormonal differences during exercise in humans. *Exp Physiol* 2004; **89**: 271–277.

148 Cremer OL, Diephuis JC, van Soest H, Vaessen PHB, Bruens MGJ, Hennis PJ *et al.* Cerebral oxygen extraction and autoregulation during extracorporeal whole body hyperthermia in humans. *Anesthesiology* 2004; **100**: 1101–1107.

149 Blomstrand E, Moller K, Secher NH, Nybo L. Effect of carbohydrate ingestion on brain exchange of amino acids during sustained exercise in human subjects. *Acta Physiol Scand* 2005; **185**: 203–209.

150 Chieregato A, Marchi M, Fainardi E, Targa L. Cerebral Arterio-venous pCO2 Difference, Estimated Respiratory Quotient, and Early Posttraumatic Outcome: Comparison With Arterio-venous Lactate and Oxygen Differences. *Journal of Neurosurgical Anesthesiology* 2007; **19**: 222–228.

151 Seifert T, Rasmussen P, Secher NH, Nielsen HB. Cerebral oxygenation decreases during exercise in humans with beta-adrenergic blockade. *Acta Physiol (Oxf)* 2009; **196**: 295–302.

152 Holbein M, Béchir M, Ludwig S, Sommerfeld J, Cottini SR, Keel M *et al.* Differential influence of arterial blood glucose on cerebral metabolism following severe traumatic brain injury. *Crit Care* 2009; **13**: R13.

153 van Hall G, Strømstad M, Rasmussen P, Jans O, Zaar M, Gam C *et al.* Blood lactate is an important energy source for the human brain. *J Cereb Blood Flow Metab* 2009; **29**: 1121–1129.

154 Espenell AEG, McIntyre IW, Gulati H, Girling LG, Wilkinson MF, Silvaggio JA *et al.* Lactate flux during carotid endarterectomy under general anesthesia: correlation with various point-of-care monitors. *Can J Anaesth* 2010; **57**: 903–912.

155 Powers WJ, Haas RH, Le T, Videen TO, Markham J, Perlmutter JS. Platelet mitochondrial complex I and I+III activities do not correlate with cerebral mitochondrial oxidative metabolism. *J Cereb Blood Flow Metab* 2011; **31**: e1–5.

156 Rasmussen P, Nybo L, Volianitis S, Moller K, Secher NH, Gjedde A. Cerebral oxygenation is reduced during hyperthermic exercise in humans. *Acta Physiol (Oxf)* 2010; **199**: 63–70.

157 Smith ZM, Krizay E, Guo J, Shin DD, Scadeng M, Dubowitz DJ. Sustained high-altitude hypoxia increases cerebral oxygen metabolism. *J Appl Physiol* 2013; **114**: 11–18.

158 Mikkelsen KH, Seifert T, Secher NH, Grøndal T, van Hall G. Systemic, Cerebral and Skeletal Muscle Ketone Body and Energy Metabolism During Acute Hyper-D-β-Hydroxybutyratemia in Post-Absorptive Healthy Males. *J Clin Endocrinol Metab* 2015; **100**: 636–643.

159 Glenn TC, Martin NA, McArthur DL, Hovda DA, Vespa P, Johnson ML *et al.* Endogenous Nutritive Support after Traumatic Brain Injury: Peripheral Lactate Production for Glucose Supply via Gluconeogenesis. *J Neurotrauma* 2015; **32**: 811–819.

160 Fabricius-Bjerre A, Overgaard A, Winther-Olesen M, Lönn L, Secher NH, Nielsen HB. Reduced cerebral oxygen-carbohydrate index during endotracheal intubation in vascular surgical patients. *Clin Physiol Funct Imaging* 2015; **35**: 404–410.

161 Lewis NCS, Bain AR, MacLeod DB, Wildfong KW, Smith KJ, Willie CK *et al.* Impact of hypocapnia and cerebral perfusion on orthostatic tolerance. *J Physiol (Lond)* 2014; **592**: 5203–5219.

162 Trangmar SJ, Chiesa ST, Stock CG, Kalsi KK, Secher NH, González-Alonso J. Dehydration affects cerebral blood flow but not its metabolic rate for oxygen during maximal exercise in trained humans. *J Physiol (Lond)* 2014; **592**: 3143–3160.

163 Tholance Y, Barcelos GK, Dailler F, Renaud B, Marinesco S, Perret-Liaudet A. Biochemical neuromonitoring of poor-grade aneurysmal subarachnoid hemorrhage: comparative analysis of metabolic events detected by cerebral microdialysis and by retrograde jugular vein catheterization. *Neurological Research* 2015; **37**: 578–587.

164 Slusher AL, Whitehurst M, Zoeller RF, Mock JT, Maharaj A, Huang CJ. Brain-Derived Neurotrophic Factor and Substrate Utilization Following Acute Aerobic Exercise in Obese Individuals. *J Neuroendocrinol* 2015; **27**: 370–376.

165 Grüne F, Kazmaier S, Hoeks SE, Stolker RJ, Coburn M, Weyland A. Argon does not affect cerebral circulation or metabolism in male humans. *PLoS ONE* 2017; **12**: e0171962.

Chapter 3: Quantitative positron emission tomography reveals regional differences in non-oxidative glucose consumption within the human brain[i]

3.1 Abstract

Glucose and oxygen metabolism are tightly coupled in the human brain, with the preponderance of the brain's glucose supply used to generate ATP via oxidative phosphorylation. A fraction of glucose is consumed outside of oxidative phosphorylation despite the presence of sufficient oxygen to do so. We refer to this process as non-oxidative glucose consumption (NOglc). A recent positron emission tomography study reported that NOglc is uniform within gray matter. Here, we analyze the same data and demonstrate robust regional differences in NOglc within gray matter, a finding consistent with previously published data.

3.2 Introduction

The energetic needs of the healthy human brain are almost entirely met by oxidative consumption of blood-borne glucose[1,2]. However, a fraction of the brain's glucose uptake does not undergo oxidative phosphorylation. This effect conventionally is quantitated using the oxygen-glucose index (OGI), which is the molar ratio of oxygen to glucose consumption. If no alternative fuels are used and all glucose undergoes complete oxidative phosphorylation, the OGI is exactly 6. However, multiple studies have shown that the OGI of the young adult human brain is less than 6, typically on the order of 5.5[3-7]. Thus, around 10% of the whole brain's glucose

[i] This chapter is slightly modified version of a previously published article: Blazey TM, Snyder AZ, Su Y, Goyal MS, Lee JJ, Vlassenko AG et al. Quantitative positron emission tomography reveals regional differences in aerobic glycolysis within the human brain. *J Cereb Blood Flow Metab* 2018; **144**: 271678X18767005.

consumption is metabolized through non-oxidative pathways. We define non-oxidative glucose consumption (NOglc) as the fraction of glucose metabolized outside of oxidative phosphorylation. NOglc is defined inversely proportional to OGI; thus areas of the brain that have high NOglc have low OGI ratios and vice versa. Note that NOglc is often referred to as aerobic glycolysis[8], which dates back to Warburg's discovery that cancer cells have high rates of glycolysis despite sufficient oxygen[9].

Prior work from our laboratory has shown that, in resting, healthy young adults, NOglc is regionally greater in prefrontal cortex, lateral parietal lobe, and the precuneus/posterior cingulate cortex, relative to the rest of the brain[8]. These regions correspond to the default mode and fronto-parietal control networks, which are areas of the cerebral cortex associated with higher-order cognition[10]. Conversely, NOglc in the cerebellum has been shown by us[8], and others[11], to be lower than in the rest of the brain. Hyder and colleagues[7] recently published a study disputing the existence of regional variability in NOglc. Using quantitative positron emission tomography (PET) techniques, Hyder et al. measured OGI in 13 normal volunteers and reported that OGI is uniform within gray matter, which implies that NOglc is uniform as well. In the following, we refer to this study as "Hyder et al.". To resolve the discrepancy between Hyder et al. and our previous findings, we reanalyzed the PET data from Hyder et al., which was generously shared with us by the original authors.

3.3 Methods

Dataset

We obtained processed, quantitative PET images of cerebral blood flow (CBF), oxygen utilization ($CMRO_2$), and glucose consumption (CMRglc) for 13 normal adult males from Hyder et al.[7] CBF and $CMRO_2$ were measured using [^{15}O]-H_2O and [^{15}O]-O_2 respectively. A two-

compartment (tissue and vascular distribution) kinetic model was used for both tracers[12,13]. No correction for recirculating [^{15}O]-H_2O was performed during [^{15}O]-O_2 modeling. CMRglc was obtained by fitting an irreversible two-compartment (free [^{18}F]-FDG and trapped [^{18}F]-FDG-6-phosophate) model to the [^{18}F]-FDG data[14]. No correction for vascular radioactivity was performed, and a lumped constant of 0.8 was used. All PET imaging data were acquired with arterial sampling, allowing for absolute quantitation of all metabolic parameters. For further methodological details please see the original publication[7]. As stated in the original report by Hyder et al.[7], all subjects gave written informed consent in accordance with the Helsinki Protocol and all experimental procedures were approved by the ethical review committees of the Central Denmark Region and the Aarhus University Hospital, Aarhus Denmark.

OGI Regional Computations

To assess regional differences in NOglc, we first calculated voxelwise OGI ($CMRO_2$/CMRglc) in each subject. We then computed regional average OGI values in several regions of interest (ROIs). Prior to computing regional means, we excluded voxels that were outside five median absolute deviations (1.11) from the gray matter median (4.83)[15]. Excluded voxels were predominantly in areas of vascular artifact or on the edges of the PET images (4.09% of all voxels were excluded). We also excluded any voxels that were not classified as gray matter in the atlas used by Hyder et al.[7]

Our primary ROI set comprised seven resting state networks (Figure 3.1A), defined in a previous resting-state functional magnetic resonance imaging study[16]. Each ROI included only voxels in which the likelihood of network identity exceeded 90%. Resting state ROIs were transformed, using FSL[17,18], into the atlas space used by Hyder et al. without alterations of the metabolic imaging data. We also created an ROI of the cerebellar gray matter within the atlas

used by Hyder et al.[7] To accommodate incomplete cerebellar coverage of the PET data, the present results are limited to portions of the cerebellum in which the OGI was measured in every subject (Figure 3.2).

Statistical Methods

All statistical analyses were conducted in R[19]. A one-way ANOVA with region as a factor and subject as a repeated measure was used to determine if brain region explained any variance in OGI. Statistical significance was determined using a *F*-test on the region factor. One sample *t*-tests were used to determine if regional OGI values were different from 6. An OGI significantly ($p<0.05$, two-tailed) less than 6 means that the probability of finding such, or more extreme, data by chance is below 5%. We took this as indication that a portion of the glucose consumption in a given region undergoes only NOglc. In the same sense, paired *t*-tests were used to assess differences in OGI between regions. We used a significant difference ($p<0.05$, two-tailed) as indication that NOglc is different between two regions. Correction for the 21 pairwise comparisons between networks was performed using False Discovery Rate (FDR) theory[20]. Reported values are means and 95% confidence intervals unless otherwise stated.

The statistical thresholds that we defined above are dependent on the power of the Hyder et al. dataset. To determine the power of the Hyder et al. data we performed a power analysis using two previously published PET datasets. All power calculations were performed using the R package pwr[21]. Sasaki et al. reported the mean difference between the cortical and cerebellar gray matter OGI to be -1.48 (SD=0.42; n=7)[11]. The 13 subjects in the Hyder et al. dataset gives us 100% power to detect an effect of this magnitude. The mean OGI difference between the cortical gray matter and the basal ganglia was found by Hatazwa et al. to be 0.38 (SD=0.93; n=7)[22]. The Hyder et al. dataset would provide only 17.2% power to detect this effect. Taken

together, these analyses reveal that we are more than sufficiently powered to detect large regional differences, but are unlikely to capture smaller effects.

3.4 Results

Aerobic Glycolysis Varies by Resting State Network

To assess regional differences in NOglc, we computed OGI in seven resting state networks (Figure 3.1A). The means for other metabolic parameters (e.g., CBF) are reported in Table 3.1. With the exception of the visual network (VIS), all resting state networks had an OGI significantly less than 6 (p<0.05), indicating the presence of NOglc. A repeated measures, one-way ANOVA revealed a highly significant difference in OGI across the brain ($F_{6,72}$ = 74.16, p < 0.001). Differences in OGI between specific network pairs are shown in Figure 1B; the RSNs are ordered by OGI and significant differences (p < 0.05, corrected) are highlighted by color. In agreement with previous work[8], the OGI was low in default mode network (DMN) and high in the visual network (VIS). Unexpectedly, the ventral attention (VAN) network had the lowest OGI. We note that regional differences were highly consistent across individuals. For example, OGI in the DMN was less than OGI in the visual network (VIS) in every subject (Figure 3.1C).

Aerobic Glycolysis in the Cerebellum

Previous studies have shown that NOglc in the cerebellum is lower than NOglc in the rest of the brain[8,11]. In the Hyder et al. data, the OGI in the superior cerebellum (see Methods) was 6.50 (± 0.67), which was not significantly different from 6.0 (t=1.63, p=0.13). The difference between the cerebellum and the rest of gray matter (5.18 ± 0.51) was significant (t=-8.70, p<0.001). As the lumped constant in the cerebellum has been reported to be approximately 1.14 times greater than in the whole brain[23], we repeated our analysis after adjusting the cerebellum OGI for this difference. After the adjustment, the cerebellar OGI was 5.70 (± 0.58), again not

significantly different from 6.0 (t=-1.12, p=0.28), but still significantly different from the rest of gray matter (t=-4.00, p=0.0018). Thus, the cerebellum is characterized by a distinct lack of NOglc.

Topography of OGI

The present results indicate that regional differences in NOglc exist between resting state networks as well as between the cerebellar and non-cerebellar gray matter. Figure 3.3A shows group averaged OGI (image obtained from the original authors) at a finer spatial scale. This figure is essentially identical to Figure 3A in Hyder et al. (reproduced here as Figure 3.3B) except for choice of color scale. Thus, presenting the identical results using a more physiologically meaningful scale (4-7 in Figure 3.3A as opposed to 1-10 in Figure 3.3B) demonstrates regional differences in OGI on inspection.

3.5 Discussion

Our reexamination of the data from Hyder et al. reveals two primary findings. First, many regions of the brain exhibit NOglc at rest. This result is consistent with both the regional PET literature[11,22] as well as with whole-brain measurements of OGI[3-6]. Second, we observed significant regional differences in NOglc between gray matter regions that were highly preserved across subjects (Figure 3.1C).

These findings are consistent with Vaishnavi et al., 2010, a previous study from our group that employed regional standardized uptake ratios[8]. The principal result of that study was that NOglc is significantly non-uniform across the brain. In particular, regions constituting the default mode network (DMN) had higher NOglc than other parts of the brain. In contrast, the cerebellum had lower NOglc. These findings are replicated here using the Hyder et al. dataset.

There are, however, a few differences between the two datasets. The fronto-parietal control network (FPC) had higher NOglc in the Vaishnavi et al. study compared to Hyder et al., and the NOglc in the ventral attention network (VAN) was much higher in the Hyder et al. data compared to Vaishnavi et al. (Figure 3.1B and C). It is not clear whether these differences are attributable to analytical approach (relative vs. quantitative PET), study population (the Hyder et al. study contained only male subjects), or other unknown factors. Therefore, although both datasets clearly support regional differences, more work is needed to resolve the discrepancies between the two studies.

On the basis of the same dataset, Hyder et al. argued that no regional differences in NOglc exist, and that findings reported by Vaishnavi et al. are artifacts attributable to the use of relative metabolic measures. The present results, obtained using the quantitative data identical to that from the Hyder et al. study, do not support this perspective. It follows that the discrepant perspectives are attributable to differences in analysis methodology. Specifically, Hyder et al. did not account for subject level variability common to all regions (e.g. use of ANOVA without a repeated measures factor). Figure 3.1C illustrates how OGI measures in two regions would appear to not be significantly different if variability attributable to subject is not taken into account.

Could the observed regional difference arise from non-biological artifacts? PET involves many technical decisions including choosing a kinetic model, accounting for vascular radioactivity, adjusting for recirculating metabolites, and correcting for the delay and dispersion of the arterial input function. Any of these factors could, in theory, produce an artefactual regional difference in NOglc. However, we think this unlikely for several reasons. First, despite the fact that there are regional differences in cerebral blood volume[24] and arterial delay[25], there is

no direct evidence that any of these technical factors produce a spatial artifact that induces regional differences in OGI. Second, using different procedures to analyze PET data, we[8] and others[11] have found regional differences in OGI similar to the present findings. Finally, additional evidence from different techniques suggests that NOglc varies throughout the brain. Using microdialysis in a transgenic mouse model of Alzheimer's disease, Bero et al. reported regional differences in lactate levels in interstitial fluid, a result consistent with regional differences in NOglc[26]. Taken together, the available evidence supports the conclusion that regional differences in OGI are of biological origin.

In the Hyder et al. dataset, NOglc accounts for 5.57 (± 2.65) μMol/hg/min, or approximately 19%, of the glucose consumption in the default mode network. From an energetic perspective, it may be surprising that NOglc accounts for so much glucose consumption in any part of the brain, as the quantity of ATP generated by NOglc is quite small compared to that generated by oxidative phosphorylation[7]. Therefore, a number of alternative explanations have been proposed, including rapid synthesis of ATP for the Na^+/K^+-ATPase[27], generation of biosynthetic intermediates necessary for myelination as well as synaptic and neuritic formation and turnover[8], alteration of cellular redox potentials[28], regulation of glycogen levels through a hypothesized glycogen shunt[29], and the uptake and recycling of glutamate by astrocytes[30,31]. The exact apportionment of NOglc among these alternatives remains uncertain.

One way to elucidate the role of NOglc in the brain is through spatial topography. Past work in our laboratory has shown that the spatial distribution of NOglc correlates with the expression of genes related to synaptic development and growth[32]. The relationship between NOglc and synaptic plasticity is particularly intriguing given previous findings relating NOglc to task performance. Madsen et al. found that whole brain NOglc was elevated both during and

after performance of the Wisconsin Card Sorting Test[33]. Our group recently expanded on this finding. We measured relative OGI in subjects before and after the performance of a covert motor learning task[34]. We found that hours after the performance of the learning task, subjects had elevated NOglc in the left Brodmann area 44, an area recruited by task performance. Furthermore, we observed a correlation between task performance and subsequent increases in NOglc. These results link focal changes in NOglc to learning and suggests that regional differences in NOglc might reflect regional differences in synaptic plasticity.

Other experiments have focused on the role of NOglc in aging and Alzheimer's disease (AD). For example, it has been shown that higher levels of neural activity lead to increased amyloid-beta production in a mouse model of AD[26]. Moreover, this effect is associated with increased lactate levels in the interstitial fluid[26]. Cross-sectional studies in humans have found that brain NOglc decreases in AD[35,36] as well as in normal aging [37] (two smaller aging studies have reported non-significant trends[38,39]). One interpretation of these findings is that the same processes that lead to high NOglc and synaptic plasticity in early life may ultimately lead to disease later in life[40,41].

Synaptic plasticity is but one of several, non-exclusive explanations for the brain's use of NOglc. Much more work is needed before NOglc in the brain is fully understood. Any explanation of NOglc will need to consider regional differences, which have now been reproduced in an independent dataset. It is our hope that this report will serve as an impetus for new research that will further elucidate the role NOglc in the brain.

3.6 Figures

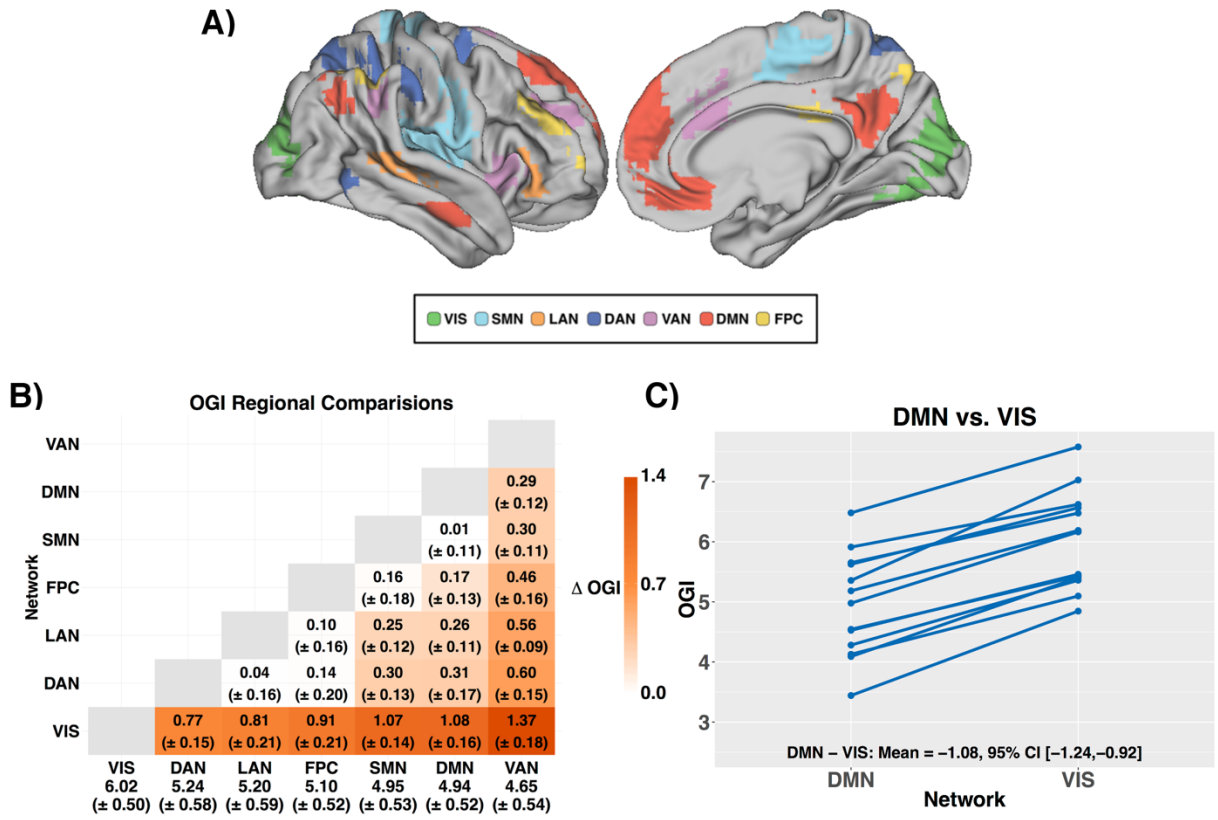

Figure 3.1: Differences in OGI between resting state networks

A) Regions of interest for each of the seven resting state networks projected on the right hemisphere cortical gray matter surface of the Conte 69 atlas[42] using Connectome Workbench[43]. Images show the right lateral and medial surfaces. **B)** Pairwise differences between each resting state network. Within each cell is the difference in OGI (ΔOGI) between resting state networks along with the 95% CI of the difference. Positive numbers indicate greater OGI (less NOglc) in the network listed on the vertical axis. Only significant differences are shown in color. The numbers along the bottom row are the mean and the 95% CI for each network. Network abbreviations: fronto-parietal control (FPC), default mode (DMN), dorsal attention (DAN), ventral attention (VAN), language (LAN), somatomotor (SMN) and visual (VIS). **(C)** Within-

subject comparison of OGI evaluated within the default mode network versus visual network. The solid blue lines connect regional measurements within a single participant. Note consistency of regional differences in OGI from subject to subject. The DMN exhibited lower OGI than the visual network (VIS) in every subject.

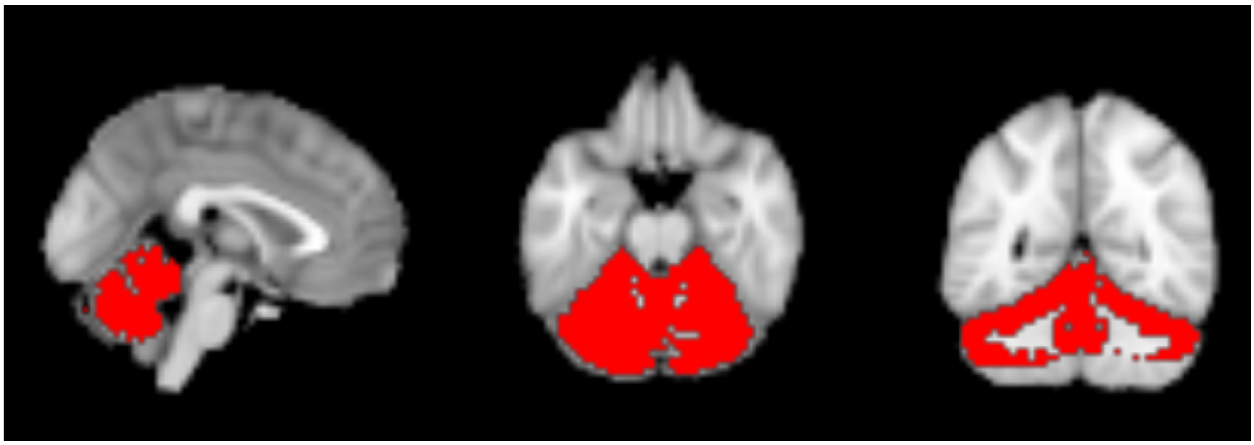

Figure 3.2: Cerebellar gray matter region of interest

Region was derived from the atlas used by Hyder et al. [7]. Only voxels for which OGI was non-zero in every subject were included. The MNI152 T1 template was resampled to the space of the PET data for anatomical reference.

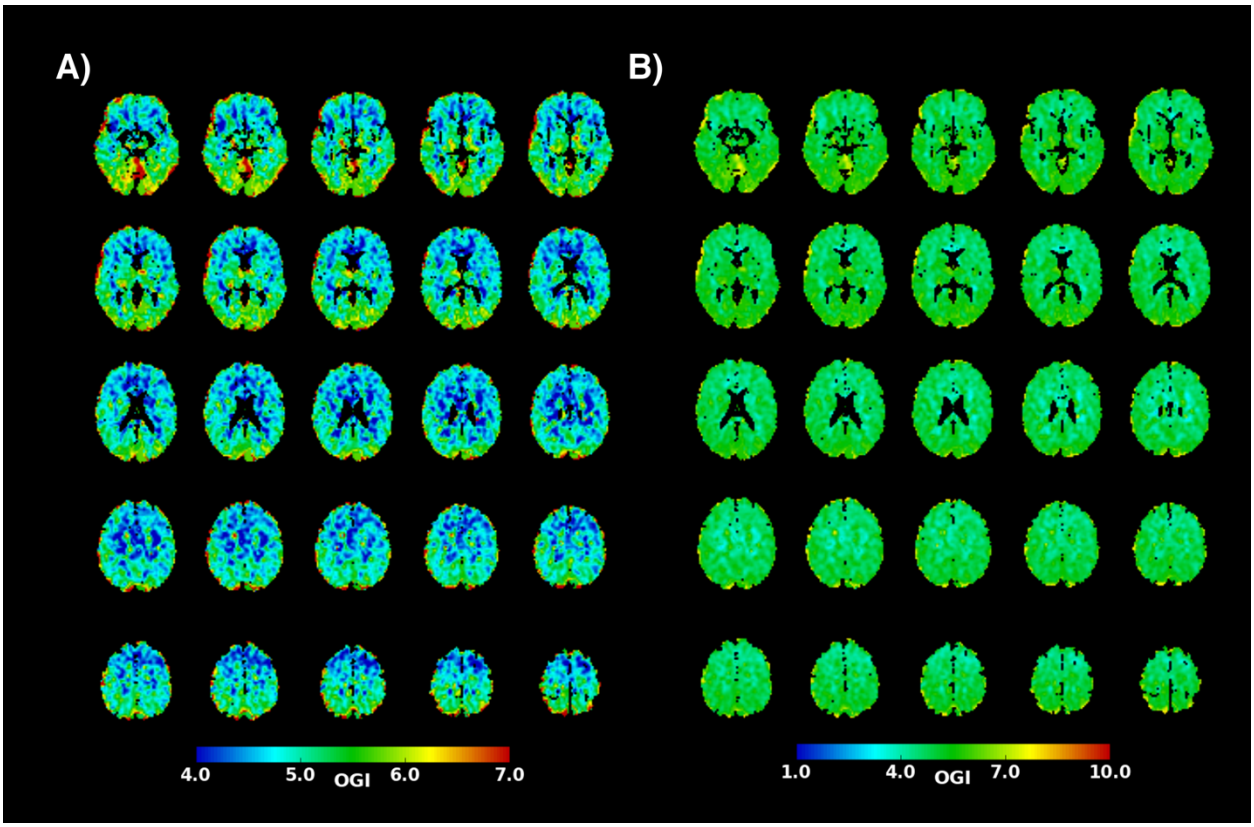

Figure 3.3: Regional topography of OGI

A) A group-averaged OGI map obtained from the authors of the Hyder et al. study. Regional differences are found throughout the brain. **B)** Replication of Figure 3A from Hyder et al., 2016 which shows little regional variation in OGI. Regional differences are masked by the use of a color scale that lacks a dynamic range which is not matched over the relevant physiologic range of the data.

3.7 Tables

Table 3.1: Means and 95% CIs for selected regions and resting state networks

Whole brain, gray matter, and white matter regions were taken from the atlas used by Hyder et al. [7]. Resting state regions were from Hacker et al. [16]. The cerebellum was excluded from all regions. Summary statistics were calculated after excluding voxels that exceed five median absolute deviations from the gray matter median[15]. The reported means for whole brain, as well as gray and white matter, are largely similar to those reported in the Hyder et al. manuscript[7].

Region	CBF (mL/hg/min)	CMRglc (μMol/hg/min)	$CMRO_2$ (μMol/hg/min)	OGI	OEF
Whole Brain	36.32 (2.89)	26.34 (1.59)	134.53 (13.76)	5.10 (0.50)	0.42 (0.04)
Gray Matter	38.31 (3.14)	27.57 (1.74)	142.51 (14.89)	5.18 (0.51)	0.42 (0.04)
White Matter	28.95 (2.11)	21.74 (1.15)	104.93 (9.79)	4.78 (0.47)	0.41 (0.04)
Dorsal Attention	37.97 (3.90)	29.00 (1.98)	150.32 (17.26)	5.24 (0.58)	0.44 (0.05)
Ventral Attention	45.40 (4.02)	32.13 (2.10)	147.13 (16.83)	4.65 (0.54)	0.37 (0.04)
Somatomotor	39.51 (3.42)	28.99 (1.81)	141.74 (16.59)	4.95 (0.53)	0.41 (0.05)
Visual	41.06 (3.35)	28.42 (2.21)	173.26 (17.46)	6.02 (0.50)	0.47 (0.05)

Fronto-Parietal Control	40.63 (3.81)	30.17 (2.08)	152.25 (16.21)	5.10 (0.52)	0.42 (0.05)
Language	41.58 (3.73)	29.88 (1.81)	152.86 (16.73)	5.20 (0.59)	0.41 (0.05)
Default Mode	41.03 (3.57)	29.67 (1.81)	144.73 (15.40)	4.94 (0.52)	0.40 (0.04)

3.8 References

1 Gibbs EL, Lennox WG, Nims LF, Gibbs FA. Arterial and cerebral venous blood arterial-venous differences in man. *J Biol Chem* 1942; **144**: 325–332.

2 Siesjö BK. *Brain energy metabolism*. John Wiley & Sons, 1978.

3 Cohen PJ, Alexander SC, Smith TC, Reivich M, Wollman H. Effects of hypoxia and normocarbia on cerebral blood flow and metabolism in conscious man. *J Appl Physiol* 1967; **23**: 183–189.

4 Raichle ME, Posner JB, Plum F. Cerebral blood flow during and after hyperventilation. *Arch Neurol* 1970; **23**: 394–403.

5 Boyle PJ, Scott JC, Krentz AJ, Nagy RJ, Comstock E, Hoffman C. Diminished brain glucose metabolism is a significant determinant for falling rates of systemic glucose utilization during sleep in normal humans. *J Clin Invest* 1994; **93**: 529–535.

6 Rasmussen P, Wyss MT, Lundby C. Cerebral glucose and lactate consumption during cerebral activation by physical activity in humans. *FASEB J* 2011; **25**: 2865–2873.

7 Hyder F, Herman P, Bailey CJ, Møller A, Globinsky R, Fulbright RK *et al.* Uniform distributions of glucose oxidation and oxygen extraction in gray matter of normal human brain: No evidence of regional differences of aerobic glycolysis. *J Cereb Blood Flow Metab* 2016; **36**: 903–916.

8 Vaishnavi SN, Vlassenko AG, Rundle MM, Snyder AZ, Mintun MA, Raichle ME. Regional aerobic glycolysis in the human brain. *Proc Natl Acad Sci USA* 2010; **107**: 17757–17762.

9 Warburg O. On the origin of cancer cells. *Science* 1956; **123**: 309–314.

10 Zhang D, Raichle ME. Disease and the brain's dark energy. *Nat Rev Neurol* 2010; **6**: 15–28.

11 Sasaki H, Kanno I, Murakami M, Shishido F, Uemura K. Tomographic mapping of kinetic rate constants in the fluorodeoxyglucose model using dynamic positron emission tomography. *J Cereb Blood Flow Metab* 1986; **6**: 447–454.

12 Ohta S, Meyer E, Thompson CJ, Gjedde A. Oxygen consumption of the living human brain measured after a single inhalation of positron emitting oxygen. *J Cereb Blood Flow Metab* 1992; **12**: 179–192.

13 Ohta S, Meyer E, Fujita H, Reutens DC, Evans A, Gjedde A. Cerebral [15O]water clearance in humans determined by PET: I. Theory and normal values. *J Cereb Blood Flow Metab* 1996; **16**: 765–780.

14 Kuwabara H, Gjedde A. Measurements of glucose phosphorylation with FDG and PET are not reduced by dephosphorylation of FDG-6-phosphate. *J Nucl Med* 1991; **32**: 692–698.

15 Leys C, Ley C, Klein O, Bernard P, Licata L. Detecting outliers: Do not use standard deviation around the mean, use absolute deviation around the median. *J Exp Soc Psychol* 2013; **49**: 764–766.

16 Hacker CD, Laumann TO, Szrama NP, Baldassarre A, Snyder AZ, Leuthardt EC *et al.* Resting state network estimation in individual subjects. *Neuroimage* 2013; **82**: 616–633.

17 Jenkinson M, Smith S. A global optimisation method for robust affine registration of brain images. *Med Image Anal* 2001; **5**: 143–156.

18 Jenkinson M, Beckmann CF, Behrens TEJ, Woolrich MW, Smith SM. FSL. *Neuroimage* 2012; **62**: 782–790.

19 R Core Team. R: A Language and Environment for Statistical Computing. Vienna, Austria, 2017https://www.R-project.org/.

20 Benjamini Y, Hochberg Y. Controlling the false discovery rate: a practical and powerful approach to multiple testing. *J R Stat Soc Series B Stat Methodol* 1995; **57**: 289–300.

21 Champely S. pwr. https://CRAN.R-project.org/package=pwr.

22 Hatazawa J, Ito M, Matsuzawa T, Ido T, Watanuki S. Measurement of the ratio of cerebral oxygen consumption to glucose utilization by positron emission tomography: its consistency with the values determined by the Kety-Schmidt method in normal volunteers. *J Cereb Blood Flow Metab* 1988; **8**: 426–432.

23 Graham MM, Muzi M, Spence AM, O'Sullivan F, Lewellen TK, Link JM *et al.* The FDG lumped constant in normal human brain. *J Nucl Med* 2002; **43**: 1157–1166.

24 Grubb RL, Raichle ME, Higgins CS, Eichling JO. Measurement of regional cerebral blood volume by emission tomography. *Annals of Neurology* 1978; **4**: 322–328.

25 Iida H, Higano S, Tomura N, Shishido F, Kanno I, Miura S *et al.* Evaluation of regional differences of tracer appearance time in cerebral tissues using [15O] water and dynamic positron emission tomography. *J Cereb Blood Flow Metab* 1988; **8**: 285–288.

26 Bero AW, Yan P, Roh JH, Cirrito JR, Stewart FR, Raichle ME *et al.* Neuronal activity regulates the regional vulnerability to amyloid-β deposition. *Nat Neurosci* 2011; **14**: 750–756.

27 Pellerin L, Magistretti PJ. Excitatory amino acids stimulate aerobic glycolysis in astrocytes via an activation of the Na+/K+ ATPase. *Dev Neurosci* 1996; **18**: 336–342.

28 Cerdán S, Rodrigues TB, Sierra A, Benito M, Fonseca LL, Fonseca CP *et al.* The redox switch/redox coupling hypothesis. *Neurochem Int* 2006; **48**: 523–530.

29 Shulman RG, Hyder F, Rothman DL. Cerebral energetics and the glycogen shunt: neurochemical basis of functional imaging. *Proc Natl Acad Sci USA* 2001; **98**: 6417–6422.

30 Sonnewald U. Glutamate synthesis has to be matched by its degradation - where do all the carbons go? *J Neurochem* 2014; **131**: 399–406.

31 Dienel GA, McKenna MC. A dogma-breaking concept: glutamate oxidation in astrocytes is the source of lactate during aerobic glycolysis in resting subjects. *J Neurochem* 2014; **131**: 395–398.

32 Goyal MS, Hawrylycz M, Miller JA, Snyder AZ, Raichle ME. Aerobic glycolysis in the human brain is associated with development and neotenous gene expression. *Cell Metab* 2014; **19**: 49–57.

33 Madsen PL, Hasselbalch SG, Hagemann LP, Olsen KS, Bülow J, Holm S *et al.* Persistent resetting of the cerebral oxygen/glucose uptake ratio by brain activation: evidence obtained with the Kety-Schmidt technique. *J Cereb Blood Flow Metab* 1995; **15**: 485–491.

34 Shannon BJ, Vaishnavi SN, Vlassenko AG, Shimony JS, Rutlin J, Raichle ME. Brain aerobic glycolysis and motor adaptation learning. *Proc Natl Acad Sci USA* 2016; **113**: E3782–91.

35 Fukuyama H, Ogawa M, Yamauchi H, Yamaguchi S, Kimura J, Yonekura Y *et al.* Altered cerebral energy metabolism in Alzheimer's disease: a PET study. *J Nucl Med* 1994; **35**: 1–6.

36 Ogawa M, Fukuyama H, Ouchi Y, Yamauchi H, Kimura J. Altered energy metabolism in Alzheimer's disease. *Journal of the Neurological Sciences* 1996; **139**: 78–82.

37 Goyal MS, Vlassenko AG, Blazey TM, Su Y, Couture LE, Durbin TJ *et al.* Loss of Brain Aerobic Glycolysis in Normal Human Aging. *Cell Metab* 2017; **26**: 353–360.e3.

38 Dastur DK. Cerebral blood flow and metabolism in normal human aging, pathological aging, and senile dementia. *J Cereb Blood Flow Metab* 1985; **5**: 1–9.

39 Fisher JP, Hartwich D, Seifert T, Olesen ND, McNulty CL, Nielsen HB *et al.* Cerebral perfusion, oxygenation and metabolism during exercise in young and elderly individuals. *J Physiol (Lond)* 2013; **591**: 1859–1870.

40 Buckner RL, Snyder AZ, Shannon BJ, LaRossa G, Sachs R, Fotenos AF *et al.* Molecular, structural, and functional characterization of Alzheimer's disease: evidence for a relationship between default activity, amyloid, and memory. *J Neurosci* 2005; **25**: 7709–7717.

41 Bufill E, Agustí J, Blesa R. Human neoteny revisited: The case of synaptic plasticity. *Am J Hum Biol* 2011; **23**: 729–739.

42 Van Essen DC, Glasser MF, Dierker DL, Harwell J, Coalson T. Parcellations and hemispheric asymmetries of human cerebral cortex analyzed on surface-based atlases. *Cereb Cortex* 2012; **22**: 2241–2262.

43 Marcus DS, Harms MP, Snyder AZ, Jenkinson M, Wilson JA, Glasser MF *et al.* Human Connectome Project informatics: Quality control, database services, and data visualization. *Neuroimage* 2013; **80**: 202–219.

Chapter 4: Regional changes in cerebral blood flow and glucose metabolism during hypoglycemia

4.1 Abstract

In healthy individuals at rest, the cerebral metabolic rate of glucose consumption (CMRglc) is tightly coupled with cerebral blood flow (CBF). However, early studies showed that global CMRglc decreases more than global CBF in patients experiencing profound hypoglycemia. Whether this relationship holds in all brain regions is unclear, as there are few regional measurements of CMRglc during hypoglycemia in humans. However, several investigators have shown that changes in CBF in humans during hypoglycemia are confined to just a few brain regions. To determine whether regional changes in glucose metabolism match changes in CBF, we used 1-[^{11}C]-D-glucose and [^{15}O]-H_2O PET to measure regional glucose metabolism and blood flow in healthy young adults undergoing hypoglycemic-hyperinsulinemic glucose clamps. We found that moderate hypoglycemia significant decreased CMRglc by approximately 20-30% in every brain region examined. Other aspects of glucose metabolism, such as glucose influx and tissue concentration, were also decreased in every region. Changes in CBF (~10%) were generally smaller than changes in CMRglc (~20%) and were only significantly different from euglycemia in a few regions. Our results indicate that hypoglycemia does not alter CBF to the same degree as CMRglc during hypoglycemia. Furthermore, they suggest that the purpose of focal increases in CBF during hypoglycemia is not to maintain CMRglc despite low glucose availability.

4.2 Introduction

Blood-borne glucose is the brain's primary energy source[1], with other fuel sources such as glycogen[2], ketone bodies[3], or lactate[4] contributing only small amounts under normal conditions. Therefore, the regulation of blood-glucose level is critical for proper brain function[5]. Acute hypoglycemia has several known neurological effects, including confusion, drowsiness, speech difficulties, and lack of coordination[6]. If blood glucose drops too low from its normal value of ~90 $mg \cdot dL^{-1}$, seizures, coma, and even death, can occur[5,7].

Due to the counterregulatory responses of insulin, glucagon, epinephrine, and other hormones[8], the incidence of hypoglycemia is rare in non-diabetic healthy individuals[9]. Hypoglycemic episodes are relatively common[10], however, in individuals with type-1 diabetes (T1DM), who experience mild treatment-related hypoglycemia nearly twice a week[11]. Hypoglycemia can be particularly problematic for the approximately 25% of individuals with T1DM that experience hypoglycemic unawareness[12], or the failure to develop hypoglycemia-related symptoms. Without the warning provided by symptoms, individuals fail to take action to counter hypoglycemia (e.g., food consumption)[10], which increases the risk of a more serious hypoglycemic episode[13].

Due to its potentially serious consequences, the impact of hypoglycemia on human brain metabolism is the subject of a large body of literature (e.g., see [14,15]). The relationship between cerebral blood flow (CBF) and hypoglycemia has been particularly well-studied. Several early studies reported that compared to the cerebral metabolic rate of glucose (CMRglc), global CBF (i.e. whole-brain) is relatively stable during profound hypoglycemia (~30 $mg \cdot dL^{-1}$)[16,17]. Studies during mild hypoglycemia have reported mixed results, with some studies reporting no change in global CBF in healthy controls,[18-22], while others have reported increases[23-25] or decreases[26]. Studies examining regional changes in CBF have generally been more consistent (for divergent

findings see[23,25,27]). In both healthy controls[26,28] and individuals with T1DM[22,29-31], relative increases in CBF have been reported in a common set of brain regions including the thalamus, globus pallidus, and medial prefrontal cortex.

The majority of studies examining CMRglc during hypoglycemia in humans have examined only global effects. These studies have found that CMRglc begins to decrease at blood glucose levels around 50 $mg \cdot dL^{-1}$[18-20,32,33], with large decreases seen during profound hypoglycemia[16,17,34]. The primary method used to measure regional CMRglc in humans is [^{18}F]-fluorodeoxyglucose (FDG) positron emission tomography (PET). Because glucose is not directly used as a tracer, a correction factor, called the lumped constant (LC), must be used to accurately measure CMRglc with FDG[35]. Unfortunately, the LC changes dramatically during hypoglycemia[36], which limits the usefulness of FDG in subjects with low blood glucose concentrations. An alternative technique that avoids this complication is to use radiolabeled glucose. Very few studies, however, have used radiolabeled glucose to examine regional human brain metabolism during hypoglycemia. Perhaps the only exception is the combined work of Gutniak et al. and Blomqvist et al [18,37]. The original report by Gutniak et al. measured CMRglc in several large regions using [U-^{11}C]-glucose PET and found that CMRglc declined by 30-40% in every region[37]. Later Blomqvist et al. performed a voxelwise analysis of the same data to confirm the uniform decline in CMRglc on a much finer spatial scale[18].

The uniform decline in CMRglc during hypoglycemia reported by Gutniak et al. and Blomqvist et al. is in contrast to the focal CBF changes that predominate the literature[14,15]. A uncoupling between CBF and CMRglc changes might be surprising given the tight spatial correlation between the two parameters under normal euglycemic conditions[38,39]. It would, however, be consistent with the fact that during profound hypoglycemia, changes in global

CMRglc are much more pronounced than changes in either CBF or oxygen consumption[16,17,34,40]. Moreover, it has been proposed that the purpose of CBF changes during hypoglycemia in not to provide the brain with more glucose. Rather, CBF changes as a part of the brain's counterregulatory hormonal response to hypoglycemia[41,42]. To determine whether brain glucose metabolism changes during hypoglycemia are regionally-specific or uniform, we used measured regional glucose metabolism with 1-[^{11}C]-D-glucose and regional CBF with [^{15}O]-H_2O PET during stepped hypoglycemia in healthy participants. As a true glucose tracer, 1-[^{11}C]-D-glucose enables quantitative estimates of CMRglc, glucose influx, free glucose concentration, and glucose extraction regardless of blood glucose level.

4.3 Methods

The original source for the data analyzed in this report is a previous study examining the relationship between hypoglycemia, whole-brain glucose metabolism, and counterregulatory hormones[33]. For further methodical detail, please see the cited reference.

Participants

A total of eighteen participants were included in this study. All participants were healthy young adults without a history of diabetes. Participants were randomly assigned to one of two groups. Subjects in the first group received hyperinsulinemic glucose clamps first at 90 mg·dL^{-1} and then at 60 mg·dL^{-1}. This group consisted of 10 individuals (6 female, 4 male) with an average age of 28.9 (SD 6.9) years and a BMI of 24.4 (SD 3.6) kg·m^{-2}. The second group consisted of 8 subjects (2 female, 6 male) who received glucose clamps at 75 mg·dL^{-1}and 45 mg·dL^{-1}. The average age was 27.6 (SD 8.2) years and a BMI of 24.0 (SD 2.8) kg·m^{-2}. All participants gave written informed consent.

Experimental design

Subjects reported in the morning after fasting overnight for 10 hours. Intravenous catheters were placed into the antecubital veins of both arms. The first catheter was used for the infusion of insulin, glucose, and potassium chloride, and the second for the injection of radioactive tracers. An arterial line was placed into the radial artery of one forearm for the collection of arterial input data. Subjects were then taken to the PET scanner, where the hyperinsulinemic glucose clamps were started after 30 minutes of supine rest. Human insulin was infused at 2.0 $mU \cdot kg^{-1} \cdot min^{-1}$ and 20% glucose was infused at a rate necessary to achieve the target glucose level. The first glucose clamp (90 or 75 $mg \cdot dL^{-1}$) was immediately followed by the second clamp (60 or 45 $mg \cdot dL^{-1}$). Each clamp lasted for 2 hours. During the clamping procedure, symptom scores and the arterial concentrations of epinephrine, norepinephrine, insulin, C-peptide, glucagon, cortisol, fatty acids, B-hydroxybutyrate, and lactate were measured every 30 minutes. All experimental procedures were approved by the Washington University School of Medicine Human Research Protection Office for compliance with the Helsinki Declaration of 1975.

Image acquisition

PET scanning began 20 minutes after blood glucose was maintained at the target level for twenty minutes. First, attenuation was measured with [^{68}Ge]-[^{68}Ga]-rotating rod sources. Next, subjects inhaled 22 ± 4 mCi of [^{15}O]-CO for the measurement of cerebral blood volume (CBV) [43]. A single 5-minute long emission frame was acquired starting 2 minutes after inhalation. Cerebral blood flow (CBF) was then measured with the injection of 19 ± mCi of [^{15}O]-H_2O [44]. The dynamic acquisition consisted of 60 2-second frames acquired immediately following injection. Finally, cerebral glucose metabolism was measured via the injection of 10 ± 3 mCi of 1-[^{11}C]-D-glucose[45]. The emission data was split into 45 frames spanning 60 minutes (16 x 30 s,

8 x 60 s, 16 x 120 s, 4 x 180s). All PET data was acquired with a ECAT EXACT HR+ PET scanner (Siemens/CTI, Knoxville, TN) in 3D mode with retraction of interslice septa and reconstructed using a filtered back-projection[46]. During [^{15}O]-CO and [^{15}O]-H_2O acquisition, arterial input data was automatically sampled from the radial artery at a rate of 5 mL·min^{-1}. During the 1-[^{11}C]-D-glucose scan, manual arterial samples were acquired every 10-15 seconds during the first 3 minutes and every 10-15 minutes thereafter. The same PET scanning protocol was performed during both glucose clamps. Following the completion of the glucose clamping experiment, a high resolution T1-weighted MPRAGE was acquired using a Siemens 3T Trio (2400 ms TR, 3.16 ms TE, 256 x 256 x 176 FOV, 1 mm^3 voxels).

Image analysis

All PET data was smoothed with a 5 mm isotropic Gaussian kernel to create images with an approximate resolution of 8 mm isotropic voxels[47]. After smoothing, the dynamic 1-[^{11}C]-D-glucose data was motion-corrected using previously described in-house software[48,49]. A mean image across time was then created for each PET series, resulting in two images for each tracer. Within each tracer, the average images were registered to each other by minimizing the error between the forward (image 1 -> image 2) and backward (image 2 -> to image 1) registrations[48]. Once aligned, an average within-tracer image was computed and registered to the high-resolution T1-weighted image using a vector gradient algorithm[50].

The T1-weighted image was segmented using Freesurfer 5.1[51] to create 48 non-overlapping cortical and subcortical regions of interest (ROIs; Figure 4.1).The Desikan atlas[52] was used to define 34 gyral-based cortical gray matter ROIs. Separate ROIs were created for subcortical gray regions (thalamus, caudate, putamen, pallidum, hippocampus, amygdala, and nucleus accumbens) and white matter (deep, superficial, corpus callosum)[53]. ROIs were also

created for cerebellar gray and white matter. Finally, the brainstem and ventral dienecephalon were separated into two ROIs. All ROIs were averaged across the cerebral hemispheres. The tissue class (white matter, gray matter, and CSF) of each voxel was determined separately using FSL's[54] FAST[55].

A previously published and validated four-compartment model[45] was used to describe the 1-[^{11}C]-D-glucose data:

$$C_T(t) = CBV \cdot C_a(t) + \int_0^t C_a(\tau) \cdot r(t-\tau)\, d\tau \qquad (4.1)$$

$$r(t) = \alpha e^{-\beta t} + K_1 k_3 \left[\frac{e^{-k_4 t}}{(\beta - k_4)} + \frac{k_4 \cdot e^{-k_4 t}}{(\beta - k_4)(k_5 - k_4)} + \frac{k_4 \cdot e^{-k_5 t}}{(\beta - k_5)(k_4 - k_5)}\right] \qquad (4.2)$$

where $C_T(t)$ is the average tracer concentration within the ROI at time t, $C_a(t)$ is the arterial tracer concentration, and $r(t)$ is the tissue impulse response function. The α and β terms are products of the model's five rate constants (K_1, k_2, k_3, k_4, and k_5): $\alpha = K_1 \left[1 - \frac{k_3}{(\beta - k_4)} + \frac{k_3 k_4}{(k_4 - \beta)(k_5 - \beta)}\right]$, $\beta = k_2 + k_3$. To simplify the model fitting, k_5 was assumed to equal CBF/CBV. The remaining rate constants were estimated for all 48 FreeSurfer ROIs using nonlinear least squares. Following Graham et al., we chose to optimize $\frac{K_1}{(k_2 + k_3)}$ instead of k_2[56]. Prior to regional fitting, the delay between the input function, $C_a(t)$, and the PET data was corrected for by fitting equation 4.1 to the average whole-brain tissue activity curve with the addition of a delay term. In accordance with previous procedures, all 1-[^{11}C]-D-glucose modeling was done with whole-blood arterial tracer concentration without correction for radiometabolities[33,45,57].

CBF was computed for each ROI using a one-compartment, two parameter model[44]:

$$C_T(t) = f \int_0^t C_a(\tau) \cdot e^{-\frac{f}{\lambda}(t-\tau)}\, d\tau \qquad (4.3)$$

where f is CBF and λ is the blood brain partition coefficient. Before performing a nonlinear least squares fit on equation 4.3, the arterial input function, C_a, was corrected for delay and dispersion. Correction for the dispersion between the automatic blood sampler and the radial artery was performed by assuming that the measured input function, C_m, is the convolution of the actual input function, C_a, with a measured kernel h[58]:

$$C_m(t) = \int_0^t C_a(\tau) \cdot h(t-\tau)\, d\tau \qquad (4.4)$$

Therefore, the reconstruction of C_a is a deconvolution problem. This problem was solved by assuming that C_a follows the form described by Golish et al.[59], and then minimizing the difference between C_m and the right hand side of equation 4.4 with nonlinear least squares. Delay between C_a and the [^{15}O]-H_2O PET data was corrected for using the same procedure as the 1-[^{11}C]-D-glucose data.

CBV (in mL·hg^{-1}) was computed for each voxel using the following equation[43]:

$$CBV = \frac{\int_{t_1}^{t_2} C_T(\tau)\, d\tau \cdot 100}{\int_{t_1}^{t_2} C_a(\tau)\, d\tau \cdot R \cdot d_T \cdot d_B} \qquad (4.5)$$

where R is the ratio of cerebral small to large vessel hematocrit and d_T and d_B are the densities of tissue and blood respectively. The values for these constants were set according to Martin et al.[43]: $R = 0.85$, $d_T = d_B = 1.05 \frac{g}{mL}$. As CBV was not a parameter of interest and only needed to solve equation 4.1, we utilized a simple strategy to minimize the impact that noise in the CBV quantification had on our results. All voxels with a CBV less than 6 were replaced with the mean CBV value of their respective tissue class (white, gray, or CSF). All voxels with a CBV greater

or equal to 6 were replaced with the mean of all such voxels. The resultant image was then smoothed with 5 mm isotropic Gaussian kernel prior to computing the mean CBV within each FreeSurfer ROI. Without this correction fitting the C11-glucose model (Eq. 1 and 2) was often unstable, as low values of CBV from noisy voxels produced unrealistically high values of k_5.

All optimization was performed using the *optimize* package in SciPy [60]. Uniform weights were used for all nonlinear least square fits.

Metabolic parameters

The rate constants estimated from the regional 1-[^{11}C]-D-glucose data were used to estimate five distinct parameters: 1) cerebral metabolic rate of glucose (CMRglc), 2) glucose influx, 3) free glucose concentration, 4) glucose first-pass extraction (E_{fp}), and 5) net glucose extraction (E_{net}). These quantities were computed as follows[45,61]:

$$CMRglc = \frac{K_1 k_3}{(k_2+k_3)} \cdot C_b \qquad (4.6)$$

$$Influx = K_1 C_b \qquad (4.7)$$

$$Concentration = \frac{K_1}{(k_2+k_3)} \cdot C_b \qquad (4.8)$$

$$E_{fp} = \frac{K_1}{CBF} \qquad (4.9)$$

$$E_{\boldsymbol{net}} = \frac{K_1 k_3}{(k_2+k_3)\cdot CBF} \qquad (4.10)$$

C_b, the arterial whole blood glucose concentration, was estimated using C_p, the measured arterial plasma glucose concentration[45,62]: $C_b = C_p(1 - 0.3 \cdot hematocrit)$. We also computed whole-brain normalized estimates of each parameter by dividing each regional value by the volume-weighted mean across regions.

Statistics

For each region, the relationship between C_p and CMRglc, glucose influx, glucose concentration, CBF, E_{fp}, and E_{net} was assessed using a multivariate linear mixed model[63]:

$$Y_{ij} = X_{ij}\beta + b_i + e_{ij} \qquad (4.11)$$

where Y_{ij} is a 6 x 1 vector containing the metabolic parameter estimates for subject *i* during glucose clamp *j*. X_{ij} is a 1 x p row vector containing the fixed effect regressors. Here, p = 3 as X_{ij} is made up of three regressors: 1) Intercept (β_0), 2) C_p (β_1), and 3) A restricted cubic spline term with boundary knots at the 0.1 and 0.9 quantiles and an interior knot at the 0.5 quantile (β_2)[64]. The spline regressor was added to allow for a nonlinear relationship between C_p and any of the metabolic parameters. Prior to fitting, the data in Y and X were standardized so that each metabolic parameter and fixed effects regressor had a mean of zero and a SD of 1. The fixed effect regression coefficients are in the p x 6 matrix β. The 1 x 6 row vector b_i contains a subject specific random intercept for each metabolic parameter. Finally e_{ij} is a 1 x 6 row vector of independent and identically distributed errors. The random intercept terms were assumed to come from a multivariate normal distribution: $b_i \sim Normal(0, D)$, where D is a 6 x 6 unstructured covariance matrix. Note that even though our model assumes the residual errors for each parameter are identical and independent, covariance between the parameters can be accounted for through their random intercepts[63].

Equation 4.11 was fit separately to the data from each FreeSurfer ROI using a Bayesian Hamilton Markov chain Monte Carlo (MCMC) with Stan[65]. The fixed effect coefficients where given a broad normal prior with a mean of 0 and a SD of 5. A half-Cauchy distribution with a

location of 0 and a scale of five was used as the prior for the residual error term. For modeling purposes, the random effects covariance matrix was decomposed into a 6x6 correlation matrix and a vector of SDs [66]. The correlation matrix was given a LKJ Cholesky[67] prior with a shape of 1.0, which implies a uniform prior density for the correlation between the random effect parameters[68]. A half-Cauchy distribution with a location of 0 and a scale of five was used for the standard deviation parameters. Fitting was performed with four independent MCMC chains consisting of 5,000 iterations. The first 2,500 iterations of each chain were removed as warm-up, leaving a total of 10,000 iterations available for inference. The Gelman-Rubin $\hat{R}$ statistic was used to check that all four MCMC chains had converged [69,70]. $\hat{R}$ is the ratio of within to between chain variance and should equal 1 after convergence. The $\hat{R}$ for all reported parameters was close to 1.0 for every regional fit (range=0.9996 to 1.036).

Regional CBF data was missing for three clamp studies. A univariate mixed model was used to interpolate the missing CBF values for each FreeSurfer region. The model consisted of a single random intercept and the same fixed effect regressors as equation 4.11. All fitting was performed using the R[71] package *lme4*[72]. The interpolated CBF values were used to optimize equation 4.1 and to compute E_{fp} and E_{net}. They were not used to assess the relationship between CBF and C_p with equation 4.11. Therefore, all inference for changes in CBF was based on 33 data points and not 36 like the other metabolic parameters. To account for the missing CBF data, the Bayesian formulation of equation 4.11 included the missing data points as free parameters.

For each region, the overall association between C_p and each of the six metabolic parameters (CMRglc, glucose influx, glucose concentration, CBF, E_{fp}, and $E_{net)}$ was tested by computing the 95% highest density region of the joint distribution between β_1 and β_2 (Figure

4.2). A significant relationship was reported if the coordinate $\beta_1 = 0.0$, $\beta_2 = 0.0$ was outside of the 95% region. For example, a significant relationship between C_p and CMRglc would indicate that CMRglc changes as a function of blood glucose level. The R package *ks* was used estimate the 95% highest density regions[73]. If a significant relationship with C_p was found, than the marginal highest density interval (HDI) for the cubic spline term β_2 was computed[74]. There was significant evidence for a nonlinear relationship with C_p if the 95% HDI of β_2 did not overlap 0.0. A nonlinear relationship with C_p indicates that that change in the metabolic parameter (e.g. CMRglc) cannot be described by a simple linear function. To visualize the effect of hypoglycemia, an image of the difference between euglycemia and hypoglycemia was made by computing the difference between the model prediction at C_p= 90 mg·dL^{-1} and at C_p = 45 mg·dL^{-1} for each ROI. Spearman rank order correlations were used to assess the spatial correspondence between maps of metabolic change (e.g., CMRglc vs. CBF). Due to the autocorrelation present between brain regions[75], as well as differences in ROI sizes, *p*-values for the correlation coefficients were not computed. Unless otherwise stated, all values are posterior medians and HDIs.

4.4 Results

Regional changes in metabolism

Figure 4.3 shows the individual CMRglc, glucose influx, glucose concentration, CBF, E_{fp}, and E_{net} data in both the precuneus and deep white matter along with the population average fits from the multivariate linear mixed model. We chose the precuneus as an example gray matter region as it has one of the highest CMRglc at euglycemia. CMRglc, influx, and concentration dropped along with C_p in both the precuneus and deep white matter (Figure 4.3A-C).

Conversely, E_{net} increased with decreasing C_p (Figure 4.3F). CBF and E_{fp} showed less pronounced changes during hypoglycemia (Figure 4.3D-E).

To quantify this impression, we tested for the presence of a significant relationship between C_p and each metabolic parameter in 48 separate FreeSurfer ROIs (see Methods). A significant relationship was found between C_p and CMRglc (Figure 4.4B), glucose influx (Figure 4.5B), glucose concentration (Figure 4.6B), and E_{net} (Figure 4.7B) in every region tested. A significant nonlinear relationship between C_p and CMRglc was found for most (35/48), but not all, regions (Figure 4.4C). The regions showing only a linear relationship include both gray (amygdala, entorhinal cortex, and globus pallidus) and white (cerebellar white matter, corpus callosum, and deep white matter) matter. No region showed a nonlinear relationship between C_p and glucose influx (Figure 4.5C) or concentration (Figure 4.6C), and only the globus pallidus had a significant nonlinear association between C_p and E_{net} (Figure 4.7C).

Quantitative changes in E_{fp} and CBF were not nearly so widespread. Significant increases in E_{fp} with decreasing C_p were found in 17 out of 48 regions (Figure 4.8B). Both cortical and cerebellar gray and white matter regions displayed increases in E_{fp}, though the only subcortical gray matter region which increased its first-pass extraction was the caudate. No evidence was found for a nonlinear relationship between C_p and E_{fp} (Figure 4.8C). A significant relationship between CBF and C_p was found in only nine regions (Figure 4.9B). Significant decreases in CBF with hypoglycemia were found in the banks of the superior temporal sulcus, caudal anterior cingulate, interior temporal cortex, posterior cingulate, superior temporal cortex, frontal pole, transverse temporal cortex, and nucleus accumbens. A significant increase was found only in the

globus pallidus, which was also the only region with a significant nonlinear relationship between C_p and CBF (Figure 4.9C).

As many previous studies have reported relative changes in blood flow during hypoglycemia[22,26,28], we repeated our previous analysis of CBF changes after first normalizing each CBF image by its global mean. A relative decrease in CBF was observed in the posterior cingulate, while relative increases were found in the thalamus, globus pallidus, brainstem, and ventral diencephalon (Figure 4.10B).

Discrepancies between CMRglc and CBF changes

To further investigate the discrepancy between the widespread changes in CMRglc (Figure 4) and the focal changes of CBF (Figures 7,10), we first correlated euglycemic metabolic values with the difference between euglycemia and hypoglycemia over all ROIs (see Methods). CMRglc, influx, and concentration all showed strong negative correlations. Regions with the greatest baseline values displayed the greatest changes during hypoglycemia (Figure 4.11A-C). Conversely, CBF, E_{fp}, and E_{net}, the parameters which are directly dependent on blood flow, showed only modest correlations (Figure 4.11D-F), with the association between baseline and change in E_{fp} being particularly weak (Figure 4.11E).

Next, we correlated regional changes in CMRglc with regional changes in CBF. Changes in CBF and CMRglc showed only modest regional correlations, both quantitatively (Figure 4.12A), and expressed as percent change (Figure 4.12B). This is in contrast with euglycemia, where regional CBF and CMRglc were tightly correlated (ρ = 0.86). Nearly every region exhibited CMRglc decreases in the 20-25% range, with the exception of deep white matter and the corpus collosum, the two regions with the lowest CMRglc at euglycemia (Figure 4.12B). Consistent with previous relative analysis (Figure 4.10B), CBF in most regions decreased

slightly, with the exception of the thalamus, globus pallidus, brainstem, and ventral diencephalon (Figure 4.12B), where CBF increased.

4.5 Discussion

Overview

A previous analysis of the same data analyzed here found whole-brain decreases in CMRglc, glucose influx, and free glucose concentration, an increase in E_{net}, and no change in CBF during moderate hypoglycemia (45 $mg \cdot dL^{-1}$)[33]. Importantly, changes in counterregulatory hormones (epinephrine and glucagon) were observed before changes in CMRglc. However, that study did not report any regional changes in metabolism during hypoglycemia. Here we found that hypoglycemia decreases CMRglc, glucose influx, and glucose concentration, and increases E_{net}, in every brain region we examined. Hypoglycemia induced changes in E_{fp}, and especially CBF, were more regionally specific. Decreases in CMRglc, glucose influx, and glucose concentration correlated strongly with baseline values, whereas changes in CBF, E_{fp}, and E_{net} showed only modest correlations. Regional changes in CMRglc did not correlate with regional changes in CBF, suggesting a difference between glucose metabolism and blood flow in the response to hypoglycemia. Finally, we found that glucose concentration in the cerebellum was much greater than any other brain region.

Glucose Metabolism

Our finding that hypoglycemia decreases CMRglc in all brain regions is consistent with two previous paired studies in humans[18,37]. These studies reported that CMRglc declines by approximately 40% in all regions during an insulin-induced hypoglycemia of 50 $mg \cdot dL^{-1}$. Uniform declines in CMRglc are also found during short-term starvation, a condition that results in mild hypoglycemia[76,77]. Multiple studies in rats have also reported nearly uniform decreases in

CMRglc during hypoglycemia[78-80]. A few exceptions were observed in each study. Abdul-Rahman and Siesjö reported that CMRglc in the hypothalamus and the cerebellum did not decline even after 30 minutes in an insulin-induced hypoglycemic coma[78]. Pelligrino et al. also reported that cerebellar CMRglc was maintained during modest hypoglycemia (approximately 40 $mg \cdot dL^{-1}$) [80]. Conversely, Bryan et al. reported CMRglc did not decrease in the pyramidal tracts[79], even when blood glucose was lowered to nearly 25 $mg \cdot dL^{-1}$. An outlier to the studies discussed above is the work of Suda et al., who found much more variable changes CMRglc during moderate hypoglycemia (approximately 43 $mg \cdot dL^{-1}$)[81]. After Bonferroni correction for multiple comparisons, significant declines in CMRglc were found only in the dentate gyrus of the hippocampus and in several brainstem regions. Absolute CMRglc, however, declined in every region but the superior colliculus and the dentate nucleus of the cerebellum. It is possible that some of the variability in these results is due to differences in the degree of hypoglycemia. Indeed, Bryan et. al found that CMRglc declined only in a few regions when the blood glucose level was at 35 $mg \cdot dL^{-1}$, whereas all regions exhibited declines with more pronounced hypoglycemia.

Compared to CMRglc, the literature on regional changes in quantitative glucose influx, concentration, or extraction is relatively sparse. Indeed, this report is, to the best of our knowledge, the first to examine this question in humans. There are, however, relevant studies in animal models. In agreement with our results, hypoglycemia has been shown to reduce the free glucose concentration throughout the brain in mice[82,83] and rats[84,85]. Interestingly, Paschen et al. found that the brain stem, hypothalamus, and thalamus still have some free glucose concentration even during deep hypoglycemia. As far as we are aware, this finding has not been replicated. LaManna and Harik found that glucose influx and E_{fp} decreased in the frontal and parietal

cortices, cerebellum, and hippocampus[86]. This is only partially consistent with our results, as we did not find a significantly increase in hippocampal E_{fp}. We are not aware of any data on regional changes in E_{net} during hypoglycemia, but our results are agreement with previous studies showing global increases[33,45,87].

We also found that the relationship between plasma glucose and CMRglc was nonlinear in most brain regions, with CMRglc changing little until plasma glucose was lowered to around 45 $mg \cdot dL^{-1}$. This is consistent with the finding that glucose metabolism is largely maintained during modest hypoglycemia in humans[19,32,33] and in animal models[45,78,79]. A nonlinear relationship between CMRglc and plasma glucose is expected under normal conditions, as cerebral glucose influx far outstrips glucose consumption, and therefore, glucose consumption only declines once CMRglc and influx are nearly equal[88]. Conversely, we found little evidence for nonlinearity in any of the other parameters that we examined. No regions had a significant nonlinear relationship with glucose influx, glucose concentration, or E_{fp}, and only the globus pallidus had a nonlinear relationship with E_{net}.

Our finding of linear changes in glucose influx and concentration generally agrees with the literature. Several studies using a variety of techniques have found that brain glucose concentration is linear with respect to plasma glucose over a wide range[85,89-93]. Two studies in rats reported that changes in brain glucose influx are largely linear in the blood glucose range we studied here, before saturating at higher concentrations[86,94]. Using a similar experimental design to ours, Powers et al. also showed a roughly linear decline in glucose influx in macaques[45]. Our results are somewhat in conflict with previous studies of glucose first-pass extraction in animal models[86,95,96]. These studies found a nonlinear relationship between E_{fp} and blood glucose levels, with large increases in E_{fp} during more profound hypoglycemia. Here, although E_{fp} did increase

in many regions, the increase was fairly small and did not deviate significantly from linearity. It is likely that, if we had studied more profound levels of hypoglycemia, larger changes in E_{fp} would have been observed.

Cerebral Blood Flow

Unlike glucose metabolism, alterations in CBF were restricted to a select set of regions. Quantitative decreases in CBF were found in a handful of cortical regions, including the caudal anterior cingulate, inferior temporal cortex, and posterior cingulate, as well as in the nucleus accumbens. Nwokolo et al. also reported that hypoglycemia decreases CBF in the temporal lobe[97], prefrontal cortex[42,97], and globus pallidus[42]. We also found that relative to the rest of the brain, the CBF response to hypoglycemia was significantly lower in the posterior cingulate and significantly higher in the thalamus, globus pallidus, brainstem, and ventral diencephalon. In both healthy and in individuals with T1DM, hypoglycemia has been shown to increase relative blood flow in the thalamus[26,28-31,98-100], medial prefrontal cortex[26,28,31,99], globus pallidus[26,28,31], and anterior cingulate cortex[28,31]. Although we did find a relative decrease in the posterior cingulate[29], we did not find any relative increases in CBF in the cerebral cortex. One possible explanation is that hypoglycemia was not maintained long enough to alter blood flow in these regions. In support of this hypothesis, two recent studies found that regional increases in CBF become more pronounced the longer hypoglycemia is maintained[28,31]. However, relative decreases in MPFC CBF have been found using a protocol similar to the one we used here[42].

Research in animal models have also found regional variability in the CBF response to hypoglycemia[79,88,101]. There are, however, a few important discrepancies from the human literature. First, animal model studies have generally found that hypoglycemia increases global CBF[79,92,101-104]. The human literature is much more mixed[15], with a large number of studies

reporting no change in global CBF during mild to moderate hypoglycemia [18-22,105]. It is tempting to argue that the reason for this discrepancy is that human studies do not measure CBF at low enough levels of hypoglycemia. Multiple studies in rats have shown that, although CBF increases rapidly once the blood glucose level drops below 40 $mg \cdot dL^{-1}$, it is relatively stable above this point[79,92,104]. A few human studies have found that whole-brain CBF increases once blood glucose is lowered below 40 $mg \cdot dL^{-1}$[23-25,34]. However, other studies have reported small and/or non-significant changes in subjects whose blood glucose is low enough to induce a hypoglycemic coma[16,17]. Whether increased CBF during hypoglycemia is a species specific phenomenon, or a by-product of different measurement techniques, remains to be determined. Second, studies in animal models have consistently reported that hypoglycemia increases CBF in nearly every region of the brain[79,101,103,104]. There is, however, regional variability in the magnitude of the increase. For example, particularly large increases in CBF have been found in the cerebellum[101,103] and the thalamus[79,101]. This is in contrast with the human literature, which has consistently shown that hypoglycemia selectively increases CBF in a network of regions including the thalamus and medial prefrontal cortex [15]. Part of this difference may be that unlike animal studies, studies in humans have tended to report regional changes relative to the whole-brain[22,26,28-31]. Normalization is unlikely to fully account for the discrepancy, however, as we, in agreement two other studies[42,97], did not observe CBF changes in every region even with quantitative CBF. It is also possible that a species difference may explain the discrepancy between animal and human studies. Metabolic rates are higher in rodents[106], so it is conceivable that they are more effected by hypoglycemia than humans.

Metabolic coupling during hypoglycemia

Our results show clearly that during hypoglycemia there is an uncoupling between regional changes in glucose metabolism and CBF. Glucose metabolism was altered in every

region we examined, while CBF was changed in smaller set of regions. Furthermore, there was only a modest regional correlation between changes in CMRglc and changes in CBF. This suggests that the purpose of increased CBF during hypoglycemia is not, at least completely, to increase the supply of glucose to the brain. A similar proposal was made by Powers et al., who found that the increase in CBF in the somatosensory cortex during tactile stimulation was the same in euglycemic and mildly hypoglycemic (~60 $mg \cdot dL^{-1}$) subjects[107]. If CBF increased during hypoglycemia in order to prevent a fall in glucose consumption, one would expect CMRglc to be relatively maintained in regions with increased CBF (e.g. the globus pallidus). Instead, we found that declines in CMRglc were largely determined by baseline metabolic rates, and that most regions declined by a little over 20% once the blood glucose level was lowered to 45 $mg \cdot dL^{-1}$. In contrast, CBF fell in most regions by around 10% and baseline CBF was much less predictive of CBF changes. It is possible that CBF increases in order to supply the brain with alternative fuels such as lactate or ketone bodies. We are not able to rule out this possibility with our present data. However, studies measuring whole-brain changes in metabolism have reported that lactate and β-hydroxybutyrate can account for only a modest proportion of the brain's metabolic rate during insulin induced hypoglycemia[20,87]. Furthermore, the plasma concentrations of both lactate and β-hydroxybutyrate were not significantly altered by hypoglycemia in our study[33]. This makes it unlikely that either substance was being used as an alternative, as the consumption of both lactate[108] and β-hydroxybutyrate[3]is limited strongly by plasma concentration.

An alternative hypothesis is that focal increases in CBF are part the sympathetic counterregulatory hormonal response to hypoglycemia[109]. In healthy individuals, hypoglycemia is counteracted by the release of several key hormones, the foremost of which is insulin[8].

However, hypoglycemia is also accompanied by the release of glucagon, epinephrine, growth hormone, and cortisol. If the release of these hormones fails to restore the blood glucose to normal levels, then cognitive decline begins to occur[110]. It has been proposed[109] that these counterregulatory responses are regulated by a network of brain regions consisting largely of the thalamus and medial prefrontal cortex. Consistent with this idea, acute hypoglycemia has been show to increase CBF in the thalamus and medial prefrontal cortex[22,26,28,30,42,99], and there is a positive correlation between thalamic CBF and autonomic symptom scores during hypoglyemia[97] . Both the thalamus and medial prefrontal cortex are part of a network of regions that, along with the hypothalamus, regulate the brain's autonomic response to sensory stimuli[111]. Furthermore, Arbelaez et al. reported that while recurrent hypoglycemia attenuates hormonal responses in healthy individuals, it actually augments the increase in thalamic CBF that is normally seen during acute hypoglycemia[98]. Based on this finding, and the assumption that increased CBF is a marker of increased neural activity, Arbelaez et al. proposed that hormonal responses are blunted by repeated hypoglycemia because of increased inhibition of the hypothalamus by the thalamus[98]. More work is needed to confirm this hypothesis, however, as more recent studies have reported that the increase in thalamic CBF during hypoglycemia is blunted, not increased, in type-1 diabetics with hypoglycemic unawareness[22,30].

The fact that hypoglycemia effects oxygen metabolism much less than glucose metabolism is well established[16,17,34,40]. This disconnect is particularly prevalent during extreme hypoglycemia, where the molar ratio of oxygen-to-glucose metabolism (OGI) rises well above its theoretical value of 6.0[102,112,113]. In the normal resting brain, OGI is approximately 5.5, which indicates that nearly 10% of the brain's glucose metabolism is consumed via non-oxidative pathways[114]. OGI values greater than 6.0 indicate that the brain is oxidizing energy sources other

than glucose[106]. Studies have shown that that the rat brain quickly uses its supply of free glucose, glycogen, lactate, and pyruvate during profound acute hypoglycemia[82-84,115,116]. After this point, endogenous amino acids, such as glutamine[102], and phospholipids[113] are used to maintain ATP concentration until the onset of hypoglycemic coma. Although glucose consumption is reduced more than oxygen consumption even in moderate hypoglycemia[20], how oxidative metabolism is maintained in this condition is not fully understood. Lubow et al. estimated that lactate uptake could account for up to 25% of the brain's glucose deficit during moderate hypoglycemia[20]. Glycogen has also been suggested as a potential fuel source[117-119], though it is unclear how long it can used as fuel source as glycogen is largely restricted to astrocytes[120] and is present in fairly small amounts[2]. It is likely that oxidative metabolism is maintained by some combination of these and other fuels[121]. Part of the glucose debt that occurs during moderate hypoglycemia could be paid by reducing the approximately 10% of glucose metabolism that is non-oxidative[114]. Although this idea has not been tested, it would help to support whether non-oxidative glucose consumption is involved in learning, synaptic plasticity, and development[122,123] (but see[124]).

Cerebellar Metabolism

We did not expect to find such a striking difference in free glucose concentration between the cerebellum and other brain regions (Figure 4.6A, Figure 4.11C). At euglycemia, the average free glucose concentration in the cerebellar cortex was 0.68 $\mu Mol \cdot g^{-1}$, compared to 0.42 $\mu Mol \cdot g^{-1}$for the cerebral cortex. Regional differences in free glucose concentration have not been well-studied in humans. There are, however, some exceptions. Heikkilä et al. found that compared to the cerebral cortex, the ratio of free brain glucose to water was twice as high in the cerebellum[125]. Herzog et al. reported that the concentration of both free glucose and glycogen was higher in the cerebellar cortex[126]. Similar results have been obtained in animal models as well[82-84,127], although it should be noted that the differences are smaller than what has been

ported in humans, and that other studies have failed to find any difference[80,85]. Higher glucose concentration in the cerebellum is relevant for two reasons. First, the cerebellum seems to respond differently to hypoglycemia than other brain regions. There is evidence that CMRglc in the rat cerebellum is maintained during both moderate[80] and profound hypoglycemia[78]. Although we did not replicate this finding in our study, it is possible that our subjects were hypoglycemic too long for the cerebellum's higher free glucose concentration to serve as an effective buffer. The cerebellum is also more resistant to hypoglycemia induced decreases in ATP[84,128] and protein synthesis[129]. Finally, the cerebellum appears to be more resistant to hypoglycemia-induced cell death than other brain regions. Prolonged severe hypoglycemia causes neuronal death throughout the cortex and subcortex[130-132], with neuronal loss in the dentate gyrus being a defining feature. In contrast, cerebellar neurons, particularly Purkinje cells and granule cells, are largely intact even after extended periods of profound hypoglycemia[128,131]. Given these results, one hypothesis is that higher levels of free glucose provide the cerebellum with some resistance to hypoglycemia. The role of free glucose in preserving energy metabolism is likely minor though, as the cerebellum's glucose concentration of 0.68 $\mu Mol \cdot g^{-1}$ is small compared to its baseline metabolic rate of 20.5 $\mu Mol \cdot hg^{-1} \cdot min^{-1}$.

Second, the higher glucose concentration in the cerebellum is relevant to studies using FDG PET to measure brain glucose metabolism. The LC for FDG has traditionally been assumed to be the same for all brain regions[35]. Multiple studies have shown that the LC decreases as brain free glucose concentration increases[133,134]. This suggests that the higher free glucose in the cerebellum would result in a lower LC than the rest of the brain, which is exactly what was found by Graham et al[56]. Our results support the findings of Graham et al. and suggest that studies using FDG to study cerebellar metabolism need to account for regional differences in the

LC. In particular, if the same LC is used to measure CMRglc in all brain regions, then cerebellar CMRglc will be underestimated relative to other regions.

Limitations

A few caveats should be considered when interpreting our results. First, our ability to detect regional effects was limited by our small sample size. This fact, combined with the difficulty in fitting a model with four compartments and four free parameters, limited our examination of regional changes to larger ROIs. Therefore, it is possible that we missed changes in smaller regions that were not uniquely defined in our region set (e.g., hypothalamus). Second, our experimental design was set up so that each subject was studied during only two glucose clamps. As a result, we did not observe in a single subject the transition from euglycemia (90 $mg \cdot dL^{-1}$) to moderate hypoglycemia (45 $mg \cdot dL^{-1}$). All inferences are therefore based on population level statistics. Third, the first glucose clamp for each subject was always at a higher blood glucose level than the second clamp. This is concerning as order effects have been reported with FDG PET[135,136], although the direction is not always consistent. A systematic order effect would result in biased estimates of metabolic change during hypoglycemia. Finally, our study was limited to observing changes in total glucose metabolism during hypoglycemia. We did not collect any data on oxygen metabolism to see if hypoglycemia decreased glycolytic glucose metabolism to a greater extent than oxidative glucose consumption. We also did not acquire any data that would enable us to determine the metabolic fates of glucose during hypoglycemia. Such analyzes would be possible using other techniques, such as labeled ^{13}C-labled glucose in humans[32] or at an much finer resolution using metabolic flux analysis *in vitro*[137,138].

Conclusion

We found that moderate hypoglycemia produces uniform declines in brain glucose metabolism while only altering CBF in a select set of regions. Therefore, it appears that maintaining CMRglc is not the primary driving force behind focal increases in CBF during hypoglycemia. Instead, our results are consistent with the hypothesis that focal increases in CBF are part of the sympathetic counterregulatory response to hypoglycemia. Elucidating exactly how CBF modules this counterregulatory response is an important topic for future studies.

4.6 Figures

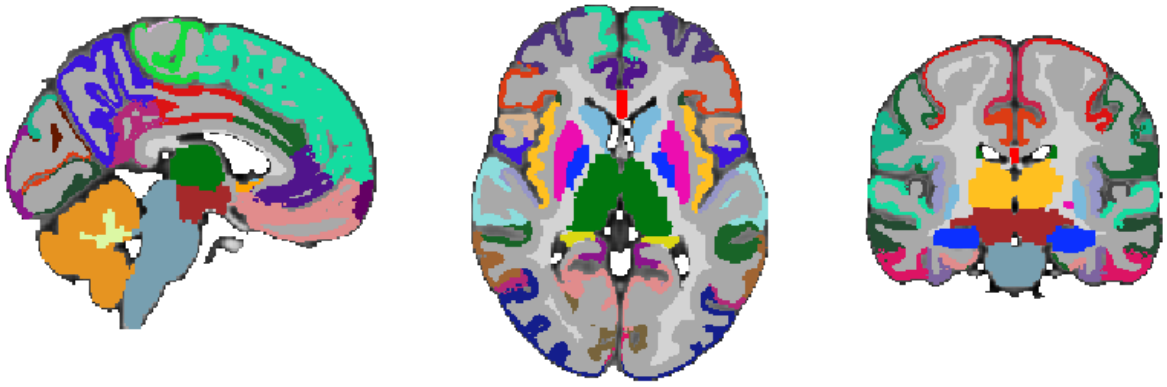

Figure 4.1: Freesurfer generated regions of interest (ROIs)

The ROI set consisted 48 non-overlapping regions that were averaged across the cerebral hemispheres. The cortical gray matter was parcellated in to 34 regions[52], the subcortical gray matter into 7 ROIs (thalamus, caudate, putamen, pallidum, hippocampus, pallidum, hippocampus, amygdala, and nucleus accumbens), and the white matter into 3 (deep white matter, cortical white matter, and corpus callosum). The cerebellum was also divided into white and gray ROIs. The remaining two regions were the brain stem and the ventral diencephalon.

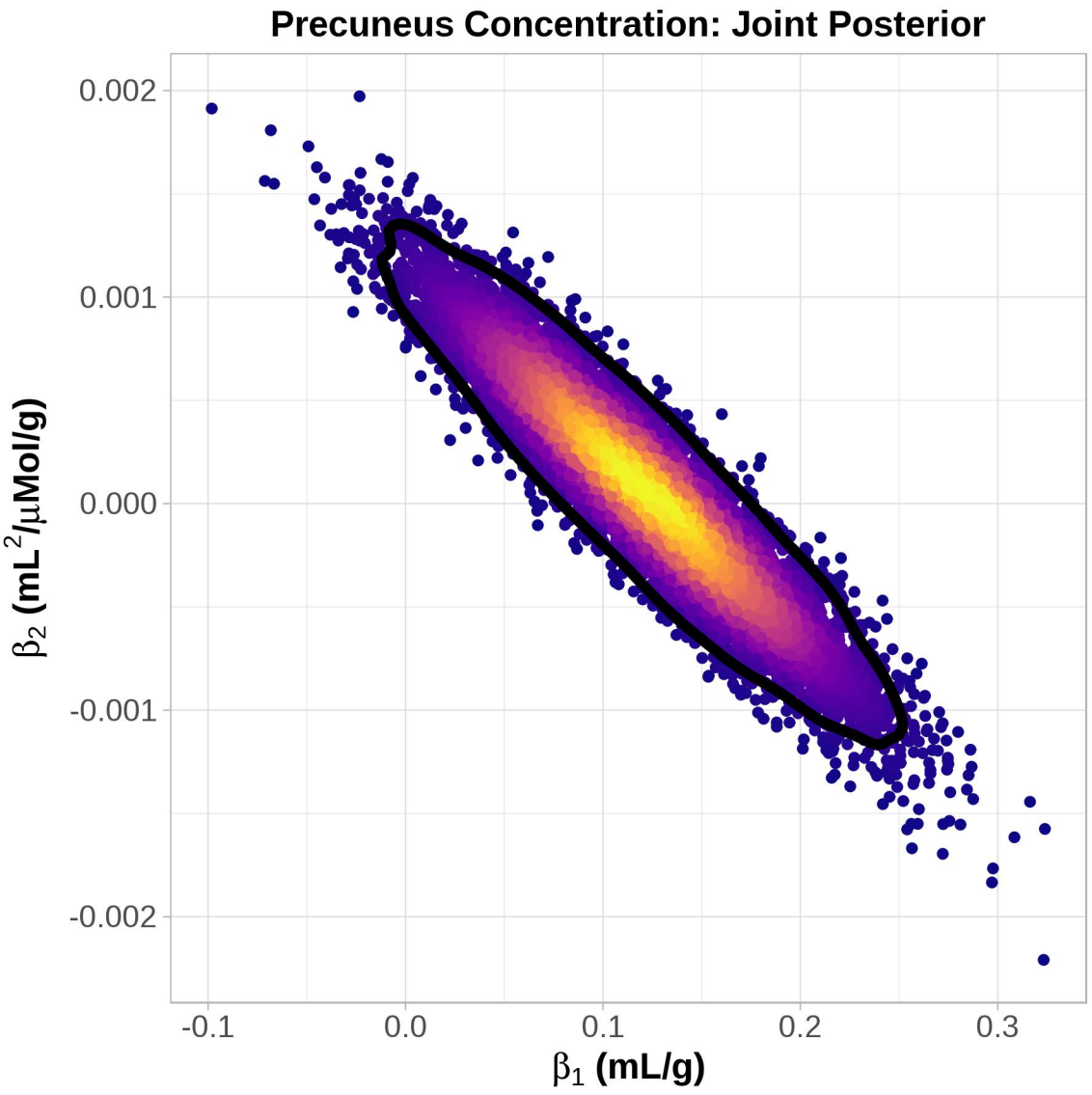

Figure 4.2: Joint parameter distribution

Each dot represents a single posterior sample from the Bayesian Markov-chain Monte Carlo (MCMC) used to model the change in brain free glucose concentration during hypoglycemia (see Methods). The x-axis is the coefficient for a linear relationship between plasma glucose (C_p) and glucose concentration in the precuneus, while the y-axis is the coefficient for a nonlinear association (a restricted cubic spline). The color indicates density, with yellow indicating the area of highest density. To assess whether there was any relationship between C_p and glucose

concentration, the 95% confidence region (black line) was computed (see Methods). A relationship between C_p and glucose concentration was significant if the point (0.0, 0.0) was outside of the 95% confidence region. In this example, (0.0, 0.0) is well outside the 95% confidence region, so we can infer that the glucose concentration in the precuneus decreases significantly as blood glucose level decreases

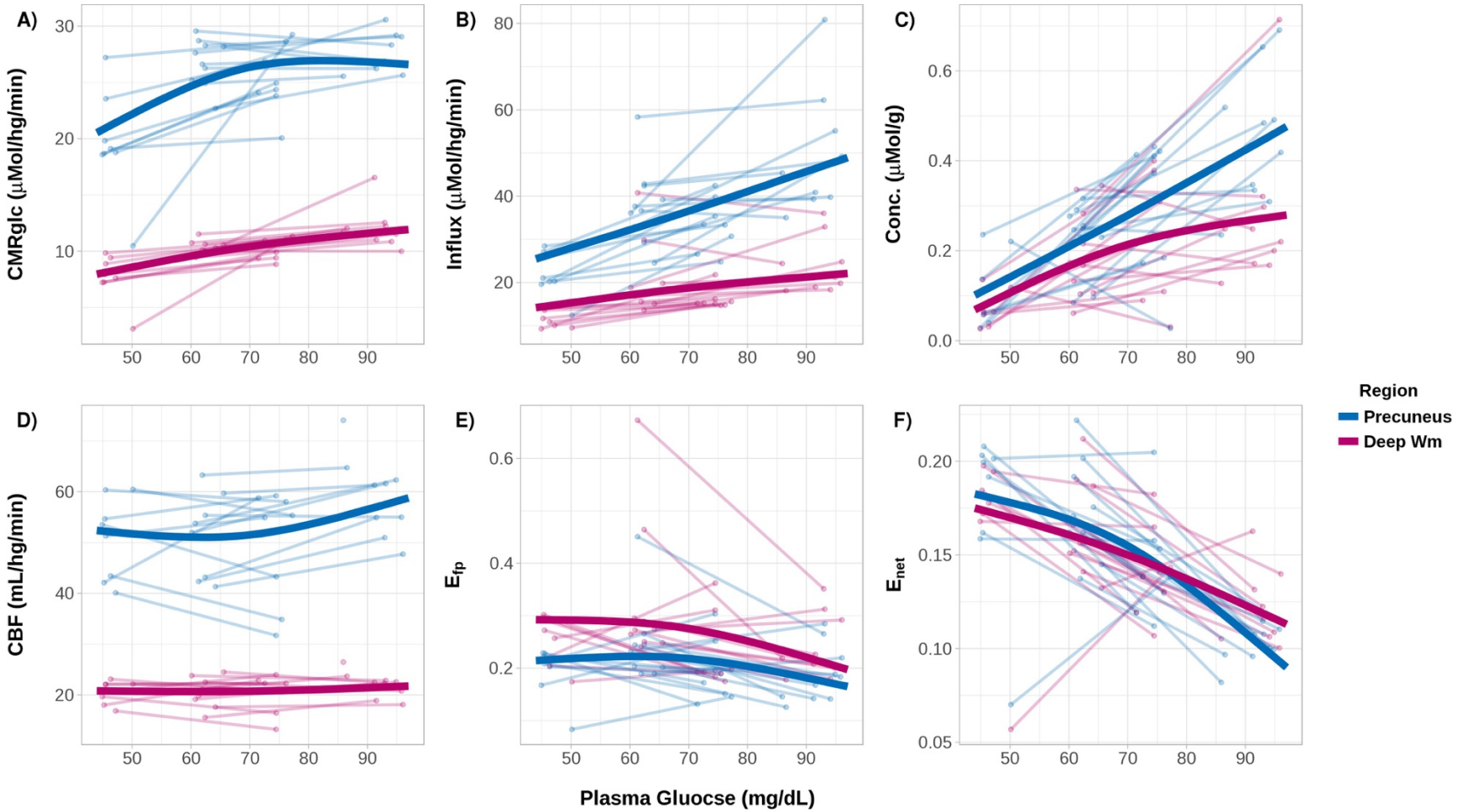

Figure 4.3: Hypoglycemia induced metabolic changes

A) CMRglc, **B)** glucose influx, **C)** glucose concentration, **D)** CBF, **E)** E_{fp}, and **F)** E_{net} as a function of hypoglycemia. Dots are individual data points, and light lines connect the data from individual subjects. Solid lines are the population median (see Methods).

Data from the precuneus is shown in blue and deep white matter in red. Hypoglycemia induced pronounced changes in **A)** CMRglc, **B)** Influx, **C)** Concentration, and **F)** E_{net}. Changes in **D)** CBF and **E)** E_{fp} were less marked.

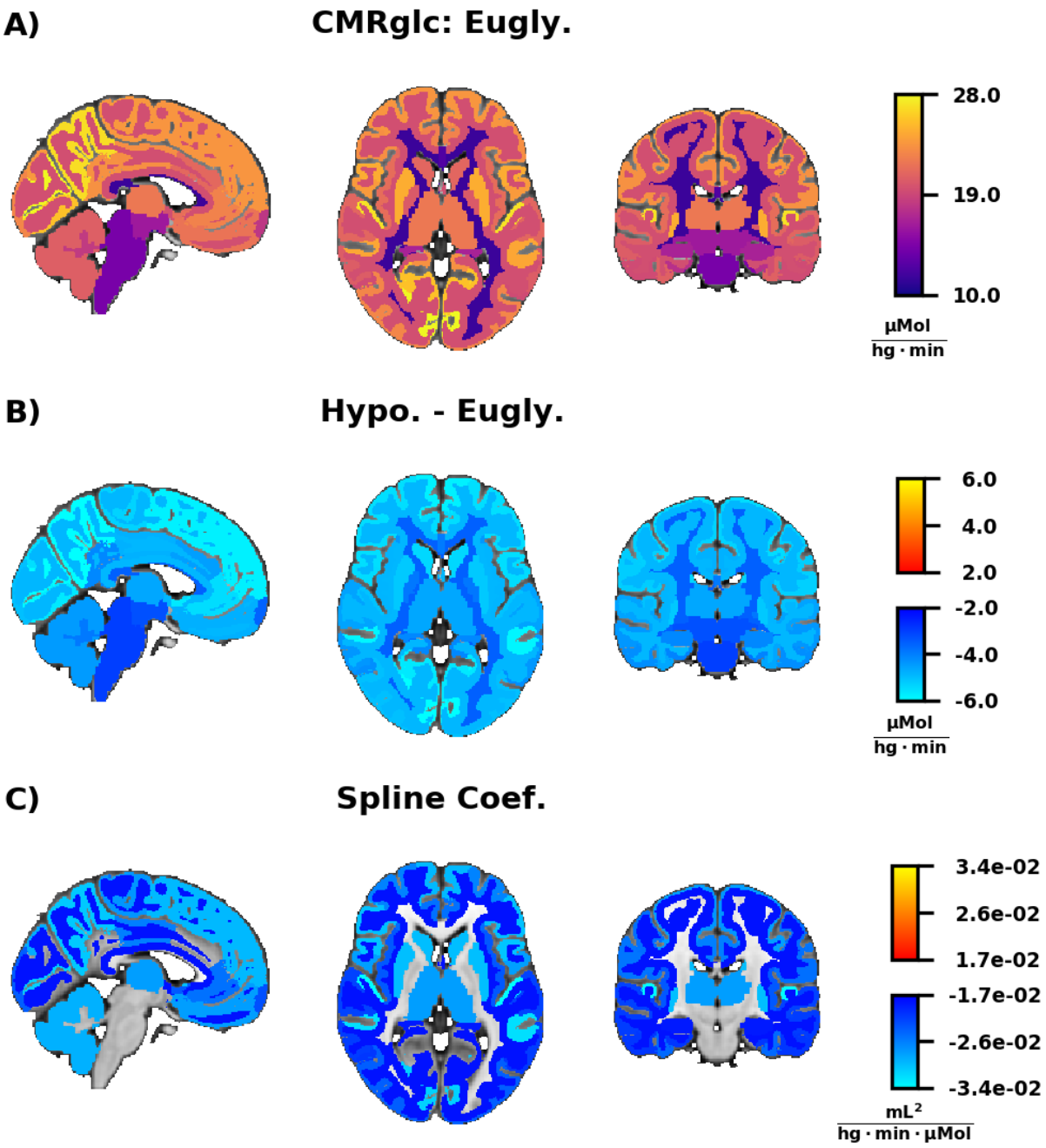

Figure 4.4: Regional CMRglc

A) Map of regional CMRglc during euglycemia (C_p = 90 mg/dL). Values were computed using the linear mixed model described in the Methods section of the text. Regions were averaged across hemispheres so the map is symmetric by definition. **B)** Estimated difference between

CMRglc at hypoglycemia (C_p = 45 mg/dL) and euglycemia. Only regions where there was a significant association between C_p and plasma glucose are shown. Note that CMRglc fell during hypoglycemia in every single region (48/48). **C)** Coefficient for the natural cubic spline term of the linear mixed model. Regions were the highest density interval (HDI) for the spline coefficient overlapped zero are not shown (13/48).

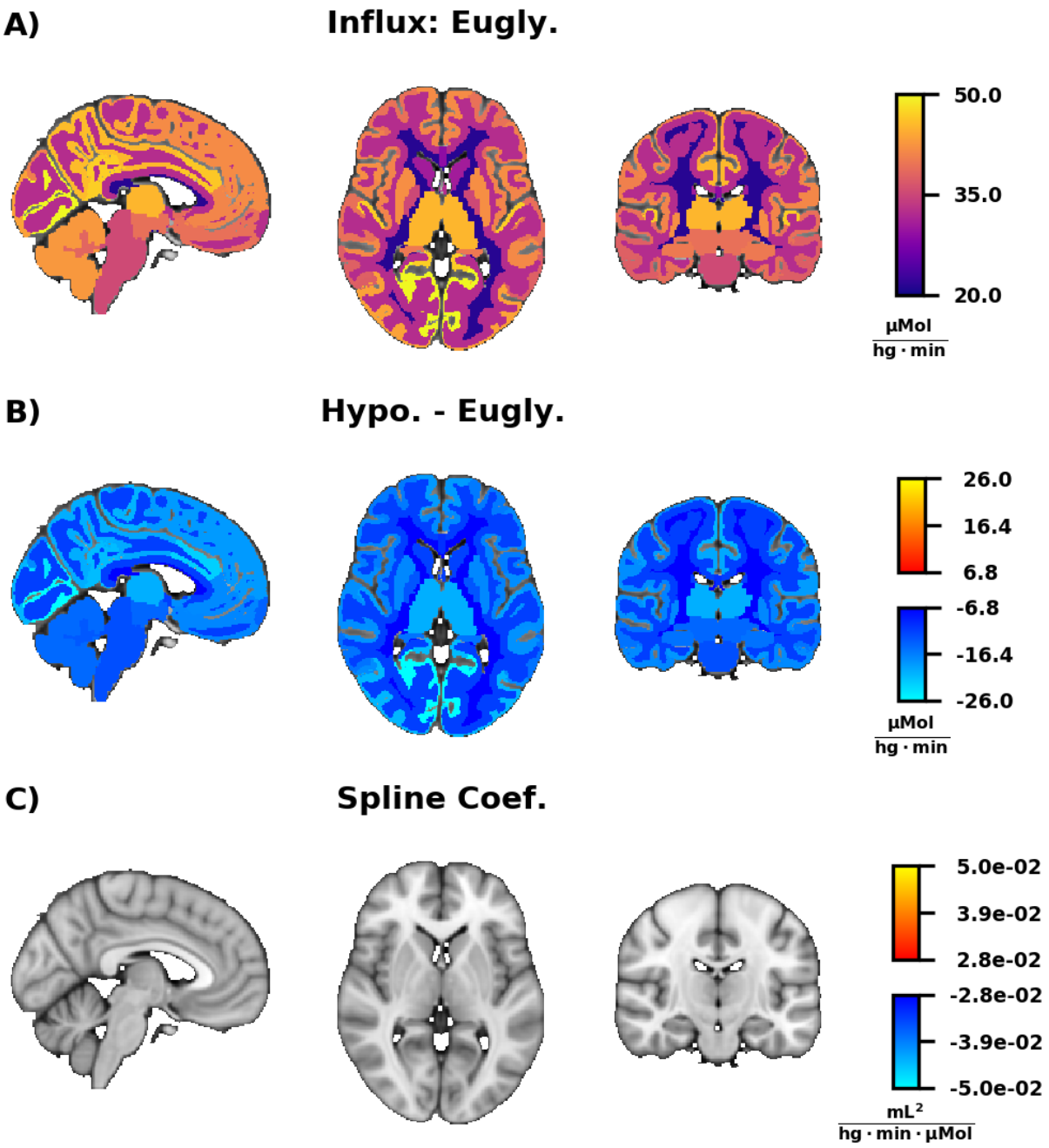

Figure 4.5: Regional glucose influx

Figure convention as in Figure 4.4. Similar to CMRglc (Figure 4.4), glucose influx decreased in every brain region with hypoglycemia.

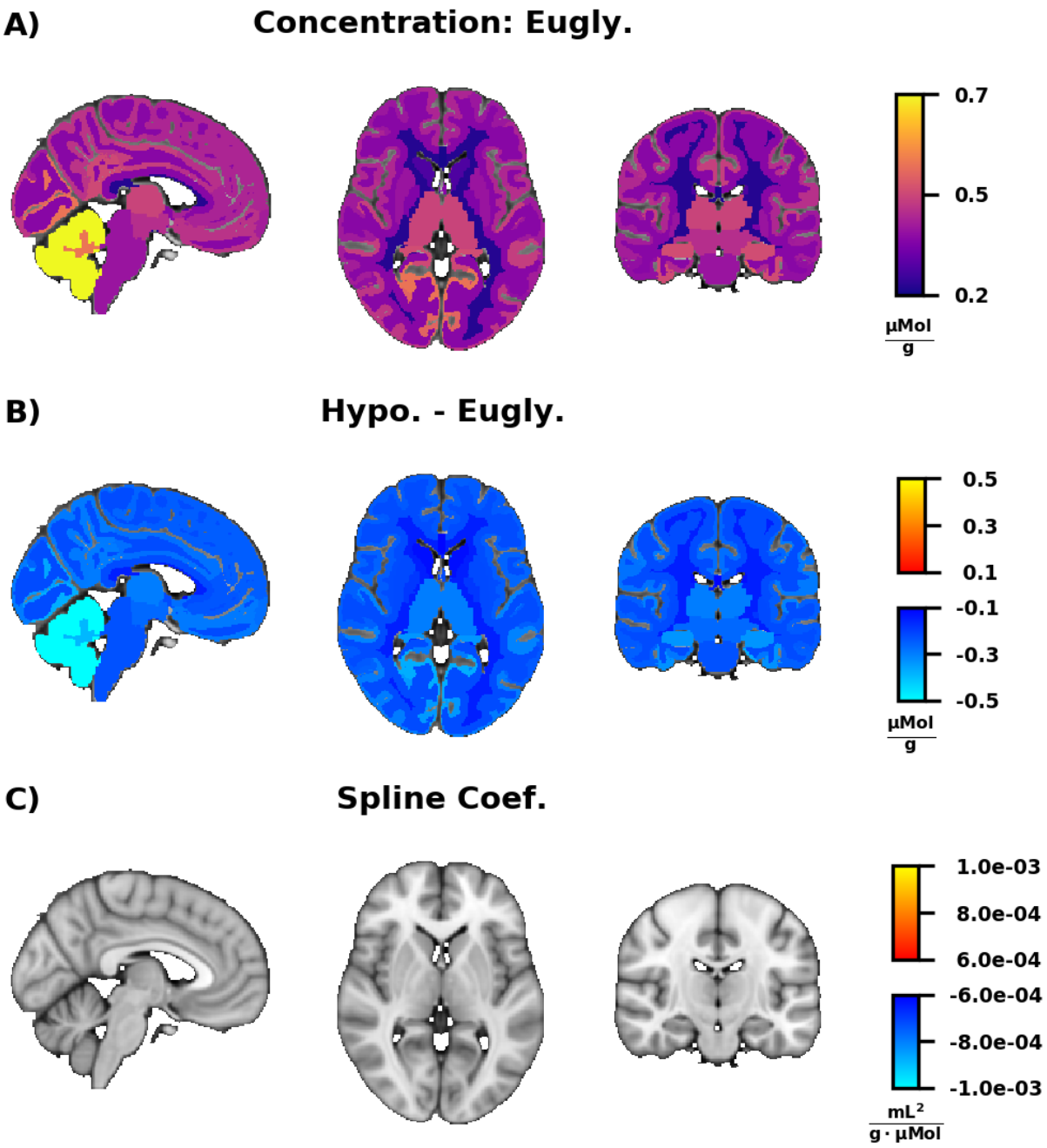

Figure 4.6: Regional glucose concentration

Figure convention as in Figure 4.4. **B)** Similar to CMRglc (Figure 4.4), glucose concentration decreased in every brain region with hypoglycemia.

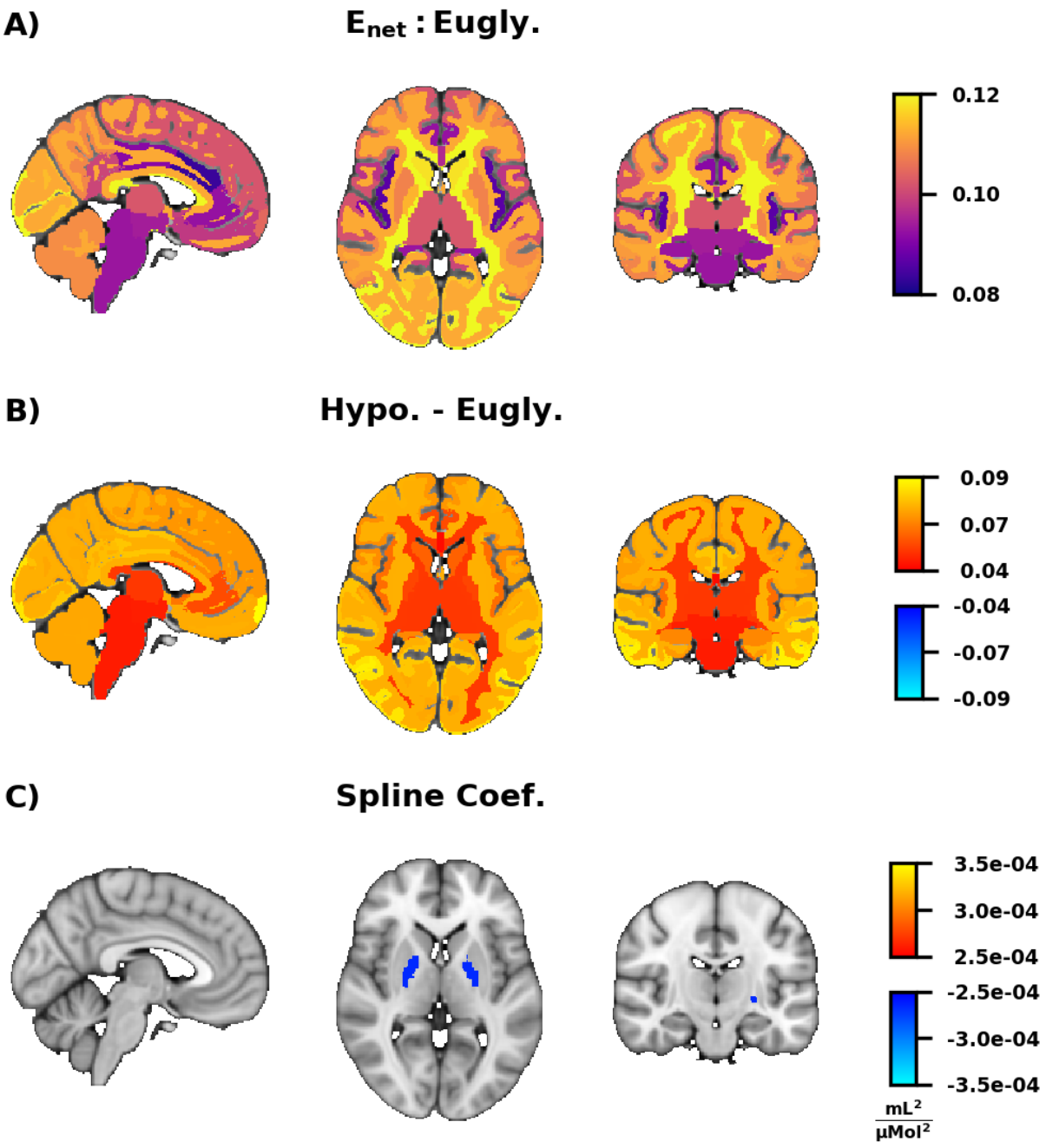

Figure 4.7: Regional E_{net}

Figure convention as in Figure 4.4. **B)** Unlike CMRglc (Figure 4.4), E_{net} increased in every brain region with hypoglycemia.

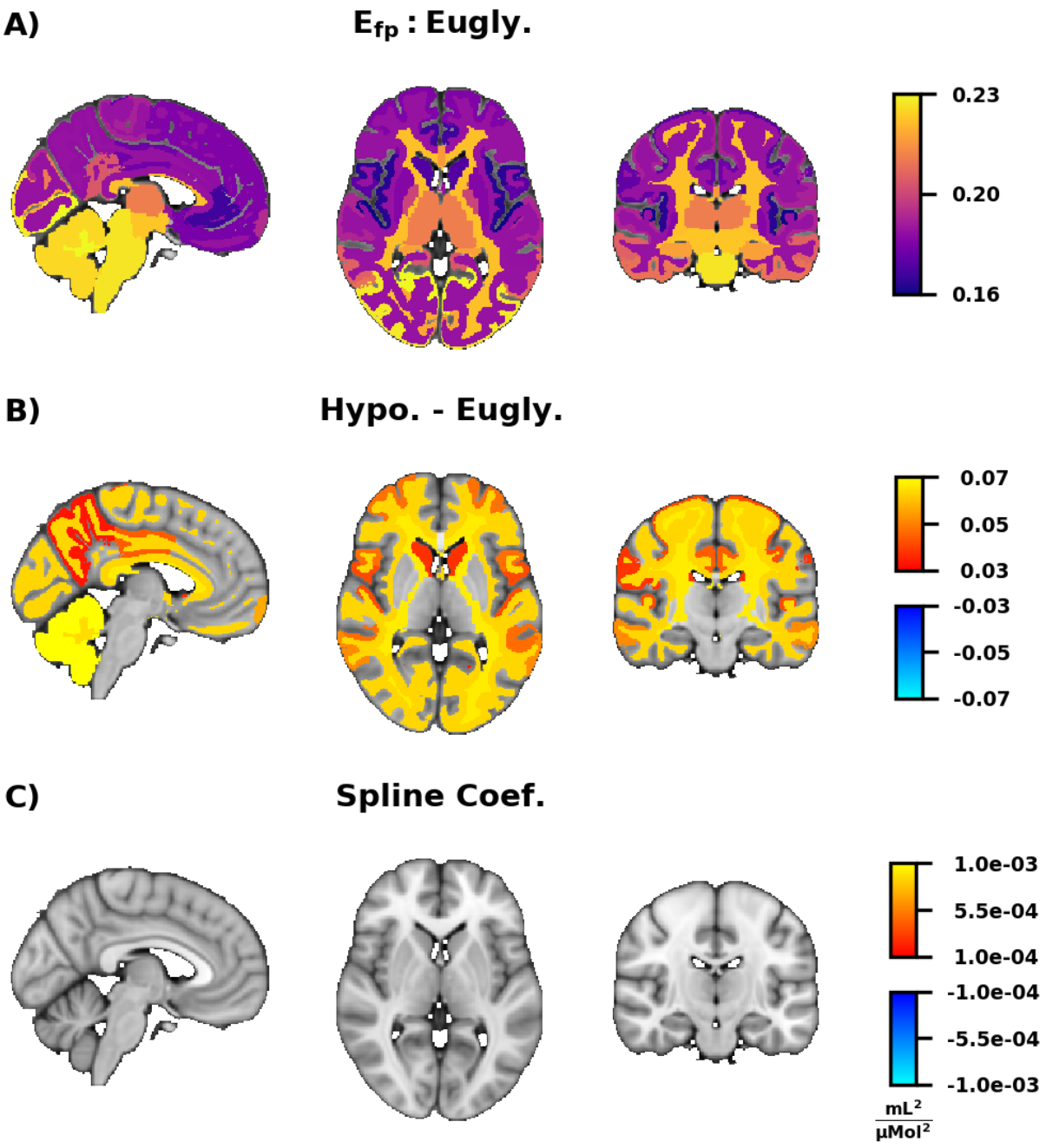

Figure 4.8: Regional E_{fp}

Figure convention as in Figure 4.4. **B)** Unlike E_{net} (Figure 4.7), E_{fp} did not significantly increase in all regions during hypoglycemia. Particularly notable absences are subcortical gray matter regions (e.g,. thalamus) and the brain stem.

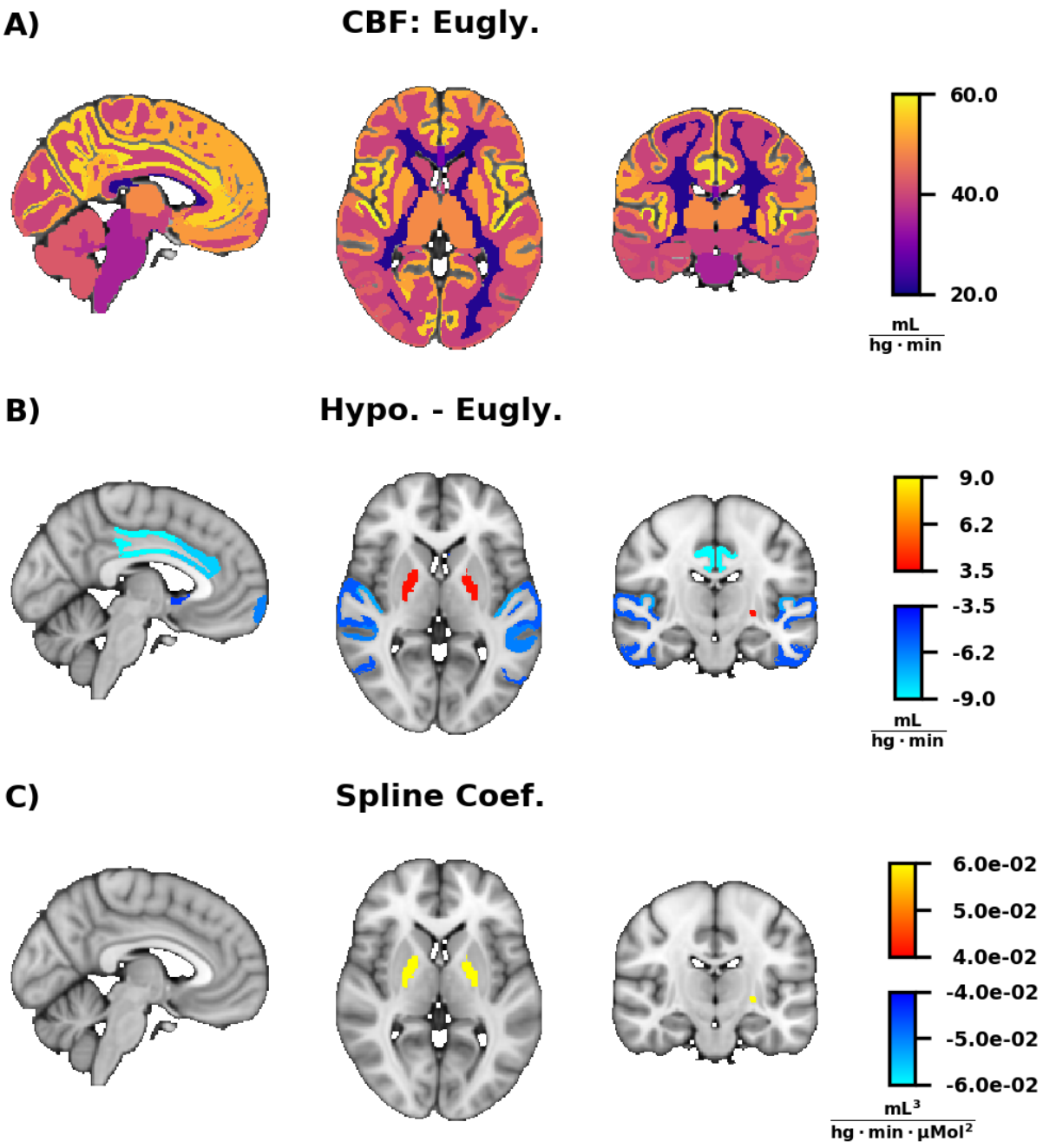

Figure 4.9: Regional CBF

Figure convention as in Figure 4.4. **B)** Unlike CMRglc (Figure 4.4), changes in CBF during hypoglycemia were confined to only a few regions.

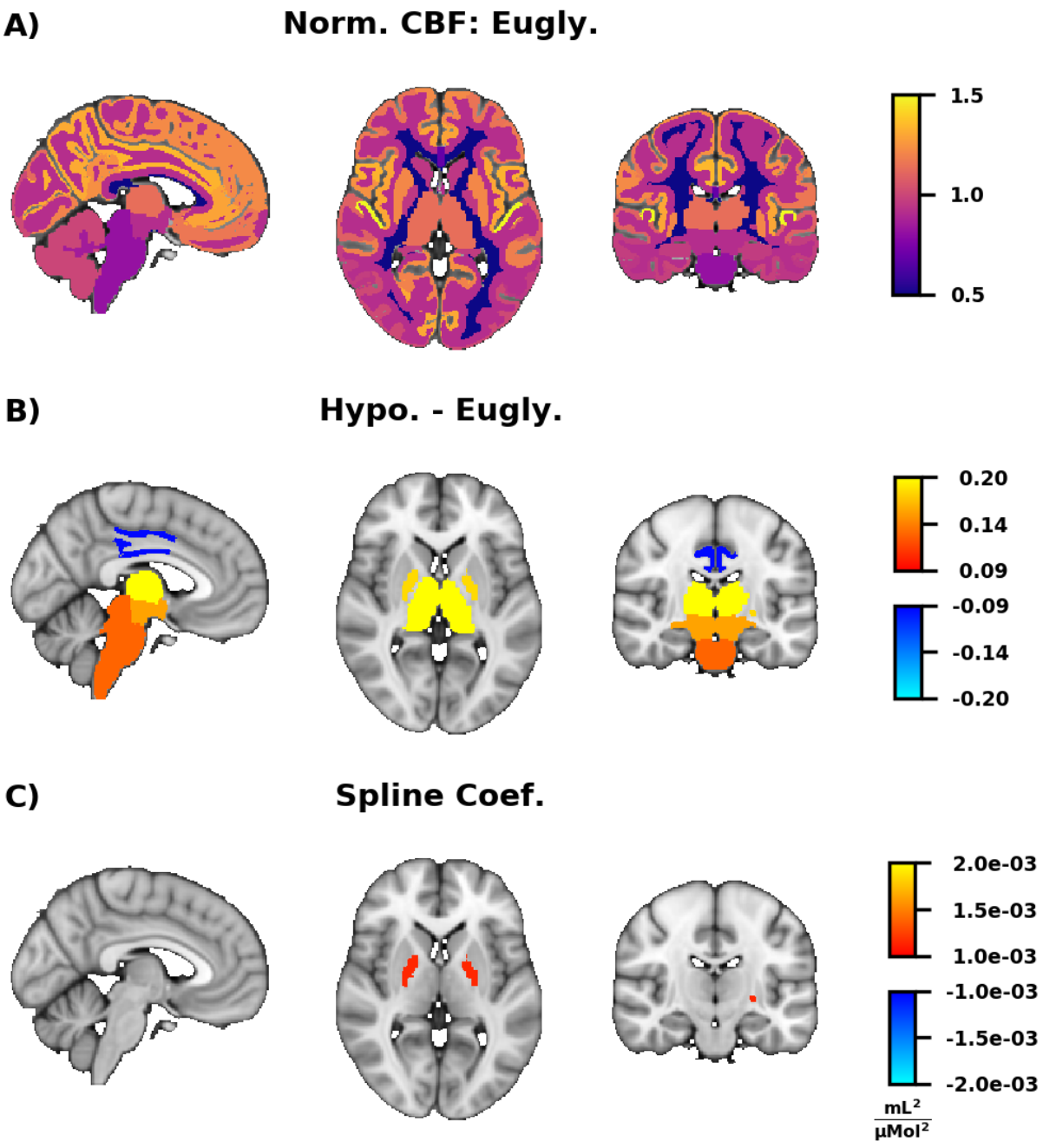

Figure 4.10: Regional normalized CBF

CBF values are normalized relative to the whole-brain mean (see Methods). Figure convention as in Figure 4.4 . **B)** Compared to absolute CBF (Figure 4.9B), normalization revealed additional regions where hypoglycemia increased CBF. Particularly prominent are the brain stem and the thalamus.

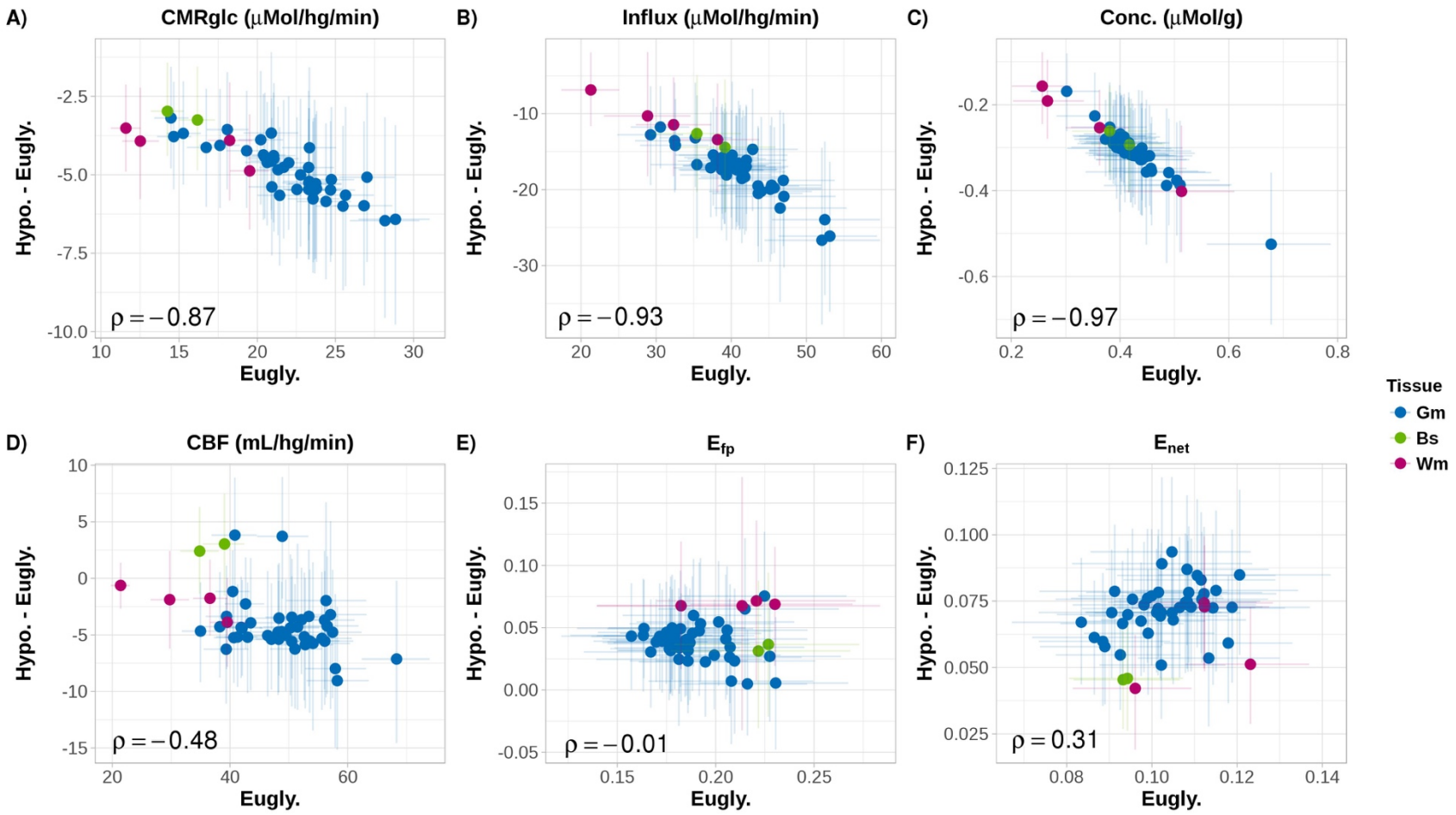

Figure 4.11: Variable spatial correspondence between maps of baseline metabolism and hypoglycemia induced change

Spatial correlation between maps of euglycemia (C_p = 90 mg/dL) and change (90 mg/dL – 45 mg/dL) for **A)** CMRglc, **B)** glucose influx, **C)** glucose concentration, **D)** CBF, **E)** E_{fp}, and **F)** E_{net}. Each point is the linear mixed model estimate for a single FreeSurfer

region. Blue dots are gray matter, red dots are white matter, and green dots are the brain stem/ventral dienecephalon. Light lines are 95% highest density intervals. Strong correlations between baseline and change were found for **A)** CMRglc, **B)** influx, and **C)** concentration but not for **D)** CBF, **E)** E_{fp}, or **F)** E_{net}.

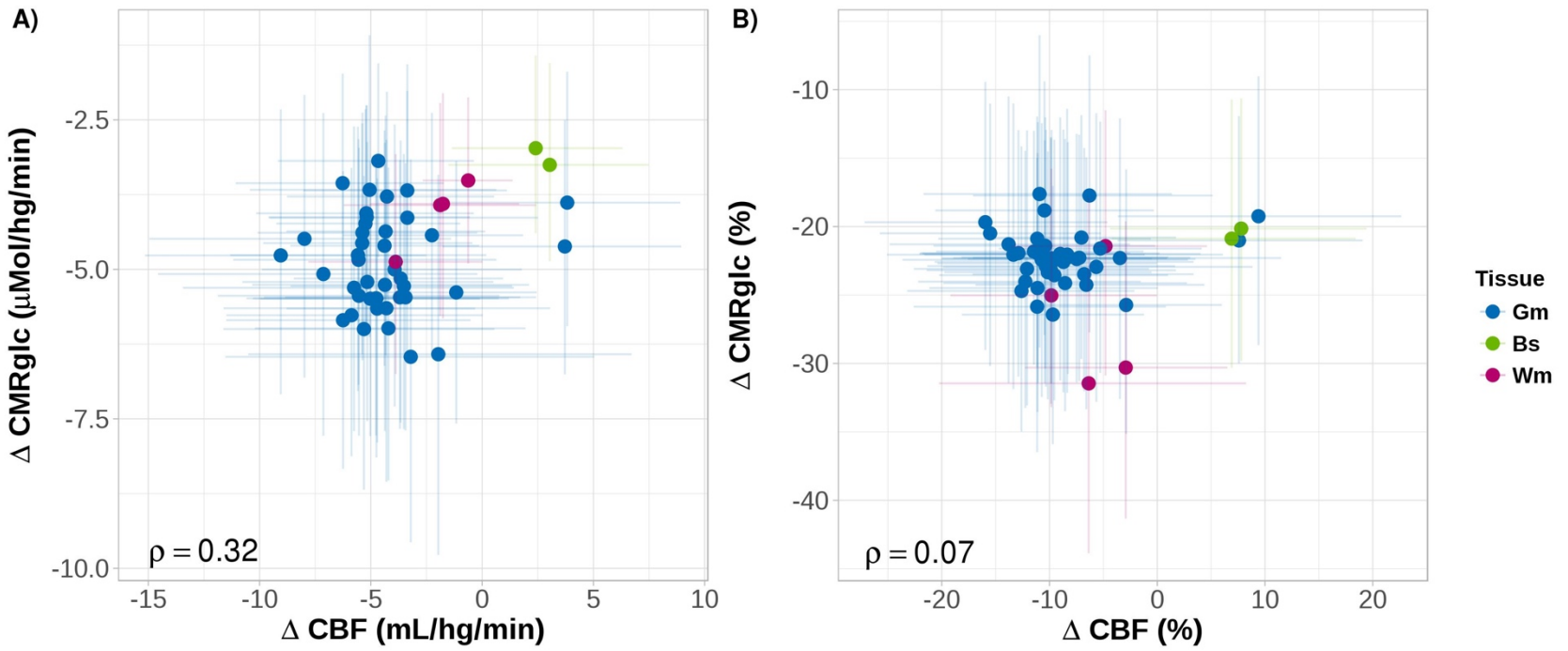

Figure 4.12: Lack of a strong spatial correspondence between regional CBF and CMRglc changes

Each dot represents the linear mixed model estimate for the difference between euglycemia (C_p = 90 mg/dL) and hypoglycemia (C_p = 45 mg/dL) for a single FreeSurfer region. Blue dots are gray matter, red dots are white matter, and green dots are the brain stem/ventral diencephalon. Light lines are 95% highest density intervals. **A)** Only a modest correlation was found the between map of CBF change and the map of CMRglc change. **B)** Expressed as a percent change, the spatial correspondence between the two maps is even weaker. The cluster of four regions on the right of **B)** are the thalamus, globus pallidus, brainstem, and ventral diencephalon. The two regions at the bottom of **B)** are the deep white matter and corpus callosum.

4.7 References

1 Gibbs EL, Lennox WG, Nims LF, Gibbs FA. Arterial and cerebral venous blood arterial-venous differences in man. *J Biol Chem* 1942; **144**: 325–332.

2 Öz G, DiNuzzo M, Kumar A, Moheet A, Seaquist ER. Revisiting Glycogen Content in the Human Brain. *Neurochem Res* 2015; **40**: 2473–2481.

3 Courchesne-Loyer A, Croteau E, Castellano C-A, St-Pierre V, Hennebelle M, Cunnane SC. Inverse relationship between brain glucose and ketone metabolism in adults during short-term moderate dietary ketosis: A dual tracer quantitative positron emission tomography study. *J Cereb Blood Flow Metab* 2017; **37**: 2485–2493.

4 Boumezbeur F, Petersen KF, Cline GW, Mason GF, Behar KL, Shulman GI *et al.* The contribution of blood lactate to brain energy metabolism in humans measured by dynamic 13C nuclear magnetic resonance spectroscopy. *J Neurosci* 2010; **30**: 13983–13991.

5 Cryer PE, Davis SN, Shamoon H. Hypoglycemia in diabetes. *Diabetes Care* 2003; **26**: 1902–1912.

6 Deary IJ, Hepburn DA, MacLeod KM, Frier BM. Partitioning the symptoms of hypoglycaemia using multi-sample confirmatory factor analysis. *Diabetologia* 1993; **36**: 771–777.

7 Deckert T, Poulsen JE, Larsen M. Prognosis of diabetics with diabetes onset before the age of thirty-one. I. Survival, causes of death, and complications. *Diabetologia* 1978; **14**: 363–370.

8 Cryer PE. Glucose counterregulation: prevention and correction of hypoglycemia in humans. *Am J Physiol* 1993; **264**: E149–55.

9 Nirantharakumar K, Marshall T, Hodson J, Narendran P, Deeks J, Coleman JJ *et al.* Hypoglycemia in non-diabetic in-patients: clinical or criminal? *PLoS ONE* 2012; **7**: e40384.

10 Cryer PE. Banting Lecture. Hypoglycemia: the limiting factor in the management of IDDM. *Diabetes* 1994; **43**: 1378–1389.

11 Pedersen-Bjergaard U, Pramming S, Heller SR, Wallace TM, Rasmussen ÅK, Jørgensen HV *et al.* Severe hypoglycaemia in 1076 adult patients with type 1 diabetes: influence of risk markers and selection. *Diabetes Metab Res Rev* 2004; **20**: 479–486.

12 Gerich JE, Mokan M, Veneman T, Korytkowski M, Mitrakou A. Hypoglycemia unawareness. *Endocr Rev* 1991; **12**: 356–371.

13 Gold AE, MacLeod KM, Frier BM. Frequency of severe hypoglycemia in patients with type I diabetes with impaired awareness of hypoglycemia. *Diabetes Care* 1994; **17**: 697–703.

14 Cheah Y-S, Amiel SA. Metabolic neuroimaging of the brain in diabetes mellitus and hypoglycaemia. *Nat Rev Endocrinol* 2012; **8**: 588–597.

15 Rooijackers HMM, Wiegers EC, Tack CJ, van der Graaf M, de Galan BE. Brain glucose metabolism during hypoglycemia in type 1 diabetes: insights from functional and metabolic neuroimaging studies. *Cell Mol Life Sci* 2016; **73**: 705–722.

16 Kety SS, Woodford RB. Cerebral blood flow and metabolism in schizophrenia; the effects of barbiturate semi-narcosis, insulin coma and electroshock. *Am J Psychiatry* 1948; **104**: 765–770.

17 Eisenberg S, Seltzer HS. The cerebral metabolic effects of acutely induced hypoglycemia in human subjects. *Metabolism* 1962; **11**: 1162–1168.

18 Blomqvist G, Gjedde A, Gutniak M, Grill V, Widén L, Stone-Elander S *et al.* Facilitated transport of glucose from blood to brain in man and the effect of moderate hypoglycaemia on cerebral glucose utilization. *Eur J Nucl Med* 1991; **18**: 834–837.

19 Boyle PJ, Nagy RJ, O'Connor AM, Kempers SF, Yeo RA, Qualls C. Adaptation in brain glucose uptake following recurrent hypoglycemia. *Proc Natl Acad Sci USA* 1994; **91**: 9352–9356.

20 Lubow JM, Piñón IG, Avogaro A, Cobelli C, Treeson DM, Mandeville KA *et al.* Brain oxygen utilization is unchanged by hypoglycemia in normal humans: lactate, alanine, and leucine uptake are not sufficient to offset energy deficit. *Am J Physiol Endocrinol Metab* 2006; **290**: E149–E153.

21 Lee JJ, Khoury N, Shackleford AM, Nelson S, Herrera H, Antenor-Dorsey JA *et al.* Dissociation Between Hormonal Counterregulatory Responses and Cerebral Glucose Metabolism During Hypoglycemia. *Diabetes* 2017; **66**: 2964–2972.

22 Wiegers EC, Becker KM, Rooijackers HM, Samson-Himmelstjerna von FC, Tack CJ, Heerschap A *et al.* Cerebral blood flow response to hypoglycemia is altered in patients with type 1 diabetes and impaired awareness of hypoglycemia. *J Cereb Blood Flow Metab* 2017; **37**: 1994–2001.

23 Tallroth G, Ryding E, Agardh CD. Regional cerebral blood flow in normal man during insulin-induced hypoglycemia and in the recovery period following glucose infusion. *Metab Clin Exp* 1992; **41**: 717–721.

24 Kerr D, Stanley JC, Barron M, Thomas R, Leatherdale BA, Pickard J. Symmetry of cerebral blood flow and cognitive responses to hypoglycaemia in humans. *Diabetologia* 1993; **36**: 73–78.

25 Eckert B, Ryding E, Agardh CD. Sustained elevation of cerebral blood flow after hypoglycaemia in normal man. *Diabetes Research and Clinical Practice* 1998; **40**: 91–100.

26 Teves D, Videen TO, Cryer PE, Powers WJ. Activation of human medial prefrontal cortex during autonomic responses to hypoglycemia. *Proc Natl Acad Sci USA* 2004; **101**: 6217–6221.

27 Tallroth G, Ryding E, Agardh CD. The influence of hypoglycaemia on regional cerebral blood flow and cerebral volume in type 1 (insulin-dependent) diabetes mellitus. *Diabetologia* 1993; **36**: 530–535.

28 Teh MM, Dunn JT, Choudhary P, Samarasinghe Y, Macdonald I, O'Doherty M *et al.* Evolution and resolution of human brain perfusion responses to the stress of induced hypoglycemia. *Neuroimage* 2010; **53**: 584–592.

29 MacLeod KM, Gold AE, Ebmeier KP, Hepburn DA, Deary IJ, Goodwin GM *et al.* The effects of acute hypoglycemia on relative cerebral blood flow distribution in patients with type I (insulin-dependent) diabetes and impaired hypoglycemia awareness. *Metab Clin Exp* 1996; **45**: 974–980.

30 Mangia S, Tesfaye N, De Martino F, Kumar AF, Kollasch P, Moheet AA *et al.* Hypoglycemia-induced increases in thalamic cerebral blood flow are blunted in subjects with type 1 diabetes and hypoglycemia unawareness. *J Cereb Blood Flow Metab* 2012; **32**: 2084–2090.

31 Dunn JT, Choudhary P, Teh MM, Macdonald I, Hunt KF, Marsden PK *et al.* The impact of hypoglycaemia awareness status on regional brain responses to acute hypoglycaemia in men with type 1 diabetes. *Diabetologia* 2018; **61**: 1676–1687.

32 van de Ven KCC, de Galan BE, van der Graaf M, Shestov AA, Henry P-G, Tack CJJ *et al.* Effect of acute hypoglycemia on human cerebral glucose metabolism measured by ^{13}C magnetic resonance spectroscopy. *Diabetes* 2011; **60**: 1467–1473.

33 Lee JJ, Khoury N, Shackleford AM, Nelson S, Herrera H, Antenor-Dorsey JA *et al.* Dissociation Between Hormonal Counterregulatory Responses and Cerebral Glucose Metabolism During Hypoglycemia. *Diabetes* 2017; **66**: 2964–2972.

34 Porta PD, Maiolo AT, Negri VU, Rossella E. Cerebral Blood Flow and Metabolism in Therapeutic Insulin Coma. *Metab Clin Exp* 1964; **13**: 131–140.

35 Sokoloff L, Reivich M, Kennedy C, Rosiers Des MH, Patlak CS, Pettigrew KD *et al.* The [14C]Deoxyglucose Method for the Measurement of Local Cerebral Glucose Utilization: Theory, Procedure, and Normal Values in the Conscious and Anesthetized Albino Rat. *J Neurochem* 1977; **28**: 897–916.

36 Schuier F, Orzi F, Suda S, Lucignani G, Kennedy C, Sokoloff L. Influence of plasma glucose concentration on lumped constant of the deoxyglucose method: effects of hyperglycemia in the rat. *J Cereb Blood Flow Metab* 1990; **10**: 765–773.

37 Gutniak M, Blomqvist G, Widén L, Stone-Elander S, Hamberger B, Grill V. D-[U-11C]glucose uptake and metabolism in the brain of insulin-dependent diabetic subjects. *Am J Physiol* 1990; **258**: E805–12.

38 Hyder F, Herman P, Bailey CJ, Møller A, Globinsky R, Fulbright RK *et al.* Uniform distributions of glucose oxidation and oxygen extraction in gray matter of normal human brain: No evidence of regional differences of aerobic glycolysis. *J Cereb Blood Flow Metab* 2016; **36**: 903–916.

39 Henriksen OM, Vestergaard MB, Lindberg U, Aachmann-Andersen NJ, Lisbjerg K, Christensen SJ *et al.* Interindividual and regional relationship between cerebral blood flow and glucose metabolism in the resting brain. *J Appl Physiol* 2018; **43**: 1157.

40 Gottstein U, Held K. The effect of insulin on brain metabolism in metabolically healthy and diabetic patients. *Klin Wochenschr* 1967; **45**: 18–23.

41 Cryer PE, Arbelaez AM. Hypoglycemia-Associated Autonomic Failure in Diabetes. In: *Pheochromocytomas, Paragangliomas and Disorders of the Sympathoadrenal System*. Humana Press, Cham: Cham, 2018, pp 183–199.

42 Arbelaez AM, Su Y, Thomas JB, Hauch AC, Hershey T, Ances BM. Comparison of regional cerebral blood flow responses to hypoglycemia using pulsed arterial spin labeling and positron emission tomography. *PLoS ONE* 2013; **8**: e60085.

43 Martin WR, Powers WJ, Raichle ME. Cerebral blood volume measured with inhaled C15O and positron emission tomography. *J Cereb Blood Flow Metab* 1987; **7**: 421–426.

44 Raichle ME, Martin WR, Herscovitch P, Mintun MA, Markham J. Brain blood flow measured with intravenous H2(15)O. II. Implementation and validation. *J Nucl Med* 1983; **24**: 790–798.

45 Powers WJ, Dagogo-Jack S, Markham J, Larson KB, Dence CS. Cerebral transport and metabolism of 1-11C-D-glucose during stepped hypoglycemia. *Annals of Neurology* 1995; **38**: 599–609.

46 Cherry SR, Dahlbom M. PET: Physics, Instrumentation, and Scanners. In: *PET*. Springer, New York, NY: New York, NY, 2004, pp 1–124.

47 Joshi A, Koeppe RA, Fessler JA. Reducing between scanner differences in multi-center PET studies. *Neuroimage* 2009; **46**: 154–159.

48 Eisenstein SA, Koller JM, Piccirillo M, Kim A, Antenor-Dorsey JAV, Videen TO *et al.* Characterization of extrastriatal D2 in vivo specific binding of [^{18}F](N-methyl)benperidol using PET. *Synapse* 2012; **66**: 770–780.

49 Su Y, Blazey TM, Snyder AZ, Raichle ME, Marcus DS, Ances BM *et al.* Partial volume correction in quantitative amyloid imaging. *Neuroimage* 2015; **107**: 55–64.

50 Rowland DJ, Garbow JR, Laforest R, Snyder AZ. Registration of [18F]FDG microPET and small-animal MRI. *Nuclear Medicine and Biology* 2005; **32**: 567–572.

51 Fischl B. FreeSurfer. *Neuroimage* 2012; **62**: 774–781.

52 Desikan RS, Ségonne F, Fischl B, Quinn BT, Dickerson BC, Blacker D *et al.* An automated labeling system for subdividing the human cerebral cortex on MRI scans into gyral based regions of interest. *Neuroimage* 2006; **31**: 968–980.

53 Fischl B, Salat DH, Busa E, Albert M, Dieterich M, Haselgrove C *et al.* Whole brain segmentation: automated labeling of neuroanatomical structures in the human brain. *Neuron* 2002; **33**: 341–355.

54 Jenkinson M, Beckmann CF, Behrens TEJ, Woolrich MW, Smith SM. FSL. *Neuroimage* 2012; **62**: 782–790.

55 Zhang Y, Brady M, Smith S. Segmentation of brain MR images through a hidden Markov random field model and the expectation-maximization algorithm. *IEEE Trans Med Imaging* 2001; **20**: 45–57.

56 Graham MM, Muzi M, Spence AM, O'Sullivan F, Lewellen TK, Link JM *et al.* The FDG lumped constant in normal human brain. *J Nucl Med* 2002; **43**: 1157–1166.

57 Segel SA, Fanelli CG, Dence CS, Markham J, Videen TO, Paramore DS *et al.* Blood-to-brain glucose transport, cerebral glucose metabolism, and cerebral blood flow are not increased after hypoglycemia. *Diabetes* 2001; **50**: 1911–1917.

58 Hutchins GD, Hichwa RD, Koeppe RA. A continuous flow input function detector for $H_2{}^{15}O$ blood flow studies in positron emission tomography. *IEEE T Nucl Sci* 1986; **33**: 546–549.

59 Golish SR, Hove JD, Schelbert HR, Gambhir SS. A fast nonlinear method for parametric imaging of myocardial perfusion by dynamic (13)N-ammonia PET. *J Nucl Med* 2001; **42**: 924–931.

60 Jones E, Oliphant T, Peterson P, others. SciPy: Open Source Scientific Tools for Python. 2001.

61 Blomqvist G, Stone-Elander S, Halldin C, Roland PE, Widén L, Lindqvist M *et al.* Positron emission tomographic measurements of cerebral glucose utilization using [1-11C]D-glucose. *J Cereb Blood Flow Metab* 1990; **10**: 467–483.

62 Dillon RS. Importance of the hematocrit in interpretation of blood sugar. *Diabetes* 1965; **14**: 672–674.

63 Verbeke G, Fieuws S, Molenberghs G, Davidian M. The analysis of multivariate longitudinal data: A review. *Statistical Methods in Medical Research* 2014; **23**: 42–59.

64 Harrell FE Jr. Hmisc: Harrell Miscellaneous. https://CRAN.R-project.org/package=Hmisc.

65 Carpenter B, Gelman A, Hoffman MD, Lee D, Goodrich B, Betancourt M *et al.* Stan: A Probabilistic Programming Language. *J Stat Soft* 2017; **76**: 1–32.

66 Barnard J, McCulloch R, Meng XL. Modeling covariance matrices in terms of standard deviations and correlations, with application to shrinkage. *Statistica Sinica* 2000. doi:10.2307/24306780.

67 Lewandowski D, Kurowicka D, Joe H. Generating random correlation matrices based on vines and extended onion method. *Journal of Multivariate Analysis* 2009; **100**: 1989–2001.

68 Stan Development Team. Stan Modeling Language. 2016. https://mc-stan.org/users/documentation/.

69 Gelman A, Rubin DB. Inference from iterative simulation using multiple sequences. *Statistical science* 1992; **7**: 457–511.

70 Brooks SP, Gelman A. General methods for monitoring convergence of iterative simulations. *Journal of Computational and Graphical Statistics* 1998; **7**: 434–455.

71 R Core Team. R: A Language and Environment for Statistical Computing. Vienna, Austria, 2017 https://www.R-project.org/.

72 Bates D, Mächler M, Bolker B, Walker S. Fitting Linear Mixed-Effects Models Using lme4. *J Stat Soft* 2015; **67**: 1–48.

73 Duong T. ks: Kernel Smoothing. https://CRAN.R-project.org/package=ks.

74 Kruschke JK. *Doing Bayesian Data Analysis*. 2nd ed. Academic Press, 2014.

75 Alexander-Bloch AF, Shou H, Liu S, Satterthwaite TD, Glahn DC, Shinohara RT *et al.* On testing for spatial correspondence between maps of human brain structure and function. *Neuroimage* 2018; **178**: 540–551.

76 Redies C, Hoffer LJ, Beil C, Marliss EB, Evans AC, Lariviere F *et al.* Generalized decrease in brain glucose metabolism during fasting in humans studied by PET. *Am J Physiol* 1989; **256**: E805–10.

77 Hasselbalch SG, Knudsen GM, Jakobsen J, Hageman LP, Holm S, Paulson OB. Brain metabolism during short-term starvation in humans. *J Cereb Blood Flow Metab* 1994; **14**: 125–131.

78 Abdul-Rahman A, Siesjö BK. Local cerebral glucose consumption during insulin-induced hypoglycemia, and in the recovery period following glucose administration. *Acta Physiol Scand* 1980; **110**: 149–159.

79 Bryan RM, Hollinger BR, Keefer KA, Page RB. Regional cerebral and neural lobe blood flow during insulin-induced hypoglycemia in unanesthetized rats. *J Cereb Blood Flow Metab* 1987; **7**: 96–102.

80 Pelligrino DA, Segil LJ, Albrecht RF. Brain glucose utilization and transport and cortical function in chronic vs. acute hypoglycemia. *Am J Physiol* 1990; **259**: E729–35.

81 Suda S, Shinohara M, Miyaoka M, Lucignani G, Kennedy C, Sokoloff L. The lumped constant of the deoxyglucose method in hypoglycemia: effects of moderate hypoglycemia on local cerebral glucose utilization in the rat. *J Cereb Blood Flow Metab* 1990; **10**: 499–509.

82 Ferrendelli JA, Chang MM. Brain metabolism during hypoglycemia. Effect of insulin on regional central nervous system glucose and energy reserves in mice. *Arch Neurol* 1973; **28**: 173–177.

83 Gorell JM, Dolkart PH, Ferrendelli JA. Regional levels OF glucose, amino acids, high energy phosphates, AND cyclic nucleotides in the central nervous system during hypoglycemic stupor and behavioral recovery. *J Neurochem* 1976; **27**: 1043–1049.

84 Ratcheson RA, Blank AC, Ferrendelli JA. Regionally Selective Metabolic Effects of Hypoglycemia in Brain. *J Neurochem* 1981; **36**: 1952–1958.

85 Paschen W, Siesjö BK, Ingvar M, Hossmann KA. Regional differences in brain glucose content in graded hypoglycemia. *Neurochemical Pathology* 1986; **5**: 131–142.

86 LaManna JC, Harik SI. Regional comparisons of brain glucose influx. *Brain Res* 1985; **326**: 299–305.

87 Wahren J, Ekberg K, Fernqvist-Forbes E, Nair S. Brain substrate utilisation during acute hypoglycaemia. *Diabetologia* 1999; **42**: 812–818.

88 Siesjö BK. Hypoglycemia, brain metabolism, and brain damage. *Diabetes Metab Rev* 1988; **4**: 113–144.

89 Gruetter R, Novotny EJ, Boulware SD, Rothman DL, Mason GF, Shulman GI *et al.* Direct measurement of brain glucose concentrations in humans by 13C NMR spectroscopy. *Proc Natl Acad Sci USA* 1992; **89**: 1109–1112.

90 Gruetter R, Ugurbil K, Seaquist ER. Steady-state cerebral glucose concentrations and transport in the human brain. *J Neurochem* 1998; **70**: 397–408.

91 Seaquist ER, Damberg GS, Tkac I, Gruetter R. The Effect of Insulin on In Vivo Cerebral Glucose Concentrations and Rates of Glucose Transport/Metabolism in Humans. *Diabetes* 2001; **50**: 2203–2209.

92 Choi IY, Lee SP, Kim SG, Gruetter R. In vivo measurements of brain glucose transport using the reversible Michaelis-Menten model and simultaneous measurements of cerebral blood flow changes during hypoglycemia. *J Cereb Blood Flow Metab* 2001; **21**: 653–663.

93 van de Ven KCC, van der Graaf M, Tack CJ, Heerschap A, de Galan BE. Steady-state brain glucose concentrations during hypoglycemia in healthy humans and patients with type 1 diabetes. *Diabetes* 2012; **61**: 1974–1977.

94 Gjedde A. Rapid steady-state analysis of blood-brain glucose transfer in rat. *Acta Physiol Scand* 1980; **108**: 331–339.

95 Crone C. Facilitated transfer of glucose from blood into brain tissue. *J Physiol (Lond)* 1965; **181**: 103–113.

96 Cutler RW, Sipe JC. Mediated transport of glucose between blood and brain in the cat. *Am J Physiol* 1971; **220**: 1182–1186.

97 Nwokolo M, Amiel SA, O'Daly O, Byrne ML, Wilson BM, Pernet A *et al.* Hypoglycemic thalamic activation in type 1 diabetes is associated with preserved symptoms despite reduced epinephrine. *J Cereb Blood Flow Metab* 2019; : 271678X19842680.

98 Arbelaez AM, Powers WJ, Videen TO, Price JL, Cryer PE. Attenuation of counterregulatory responses to recurrent hypoglycemia by active thalamic inhibition: a mechanism for hypoglycemia-associated autonomic failure. *Diabetes* 2008; **57**: 470–475.

99 Arbelaez AM, Rutlin JR, Hershey T, Powers WJ, Videen TO, Cryer PE. Thalamic activation during slightly subphysiological glycemia in humans. *Diabetes Care* 2012; **35**: 2570–2574.

100 Wiegers EC, Rooijackers HM, Tack CJ, Heerschap A, de Galan BE, van der Graaf M. Brain Lactate Concentration Falls in Response to Hypoglycemia in Patients With Type 1 Diabetes and Impaired Awareness of Hypoglycemia. *Diabetes* 2016; **65**: 1601–1605.

101 Abdul-Rahman A, Agardh CD, Siesjö BK. Local cerebral blood flow in the rat during severe hypoglycemia, and in the recovery period following glucose injection. *Acta Physiol Scand* 1980; **109**: 307–314.

102 Norberg K, Siesiö BK. Oxidative metabolism of the cerebral cortex of the rat in severe insulin-induced hypoglycaemia. *J Neurochem* 1976; **26**: 345–352.

103 Siesjö BK, Pelligrino D. Regional differences in vascular autoregulation in the rat brain in severe insulin-induced hypoglycemia. *J Cereb Blood Flow Metab* 1983; **3**: 478–485.

104 Horinaka N, Artz N, Jehle J, Takahashi S, Kennedy C, Sokoloff L. Examination of potential mechanisms in the enhancement of cerebral blood flow by hypoglycemia and pharmacological doses of deoxyglucose. *J Cereb Blood Flow Metab* 1997; **17**: 54–63.

105 Powers WJ, Boyle PJ, Hirsch IB, Cryer PE. Unaltered cerebral blood flow during hypoglycemic activation of the sympathochromaffin system in humans. *Am J Physiol* 1993; **265**: R883–7.

106 Siesjö BK. *Brain energy metabolism*. John Wiley & Sons, 1978.

107 Powers WJ, Hirsch IB, Cryer PE. Effect of stepped hypoglycemia on regional cerebral blood flow response to physiological brain activation. *Am J Physiol* 1996; **270**: H554–9.

108 van Hall G, Strømstad M, Rasmussen P, Jans O, Zaar M, Gam C *et al.* Blood lactate is an important energy source for the human brain. *J Cereb Blood Flow Metab* 2009; **29**: 1121–1129.

109 Cryer PE. Mechanisms of hypoglycemia-associated autonomic failure in diabetes. *N Engl J Med* 2013; **369**: 362–372.

110 Schwartz NS, Clutter WE, Shah SD, Cryer PE. Glycemic thresholds for activation of glucose counterregulatory systems are higher than the threshold for symptoms. *J Clin Investig* 1987; **79**: 777–781.

111 Ongür D, Price JL. The organization of networks within the orbital and medial prefrontal cortex of rats, monkeys and humans. *Cereb Cortex* 2000; **10**: 206–219.

112 Pappenheimer JR, Setchell BP. Cerebral glucose transport and oxygen consumption in sheep and rabbits. *J Physiol (Lond)* 1973; **233**: 529–551.

113 Agardh CD, Chapman AG, Nilsson B, Siesjö BK. Endogenous substrates utilized by rat brain in severe insulin-induced hypoglycemia. *J Neurochem* 1981; **36**: 490–500.

114 Blazey TM, Snyder AZ, Goyal MS, Vlassenko AG, Raichle ME. A systematic meta-analysis of oxygen-to-glucose and oxygen-to-carbohydrate ratios in the resting human brain. *PLoS ONE* 2018; **13**: e0204242.

115 Lewis LD, Ljunggren B, Norberg K, Siesjö BK. Changes in carbohydrate substrates, amino acids and ammonia in the brain during insulin-induced hypoglycemia. *J Neurochem* 1974; **23**: 659–671.

116 Ghajar JB, Plum F, Duffy TE. Cerebral oxidative metabolism and blood flow during acute hypoglycemia and recovery in unanesthetized rats. *J Neurochem* 1982; **38**: 397–409.

117 Choi I-Y, Seaquist ER, Gruetter R. Effect of hypoglycemia on brain glycogen metabolism in vivo. *Journal of Neuroscience Research* 2003; **72**: 25–32.

118 Suh SW, Bergher JP, Anderson CM, Treadway JL, Fosgerau K, Swanson RA. Astrocyte glycogen sustains neuronal activity during hypoglycemia: studies with the glycogen phosphorylase inhibitor CP-316,819 ([R-R*,S*]-5-chloro-N-[2-hydroxy-3-(methoxymethylamino)-3-oxo-1-(phenylmethyl)propyl]-1H-indole-2-carboxamide). *J Pharmacol Exp Ther* 2007; **321**: 45–50.

119 Öz G, Kumar A, Rao JP, Kodl CT, Chow L, Eberly LE *et al.* Human brain glycogen metabolism during and after hypoglycemia. *Diabetes* 2009; **58**: 1978–1985.

120 Vilchez D, Ros S, Cifuentes D, Pujadas L, Vallès J, García-Fojeda B *et al.* Mechanism suppressing glycogen synthesis in neurons and its demise in progressive myoclonus epilepsy. *Nat Neurosci* 2007; **10**: 1407–1413.

121 Amaral AI. Effects of hypoglycaemia on neuronal metabolism in the adult brain: role of alternative substrates to glucose. *J Inherit Metab Dis* 2013; **36**: 621–634.

122 Goyal MS, Hawrylycz M, Miller JA, Snyder AZ, Raichle ME. Aerobic glycolysis in the human brain is associated with development and neotenous gene expression. *Cell Metab* 2014; **19**: 49–57.

123 Shannon BJ, Vaishnavi SN, Vlassenko AG, Shimony JS, Rutlin J, Raichle ME. Brain aerobic glycolysis and motor adaptation learning. *Proc Natl Acad Sci USA* 2016; **113**: E3782–91.

124 Benveniste H, Dienel G, Jacob Z, Lee H, Makaryus R, Gjedde A *et al.* Trajectories of Brain Lactate and Re-visited Oxygen-Glucose Index Calculations Do Not Support Elevated Non-oxidative Metabolism of Glucose Across Childhood. *Front Neurosci* 2018; **12**: 631.

125 Heikkilä O, Mäkimattila S, Timonen M, Groop P-H, Heikkinen S, Lundbom N. Cerebellar glucose during fasting and acute hyperglycemia in nondiabetic men and in men with type 1 diabetes. *Cerebellum* 2010; **9**: 336–344.

126 Herzog RI, Chan O, Yu S, Dziura J, McNay EC, Sherwin RS. Effect of acute and recurrent hypoglycemia on changes in brain glycogen concentration. *Endocrinology* 2008; **149**: 1499–1504.

127 Cremer JE, Cunningham VJ, Seville MP. Relationships between extraction and metabolism of glucose, blood flow, and tissue blood volume in regions of rat brain. *J Cereb Blood Flow Metab* 1983; **3**: 291–302.

128 Agardh CD, Kalimo H, Olsson Y, Siesjö BK. Hypoglycemic brain injury: metabolic and structural findings in rat cerebellar cortex during profound insulin-induced hypoglycemia and in the recovery period following glucose administration. *J Cereb Blood Flow Metab* 1981; **1**: 71–84.

129 Weigel K, Gartzen D, Kleihues P. Regional heterogeneity of L-[3-(3)H]tyrosine incorporation into rat brain proteins during severe hypoglycemia. *J Cereb Blood Flow Metab* 1982; **2**: 249–253.

130 Auer RN, Olsson Y, Siesjö BK. Hypoglycemic brain injury in the rat. Correlation of density of brain damage with the EEG isoelectric time: a quantitative study. *Diabetes* 1984; **33**: 1090–1098.

131 Auer RN, Hugh J, Cosgrove E, Curry B. Neuropathologic findings in three cases of profound hypoglycemia. *Clin Neuropathol* 1989; **8**: 63–68.

132 Auer RN. Hypoglycemic brain damage. *Forensic Sci Int* 2004; **146**: 105–110.

133 Crane PD, Pardridge WM, Braun LD, Nyerges AM, Oldendorf WH. The interaction of transport and metabolism on brain glucose utilization: a reevaluation of the lumped constant. *J Neurochem* 1981; **36**: 1601–1604.

134 Gjedde A. Calculation of cerebral glucose phosphorylation from brain uptake of glucose analogs in vivo: a re-examination. *Brain Res* 1982; **257**: 237–274.

135 Tyler JL, Strother SC, Zatorre RJ, Alivisatos B, Worsley KJ, Diksic M *et al.* Stability of regional cerebral glucose metabolism in the normal brain measured by positron emission tomography. *J Nucl Med* 1988; **29**: 631–642.

136 Stapleton JM, Morgan MJ, Liu X, Yung BC, Phillips RL, Wong DF *et al.* Cerebral glucose utilization is reduced in second test session. *J Cereb Blood Flow Metab* 1997; **17**: 704–712.

137 Amaral AI, Teixeira AP, Håkonsen BI, Sonnewald U, Alves PM. A comprehensive metabolic profile of cultured astrocytes using isotopic transient metabolic flux analysis and C-labeled glucose. *Front Neuroenergetics* 2011; **3**: 5.

138 Amaral AI, Teixeira AP, Sonnewald U, Alves PM. Estimation of intracellular fluxes in cerebellar neurons after hypoglycemia: importance of the pyruvate recycling pathway and glutamine oxidation. *Journal of Neuroscience Research* 2011; **89**: 700–710.

Chapter 5: Hyperglycemia selectively alters cerebral glucose metabolism in white matter and brain stem

5.1 Abstract

At normal blood glucose levels, glucose influx into the brain greatly exceeds it basal metabolic rate. Despite this fact, hyperglycemia alters cerebral glucose metabolism. To investigate this surprising finding, we performed PET and MRI imaging in participants undergoing euglycemic (90-100 $mg \cdot dL^{-1}$ and hyperglycemic (250-300 $mg \cdot dL^{-1}$) glucose clamps with basal insulin replacement. Hyperglycemia significantly altered the topography of brain glucose metabolism measured with [^{18}F]-FDG PET. Relative to the rest of the brain, glucose consumption increased in white matter and in cerebellar and medial temporal lobe gray matter. Conversely, relative glucose consumption decreased throughout the rest of gray matter. The change in the topography of glucose metabolism was caused by a quantitative increase in the cerebral metabolic rate of glucose (CMRglc) in white matter and the brain stem. Hyperglycemia did not change the topographies of blood flow, blood volume, oxygen consumption, or oxygen extraction measured with PET. Quantitative cerebral blood flow (CBF), measured with pseudo-continuous arterial spin labeling (pCASL) MRI, also was not affected by hyperglycemia. As hyperglycemia did not alter the topography of oxygen consumption, the ratio of relative oxygen-to-glucose consumption decreased in the white matter and brain stem, which suggests that the increase in CMRglc in these regions is due to non-oxidative glucose consumption.

5.2 Introduction

The fact that glucose is the brain's primary fuel source[1] makes transport of glucose between the blood and brain critically important. Glucose is transported across the blood-brain barrier by facilitated diffusion through the GLUT1 transporter[2]. Therefore, the flux of glucose into the brain is dependent on the concentration of glucose in the blood. Fortunately, at normal blood glucose concentrations, the transport of glucose into the brain far exceeds the brain's baseline metabolic requirements[3]. As a result, the brain is relatively insensitive to small decreases in plasma glucose concentration, with glucose consumption only dropping after moderate hypoglycemia has occurred[4,5].

Given that the brain normally receives more than enough glucose to meet its needs, one would predict that increasing the blood glucose concentration would not have an effect on brain glucose consumption. Several studies, however, suggest that this may not be the case. Mild hyperglycemia has been shown to alter the relative uptake pattern of [^{18}F]-FDG, a PET tracer used for the measurement of regional glucose metabolism[6]. Kawasaki et al. found that, relative to the brain as a whole, acute mild hyperglycemia decreases [^{18}F]-FDG uptake throughout cortical gray matter[7]. This finding has since been replicated multiple times, both by the same research group[8-11], and by independent investigators[12].

Although intriguing, these studies are limited by the lack of quantitative estimates of the cerebral metabolic rate of glucose (CMRglc). Instead, CMRglc was approximated by computing the ratio of [^{18}F]-FDG uptake within a brain region to [^{18}F]-FDG uptake within a reference region. With this approach, all metabolic measurements are not absolute, but are relative to the reference region. As a result, it is unclear if glucose consumption is decreasing in cortical gray matter during acute hyperglycemia, or if it is simply changing less than the reference region. The extant literature favors the later possibility. With one possible exception[13], all the studies

measuring absolute CMRglc during acute hyperglycemia in humans have reported whole-brain increases[10,14-16], although only in the report by Blomqvist et al. was the increase significant[15]. Furthermore, studies in both rats [17,18] and humans[10,15,16] have failed to report significant regional decreases in CMRglc. In fact, Blomqvist et al. found that CMRglc actually increased in every region examined[15]. Interestingly, Blomqvist et al. also reported an inverse relationship between baseline CMRglc and the change induced by acute hyperglycemia, with the largest increases in CMRglc occurring in regions with the lowest baseline rates[15]. For example, CMRglc in white matter increased by approximately 50%, which is much greater than the whole-brain average increase of around 20%. A similarly large increase in white matter CMRglc was also reported by Hasselbalch et al., where the centrum semiovale was the only region where CMRglc was significantly altered by acute hyperglycemia[16].

Taken together, the results of the studies discussed above suggest that, in humans, acute hyperglycemia modestly increases global cerebral glucose consumption, with larger increases occurring in regions with lower baseline metabolic rates. This conclusion is consistent with a previous analysis of regional CMRglc data in hyperglycemic rats[19]. It also explains why many studies have found that acute hyperglycemia decreases glucose metabolism in cortical gray matter relative to the rest of the brain. Cortical gray matter regions have high basal CMRglc, and therefore CMRglc changes much less during hyperglycemia than in regions, such as white matter, where basal CMRglc is low. This is essentially what was recently found by Ishibashi et al.[10]. The authors first reported that there we no significant decreases in CMRglc in several gray matter regions[10] during mild hyperglycemia. After normalizing the CMRglc images by the whole-brain mean, however, decreases were found in several regions, including in the precuneus and posterior cingulate[10]. The most straightforward explanation of these finding is not that

CMRglc is decreasing in these regions; rather, it is simply increasing less than the rest of the brain.

If hyperglycemia is increasing CMRglc in regions with low basal metabolic rates, it is unclear what effect it is having on other aspects of cerebral metabolism. Although studies in animal models have reported that hyperglycemia decreases cerebral blood flow (CBF) throughout the entire brain[20,21], the findings in humans have not been so consistent. Multiple studies have reported that the whole-brain average CBF does not change with hyperglycemia[13,14,16,22]. Moreover, although significant regional changes in blood flow have been reported[8,23], the set of affected brain regions differed between studies. Even less clarity exists on changes in the cerebral rate of oxygen consumption ($CMRO_2$). Two initial reports found that global $CMRO_2$ was unaltered by hyperglycemia[13,14], whereas a recent study found that it was significantly decreased[22]. We know of no data examining regional changes in oxygen consumption during hyperglycemia.

Several studies from our laboratory have highlighted the importance of measuring changes in glucose consumption, blood flow, and oxygen consumption under the same conditions[24-26]. Although these quantities are normally tightly coupled at rest[27], they do not always remain so during brief episodes of increased brain activity[24] or during more sustained changes in brain structure and function across the life-span[25,26]. To explore the possibility that acute hyperglycemia selectively affects key components of brain metabolism, we acquired regional measurements of glucose metabolism, oxygen metabolism, blood flow, and blood volume during euglycemic and hyperglycemic glucose clamps in normal, young-adult humans.

5.3 Methods

Participants

Data from twenty-six participants are included in this report. Participants were healthy young adults with a mean BMI of 25.3 (SD 3.3) and no history of diabetes. The participants (females=15, males=11) had an average age of 35.1 years (SD 10.2). Complete data during both the euglycemic and hyperglycemic clamp conditions were obtained for most, but not all, participants. The total number of subjects for each metabolic parameter of interest is listed in Table 5.1. All participants gave written informed consent. Experimental procedures were approved by the Washington University School of Medicine Human Research Protection Office and were compliant with the Helsinki Declaration of 1975.

Experimental design

The target plasma glucose level was 90-100 $mg \cdot dL^{-1}$ for the euglycemic clamp and 250-300 $mg \cdot dL^{-1}$ for the hyperglycemic clamp. The majority of participants (18/26) were scanned during both clamp conditions. The condition order was counterbalanced across participants. Three participants had data from two separate euglycemic clamp visits. The second euglycemic visit was acquired as part of a separate study exploring the effect of hyperinsulinemia on brain metabolism. Any data points from repeated euglycemic visits were averaged together prior to subsequent analysis. The median time between visits was 34.0 days with a range of 7.0 – 966.0 days.

All participants were admitted to the Washington University in St. Louis Clinical Research Unit after fasting overnight for at least 10 hours. An arterial line was placed into the radial artery to allow for the sampling of arterial tracer concentration. Plasma insulin, c-peptide, β-hydroxybutyrate, lactate, and pyruvate levels were measured via the arterial line every 30 minutes. An intravenous catheter was then placed into each arm. The first catheter was placed in a vein in the dorsal forearm and used for radiotracer injection. The second catheter was

positioned in an forearm vein and was used for infusion of octreotide, insulin, dextrose (20%), glucagon, and potassium. Dextrose was infused at a variable rate determined by the clamp condition and plasma glucose measurements taken every 5 minutes. Octreotide, a somatostatin analogue, was infused at a rate of 30 $ng \cdot kg^{-1} \cdot min^{-1}$ to suppress endogenous secretion of insulin, glucagon, and growth hormone[28]. Plasma insulin and glucagon were maintained with continuous infusions of 0.1 $mU \cdot kg^{-1} \cdot min^{-1}$ and 1.0 $ng \cdot kg^{-1} \cdot min^{-1}$ respectively. Finally, potassium chloride was given at a rate of 5 $mmol \cdot h^{-1}$ to prevent insulin-induced hypokalemia[29].

Image Acquisition

PET and MRI data were acquired simultaneously using a Siemens Biograph PET/MRI. PET data acquisition began after the desired plasma glucose level was reached. First, approximately 25 mCi of $[^{15}O]$-H_2O was injected for the measurement of blood flow. Cerebral oxygen metabolism and blood volume were assessed with the inhalation of 25 mCi of $[^{15}O]$-O_2 or $[^{15}O]$-CO respectively. Repeat scans were obtained for all three tracers if possible. All the $[^{15}O]$ tracers imaging data was acquired using a dynamic acquisition that started prior to tracer administration. $[^{15}O]$-H_2O and $[^{15}O]$-O_2 scans lasted for five minutes, whereas the $[^{15}O]$-CO scan went for seven minutes. Following the $[^{15}O]$ scans, 5 mCi of $[^{18}F]$-FDG was injected, and cerebral glucose metabolism was measured using a 60 minute dynamic PET scan. For attenuation correction, a Siemens Biograph 40 PET/CT was used to acquire a CT image of the head (120 keV, 25 effective mAs, voxel size = 0.59 x 0.59 x 3.0 mm, acquisition matrix = 512 x 512 x 74 mm voxels). From the CT image, μ-maps were created by converting the CT Hounsfield values into attenuation coefficients[30,31].

Concurrent with the $[^{15}O]$-H_2O PET scans, quantitative cerebral blood flow (CBF) was measured using pseudo-continuous arterial spin labeling (pCASL). 2D pCASL acquisition

included 80 images, each with 20 slices, voxel size 3.4 x 3.4 x 5.0 mm, and a 64 x 64 mm in plane acquisition matrix. The TR was 4.0 seconds, the TE 12.0 milliseconds, and an acceleration factor of 2.0 was applied. Two separate pCASL runs were acquired during each study visit. A gradient echo field map was also acquired in a subset of subjects (16/24) to allow for the correction for EPI distortions (TR = 646.0 ms. TE 1 = 5.19 ms, TE 2 = 7.65 ms, slices = 45, voxel size = 1.7 x 1.7 x 3.0, acquisition matrix = 212 x 212 mm. A sagittal high resolution T1-weighted MPRAGE was also obtained (TR = 2400 ms, TE = 2.13 ms, FOV = 256 x 256 x 176 mm, voxel size = 1.0 x 1.0 x 1.0 mm).

Image Analysis

Structural MRI

FreeSurfer 5.3[32] was used to segment the T1-weighted structural image from each subject's first study visit into 48 non-overlapping and bilaterally symmetric cortical regions **(**Figure 2.1). Cortical gray matter was parcellated into 34 gray-based regions of interest (ROIs), according to the Desikan atlas[33]. The remaining gray matter ROIs comprised seven subcortical gray matter regions (amygdala, caudate, hippocampus, nucleus accumbens, pallidum, putamen, and thalamus), and the cerebellum[34]. White matter was divided into cerebellar white, cortical white matter, the corpus callosum, and deep white matter. The cortical white matter region was created by combining all of the superficial white matter regions that are part of FreeSurfer's standard output. Finally, separate ROIs were created for the brain stem and ventral diencephalon. Each subject's T1-weighted image was also nonlinearly aligned to MNI152 atlas space using a combination of FLIRT[35] and FNIRT in FSL[36]. To increase SNR, atlas registration was performed using an T1-weighted average image that was created by rigidly aligning images obtained at both study visits.

pCASL MRI

Preprocessing of the pCASL data began with correction for odd-even slice intensity artifacts[37]. For each ASL run, non-labeled frames were used to compute separate scaling factors for odd and even slices. These scaling factors where then applied to both the control and labeled frames to remove any systematic odd-even slice intensity artifacts. Images were then motion corrected using FSL's mclirt tool with the temporal mean image as the target[38]. Following the recommendation of Wang et al., motion correction was performed separately for label and control frames[39]. After motion correction, FSL's flirt was used to compute a rigid body transformation between the average label and average control images. A rigid body transformation was then computed between the realigned pCASL timeseries and each's subject's average T1-weighted image using FSL's flirt. For subjects where field maps were acquired, the field map magnitude image was used as an intermediary between the pCASL and T1 images. All transformations were then combined, and the pCASL time series was resampled to MNI152 2mm atlas space in a single step.

Once in atlas space, a high pass (0.08 Hz) temporal filter was applied to the pCASL data. Sinc subtraction was then used to create perfusion weighted images[40]. The perfusion weighted images were converted to voxelwise quantitative cerebral blood flow (CBF) using a one compartment model[41,42]:

$$CBF = \frac{6000 \cdot \lambda \cdot (SI_{control} - SI_{label}) \cdot e^{\frac{PLD}{T_{1,blood}}}}{2 \cdot \alpha \cdot T_{1,blood} \cdot SI_{PD} \cdot (1 - e^{\frac{-\tau}{T_{1,blood}}})} \text{ [mL/hg/min]} \qquad (5.1)$$

Where α is the labeling efficiency (0.85), λ is the blood/brain partition coefficient for water (0.9), $SI_{control}$ and SI_{label} are the control and label image intensities, SI_{PD} is the intensity from a

proton-density image, PLD is the post labeling delay (1.5 sec), τ is the labeling duration (1.517 sec), and $T_{1,blood}$ is the longitudinal relaxation rate of blood (1.65 sec). The values for α, λ, and $T_{1,blood}$ were set according to the recommendations of Alsop et al.[42]. SI_{PD} was approximated by taking the average of the control images[43]. When computing the mean CBF for a single pCASL run, a weighting scheme was applied to down weight frames where subject motion produced large global shifts in image intensity[43]. The mean difference in global noise between control and label images (-43.77 ± 107.80) between hyperglycemic (290.19 ± 88.80) and euglycemic (333.96 ± 80.97) runs was not significantly different from zero (p = 0.434). The median CBF was calculated over the whole-brain as well within each of the 48 FreeSurfer ROIs.

PET Preprocessing

All PET reconstruction was performed using the ordered-subset expectation maximization (OSEM) algorithm[44] implemented in Siemens e7tools. Our PET reconstruction strategy consisted of two stages. In the first stage, the listmode data was scatter corrected and reconstructed without attenuation correction. All of the [^{15}O] PET data was reconstructed into 30 second frames. The [^{18}F]-FDG reconstruction consisted of ten 30 second frames followed by 55 60 second frames. Attenuation correction was not done at this stage because motion between frames precluded the use of a single μ-map for all frames.

To correct for between-frame motion, we used a modified version of a previously published strategy[45]. Briefly, within each tracer each frame was registered to every other frame. From this set of pairwise registrations, a linear system was created from which it was possible to compute the least squares transformation between any two frames. These transformations were used to align the previously computed μ-map with the time-resolved PET sinograms. The aligned μ-maps were used in the second stage of reconstruction to create time-sliced PET images

with attenuation, decay, and scatter correction. The use of motion and attenuated correction in the second stage allowed us to use shorter time bins for PET reconstruction. The final [^{15}O]-H_2O and [^{15}O]-O_2 images were reconstructed into 40 three second frames followed by 18 ten second frames. The [^{15}O]-CO data was reconstructed into 40 three second frames and then 30 ten second frames. Finally, the [^{18}F]-FDG scan was separated into 12 ten second frames, six 30 second frames, and 55 60 second frames.

After reconstruction, the motion corrected time series for each tracer was summed across time to create a single 3D PET image. Within individual participants, the sum images for each tracer were aligned to each other using rigid body registration[46]. After alignment, the sum images were averaged to create a mean image for each tracer. The mean [^{18}F]-FDG image was then brought into alignment with the T1-weighted image using rigid body registration and a vector gradient algorithm[47]. The final linear transformation within computed by minimizing the error between the forward ([^{18}F]-FDG -> T1) and backward (T1 -> [^{18}F]-FDG) transformations[45]. The same procedure was used to align the [^{15}O] sum images to the [^{18}F]-FDG sum image. The computed transformations were combined and used to resample each PET time series into MNI152 2mm atlas space.

Relative PET

Standardized uptake values ratios (SUVRs) were computed for each tracer. SUVR is a semi-quantitative measure where the tracer uptake at each brain region is reported relative to a reference region. SUVR is useful in examining changes in the topography of brain metabolism, but not absolute changes. When computing an SUVR one must select both a reference region and the time window over which to sum the tracer counts. The whole-brain (excluding the lateral ventricles) was used a reference region for all SUVR analyses. Specific time windows were

selected for each tracer. For [^{18}F]-FDG, a time window from 40 to 60 minutes post injection was chosen. A sixty second window, starting approximately after the bolus reached the brain, was used for the [^{15}O]-H_2O and [^{15}O]-O_2 data. A one minute window starting 180 seconds after the bolus reached the brain was used for the [^{15}O]-CO scans. All SUVR images were computed in native space and then resampled to MNI152 2mm space. To minimize the impact of vascular artifact on our SUVR measurements of oxygen metabolism, a voxelwise spatial regression was run using the resampled [^{15}O]-O_2 SUVR as a dependent variable and [^{15}O]-H_2O and [^{15}O]-CO SUVR as independent variables[48]. The [^{15}O]-O_2 SUVR was adjusted by subtracting from it the product of the [^{15}O]-CO SUVR and its regression coefficient. An SUVR approximation of OEF (rOEF) was calculated by dividing the adjusted [^{15}O]-O_2 SUVR by the product of the [^{15}O]-H_2O SUVR and its regression coefficient. Finally, a SUVR estimate of the relative oxygen-to-glucose index (rOGI) was computed by dividing the [^{15}O]-O_2 SUVR by the [^{18}F]-FDG SUVR. Prior to any statistical comparisons, all atlas space SUVR images are were normalized to a whole-brain mean of 1.0 and smoothed with a 5 mm FWHM gaussian kernel.

Quantitative PET

We were able to obtain quantitative estimates of CMRglc in a subset of participants in whom hand drawn arterial samples were acquired during the [^{18}F]-FDG scan. Given the greater noise at the voxel level, we chose to limit our quantitative analysis to ROIs. All ROIs were resampled to the space of the [^{18}F]-FDG data. A reversible two-compartment model was fit to the dynamic [^{18}F]-FDG from each ROI[6]. The first compartment is thought to represent free [^{18}F]-FDG in the brain, while the second is [^{18}F]-FDG that has been metabolized to [^{18}F]-FDG-6-phosophate. The model includes four rates constants (K_1, k_2, k_3, and k_4) and an additional term, V_b, that accounts for arterial blood volume. K_1 and k_3 describe influx from the blood and first

compartment, respectively. Loss of tracer from the first compartment is described by k_2, and efflux from the second compartment to the first is designated by k_4. Prior to model fitting, the time delay between the arterial samples and the [^{18}F]-FDG data was accounted for by fitting a one-compartment model to the first sixty seconds (post bolus arrival) of the [^{18}F]-FDG data[49]. This one-compartment model included a shift term that accounted for the temporal delay. The whole-brain time activity curve was used to determine the shift, which was then applied to all regional fits. Model fitting was performed using non-weighted nonlinear least squares using the limited-memory BFGS algorithm[50] implemented in Numerical Python[51]. Following the recommendation of Wu et al[52], a lumped constant of 0.81 was used to calculate CMRglc.

Statistics

All statistical analyses were done using the R[53] programming language. A linear mixed model with a fixed effect for clamp condition and a random intercept for subject was used to determine if differences in brain metabolism between conditions were statistically significant. No other covariates were added to the model. The voxelwise mixed models were fit using the nlme package[54], whereas the ROI models used lme4[55]. For the lme4 models, *p*-values were calculated using the lmerTest package[56], which implements Satterthwaite's method for determining the degrees of freedom in a mixed model. The difference between conditions was considered significant when the *p*-value was less than 0.05. Multiple comparison across space were accounted for by controlling the False Discovery Rate (FDR) at 0.05[57]. No multiple comparisons adjustment was made for the multiple modalities that were considered.

The lme4 package was used to perform a piecewise linear regression on the plasma glucose and insulin data that was obtained during the glucose clamps. The fixed effects included time, clamp condition, and the interaction between time and condition. There were two

regressors, one for each condition, that allowed for the slope of the regression line to vary after a breakpoint. The breakpoint was fixed at 90 minutes. We also included a random intercept for study visit nested within subject. Slopes that were different from 0.0 at the $p < 0.05$ level (no correction for multiple comparisons) were considered significant. Spearman correlation was used to quantify the degree of spatial correspondence between baseline metabolism and the change induced by hyperglycemia. All reported values are means and 95% confidence intervals (Cis) unless otherwise stated.

5.4 Results

Blood glucose and insulin levels

The time-courses for plasma glucose and insulin during the glucose clamps are shown in Figure 5.1. All measurements excluding the initial baseline measurements were taken after the target plasma glucose level had been reached. There was no significant difference found between conditions (euglycemia, hyperglycemia) in baseline plasma glucose (97.7 ± 3.5 mg·dL^{-1}; p=0.61) or insulin (42.6 ± 11.0 pmol·L^{-1}; p=0.95). The target plasma glucose levels were achieved in both conditions, with the blood glucose level reaching 300 mg·dL^{-1} in the hyperglycemic clamp and remaining near 100 mg·dL^{-1} in the euglycemic clamp (Figure 5.1A).

However, in both conditions plasma glucose rose slightly above the target concentration during the beginning of the glucose clamp and then slow decreased throughout the study period (Figure 5.1A). The time-course for plasma insulin during the euglycemic clamp exhibited a similar behavior (Figure 5.1B). To quantify this impression, we performed a piecewise linear regression where the slope of the regression line was allowed to differ after 90 minutes into the glucose clamp (see Methods). Table 5.2 reports the slope for each segment. For the first 90 minutes, plasma glucose and insulin increased significantly with time in both conditions ($p <$

0.05). However after 90 minutes, plasma glucose decreased with time during both clamps ($p < 0.01$) and plasma insulin decreased in the euglycemic condition ($p < 0.0001$). Plasma insulin continued to increase with time after 90 minutes during the hyperglycemic clamp ($p < 0.0001$). Importantly, insulin levels never approached values typically seen after a carbohydrate meal (Figure 5.1B).

Changes in the topography of brain metabolism

To assess regional changes in brain metabolism, whole brain normalized SUVR images were computed from the [^{18}F]-FDG, [^{15}O]-H_2O, [^{15}O]-O_2, and [^{15}O]-CO data (see Methods). The group average image of glucose consumption during hyperglycemia (Figure 5.2A) had much less contrast than the average image during euglycemia (Figure 5.2B). After correcting for multiple comparisons (FDR 0.05), significant differences between the two conditions were found throughout the brain (Figure 5.2C). Glucose consumption generally decreased relative to the rest of the brain in gray matter and increased in white matter. There were, however, exceptions. Relative glucose consumption increased in the gray matter of the medial temporal lobe and the cerebellum (Figure 5.2C). Despite the changes in the topography of glucose consumption, hyperglycemia did not alter the topography of blood flow (Figure 5.3), oxygen consumption (Figure 5.4), oxygen extraction (Figure 5.5), or blood volume (Figure 5.6). As the topography of oxygen consumption was unaffected by hyperglycemia (Figure 5.4), changes in the ratio of relative oxygen-to-glucose metabolism (rOGI) were essentially opposite to those found for glucose metabolism (Figure 5.7). rOGI significantly increased in gray matter, with the exception of the cerebellum and medial temporal lobe, and significantly decreased in white matter (Figure 5.7C).

To eliminate the possibility that the limited SNR at the voxelwise level prevented us from detecting changes in the topography of brain metabolism, we performed a ROI analysis on the regional PET data (Figure 5.8). Two ROIs were created. The first ROI contained voxels where relative glucose consumption increased, and the second voxels were the relative glucose consumption decreased (Figure 5.8A). The values within these two ROIs for each metabolic parameter are shown in Figure 5.8B-G. A significant ($p < 0.0001$) change with hyperglycemia was found in both ROIs for glucose consumption (Figure 5.8B) and rOGI (Figure 5.8G). No significant differences were found in either ROI for blood flow (Figure 5.8C), oxygen consumption (Figure 5.8D), rOEF (Figure 5.8E), or blood volume (Figure 5.8F).

Quantitative changes in brain metabolism

The analyses in Figures 1-7 show that the topographies of glucose consumption and rOGI are altered by hyperglycemia, whereas the topographies of cerebral blood flow, oxygen consumption, oxygen consumption, and blood volume are unchanged. To explore the quantitative basis of these changes, we obtained quantitative estimates of cerebral glucose consumption and blood flow (see Methods). We first examined quantitative changes for the brain as a whole as well as within the same two ROIs as Figure 5.8 **(**Figure 5.9**)**. Although the whole-brain CMRglc at hyperglycemia (27.3 ± 2.0 $\mu Mol \cdot hg^{-1} \cdot min^{-1}$) was slightly higher than at euglycemia (25.1 ± 2.1 $\mu Mol \cdot hg^{-1} \cdot min^{-1}$), the difference ($2.18 \pm 2.84$ $\mu Mol \cdot hg^{-1} \cdot min^{-1}$) was not significant ($p = 0.151$; Figure 5.9A). We did, however, find significant decreases in the two forward rate constants K_1 and k_3, and a significant increase in the backward rate constant k_4 ($p < 0.01$; Table 5.3). CMRglc within the ROI where relative glucose consumption decreased did not change ($p = 0.207$; Figure 5.9B). However, CMRglc was significantly higher at hyperglycemia (23.7 ± 2.3 $\mu Mol \cdot hg^{-1} \cdot min^{-1}$) than at euglycemia ($18.2 \pm 2.5$ $\mu Mol \cdot hg^{-1} \cdot min^{-1}$) within the ROI where relative glucose consumption increased ($p = 0.006$; Figure 5.9B). Hyperglycemia did not

significantly ($p > 0.5$) alter CBF in either the whole-brain (Figure 5.9C) or in either ROI (Figure 5.9D).

To examine quantitative metabolic change at a finer spatial scale, we calculated CMRglc and CBF (see Methods) within 48 ROIs defined using FreeSurfer (Figure 2.1). Figure 5.10A shows the estimated change in CMRglc induced by hyperglycemia for each ROI. The only regions that were significant at the FDR 0.05 level were the brain stem, cortical white matter, corpus callosum, and deep white matter. The largest change was found in the deep white matter (9.65 ± 2.09 $\mu Mol \cdot hg^{-1} \cdot min^{-1;}$ Figure 5.10B), where hyperglycemia increased CMRglc from 15.1 $\pm$ 1.7 to 24.8 $\pm$ 1.6 $\mu Mol \cdot hg^{-1} \cdot min^{-1}$ ($p < 0.0001$). The large increase in deep white matter was part of the strong negative spatial correlation ($\rho = -0.91$) between baseline CMRglc and change in CMRglc during hyperglycemia (Figure 5.10C). Compared to CMRglc, the regional changes in CBF were smaller and less consistent (Figure 5.11). The difference in CBF between hyperglycemia and euglycemia was not significant for any region (Figure 5.11A). This was true even for regions, like the deep white matter ($p = 0.667$; Figure 5.11B), where CMRglc increased. Furthermore, the spatial correlation between baseline CBF and change in CBF ($\rho = -0.53$) was not as robust as that for CMRglc (Figure 5.11C).

5.5 Discussion

Overview

Several previous studies have examined the effect of acute hyperglycemia on regional cerebral glucose metabolism in humans[8-11,15,16]. Our study is the first, however, to examine changes in glucose metabolism along with both regional changes in both blood flow and oxygen metabolism. Measuring all three aspects of metabolism allowed us to obtain several new findings. First, we found that although acute hyperglycemia changes the topography of glucose

metabolism, it does not significantly alter the topography of blood flow or oxygen consumption. Second, because the topography of oxygen consumption was unchanged, the topography of relative oxygen-to-glucose consumption (rOGI) was altered inversely to glucose consumption. rOGI was therefore significantly increased in gray matter and decreased in white matter. Exceptions to this pattern were gray matter in the cerebellum and the medial temporal lobe, where rOGI decreased, although not as robustly as glucose consumption decreased. Third, we were able to show that although quantitative CMRglc was significantly increased in the brain stem, corpus callosum, cortical white matter, and deep white matter, no quantitative changes in CBF were found in these, or any other, regions.

Glucose consumption

As previously mentioned, multiple studies have shown that acute hyperglycemia decreases glucose consumption in most of gray matter relative to the rest of the brain[7-11,58]. We have largely replicate these findings, with two exceptions. First, contrary to the original report by Kawasaki et al.[7], glucose metabolism in the gray matter of the cerebellum and medial temporal increased relative to the rest of the brain. Second, we found additional relative increases throughout white matter. Although Kawasaki et al. did report some increases, they were either very focal or found only when gray matter was used as a reference region. Methodological differences are perhaps the most likely reason for the differences between our results and those reported elsewhere in the literature. The original study by Kawasaki et al[7], as well as its subsequent replications[8-11], made subjects mildly hyperglycemic using oral glucose consumption. This paradigm was much different from ours in several ways. First, our participants were much more hyperglycemic (~300 $mg \cdot dL^{-1}$) than the participants in the Kawasaki et al. study (~135 $mg \cdot dL^{-1}$). Second, the hyperglycemic clamp technique we used produces a relatively constant hyperglycemia. The glucose load applied by Kawasaki et al. most likely resulted in a decline in

blood glucose level during the experiment. Finally, we prevented a large rise in blood insulin levels during hyperglycemia by suppressing endogenous insulin secretion with octreotide. Insulin was then infused to keep blood concentrations within a normal range. Insulin was not controlled in the Kawasaki et al. study. Although the effect of insulin of cerebral metabolism is still a matter of active research[59], it has been reported that hyperinsulinemia can alter the regional pattern of cerebral glucose consumption[60].

We were able to use quantitative PET to verify the changes in relative glucose metabolism. Consistent with studies in humans[10,14,16] and rats[17], we found that hyperglycemia induced a small, but not significant, increase in whole-brain CMRglc. This is also generally in agreement with Blomqvist et al., who reported a significant 20% increase in global CMRglc during acute hyperglycemia[15]. In contrast, Rowe et al. found that although whole-brain CMRglc was insignificantly elevated from fasting levels 15 minutes after the consumption of a meal, it actually was significantly less than fasting values 30 minutes later[13]. Whether postprandial increases in blood glucose cause fluctuations in global CMRglc requirements confirmation. Taken as a whole, however, the literature suggests that global CMRglc increases slightly during hyperglycemia.

Regionally, we found that CMRglc was significantly elevated in the brain stem, corpus callosum, cortical white matter, and the deep white matter. This is consistent with two prior studies that have reported that CMRglc increases by approximately 40-50% in white matter during acute hyperglycemia[15,16]. CMRglc did not significantly decrease in any region, even in a large region encompassing all voxels were relative glucose consumption was found to decrease. Finally, we replicated work in humans[15] and rats[19] showing that the change in CMRglc induced by hyperglycemia is inversely correlated with baseline metabolic rates. Taken together, our

quantitative results suggest that decreases in gray matter FDG uptake (relative to the rest of the brain) during hyperglycemia do not truly reflect a decrease in metabolic rate. Rather, the metabolic rate in these regions simply changes less than other regions, which then could be interpreted as a decrease after whole-brain normalization. This is what was found by Ishibashi et al., who reported significant declines in whole-brain normalized CMRglc during hyperglycemia even though the absolute rate in these regions was increased by a small, nonsignificant amount[10]. It is possible that the metabolic rate is really declining in gray matter during hyperglycemia, but by such a small amount that we, and others[10,16], have failed to detect it. This possibility seem less likely considering another study reported significant increases in CMRglc throughout all of gray matter[15].

Blood flow and oxygen consumption

Regional increases in CMRglc during acute hyperglycemia are somewhat surprising. At euglycemia the influx of glucose into the brain exceeds its basal CMRglc[3], so one would not necessarily predict that raising the blood glucose concentration would increase glucose consumption. Combining our regional glucose consumption data with our PET measurements blood flow and oxygen consumption is helpful in understanding this surprising finding. In contrast to the changes in the topography of glucose metabolism, no changes were found in the topography of either blood flow or oxygen consumption. To confirm that this was not due to limited SNR at the voxel level, we made ROIs representing the brain regions where relative glucose metabolism was altered. Relative oxygen consumption and blood flow were unchanged within these ROIs as well. Consistent with the lack of changes in oxygen consumption and blood flow, relative blood volume and oxygen extraction were also unaffected by hyperglycemia. Finally, we measured quantitative CBF using pCASL MRI. In agreement with the relative blood

flow data, we found that, despite increases in CMRglc, hyperglycemia did not significantly alter blood flow in any region.

Although we are not aware of any studies measuring regional oxygen consumption during hyperglycemia, multiple studies have investigated regional blood flow. Studies in animal models have consistently found that hyperglycemia decreases CBF throughout the entire brain[18,20]. Reports in humans, however, are somewhat mixed. Ishibashi et al found that, relative to the rest of the brain, blood flow was reduced by approximately 2% in the frontal cortex, lateral parietal cortex, and precuneus/posterior cingulate[8] during mild hyperglycemia. A different set of regions was reported by Page et al., who found that mild hyperglycemia decreases CBF in the anterior cingulate, hypothalamus, insula, striatum, and thalamus[23]. It is not clear why our results are not in agreement with those of Ishibashi et al. or Page et al. Like Kawasaki et al., both studies used an oral glucose load to induce mild hyperglycemia, so the previously mentioned caveats with this approach apply. Ishibashi et al. also only measured relative blood flow in four small, *a priori* ROIs. It is possible that any changes in blood flow were either too small for our limited SNR voxelwise analysis or too focal for our large ROIs. However, these possibilities are not consistent with the fact that that we failed to observe any changes in quantitative CBF using both smaller ROIs and a larger sample size. Finally, although our results are not consistent with those of Page et al. and Ishibashi et al., they are in agreement with studies reporting no global change in CBF during hyperglycemia[13,14,16,22].

Non-oxidative glucose consumption

Because the spatial pattern of oxygen consumption was unaltered by hyperglycemia, rOGI changed inversely to glucose consumption. Relative to the whole-brain average, rOGI increased in gray matter and decreased in white matter. Exceptions to this pattern were gray

matter in the medial temporal lobe and cerebellum, where rOGI decreased. Overall the changes in rOGI indicate that hyperglycemia produces relative decreases in non-oxidiative glucose consumption (NOglc) in gray matter regions and relative increases in white matter regions. It should also be mentioned that hyperglycemia essentially eliminated the regional difference in rOGI between gray and white matter (Figure 5.7A-B**,** Figure 5.8G).

As we did not measure quantitative oxygen consumption, we could not verify the changes we observed in rOGI with quantitative data. To the best of our knowledge, there have been no other studies examining regional changes in non-oxidative glucose during acute hyperglycemia. Blomquist et al. argued that the increases in CMRglc during acute hyperglycemia were due to increased oxidative glucose metabolism, although this was not based on measurements of oxygen metabolism[15]. Instead, it relied on a prior validation study performed in euglycemic participants[61]. This validation study showed that, compared to arterio-venous measurements, whole-brain CMRglc measured with their [1-^{11}C]-glucose PET method was closer to 1/6th of $CMRO_2$ than it was to CMRglc[61]. If true, this would imply their method measures oxidative glucose metabolism, not total glucose consumption. Only a small number of subjects were used in that verification study, however, and no statistical comparison between the two methods were performed. Furthermore, the method used by Blomqvist et al. relied on correction factors obtained at euglycemia[15,61]. Therefore, there is reason to question whether Blomqvist et al. were able to distinguish between oxidative vs. non-oxidative glucose metabolism during hyperglycemia.

Studies measuring global changes in $CMRO_2$ during hyperglycemia have reported that it is either unaltered during acute hyperglycemia[13,14], or decreased[22]. If, as we found, there are no regional effects of hyperglycemia on oxygen metabolism, then these studies would suggest that

oxygen consumption is either unaffected or modestly decreased by hyperglycemia in all brain regions. This, in turn, would imply that the increased CMRglc, as well as the decrease in rOGI, within the white matter and brain stem reflect quantitative increases in non-oxidative, not oxidative, glucose consumption. It is less clear how to interpret the increases in rOGI we found within gray matter. It is likely that such increases simply reflect the relative decreases in glucose consumption we found in these same regions. As discussed previously, it is unlikely that CMRglc actually declines in gray matter, and therefore unlikely that NOglc decreases. Consistent with this idea, Gottstein et al. found that the whole-brain NOglc was slightly elevated, albeit not significantly, by acute hyperglycemia[14].

If NOglc is increased in white matter and brain stem during hyperglycemia, it is unclear how the additional glucose is being consumed. At normal blood glucose levels, the majority of glucose in white matter is consumed oxidatively to provide energy for non-signaling tasks (e.g., maintaining the resting membrane potential)[62]. There are, however, non-oxidative pathways for glucose consumption in the brain[63,64]. Among these pathways are glycogen synthesis, the glycolytic pathway, the pentose phosphate shunt, and the polyol pathway. The TCA cycle also produces intermediates that are used for the synthesis of amino acid and neurotransmitters, including acetylcholine, aspartate, GABA, and glutamate[64]. Interestingly, alterations in some of these pathways have been linked to hyperglycemia.

Both acute and chronic hyperglycemia have been shown to upregulate pentose phosphate activity in cultured astrocytes[65], although to our knowledge this has not been replicated *in vivo.* A recent study found that acute hyperglycemia increased the production of lactate, an end-point of the glycolytic pathway, in the hippocampus of a mouse model of Alzheimer's disease[66]. If lactate production is increased during hyperglycemia, it is unclear how it is removed from the

brain. Two studies in humans reported that lactate efflux from the brain to the blood was not significantly increased by hyperglycemia[13,14]. The glymphatic system has been proposed as an alternative route for lactate efflux[67,68], but there is no evidence suggesting that hyperglycemia increases lactate efflux through the glymphatic system. It is possible that hyperglycemia produces excess lactate which is then subsequently used as a fuel source. Recent work has indicated that lactate can play a prominent role in white matter metabolism[69]. In developing mice, lactate is taken up by oligodendrocytes and can be used to support myelination when glucose levels are low[70]. Conversely, in adult mice lactate is exported from oligodendrocytes into axons, where it is presumably used to produce ATP via oxidative phosphorylation[71,72]. A transfer of excess lactate between cell types does not, however, explain our results, which suggest that hyperglycemia causes an increase in white matter glucose consumption without a detectable increase in oxygen consumption.

Another possible explanation for increased NOglc in white matter and brain stem during hyperglycemia is an increase in the production of sorbitol and fructose through the polyol pathway. Although it plays a very minor role in the brain at normal blood glucose levels[73], polyol pathway activity has been shown to increase in animal models during both acute[74] and chronic hyperglycemia[75]. It is also interesting to note that activation of the polyol pathway is a well-known features of diabetes mellitus[76], a disease defined by chronic hyperglycemia. Increased polyol activity in diabetes results in oxidative stress[77], and contributes to the development of several complications including cardiovascular disease, retinopathy, neuropathy, and cataracts[76,78]. There is however, no direct evidence linking hyperglycemia with increased polyol activity in white matter or the brain stem. Perhaps the best evidence is the work of Hwang et al., who used magnetic resonance (MR) spectroscopy to show that acute hyperglycemia increases the

fructose concentration of the human brain by about 0.5 mMol·L^{-1}[179]. However, their measurements, which were performed in a large voxel (30 x 20 x 30 mm^3) in the occipital lobe, likely contained a combination of gray matter, white matter, and CSF. Clearly, although the literature suggests several possibilities, there is not yet sufficient evidence to explain how white matter consumes additional glucose during hyperglycemia. To resolve this issue, future studies will have to employ techniques, such as MR spectroscopy, that can track glucose consumption down metabolic pathways within specific brain regions.

Our results have implications for human health and disease. Previous studies from our research group have established that non-oxidative glucose use plays a role in aging and Alzheimer's disease (AD)[80]. Studies in humans have shown that NOglc varies between gray matter regions[48,81], and that the regions that have the most NOglc in youth are the same regions that develop the greatest amyloid plaque loads in AD[82]. Studies in mouse models of AD have also shown that regional lactate production correlates with levels of amyloid plaques[83]. We also reported recently that non-oxidative glucose use decreases substantially with aging, with the largest decreases occurring in regions which, in young adults, have the most rates of NOglc[26]. Finally, regional deposition of phosphorylated tau has been shown to be inversely correlated with NOglc in individuals with high levels of amyloid plaques[84]. Considered as a whole, these findings suggest that, although NOglc may play an important role in development, plasticity, and learning[25,85], over the course of a lifetime high levels of NOglc may increase the risk of neurodegeneration and disease. It is therefore tempting to hypothesize that elevated non-oxidative glucose use in white matter may play a role in the development of the white matter disease that is often found in individuals with Type-2 diabetes mellitus (T2DM)[86], or even that NOglc is part of the connection between T2DM and AD[59,87]. In support of the latter idea, it has

been shown that acute hyperglycemia increases both lactate and amyloid production in a mouse model of AD[66]. Determining whether NOglc is elevated in the brains of individuals with chronic hyperglycemia is an important question for future studies.

Limitations

A few limitations should be considered when interpreting our results. First, although we did show that CMRglc quantitatively increases in both the brain stem and white matter during hyperglycemia, we did not have any quantitative measurement of oxygen consumption. Quantification of $CMRO_2$ traditionally requires invasive automatic arterial sampling, which our facility only recently acquired the ability to do in a PET/MR environment. Instead we reported that, relative to the whole-brain average, there were no changes in [^{15}O]-O_2 SUVR in any brain region. Although SUVRs are not quantitative measurements, they are a commonly used technique because they do not require arterial sampling and because normalization by a reference region is useful in removing global intensity artifacts[88]. Despite the absence of quantitative $CMRO_2$ data, we believe that our data is most consist with an increase in NOglc within white matter and brain stem. As discussed previously, the increase in CMRglc, the absence of a relative decrease in oxygen consumption, the decrease in rOGI, and the fact that previous studies have failed to report an increase in global $CMRO_2$[13,14,22], all point to an increase in non-oxidative glucose use within white matter and brain stem during hyperglycemia. We do acknowledge, however, that relative PET techniques can be misleading[89]. Indeed, we have argued here that decreases in gray matter [^{18}F]-FDG uptake during hyperglycemia[7] likely do not reflect decreases in CMRglc. Our laboratory is therefore currently performing experiments necessary to quantify $CMRO_2$ and NOglc during hyperglycemia.

All of our measurements of CMRglc relied on [^{18}F]-FDG, which requires a correction factor to account for the differences in transport and phosphorylation kinetics between FDG and glucose[90]. We chose to use the same value for this correction factor, referred to as the lumped constant (LC), in both the euglycemic and hyperglycemic conditions. Direct measures of the LC in rats have shown that it decreases very slightly during hyperglycemia[91]. As lower values for the lumped constant result in larger CMRglc, this would imply that our estimates of CMRglc, and therefore AG, are underestimated during hyperglycemia. To address this possibility, we followed the strategy of van Golen et al., and adjusted the LC using data expressing the LC as a function of blood glucose level in rats[92]. This amounted to decreasing the LC by approximately 6% in hyperglycemic individuals. Adjusting the LC had essentially no impact on our regional data. We did not identify any new regions with significantly altered CMRglc, and CMRglc remained significant in all the regions where it was so without LC adjustment. The only difference that adjusting the LC introduced in our results was that the increase in global mean CMRglc, which was not significant before the adjustment ($p = 0.151$), became significant afterwards ($p = 0.018$). The difference was quantitatively minor, however, as the increase in whole-brain CMRglc with hyperglycemia changed from to 2.18 ± 2.84 to 3.98 ± 2.97 $\mu Mol \cdot hg^{-1} \cdot min^{-1}$. Given the small change in the LC during hyperglycemia, and the minimal impact it had our results, we chose to use a fixed LC for all of our analyses.

Studies in humans have reported that the LC decreases to a greater extent than what we assumed above[10,16]. As lowering the LC increases the apparent CMRglc, it is possible that, if we had assumed a smaller value for the LC during hyperglycemia, we would have found increased CMRglc in a greater number of regions. In support of this possibility, a study using [1-^{11}C]-glucose PET[15], which does not require a LC, reported increased CMRglc in all brain regions

during hyperglycemia. There is, however, reason to be skeptical of a larger decrease in the LC during hyperglycemia. The two studies reporting changes in the LC in hyperglycemic humans did not measure the LC directly[10,16]. Measuring the LC typically requires estimates of the metabolic rate of glucose and FDG in the same individuals[93,94]. Instead these studies used only [^{18}F]-FDG data along with a mathematical model[95] that assumes: 1) the ratio of the K_1 for glucose to the K_1 for FDG is known and unchanged by hyperglycemia, 2) the ratio of K_3 between glucose and FDG is similarly known and unaffected by hyperglycemia, and 3) all the glucose-6-phosophate that is created is metabolized. Although the K_1 ratio is unaffected by hyperglycemia[96], we are not aware of any study verifying the stability of the k_3 ratio. We are also not aware of any study comparing directly LC values estimated with this model with direct measurements in humans. Hasselbalch et al. did attempt to validate the model based approach[93]. However, their verification was circular as the measured LC was used to compute the k_3 ratio that was subsequently entered into the model. It should be noted, too, that even the studies that used the model-based method to correct for changes in the LC produced CMRglc results that were in agreement with ours. They found that during acute hyperglycemia: 1) whole-brain CMRglc increased by a non-significant amount[10,16], 2) gray matter CMRglc was unchanged in every region examined[10,16], and 3) CMRglc within white matter significantly increased by over 40%[16].

Finally, it should be acknowledged that all of our metabolic measurements were made in an experimental setting. Endogenous insulin and glucagon secretion were blocked using infusions of the somatostatin analog octreotide. Although somatostatin has several roles in the CNS[97], blood-brain barrier permeability for somatostatin analogs are low[98], and we know of no studies reporting changes in CBF, $CMRO_2$, or CMRglc after octreotide administration. Infusions

of glucagon and insulin were also used to were used to keep both hormones at normal values. This was done to isolate the effect of hyperglycemia on brain metabolism. However, hyperglycemia typically sharply increases the concentration of insulin in the blood. Although plasma insulin did rise slightly during our hyperglycemic clamp, it always remained lower than what is seen during an oral glucose tolerance test[99] or after the consumption of a meal[100]. As a result, our results do not mirror naturally occurring hyperglycemia. It is therefore encouraging that our results are broadly consistent with studies that do not perform basal insulin replacement[7,10,15]. Determining what, if any, differences there are in brain metabolism between hyperglycemia with and without elevated insulin will require direct studies.

Conclusion

Our work is a novel addition to studies examining the effect of acute hyperglycemia on the brain. We reported that in humans, acute hyperglycemia increases CMRglc in white matter and brain stem, without altering regional blood flow, blood volume, or oxygen metabolism. This suggests that acute hyperglycemia alters normal brain metabolism by increasing NOglc in white matter and brain stem. Expanding upon this finding is an important topic for future research. Among the most pressing questions are quantifying the increase in NOglc during acute hyperglycemia, identifying the metabolic pathways responsible for elevated non-oxidative glucose use, and determining if NOglc remains high in individuals with chronic hyperglycemia. Addressing these questions will not only further our understanding of brain metabolism during hyperglycemia, but may also clarify the emerging relationship between NOglc, AD, and T2DM[59,66,80].

5.6 Figures

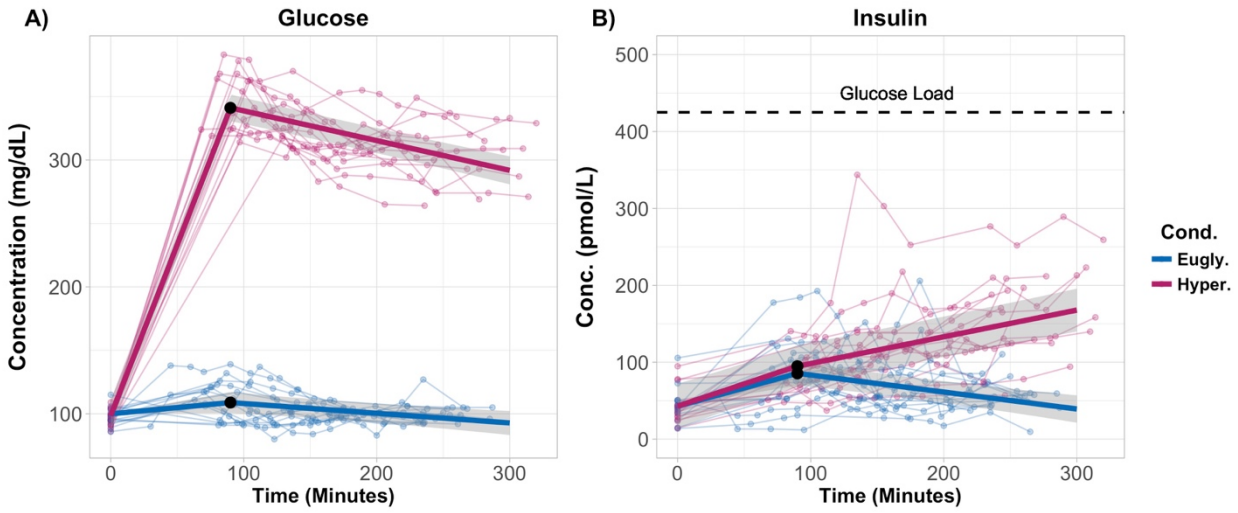

Figure 5.1: Time course of plasma glucose and insulin levels during glucose clamping

A) After the hyperglycemic clamp (red) the plasma glucose level was approximately 300 mg·dL^{-1}, whereas it remained near 100 mg·dL^{-1} during the euglycemic clamp (blue). A piecewise linear regression with a breakpoint at 90 minutes (black dot) was used to compute population estimates (thick lines) and their 95% CIs (gray ribbons). In both groups, blood glucose level increased prior to the breakpoint and then decreased afterwards (see Results). **B)** Plasma insulin also increased in both groups prior to the breakpoint. However, after the breakpoint insulin decreased during euglycemic clamp and increased in the hyperglycemic clamp. The dashed black line indicates a published value for the peak plasma insulin concentration after a 75 gram oral glucose tolerance test[99]. Note that even though plasma insulin increased throughout the hyperglycemic clamp, it was always below this value. The light lines and dots are data from individual sessions.

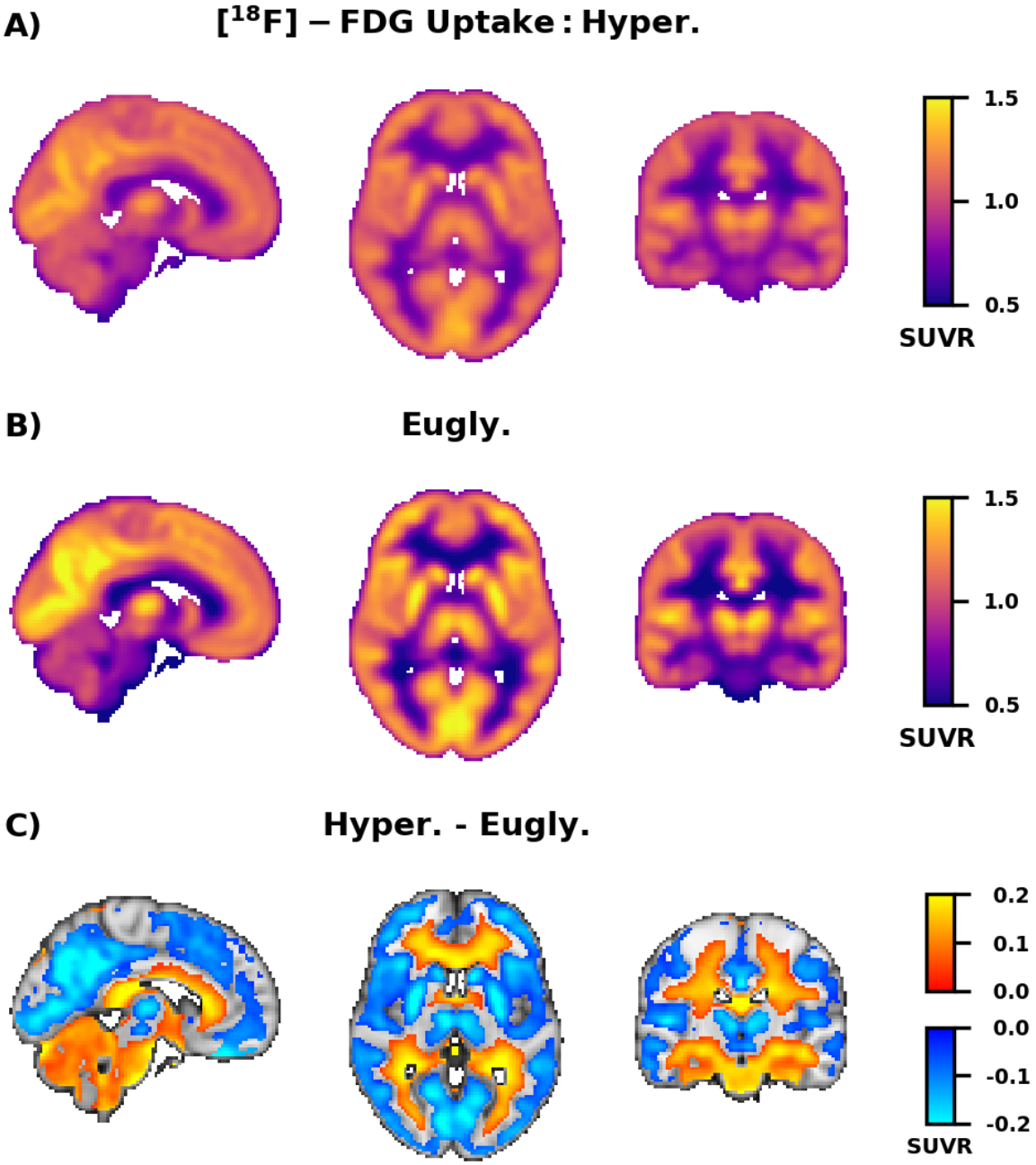

Figure 5.2: Hyperglycemia induced changes in relative glucose consumption

A) Group average (n=18) image of [^{18}F]-FDG SUVR during the euglycemic clamp. Values are normalized to the whole-brain mean. **B)** Group average (n=15) image of [^{18}F]-FDG SUVR during the hyperglycemic clamp. **C)** Group average difference in [^{18}F]FDG SUVR between the hyperglycemic and euglycemic clamp. Only voxels that are significantly different from zero after

correction for multiple comparisons (FDR 0.05) are shown in color. [^{18}F]-FDG uptake in blue voxels decreased relative to the whole brain mean during hyperglycemia, whereas orange/yellow voxels increased.

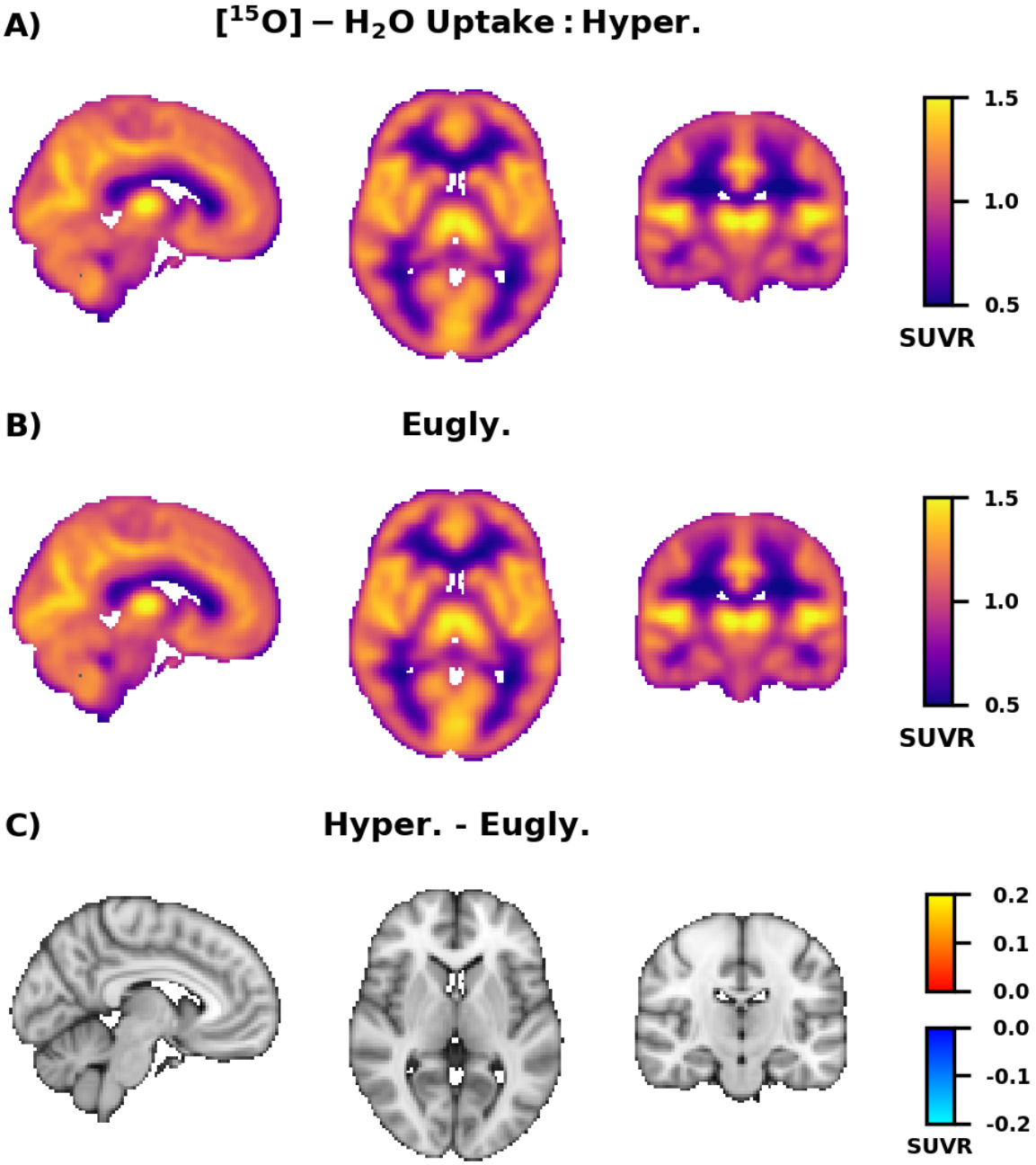

Figure 5.3: Relative cerebral blood flow measured with whole-brain normalized [^{15}O]-H_2O SUVR

All conventions as in Figure 5.2. No significant differences ($p > 0.05$) were found between **A)** euglycemia (n=19) and **B)** hyperglycemia (n=15) after **C)** correction or multiple comparisons with FDR.

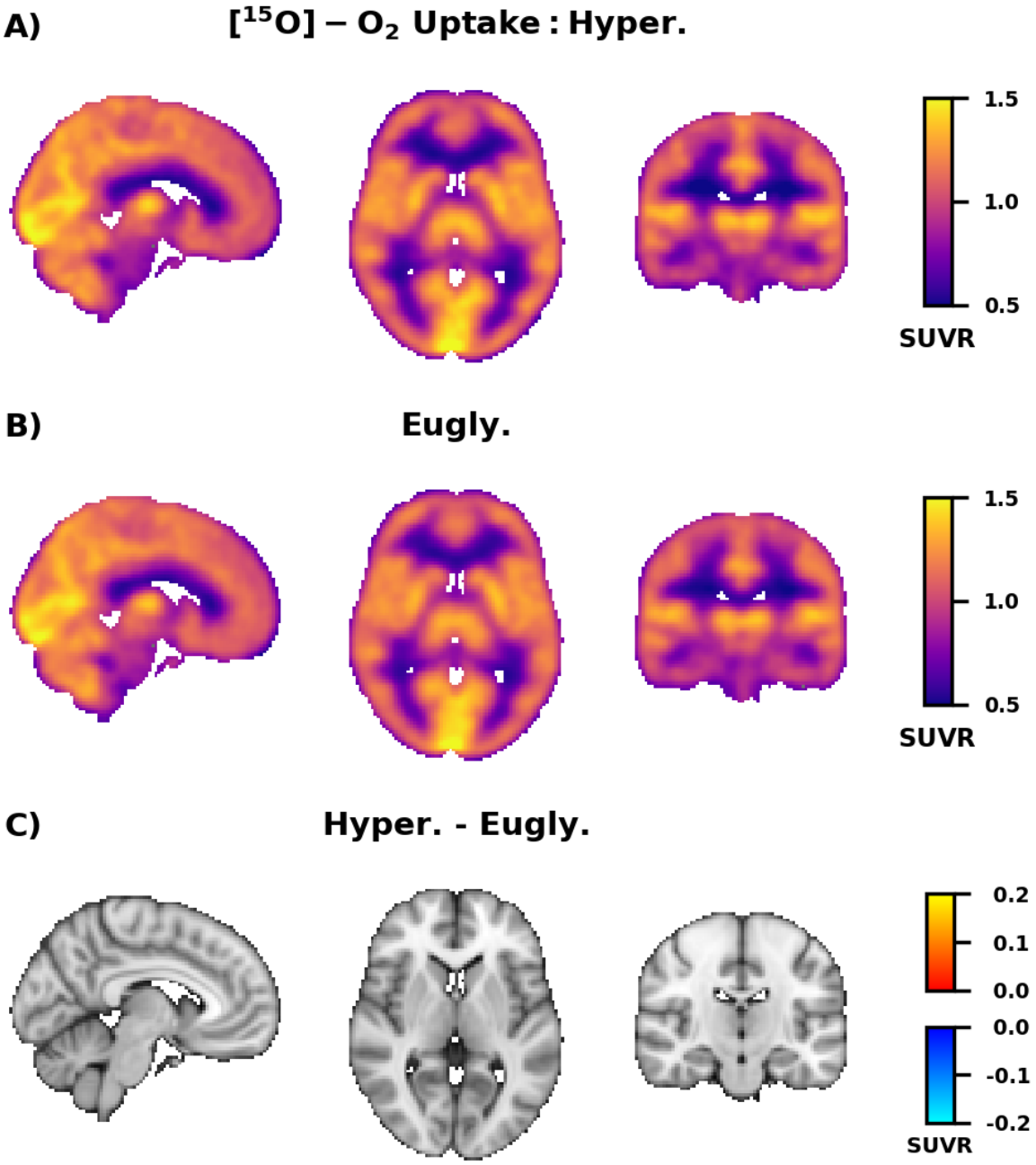

Figure 5.4: Relative oxygen consumption measured with whole-brain normalized [^{15}O]-O_2 SUVR

All conventions as in Figure 5.2. No significant differences ($p > 0.05$) were found between **A)** euglycemia (n=18) and **B)** hyperglycemia (n=14) after **C)** correction or multiple comparisons with FDR.

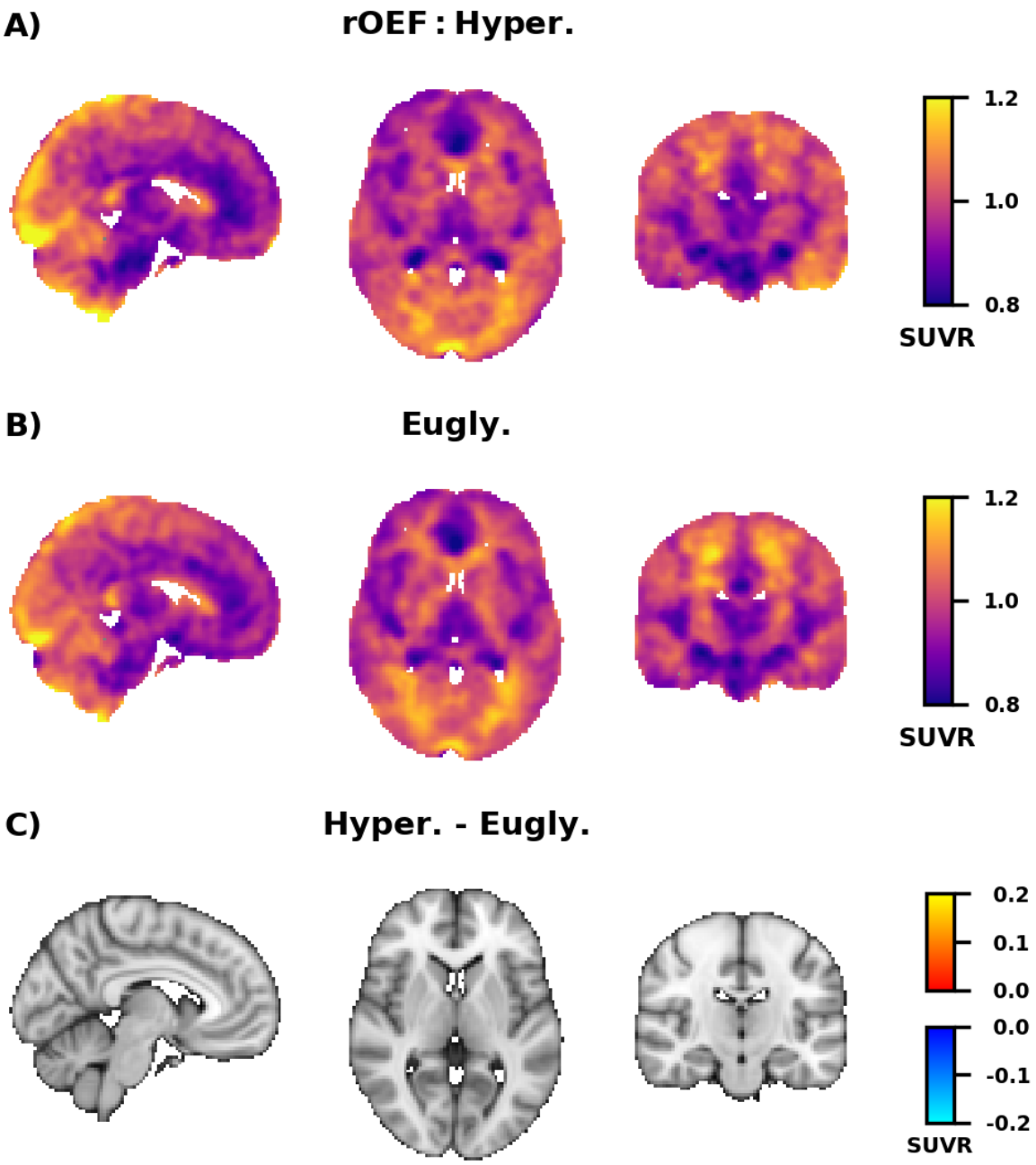

Figure 5.5: Relative oxygen extraction fraction (rOEF) measured with whole-brain normalized [^{15}O]-O_2 and [^{15}O]-H_2O SUVR

All conventions as in Figure 5.2. No significant differences ($p > 0.05$) were found between **A)** euglycemia (n=18) and **B)** hyperglycemia (n=14) after **C)** correction or multiple comparisons with FDR.

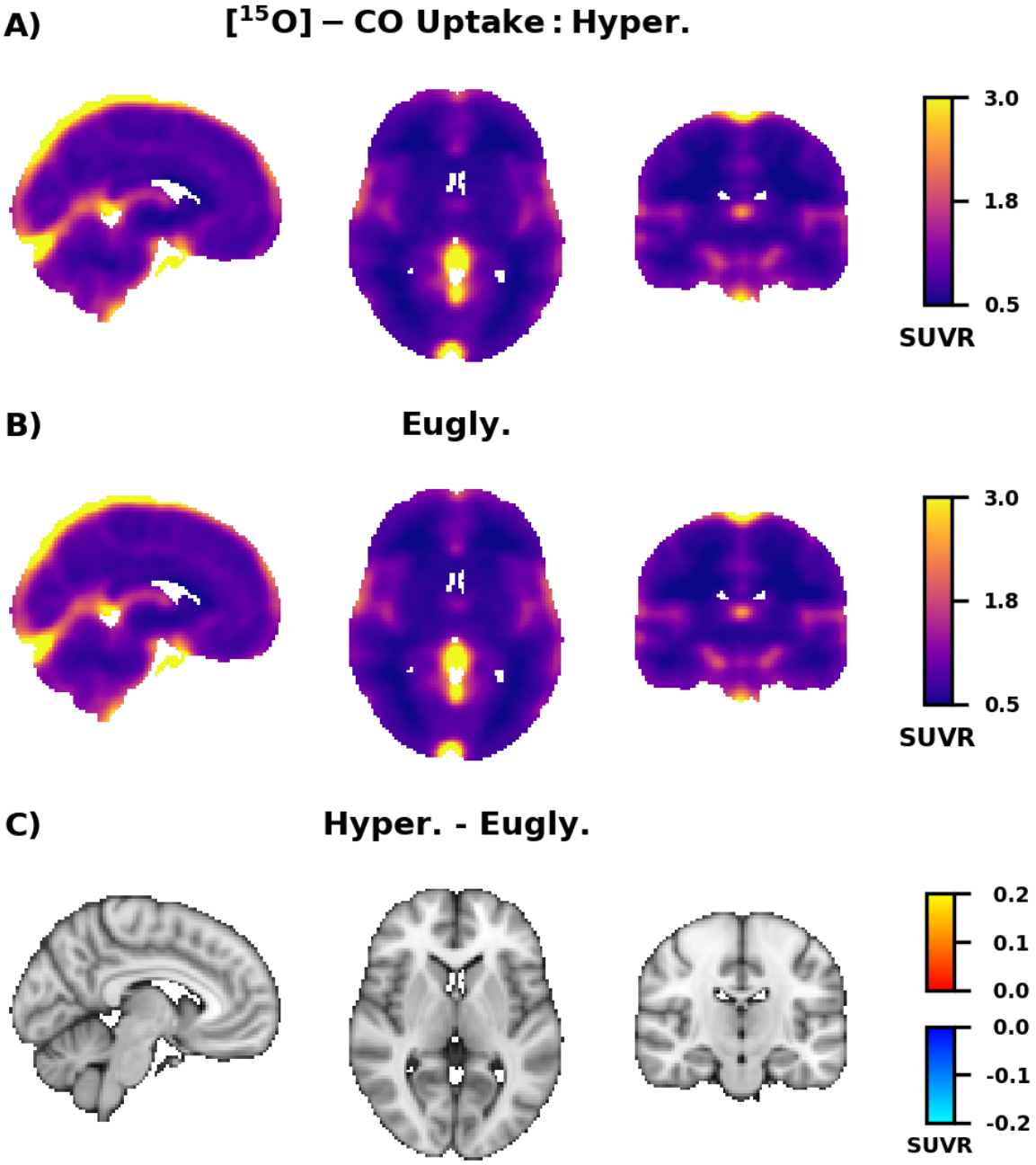

Figure 5.6: Relative cerebral blood volume measured with whole-brain normalized [^{15}O]-CO SUVR

All conventions as in Figure 5.2. No significant differences ($p > 0.05$) were found between **A)** euglycemia (n=18) and **B)** hyperglycemia (n=14) after **C)** correction or multiple comparisons with FDR.

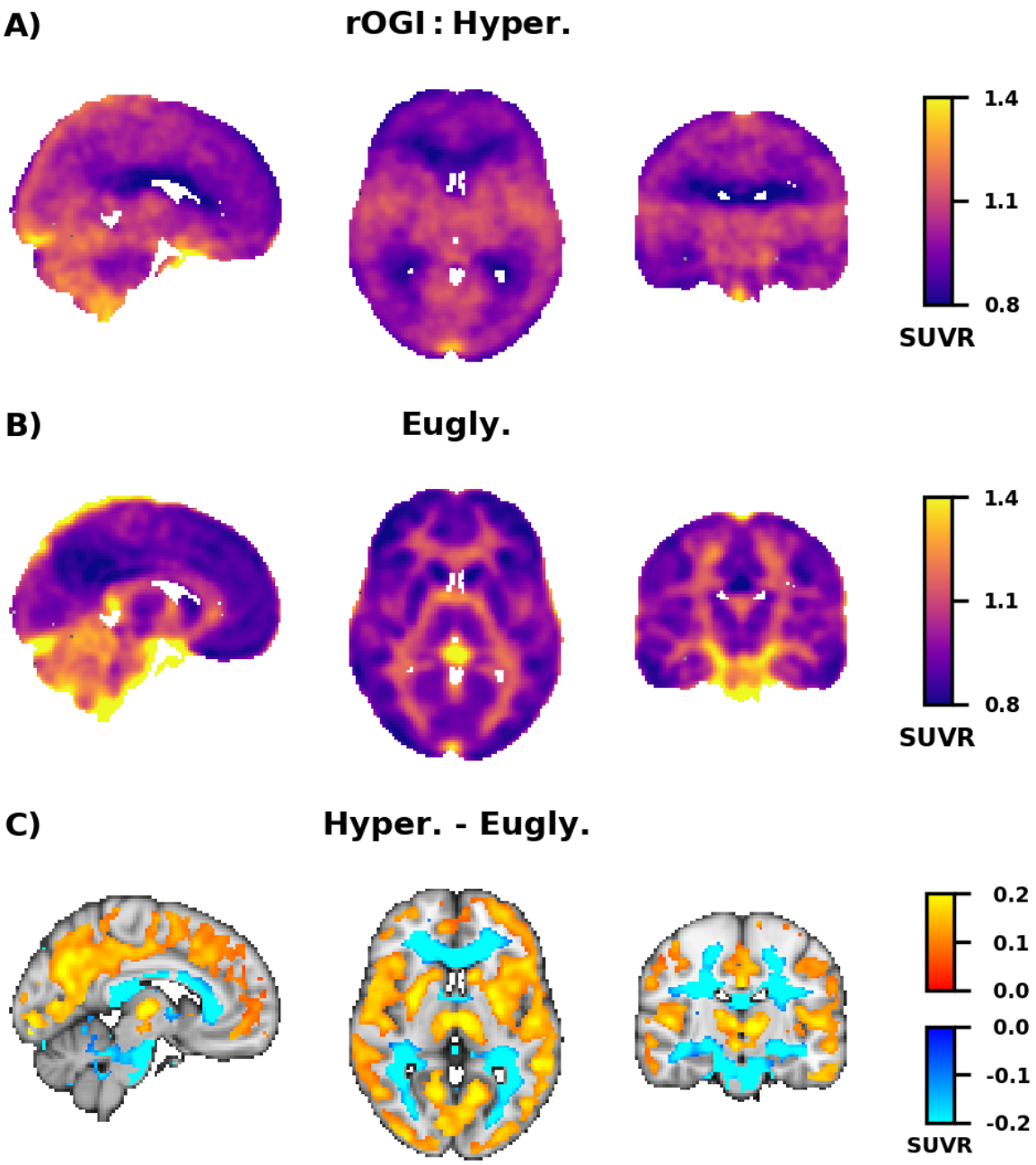

Figure 5.7: Hyperglycemia induced changes in relative oxygen-to-glucose (rOGI)

A) Group average images of rOGI during the euglycemic clamp (n=17) and **B)** hyperglycemic (n=14) clamp. rOGI was computed by taking the ratio of the [^{15}O]-O_2 SUVR and [^{18}F]-FDG SUVR images and then normalizing the result so that the whole-brain mean was equal to 1. **C)**

Group average difference in relative rOGI between the hyperglycemic and euglycemic clamp. Only voxels that are significantly different from zero after correction for multiple comparisons (FDR 0.05) are shown in color. rOGI in blue voxels decreased relative to the whole brain mean during hyperglycemia, whereas the rOGI orange/yellow voxels increased.

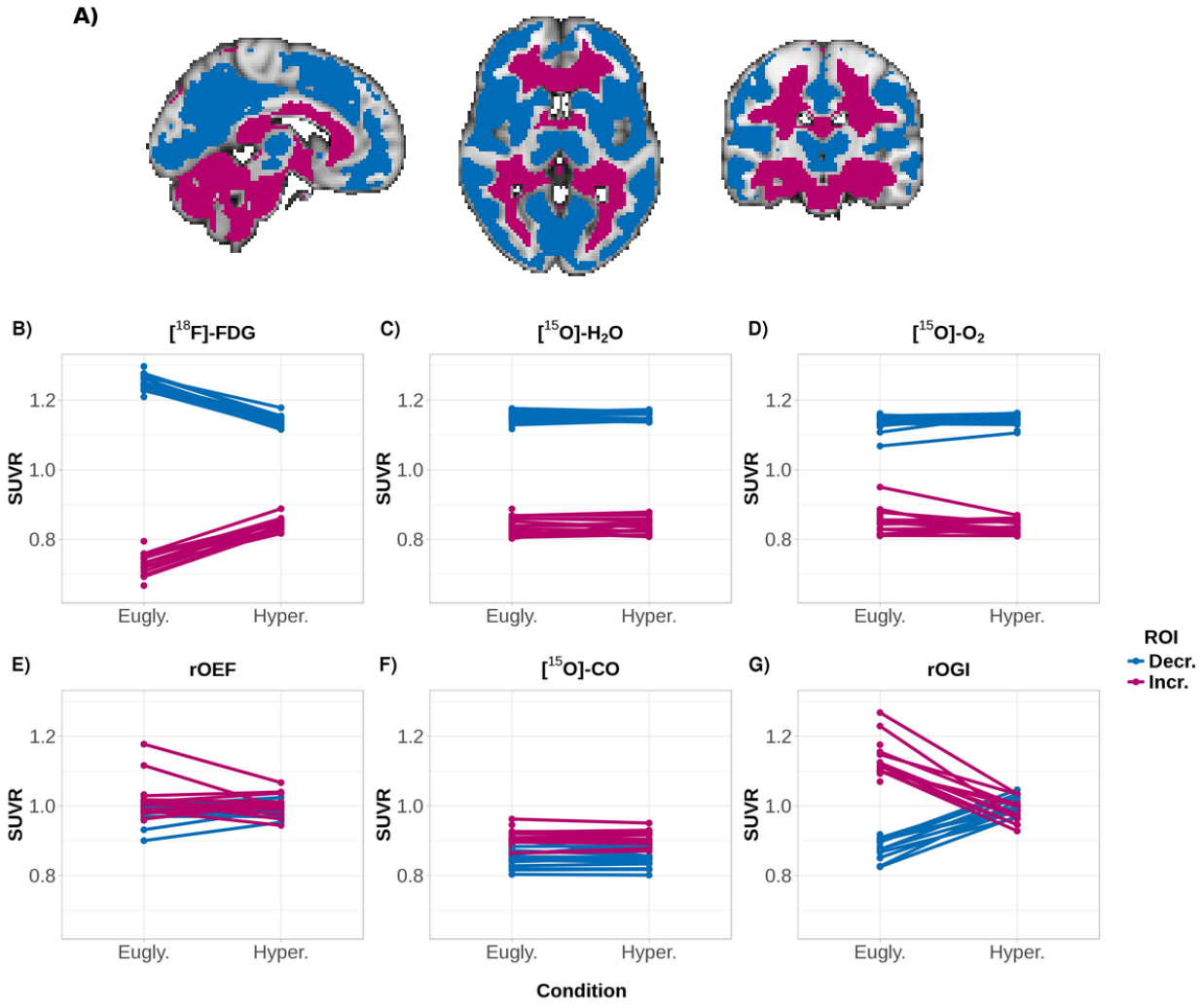

Figure 5.8: Hyperglycemia changes relative glucose consumption but not blood flow, blood volume, or oxygen metabolism

A) Regions-of-interest (ROIs) extracted from the voxelwise analysis of relative glucose consumption (Figure 5.2). The blue region is composed of voxels where relative [^{18}F]FDG SUVR decreased during hyperglycemia, and the red region is voxels were relative uptake increased. Subsequent figures show values within these ROIS for **B)** [^{18}F]-FDG SUVR (glucose consumption), **C)** [^{15}O]-H_2O SUVR (cerebral blood flow), **D)** [^{15}O]-O_2 SUVR (oxygen consumption), **E)** rOEF (ratio of [^{15}O]-O_2 and [^{15}O]-H_2O SUVR), **F)** [^{15}O]-CO SUVR (blood

volume), and **G)** rOGI (ratio of [^{15}O]-O_2 and [^{18}F]-FDG SUVR). Relative to the whole-brain, metabolic changes are only observed in glucose consumption and in rOGI. Significant ($p < 0.0001$) No changes were seen in blood flow, oxygen metabolism, or in blood volume.

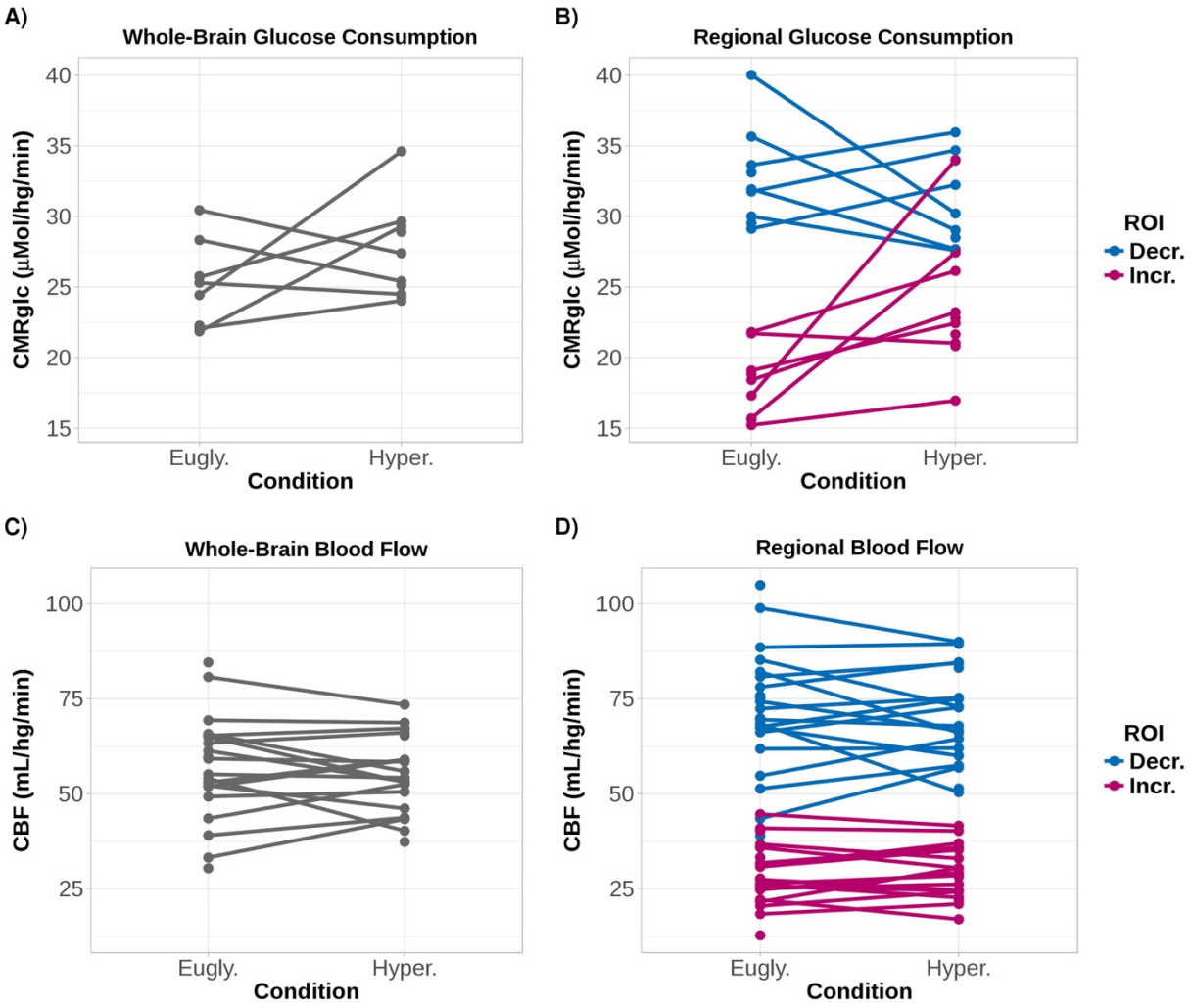

Figure 5.9: Quantitative glucose consumption and blood flow during hyperglycemia

A) Whole-brain average cerebral metabolic rate of glucose (CMRglc) during the euglycemic (25.1 ± 2.1 µMol·hg^{-1}·min^{-1}; n=9) and hyperglycemic (27.3 ± 2.0 µMol·hg^{-1}·min^{-1}; n=10) clamp conditions. The increase in CMRglc with hyperglycemia (2.18 ± 2.84 µMol·hg^{-1}·min^{-1}) did not reach significance (p = 0.151) . **B)** Regional CMRglc in the same regions as Figure 5.8A. A significant increase (p = 0.006*;* see Methods) was found with hyperglycemia in the ROI where relative glucose metabolism increased (red), but not (p = 0.207) in the ROI were relative glucose metabolism increased (blue). No significant difference in CBF (measured with ASL) were found

between euglycemia (n=22) and hyperglycemia (n=19) in either the **C)** whole-brain or **D)** the ROIs from Figure 5.8A ($p > 0.5$).

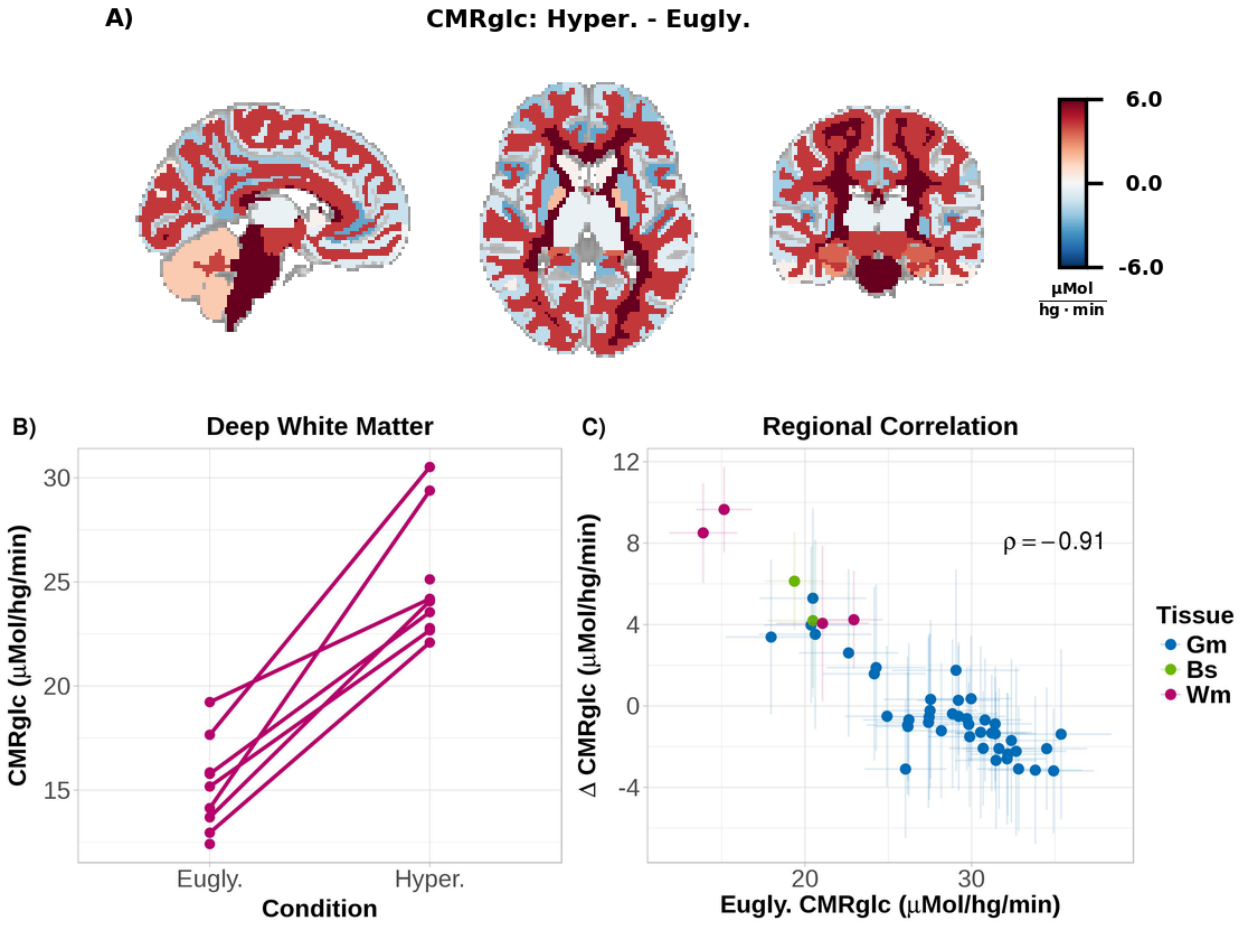

Figure 5.10: Quantitative increases in CMRglc in regions with low basal metabolic rates

A) Difference between hyperglycemia and euglycemia within 48 FreeSurfer derived ROIs (Figure 2.1). After correction for multiple comparisons using FDR, significant ($p < 0.05$) increases were found in the brain stem, cortical white matter, corpus callosum, and deep white matter. No significant decreases were found. **B)** CMRglc data from the deep white matter ROI, showing a robust increase in glucose consumption with hyperglycemia (9.65 ± 2.09 µMol·hg^{-1}·min^{-1}; $p < 0.0001$). **C)** Scatterplot of CMRglc during euglycemia vs. the difference between hyperglycemia and euglycemia. Each dot is the group estimate CMRglc within a single FreeSurfer region. Blue dots are gray matter, red dots are white matter, and green dots are the brain stem/ventral diencephalon. Lines are 95% confidence intervals. There is a strong

correlation between baseline CMRglc and hyperglycemia induced change, with the regions with the smallest baseline values showing the greatest change.

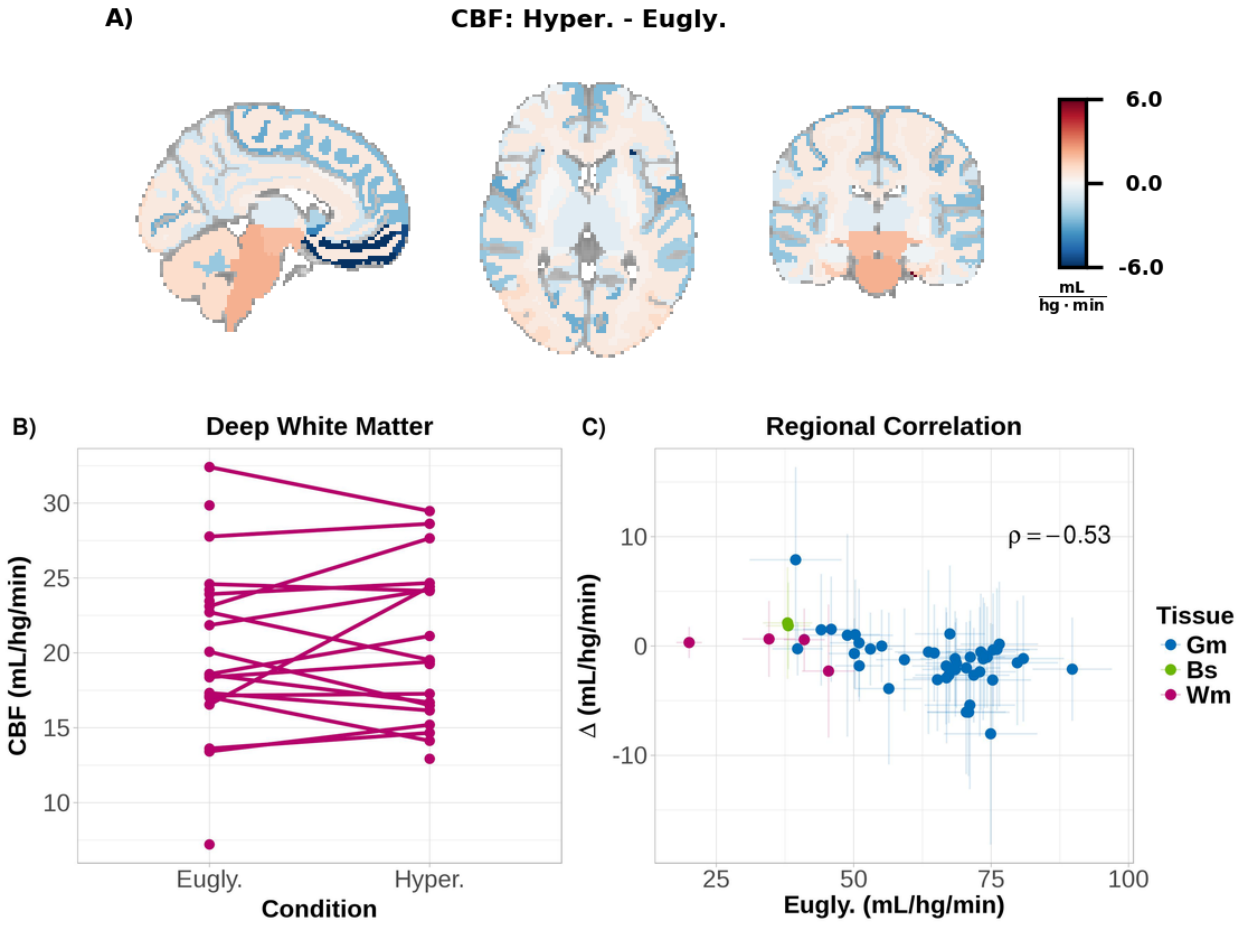

Figure 5.11: No regional changes in CBF during hyperglycemia

A) Difference in CBF between hyperglycemia and euglycemia within FreeSurfer ROIs. The change in CBF was not significant ($p > 0.05$) in any ROI after correction for multiple comparisons using FDR. **B)** Unlike CMRglc (Figure 5.10B), CBF does not increase in the deep white matter during hyperglycemia (0.32 ± 1.42 mL·hg^{-1}·min^{-1}; $p > 0.05$). **C)** Scatterplot of CBF during euglycemia vs. the difference between hyperglycemia and euglycemia. Only a moderate correlation exists between baseline CBF and the change in CBF induced by hyperglycemia. All other conventions as in Figure 5.10.

5.7 Tables

	[^{18}F]-FDG SUVR		[^{15}O]-H_2O SUVR		[^{15}O]-O_2 SUVR		rOEF SUVR		[^{15}O]-CO SUVR		rOGI SUVR		Quant. CMRglc		Quant. CBF	
ID	**Eugly.**	**Hyper.**	**Eugly.**	**Hyper.**	**Eugly.**	**Hyper.**	**Eugly.**	**Hyper.**	**Eugly.**	**Hyper.**	**Eugly.**	**Hyper.**	**Eugly.**	**Hyper.**	**Eugly.**	**Hyper.**
1	✓		✓		✓		✓		✓		✓					
2	✓	✓	✓	✓	✓	✓	✓	✓	✓	✓	✓	✓			✓	✓
3															✓	✓
4															✓	✓
5	✓		✓		✓		✓		✓		✓				✓	✓
6	✓		✓		✓		✓		✓		✓				✓	
7	✓	✓	✓	✓	✓	✓	✓	✓	✓	✓	✓	✓			✓	✓
8	✓	✓	✓	✓	✓	✓	✓	✓	✓	✓	✓	✓	✓	✓	✓	✓
9		✓	✓	✓	✓	✓	✓	✓	✓	✓		✓		✓	✓	✓
10	✓	✓	✓	✓	✓	✓	✓	✓	✓	✓	✓	✓	✓	✓	✓	✓
11	✓	✓	✓	✓	✓	✓	✓	✓	✓	✓	✓	✓	✓		✓	✓
12	✓		✓		✓		✓		✓		✓				✓	
13	✓	✓	✓	✓	✓	✓	✓	✓	✓	✓	✓	✓	✓	✓	✓	✓
14	✓	✓	✓	✓	✓	✓	✓	✓	✓	✓	✓	✓	✓	✓	✓	✓
15																
16	✓	✓	✓	✓	✓	✓	✓	✓	✓	✓	✓	✓	✓	✓	✓	✓
17	✓	✓	✓	✓	✓	✓	✓	✓	✓	✓	✓	✓	✓	✓	✓	✓
18	✓	✓	✓	✓	✓	✓	✓	✓	✓	✓	✓	✓	✓		✓	✓
19	✓	✓	✓	✓	✓	✓	✓	✓	✓	✓	✓	✓		✓	✓	✓
20		✓		✓		✓		✓		✓		✓		✓		✓
21	✓	✓	✓	✓	✓	✓	✓	✓	✓	✓	✓	✓	✓	✓	✓	✓
22															✓	
23																✓
24	✓		✓		✓		✓		✓		✓					

25															✓	
26	✓	✓	✓	✓											✓	✓
Totals	**18**	**15**	**19**	**15**	**18**	**14**	**18**	**14**	**18**	**14**	**17**	**14**	**9**	**10**	**21**	**19**

Table 5.1: Breakdown of participants with each imaging data-type

Table 5.2: Slope estimates from piecewise regression of plasma glucose and insulin time-courses

Values are means and symmetric 95% confidence intervals. All slopes are significantly different from zero at the 0.05 level without correction for multiple comparisons.

Time	Glucose ($mg \cdot dL^{-1} \cdot min^{-1}$)		Insulin ($pmol \cdot L^{-1} \cdot min^{-1}$)	
	Eugly.	**Hygly.**	**Eugly.**	**Hygly.**
Before breakpoint	0.099 ± 0.093	2.7 ± 0.094	0.47 ± 0.17	0.58 ± 0.18
After breakpoint	-0.077 ± 0.046	-0.23 ± 0.041	-0.22 ± 0.086	0.35 ± 0.077

Table 5.3: Whole-brain parameter estimates from the irreversible 2-compartment FDG model

For each parameter, a linear mixed model was used to estimate the population mean and 95% CI during both the euglycemic (n=9) and hyperglycemic (n=10) clamp. K_1 and k_3 were significantly decreased during hyperglycemia, whereas k_4 was significantly increased.

Parameter	Eugly.	Hygly.	Hygly. – Eugly.	*p*-value
K_1 ($mL \cdot hg^{-1} \cdot min^{-1}$)	11.17 ± 1.45	6.09 ± 1.37	-5.07 ± 1.82	**$3.0 \cdot 10^{-4}$**
k_2 (min^{-1})	0.28 ± 0.11	0.24 ± 0.10	-0.041 ± 0.15	$5.9 \cdot 10^{-1}$
k_3 (min^{-1})	0.14 ± 0.034	0.062 ± 0.032	-0.082 ± 0.047	**$3.3 \cdot 10^{-3}$**
k_4 (min^{-1})	0.0098 ± 0.0023	0.016 ± 0.0022	0.0070 ± 0.0031	**$7.6 \cdot 10^{-3}$**
V_b ($mL \cdot hg^{-1}$)	5.83 ± 1.27	5.25 ± 1.22	-0.57 ± 1.39	$4.6 \cdot 10^{-1}$

5.8 References

1 Gibbs EL, Lennox WG, Nims LF, Gibbs FA. Arterial and cerebral venous blood arterial-venous differences in man. *J Biol Chem* 1942; **144**: 325–332.

2 Mergenthaler P, Lindauer U, Dienel GA, Meisel A. Sugar for the brain: the role of glucose in physiological and pathological brain function. *Trends in Neurosciences* 2013; **36**: 587–597.

3 Lund-Andersen H. Transport of glucose from blood to brain. *Physiol Rev* 1979; **59**: 305–352.

4 Boyle PJ, Nagy RJ, O'Connor AM, Kempers SF, Yeo RA, Qualls C. Adaptation in brain glucose uptake following recurrent hypoglycemia. *Proc Natl Acad Sci USA* 1994; **91**: 9352–9356.

5 Lee JJ, Khoury N, Shackleford AM, Nelson S, Herrera H, Antenor-Dorsey JA *et al.* Dissociation Between Hormonal Counterregulatory Responses and Cerebral Glucose Metabolism During Hypoglycemia. *Diabetes* 2017; **66**: 2964–2972.

6 Phelps ME, Huang SC, Hoffman EJ, Selin C, Sokoloff L, Kuhl DE. Tomographic measurement of local cerebral glucose metabolic rate in humans with (F-18)2-fluoro-2-deoxy-D-glucose: validation of method. *Annals of Neurology* 1979; **6**: 371–388.

7 Kawasaki K, Ishii K, Saito Y, Oda K, Kimura Y, Ishiwata K. Influence of mild hyperglycemia on cerebral FDG distribution patterns calculated by statistical parametric mapping. *Ann Nucl Med* 2008; **22**: 191–200.

8 Ishibashi K, Kawasaki K, Ishiwata K, Ishii K. Reduced uptake of 18F-FDG and 15O-H2O in Alzheimer's disease-related regions after glucose loading. *J Cereb Blood Flow Metab* 2015; **35**: 1380–1385.

9 Ishibashi K, Onishi A, Fujiwara Y, Ishiwata K, Ishii K. Relationship between Alzheimer disease-like pattern of 18F-FDG and fasting plasma glucose levels in cognitively normal volunteers. *J Nucl Med* 2015; **56**: 229–233.

10 Ishibashi K, Wagatsuma K, Ishiwata K, Ishii K. Alteration of the regional cerebral glucose metabolism in healthy subjects by glucose loading. *Hum Brain Mapp* 2016; **37**: 2823–2832.

11 Ishibashi K, Onishi A, Fujiwara Y, Ishiwata K, Ishii K. Effects of glucose, insulin, and insulin resistance on cerebral 18F-FDG distribution in cognitively normal older subjects. *PLoS ONE* 2017; **12**: e0181400.

12 Apostolova I, Lange C, Suppa P, Spies L, Klutmann S, Adam G *et al.* Impact of plasma glucose level on the pattern of brain FDG uptake and the predictive power of FDG PET in mild cognitive impairment. *Eur J Nucl Med Mol Imaging* 2018; **45**: 1417–1422.

13 Rowe GG, Maxwell GM, Castillo CA, Freeman DJ, Crumpton CW. A study in man of cerebral blood flow and cerebral glucose, lactate and pyruvate metabolism before and after eating. *J Clin Investig* 1959; **38**: 2154–2158.

14 Gottstein U, Held K, Sebening H, Walpurger G. Der Glucoseverbrauch des menschlichen Gehirns unter dem Einfluß intravenöser Infusionen von Glucose, Glucagon und Glucose-Insulin. *Klin Wochenschr* 1965; **43**: 965–975.

15 Blomqvist G, Grill V, Ingvar M, Widén L, Stone-Elander S. The effect of hyperglycaemia on regional cerebral glucose oxidation in humans studied with [1-11C]-D-glucose. *Acta Physiol Scand* 1998; **163**: 403–415.

16 Hasselbalch SG, Knudsen GM, Capaldo B, Postiglione A, Paulson OB. Blood-brain barrier transport and brain metabolism of glucose during acute hyperglycemia in humans. *J Clin Endocrinol Metab* 2001; **86**: 1986–1990.

17 Orzi F, Lucignani G, Dow-Edwards D, Namba H, Nehlig A, Patlak CS *et al.* Local cerebral glucose utilization in controlled graded levels of hyperglycemia in the conscious rat. *J Cereb Blood Flow Metab* 1988; **8**: 346–356.

18 Duckrow RB, Bryan RM. Regional cerebral glucose utilization during hyperglycemia. *J Neurochem* 1987; **48**: 989–993.

19 Blomqvist G. Effect of hyperglycemia on rCMRglc in rats. *J Cereb Blood Flow Metab* 1995; **15**: 349–351.

20 Duckrow RB. Regional cerebral blood flow decreases during hyperglycemia. *Annals of Neurology* 1985; **17**: 267–272.

21 Duckrow RB, Beard DC, Brennan RW. Regional cerebral blood flow decreases during chronic and acute hyperglycemia. *Stroke* 1987; **18**: 52–58.

22 Xu F, Liu P, Pascual JM, Xiao G, Huang H, Lu H. Acute effect of glucose on cerebral blood flow, blood oxygenation, and oxidative metabolism. *Hum Brain Mapp* 2015; **36**: 707–716.

23 Page KA, Chan O, Arora J, Belfort-DeAguiar R, Dzuira J, Roehmholdt B *et al.* Effects of fructose vs glucose on regional cerebral blood flow in brain regions involved with appetite and reward pathways. *JAMA* 2013; **309**: 63–70.

24 Fox PT, Raichle ME, Mintun MA, Dence C. Nonoxidative glucose consumption during focal physiologic neural activity. *Science* 1988; **241**: 462–464.

25 Goyal MS, Hawrylycz M, Miller JA, Snyder AZ, Raichle ME. Aerobic glycolysis in the human brain is associated with development and neotenous gene expression. *Cell Metab* 2014; **19**: 49–57.

26 Goyal MS, Vlassenko AG, Blazey TM, Su Y, Couture LE, Durbin TJ *et al.* Loss of Brain Aerobic Glycolysis in Normal Human Aging. *Cell Metab* 2017; **26**: 353–360.e3.

27 Siesjö BK. *Brain energy metabolism*. John Wiley & Sons, 1978.

28 Krentz AJ, Boyle PJ, Macdonald LM, Schade DS. Octreotide: a long-acting inhibitor of endogenous hormone secretion for human metabolic investigations. *Metab Clin Exp* 1994; **43**: 24–31.

29 DeFronzo RA, Felig P, Ferrannini E, Wahren J. Effect of graded doses of insulin on splanchnic and peripheral potassium metabolism in man. *Am J Physiol* 1980; **238**: E421–7.

30 Kamel E, Hany TF, Burger C, Treyer V, Lonn AHR, Schulthess von GK *et al.* CT vs 68Ge attenuation correction in a combined PET/CT system: evaluation of the effect of lowering the CT tube current. *Eur J Nucl Med Mol Imaging* 2002; **29**: 346–350.

31 Su Y, Su Y, Rubin BB, Rubin BB, McConathy J, McConathy J *et al.* Impact of MR-Based Attenuation Correction on Neurologic PET Studies. *J Nucl Med* 2016; **57**: 913–917.

32 Fischl B. FreeSurfer. *Neuroimage* 2012; **62**: 774–781.

33 Desikan RS, Ségonne F, Fischl B, Quinn BT, Dickerson BC, Blacker D *et al.* An automated labeling system for subdividing the human cerebral cortex on MRI scans into gyral based regions of interest. *Neuroimage* 2006; **31**: 968–980.

34 Fischl B, Salat DH, Busa E, Albert M, Dieterich M, Haselgrove C *et al.* Whole brain segmentation: automated labeling of neuroanatomical structures in the human brain. *Neuron* 2002; **33**: 341–355.

35 Jenkinson M, Smith S. A global optimisation method for robust affine registration of brain images. *Med Image Anal* 2001; **5**: 143–156.

36 Jenkinson M, Beckmann CF, Behrens TEJ, Woolrich MW, Smith SM. FSL. *Neuroimage* 2012; **62**: 782–790.

37 Hacker CD, Laumann TO, Szrama NP, Baldassarre A, Snyder AZ, Leuthardt EC *et al.* Resting state network estimation in individual subjects. *Neuroimage* 2013; **82**: 616–633.

38 Jenkinson M, Bannister P, Brady M, Smith S. Improved optimization for the robust and accurate linear registration and motion correction of brain images. *Neuroimage* 2002; **17**: 825–841.

39 Wang Z, Aguirre GK, Rao H, Wang J, Fernández-Seara MA, Childress AR *et al.* Empirical optimization of ASL data analysis using an ASL data processing toolbox: ASLtbx. *Magn Reson Imaging* 2008; **26**: 261–269.

40 Aguirre GK, Detre JA, Zarahn E, Alsop DC. Experimental design and the relative sensitivity of BOLD and perfusion fMRI. *Neuroimage* 2002; **15**: 488–500.

41 Buxton RB, Frank LR, Wong EC, Siewert B, Warach S, Edelman RR. A general kinetic model for quantitative perfusion imaging with arterial spin labeling. *Magn Reson Med* 1998; **40**: 383–396.

42 Alsop DC, Detre JA, Golay X, Günther M, Hendrikse J, Hernandez-Garcia L *et al.* Recommended implementation of arterial spin-labeled perfusion MRI for clinical applications: A consensus of the ISMRM perfusion study group and the European consortium for ASL in dementia. *Magn Reson Med* 2015; **73**: 102–116.

43 Tanenbaum AB, Snyder AZ, Brier MR, Ances BM. A method for reducing the effects of motion contamination in arterial spin labeling magnetic resonance imaging. *J Cereb Blood Flow Metab* 2015; **35**: 1697–1702.

44 Comtat, Bataille F, Michel C, Jones JP, Sibomana M, Janeiro L *et al.* OSEM-3D Reconstruction Strategies for the ECAT HRRT. *IEEE Symposium Conference Record Nuclear Science 2004*; **6**: 3492–3496.

45 Eisenstein SA, Koller JM, Piccirillo M, Kim A, Antenor-Dorsey JAV, Videen TO *et al.* Characterization of extrastriatal D2 in vivo specific binding of [^{18}F](N-methyl)benperidol using PET. *Synapse* 2012; **66**: 770–780.

46 Snyder AZ. Difference image vs. ratio image error function forms in PET-PET realignment. In: Myers R, Cunningham V, Bailey D, Jones T (eds). *Quantification of Brain Function Using PET*. San Diego, California, 1996, pp 131–137.

47 Rowland DJ, Garbow JR, Laforest R, Snyder AZ. Registration of [18F]FDG microPET and small-animal MRI. *Nuclear Medicine and Biology* 2005; **32**: 567–572.

48 Vaishnavi SN, Vlassenko AG, Rundle MM, Snyder AZ, Mintun MA, Raichle ME. Regional aerobic glycolysis in the human brain. *Proc Natl Acad Sci USA* 2010; **107**: 17757–17762.

49 Van den Hoff J, Burchert W, Muller-Schauenburg W, Meyer GJ, Hundeshagen H. Accurate local blood flow measurements with dynamic PET: fast determination of input function delay and dispersion by multilinear minimization. *J Nucl Med* 1993; **34**: 1770–1777.

50 Byrd RH, Lu P, Nocedal J, Zhu C. A limited memory algorithm for bound constrained optimization. *SIAM Journal on Scientific Computing* 1995; **16**: 1190–1208.

51 Jones E, Oliphant T, Peterson P, others. SciPy: Open Source Scientific Tools for Python. 2001.

52 Wu H-M, Bergsneider M, Glenn TC, Yeh E, Hovda DA, Phelps ME *et al.* Measurement of the global lumped constant for 2-deoxy-2-[18F]fluoro-D-glucose in normal human

brain using [15O]water and 2-deoxy-2-[18F]fluoro-D-glucose positron emission tomography imaging. A method with validation based on multiple methodologies. *Mol Imaging Biol* 2003; **5**: 32–41.

53 R Core Team. R: A Language and Environment for Statistical Computing. https://www.R-project.org/.

54 Pinheiro J, Bates D, DebRoy S, Sarkar D, R Core Team. nlme: Linear and Nonlinear Mixed Effects Models. http://CRAN.R-project.org/package=nlme.

55 Bates D, Mächler M, Bolker B, Walker S. Fitting Linear Mixed-Effects Models Using lme4. *J Stat Soft* 2015; **67**: 1–48.

56 Kuznetsova A, Brockhoff PB, Christensen RHB. lmerTest Package: Tests in Linear Mixed Effects Models. *J Stat Soft* 2017; **82**: 1–27.

57 Benjamini Y, Hochberg Y. Controlling the false discovery rate: a practical and powerful approach to multiple testing. *J R Stat Soc Series B Stat Methodol* 1995; **57**: 289–300.

58 Impact of plasma glucose level on the pattern of brain FDG uptake and the predictive power of FDG PET in mild cognitive impairment. *Eur J Nucl Med Mol Imaging* 2018; **45**: 1417–1422.

59 Arnold SE, Arvanitakis Z, Macauley-Rambach SL, Koenig AM, Wang H-Y, Ahima RS *et al.* Brain insulin resistance in type 2 diabetes and Alzheimer disease: concepts and conundrums. *Nat Rev Neurol* 2018; **14**: 168–181.

60 Bingham EM, Hopkins D, Smith D, Pernet A, Hallett W, Reed L *et al.* The role of insulin in human brain glucose metabolism: an 18fluoro-deoxyglucose positron emission tomography study. *Diabetes* 2002; **51**: 3384–3390.

61 Blomqvist G, Stone-Elander S, Halldin C, Roland PE, Widén L, Lindqvist M *et al.* Positron emission tomographic measurements of cerebral glucose utilization using [1-11C]D-glucose. *J Cereb Blood Flow Metab* 1990; **10**: 467–483.

62 Yu Y, Herman P, Rothman DL, Agarwal D, Hyder F. Evaluating the gray and white matter energy budgets of human brain function. *J Cereb Blood Flow Metab* 2018; **38**: 1339–1353.

63 Magistretti PJ, Allaman I. A cellular perspective on brain energy metabolism and functional imaging. *Neuron* 2015; **86**: 883–901.

64 Dienel GA. Brain Glucose Metabolism: Integration of Energetics with Function. *Physiol Rev* 2019; **99**: 949–1045.

65 Takahashi S, Izawa Y, Suzuki N. Astroglial pentose phosphate pathway rates in response to high-glucose environments. *ASN Neuro* 2012; **4**. doi:10.1042/AN20120002.

66 Macauley SL, Stanley M, Caesar EE, Yamada SA, Raichle ME, Perez R *et al.* Hyperglycemia modulates extracellular amyloid-β concentrations and neuronal activity in vivo. *J Clin Invest* 2015; **125**: 2463–2467.

67 Ball KK, Cruz NF, Mrak RE, Dienel GA. Trafficking of glucose, lactate, and amyloid-beta from the inferior colliculus through perivascular routes. *J Cereb Blood Flow Metab* 2010; **30**: 162–176.

68 Lundgaard I, Lu ML, Yang E, Peng W, Mestre H, Hitomi E *et al.* Glymphatic clearance controls state-dependent changes in brain lactate concentration. *J Cereb Blood Flow Metab* 2017; **37**: 2112–2124.

69 Rinholm JE, Bergersen LH. White matter lactate--does it matter? *Neuroscience* 2014; **276**: 109–116.

70 Rinholm JE, Hamilton NB, Kessaris N, Richardson WD, Bergersen LH, Attwell D. Regulation of oligodendrocyte development and myelination by glucose and lactate. *J Neurosci* 2011; **31**: 538–548.

71 Fünfschilling U, Supplie LM, Mahad D, Boretius S, Saab AS, Edgar J *et al.* Glycolytic oligodendrocytes maintain myelin and long-term axonal integrity. *Nature* 2012; **485**: 517–521.

72 Lee Y, Morrison BM, Li Y, Lengacher S, Farah MH, Hoffman PN *et al.* Oligodendroglia metabolically support axons and contribute to neurodegeneration. *Nature* 2012; **487**: 443–448.

73 Dienel GA, Cruz NF, Sokoloff L. Metabolites of 2-deoxy-[14C]glucose in plasma and brain: influence on rate of glucose utilization determined with deoxyglucose method in rat brain. *J Cereb Blood Flow Metab* 1993; **13**: 315–327.

74 Cheng HM, González RG. The effect of high glucose and oxidative stress on lens metabolism, aldose reductase, and senile cataractogenesis. *Metab Clin Exp* 1986; **35**: 10–14.

75 Kwee IL, Igarashi H, Nakada T. Aldose reductase and sorbitol dehydrogenase activities in diabetic brain: in vivo kinetic studies using 19F 3-FDG NMR in rats. *Neuroreport* 1996; **7**: 726–728.

76 Gabbay KH. The sorbitol pathway and the complications of diabetes. *N Engl J Med* 1973; **288**: 831–836.

77 Chung SSM, Ho ECM, Lam KSL, Chung SK. Contribution of polyol pathway to diabetes-induced oxidative stress. *Journal of the American Society of Nephrology* 2003; **14**: S233–6.

78 Tang WH, Martin KA, Hwa J. Aldose reductase, oxidative stress, and diabetic mellitus. *Front Pharmacol* 2012; **3**: 87.

79 Hwang JJ, Jiang L, Hamza M, Sanchez Rangel E, Dai F, Belfort-DeAguiar R *et al.* Blunted rise in brain glucose levels during hyperglycemia in adults with obesity and T2DM. *JCI Insight* 2017; **2**. doi:10.1172/jci.insight.95913.

80 Vlassenko AG, Raichle ME. Brain aerobic glycolysis functions and Alzheimer's disease. *Clinical and Translational Imaging* 2015; **3**: 27–37.

81 Blazey TM, Snyder AZ, Su Y, Goyal MS, Lee JJ, Vlassenko AG *et al.* Quantitative positron emission tomography reveals regional differences in aerobic glycolysis within the human brain. *J Cereb Blood Flow Metab* 2018; **144**: 271678X18767005.

82 Vlassenko AG, Vaishnavi SN, Couture L, Sacco D, Shannon BJ, Mach RH *et al.* Spatial correlation between brain aerobic glycolysis and amyloid-β (Aβ) deposition. *Proc Natl Acad Sci USA* 2010; **107**: 17763–17767.

83 Bero AW, Yan P, Roh JH, Cirrito JR, Stewart FR, Raichle ME *et al.* Neuronal activity regulates the regional vulnerability to amyloid-β deposition. *Nat Neurosci* 2011; **14**: 750–756.

84 Vlassenko AG, Gordon BA, Goyal MS, Su Y, Blazey TM, Durbin TJ *et al.* Aerobic glycolysis and tau deposition in preclinical Alzheimer's disease. *Neurobiol Aging* 2018; **67**: 95–98.

85 Shannon BJ, Vaishnavi SN, Vlassenko AG, Shimony JS, Rutlin J, Raichle ME. Brain aerobic glycolysis and motor adaptation learning. *Proc Natl Acad Sci USA* 2016; **113**: E3782–91.

86 Prediabetes Is Associated With Structural Brain Abnormalities: The Maastricht Study. *Diabetes Care* 2018; **41**: 2535–2543.

87 Cheng G, Huang C, Deng H, Wang H. Diabetes as a risk factor for dementia and mild cognitive impairment: a meta-analysis of longitudinal studies. *Intern Med J* 2012; **42**: 484–491.

88 Arndt S, Cizadlo T, O'Leary D, Gold S, Andreasen NC. Normalizing counts and cerebral blood flow intensity in functional imaging studies of the human brain. *Neuroimage* 1996; **3**: 175–184.

89 Borghammer P, Aanerud J, Gjedde A. Data-driven intensity normalization of PET group comparison studies is superior to global mean normalization. *Neuroimage* 2009; **46**: 981–988.

90 Sokoloff L, Reivich M, Kennedy C, Rosiers Des MH, Patlak CS, Pettigrew KD *et al.* The [14C]Deoxyglucose Method for the Measurement of Local Cerebral Glucose Utilization: Theory, Procedure, and Normal Values in the Conscious and Anesthetized Albino Rat. *J Neurochem* 1977; **28**: 897–916.

91 Schuier F, Orzi F, Suda S, Lucignani G, Kennedy C, Sokoloff L. Influence of plasma glucose concentration on lumped constant of the deoxyglucose method: effects of hyperglycemia in the rat. *J Cereb Blood Flow Metab* 1990; **10**: 765–773.

92 van Golen LW, IJzerman RG, Hoetjes NJ, Schwarte LA, Diamant M. Cerebral blood flow and glucose metabolism measured with positron emission tomography are decreased in human type 1 diabetes. *Diabetes* 2013; **62**: 2898–2904.

93 Hasselbalch SG, Madsen PL, Knudsen GM, Holm S, Paulson OB. Calculation of the FDG lumped constant by simultaneous measurements of global glucose and FDG metabolism in humans. *J Cereb Blood Flow Metab* 1998; **18**: 154–160.

94 Graham MM, Muzi M, Spence AM, O'Sullivan F, Lewellen TK, Link JM *et al.* The FDG lumped constant in normal human brain. *J Nucl Med* 2002; **43**: 1157–1166.

95 Kuwabara H, Evans AC, Gjedde A. Michaelis-Menten constraints improved cerebral glucose metabolism and regional lumped constant measurements with [18F]fluorodeoxyglucose. *J Cereb Blood Flow Metab* 1990; **10**: 180–189.

96 Hasselbalch SG, Knudsen GM, Holm S, Hageman LP, Capaldo B, Paulson OB. Transport of D-glucose and 2-fluorodeoxyglucose across the blood-brain barrier in humans. *J Cereb Blood Flow Metab* 1996; **16**: 659–666.

97 Martel G, Dutar P, Epelbaum J, Viollet C. Somatostatinergic systems: an update on brain functions in normal and pathological aging. *Front Endocrinol (Lausanne)* 2012; **3**: 154.

98 Banks WA, Schally AV, Barrera CM, Fasold MB, Durham DA, Csernus VJ *et al.* Permeability of the murine blood-brain barrier to some octapeptide analogs of somatostatin. *Proc Natl Acad Sci USA* 1990; **87**: 6762–6766.

99 Hollenbeck C, Reaven GM. Variations in insulin-stimulated glucose uptake in healthy individuals with normal glucose tolerance. *J Clin Endocrinol Metab* 1987; **64**: 1169–1173.

100 Jenkins DJ, Leeds AR, Gassull MA, Cochet B, Alberti GM. Decrease in postprandial insulin and glucose concentrations by guar and pectin. *Ann Intern Med* 1977; **86**: 20–23.

Chapter 6: Summary and Conclusions

6.1 Summary

The goal of this thesis was to explore the relationship between cerebral blood flow (CBF), the cerebral metabolic rate of glucose consumption (CMRglc), and the cerebral metabolic rate of oxygen consumption ($CMRO_2$). In particular, I wanted to investigate the role of non-oxidative glucose consumption (NOglc) in the brain. To explore these issues, I performed the analyses that make up Chapters 2-5. Roughly speaking, these chapters can be divided into two parts. The focus of the first part, which consists of Chapters 2 and 3, is quantifying how much of the brain's glucose consumption is metabolized via non-oxidative pathways. The aim of the second part of the thesis is to determine if CBF, CMRglc, and $CMRO_2$ all are affected equally by hypoglycemia (Chapter 4) and hyperglycemia (Chapter 5).

There are three primary findings in Chapters 2 and 3. First, when considering the brain as a whole, NOglc accounts for approximately 9% of resting CMRglc. This shows that a substantial portion of the brain's glucose consumption does not undergo complete oxidative phosphorylation. Second, nearly 7% of resting whole-brain CMRglc is consumed via non-oxidative pathways that do not end in lactate transport to the venous blood. It is therefore likely that a portion of the brain's glucose consumption is directed to other pathways, including the synthesis of nucleic and amino acids. Third, the proportion of NOglc varies throughout the brain. In the precuneus and prefrontal cortex, regions that are part of the default mode network, NOglc accounts for nearly 20% of resting CMRglc. Conversely, there does not appear to be any NOglc in the cerebellum at rest.

In Chapter 4, I found a dissociation between regional changes in CBF and CMRglc during moderate hypoglycemia. Specifically, I found that hypoglycemia increases CBF in the globus pallidus and decreases CBF in the nucleus accumbens and a handful of cortical regions. In the majority of regions, however, CBF was not affected by hypoglycemia. Conversely, I found that hypoglycemia significantly decreases CMRglc in every region of the brain. Moreover, regional changes in CMRglc were highly correlated with baseline CMRglc and not changes in CBF, generally increase during hypoglycemia in order to maintain delivery of glucose. The most likely explanation of increased CBF in the thalamus, globus pallidus, brainstem, and ventral diencephalon is to promote arousal and behavioral food-seeking behaviors.

I reported in Chapter 5 that hyperglycemia produces a shift in the topography of cerebral glucose metabolism. Glucose consumption in regions with high baseline metabolic rates, such as the visual cortex, decreased relative to the rest of the brain, whereas regions with low baseline metabolic rates (e.g., white matter) increased. The major effect of hyperglycemia is a significant quantitative increase in CMRglc in cerebral white matter and brain stem. Interestingly, no changes in quantitative CBF or relative blood flow, blood volume, oxygen metabolism, or oxygen extraction were found in any brain region. Taken together, these findings suggest NOglc is elevated in the white matter and brain stem during hyperglycemia.

6.2 Significance and Future Directions

In Chapter 1, I reviewed the fairly large literature examining the relationship between cerebral metabolism and functional activity, with a particular emphasis on examples of uncoupling between CBF, CMRglc, and $CMRO_2$. This literature has conclusively shown that, although focal elevations in neural activity substantially increase CBF and CMRglc, $CMRO_2$

changes only modestly. As a result, enhanced neural activity results in a temporary increase in NOglc. The uncoupling between CBF, CMRglc, and $CMRO_2$ in responses to task paradigms is responsible for the blood oxygen dependent (BOLD) signals underlying fMRI.

Although metabolic uncoupling now is well established, there are still several outstanding questions surrounding it. The rest of this chapter will focus on three of the more prominent areas of research.

Non-oxidative glucose consumption during neural activity

One of the most important remaining questions is why task-evoked activity focally increases NOglc. In Chapter 1, I discussed several possibilities including a modified astrocyte-neuron lactate shuttle, glycogen or glutamate synthesis, lactate production, or biosynthesis of amino acids and proteins. None of the analyses included in this thesis favor any of these possibilities, as all of the data were collected in resting conditions. As I argued in Chapter 1, a complete account of NOglc during responses to task paradigms likely will need to examine several different mechanisms that operate in both neurons and glia. Furthermore, recent studies implicating the role of lactate as a signaling molecule[1,2], suggest that the role of NOglc extends beyond energy metabolism. Therefore, to further our understanding of task-related changes in NOglc, we need quantitative studies that track the creation and movement of glucose intermediates between cell types *in vivo.* Without direct evidence indicating which non-oxidative pathways are active, the reason why task performance elevates NOglc will remain unclear.

Non-oxidative glucose consumption at rest

The role of NOglc at rest has been examined to a far lesser extent than it has been during periods of increased neural activity. In Chapter 2, I reported that NOglc accounts for nearly 10%

of the brain's resting glucose consumption, replicating previous findings[3]. Although most investigators acknowledge that NOglc accounts for a portion of resting CMRglc, it is sometimes asserted that this a fairly small amount that can be safely ignored as it is due entirely to excess lactate production[4,5]. Much less common are reports that actively consider the possibility that NOglc plays a role in resting brain metabolism and function. The results presented in this thesis favor the possibility that NOglc plays an important role in the brain at rest. I found that a substantial portion of the brain's resting NOglc cannot be accounted for by lactate efflux to the venous blood. Therefore, other mechanisms must be invoked to explain why the brain is consuming glucose without complete oxidative phosphorylation.

One way to assess what role NOglc has in the resting brain is to correlate the spatial topography of NOglc with the topographies of other biological markers. A previous study from our group found a positive correlation between regional NOglc and the expression of genes related to synaptic plasticity and development[6]. This finding suggests that NOglc could be used to generate the biosynthetic intermediates necessary for synaptic plasticity. Consistent with this idea, other work from both our group[7] and others[8] has shown that NOglc is elevated hours after the performance of a learning task.

In Chapter 3, I directly quantified NOglc in several regions of the brain at rest. In regions such as the precuneus, lateral parietal cortex, and medial prefrontal cortex, NOglc accounts for as much as 20% of resting CMRglc. Conversely, there does not appear to be any NOglc in the cerebellar gray matter. Therefore, if NOglc plays a role in synaptic plasticity, its importance may vary by region. The cerebellum is of particular interest in this regard, as it has little to no NOglc despite being a classical example of plasticity in certain types of motor learning[9,10].

Given the limitations of human studies, none of the work I have presented here directly tests which cellular mechanisms underlie resting NOglc. It is likely, however, that the same mechanisms that are behind NOglc in responses to task paradigms also operate in the resting brain. Although the use of task paradigms in functional neuroimaging studies has encouraged the belief that task and rest are fundamentally different states, this is an oversimplification. Indeed, the brain is highly active even when it is not performing any overt task[11], and only a small fraction of the brain's energy is devoted to responding to external stimuli[12]. Therefore, it is parsimonious to hypothesize that the same mechanisms that are responsible for NOglc during task responses also operate at rest.

Metabolic uncoupling and altered states

As was discussed in Chapter 1, metabolic derangements often result in uncoupling between CBF, CMRglc, and $CMRO_2$. A classic example is profound hypoglycemia, which decreases global CMRglc to a much greater extent than CBF or $CMRO_2$[13]. In Chapter 4, I expanded upon this literature by examining regional CBF and CMRglc during moderate hypoglycemia. I found that, although hypoglycemia decreased CMRglc in every brain region, it decreased CBF in only a handful of regions. Interestingly, the only region where hyperglycemia increased CBF was the globus pallidus. This is in contrast to the animal literature, which has consistently reported that hypoglycemia increases global[14] and regional[15] CBF. An increase in CBF during hypoglycemia would suggest than blood flow is upregulated during hypoglycemia to increase the amount of glucose that is delivered to the brain. However, the data presented in Chapter 3 would suggest that this is not the case in humans, at least during moderate hypoglycemia.

An alternative possibility is that CBF changes during hypoglycemia are part of the brain's counterregulatory response to changes in blood glucose concentration. The release of insulin during hypoglycemia is typically followed by the release of several counterregulatory hormones, including of glucagon, epinephrine, growth hormone, and cortisol[16]. Studies examining changes in blood flow in humans have typically reported focal increases in the globus pallidus, thalamus, and medial prefrontal cortex[17-19]. Interestingly, although the hormonal response to hypoglycemia is diminished after multiple hypoglycemic episodes, the increase in CBF in the thalamus is amplified[20]. These findings have led to the hypothesis that focally increased thalamic CBF during hypoglycemia is a marker of hypothalamic inhibition[20,21]. With repeated episodes of hypoglycemia, the amount of inhibition is increased, resulting in a diminished sympathetic response[20].

However, the results shown in Chapter 4 are not entirely consistent with this hypothesis. Although hypoglycemia did increase CBF in the thalamus, the increase was not statistically significant, possibly owing to the global noise inherent in absolute quantification of CBF. CBF in the thalamus was significantly elevated from euglycemia when expressed relative to whole-brain CBF. In any case, more work is needed to establish why CBF changes during hypoglycemia. It would also be particularly interesting to measure regional oxygen consumption during hypoglycemia. As mentioned earlier, profound hypoglycemia produces little change in global $CMRO_2$[13]. If this is true during moderate hypoglycemia, it would suggest than most of the decrease in CMRglc I reported in Chapter 4 was due to a decrease in NOglc. This could have important implications especially if, as mentioned above, NOglc is involved in plasticity and learning.

In Chapter 5, I found that metabolic uncoupling is increased during acute hyperglycemia, as in hypoglycemia. Specifically, hyperglycemia altered the topography of cerebral glucose consumption, whereas the topographies of blood flow and oxygen consumption were unchanged. The change in the regional distribution of glucose consumption was due to a selective quantitative increase in CMRglc within the white matter and brain stem. Taken together, these findings suggest that, during hyperglycemia, NOglc is selectively increased in the white matter and brainstem. It is worthwhile noting that Type-2 diabetes mellitus (T2DM), which leads to chronic hyperglycemia, is associated with white matter disease[22]. Speculatively, it is possible that chronically elevated NOglc in white matter is a risk factor for the development of white matter disease in individuals with T2DM. In support of this possibility, increased concentration of sorbitol, a sugar alcohol produced from glucose via non-oxidative pathways, has been implicated in the development of diabetic retinotopy and neuropathy[23]. Therefore, determining whether individuals with T2DM have increased NOglc in white matter would be an important next step.

Finally, it is interesting to consider that both NOglc[24] and diabetes[25] have been suggested to play a role in the development of dementia. Individuals with diabetes are more likely to develop dementia[26] and chronic hyperglycemia, even in the absence of diabetes, is a risk factor for Alzheimer's disease (AD)[27]. Although alterations in NOglc have not yet been shown to be a risk factor for dementia, there is evidence that NOglc is involved in the development of amyloid plaques, one of the pathological hallmarks of AD. A previous study from our laboratory found that regions that have high levels of NOglc in healthy young adults go on to develop amyloid plaques in individuals with AD[28]. Consistent with this finding, Bero et al. reported a positive correlation between amyloid plaque loads and lactate production in a mouse model of AD[29]. In

the same model, Shannon et al. also found that hyperglycemia increases both amyloid production and lactate release in the hippocampus[30]. Other studies have reported that global NOglc is lower in both early[31] and late[32] onset AD, although both these studies involved small sample sizes (20 patients or less). A recent report from our group also found that aging decreases NOglc, particularly in regions with high rates of NOglc in young individuals[33]. Given these connections, it is tempting to argue that individuals with diabetes have an increased risk for the development of dementia, in part, because of the effect of hyperglycemia on NOglc. Detailed mechanistic studies will be required to verify whether this hypothesis has merit. A longitudinal study establishing that individuals with abnormal NOglc do go on to develop AD at higher rates would also be of great interest.

6.3 References

1 Suzuki A, Stern SA, Bozdagi O, Huntley GW, Walker RH, Magistretti PJ *et al.* Astrocyte-Neuron Lactate Transport Is Required for Long-Term Memory Formation. *Cell* 2011; **144**: 810–823.

2 Yang J, Ruchti E, Petit J-M, Jourdain P, Grenningloh G, Allaman I *et al.* Lactate promotes plasticity gene expression by potentiating NMDA signaling in neurons. *Proc Natl Acad Sci USA* 2014; **111**: 12228–12233.

3 Kety SS. The General Metabolism Of The Brain *In Vivo*. In: Richter D (ed). *Metabolism Of The Nervous System*. London, 1957, pp 221–327.

4 Seifert T, Secher NH. Sympathetic influence on cerebral blood flow and metabolism during exercise in humans. *Prog Neurobiol* 2011; **95**: 406–426.

5 Dienel GA. Brain Glucose Metabolism: Integration of Energetics with Function. *Physiol Rev* 2019; **99**: 949–1045.

6 Goyal MS, Hawrylycz M, Miller JA, Snyder AZ, Raichle ME. Aerobic glycolysis in the human brain is associated with development and neotenous gene expression. *Cell Metab* 2014; **19**: 49–57.

7 Shannon BJ, Vaishnavi SN, Vlassenko AG, Shimony JS, Rutlin J, Raichle ME. Brain aerobic glycolysis and motor adaptation learning. *Proc Natl Acad Sci USA* 2016; **113**: E3782–91.

8 Madsen PL, Hasselbalch SG, Hagemann LP, Olsen KS, Bülow J, Holm S *et al.* Persistent resetting of the cerebral oxygen/glucose uptake ratio by brain activation: evidence obtained with the Kety-Schmidt technique. *J Cereb Blood Flow Metab* 1995; **15**: 485–491.

9 Martin TA, Keating JG, Goodkin HP, Bastian AJ, Thach WT. Throwing while looking through prisms. I. Focal olivocerebellar lesions impair adaptation. *Brain* 1996; **119 (Pt 4)**: 1183–1198.

10 Hansel C, Linden DJ, D'Angelo E. Beyond parallel fiber LTD: the diversity of synaptic and non-synaptic plasticity in the cerebellum. *Nat Neurosci* 2001; **4**: 467–475.

11 Raichle ME. Neuroscience. The brain's dark energy. *Science* 2006; **314**: 1249–1250.

12 Raichle ME, Mintun MA. Brain work and brain imaging. *Annu Rev Neurosci* 2006; **29**: 449–476.

13 Kety SS, Woodford RB. Cerebral blood flow and metabolism in schizophrenia; the effects of barbiturate semi-narcosis, insulin coma and electroshock. *Am J Psychiatry* 1948; **104**: 765–770.

14 Norberg K, Siesiö BK. Oxidative metabolism of the cerebral cortex of the rat in severe insulin-induced hypoglycaemia. *J Neurochem* 1976; **26**: 345–352.

15 Abdul-Rahman A, Agardh CD, Siesjö BK. Local cerebral blood flow in the rat during severe hypoglycemia, and in the recovery period following glucose injection. *Acta Physiol Scand* 1980; **109**: 307–314.

16 Cryer PE. Glucose counterregulation: prevention and correction of hypoglycemia in humans. *Am J Physiol* 1993; **264**: E149–55.

17 Teves D, Videen TO, Cryer PE, Powers WJ. Activation of human medial prefrontal cortex during autonomic responses to hypoglycemia. *Proc Natl Acad Sci USA* 2004; **101**: 6217–6221.

18 Arbelaez AM, Rutlin JR, Hershey T, Powers WJ, Videen TO, Cryer PE. Thalamic activation during slightly subphysiological glycemia in humans. *Diabetes Care* 2012; **35**: 2570–2574.

19 Arbelaez AM, Su Y, Thomas JB, Hauch AC, Hershey T, Ances BM. Comparison of regional cerebral blood flow responses to hypoglycemia using pulsed arterial spin labeling and positron emission tomography. *PLoS ONE* 2013; **8**: e60085.

20 Arbelaez AM, Powers WJ, Videen TO, Price JL, Cryer PE. Attenuation of counterregulatory responses to recurrent hypoglycemia by active thalamic inhibition: a mechanism for hypoglycemia-associated autonomic failure. *Diabetes* 2008; **57**: 470–475.

21 Cryer PE. Mechanisms of hypoglycemia-associated autonomic failure in diabetes. *N Engl J Med* 2013; **369**: 362–372.

22 Prediabetes Is Associated With Structural Brain Abnormalities: The Maastricht Study. *Diabetes Care* 2018; **41**: 2535–2543.

23 Gabbay KH. The sorbitol pathway and the complications of diabetes. *N Engl J Med* 1973; **288**: 831–836.

24 Vlassenko AG, Raichle ME. Brain aerobic glycolysis functions and Alzheimer's disease. *Clinical and Translational Imaging* 2015; **3**: 27–37.

25 Arnold SE, Arvanitakis Z, Macauley-Rambach SL, Koenig AM, Wang H-Y, Ahima RS *et al.* Brain insulin resistance in type 2 diabetes and Alzheimer disease: concepts and conundrums. *Nat Rev Neurol* 2018; **14**: 168–181.

26 Cheng G, Huang C, Deng H, Wang H. Diabetes as a risk factor for dementia and mild cognitive impairment: a meta-analysis of longitudinal studies. *Intern Med J* 2012; **42**: 484–491.

27 Crane PK, Walker R, Hubbard RA, Li G, Nathan DM, Zheng H *et al.* Glucose levels and risk of dementia. *N Engl J Med* 2013; **369**: 540–548.

28 Vlassenko AG, Vaishnavi SN, Couture L, Sacco D, Shannon BJ, Mach RH *et al.* Spatial correlation between brain aerobic glycolysis and amyloid-β (Aβ) deposition. *Proc Natl Acad Sci USA* 2010; **107**: 17763–17767.

29 Bero AW, Yan P, Roh JH, Cirrito JR, Stewart FR, Raichle ME *et al.* Neuronal activity regulates the regional vulnerability to amyloid-β deposition. *Nat Neurosci* 2011; **14**: 750–756.

30 Macauley SL, Stanley M, Caesar EE, Yamada SA, Raichle ME, Perez R *et al.* Hyperglycemia modulates extracellular amyloid-β concentrations and neuronal activity in vivo. *J Clin Invest* 2015; **125**: 2463–2467.

31 Hoyer S, Oesterreich K, Wagner O. Glucose metabolism as the site of the primary abnormality in early-onset dementia of Alzheimer type? *J Neurol* 1988; **235**: 143–148.

32 Ogawa M, Fukuyama H, Ouchi Y, Yamauchi H, Kimura J. Altered energy metabolism in Alzheimer's disease. *Journal of the Neurological Sciences* 1996; **139**: 78–82.

33 Goyal MS, Vlassenko AG, Blazey TM, Su Y, Couture LE, Durbin TJ *et al.* Loss of Brain Aerobic Glycolysis in Normal Human Aging. *Cell Metab* 2017; **26**: 353–360.e3.